Univerzita Hradec Králové

Filozofická fakulta

Disertační práce

2022   Soňa Boriová

Univerzita Hradec Králové

Filozofická fakulta

Katedra archeologie

Fragmentation of Osteological Material in the Upper Paleolithic: Experiment and Archaeology

Disertační práce

Autor: Mgr. Soňa Boriová

Studijní program: P7109 Archeologie

Studijní obor: Archeologie

Forma studia: prezenční

Vedoucí práce: doc. Mgr. Sandra Sázelová, Ph.D.

Hradec Králové, 2022

Zadání disertační práce

Autor:	**Mgr. Soňa Boriová**
Studium:	F20DP0002
Studijní program:	P0222D120001 Archeologie
Studijní obor:	Archeologie
Název disertační práce:	**Fragmentarizácia osteologického materiálu v mladom paleolite: Experiment a archeológia**
Název disertační práce AJ:	Fragmentation of Osteological Material in the Upper Paleolithic: Experiment and Archaeology

Cíl, metody, literatura, předpoklady:

Disertační práce bude vypracovaná v souladu se Studijním a zkušebním řádem Univerzity Hradec Králové a požadavky Katedry archeologie FF UHK kladených na tento typ prací. Disertační práce bude vypracována v anglickém jazyce.

Práce se bude skládat z dvou částí, teoretické a praktické. Předmětem teoretické části bude rozšířená rešerše dostupné tuzemské i zahraniční literatury a budou představeny a rozpracovány metodické postupy a protokoly zaměřené na fragmentarizaci osteologického materiálu, z nichž bude vycházet část praktická. Praktická část bude obsahovat dvě složky. První část se bude věnovat experimentům s recentním materiálem zaměřeným na intencionální fragmentarizaci člověkem, v části druhé budou získané poznatky aplikované na vybraný osteologický materiál z paleolitické lokality regionu Dolní Věstonice – Pavlov – Milovice, např. Pavlov I.

Hlavním cílem práce je popsat a sumarizovat dosavadní znalosti k problematice fragmentarizace osteologického materiálu na archeologických lokalitách a nadvázat na aktuální práce sérií nových experimentů. Získané znalosti by měli napomoci interpretaci tafonomických jevů a fragmentarizačních vzorců pozorovaných na archeologických lokalitách ve sledovaném období.

Binford L.R. (1981). *Bones: ancient man and modern myths*. San Diego: Academic press

Johnson E. (1985). Current Developments in Bone Technology. *Advances in Archaeological Method and Theory* 8, 157-235.

Johnson E., Parmenter P.C.R., Outram A.K. (2016). A new approach to profiling taphonomic history through bone fracture analysis , with an example application to Linearbandkeramik site of Ludwinowo 7. *Journal of Archaeological Science: Reports* 9, 623-629.

Karr L.P., Outram A.K. (2012). Bone Degradation and Environment: Understanding, Assessing and Conducting Archaeological Experiments Using Modern Animal Bones. *International Journal of Osteoarchaeology* 25(2), 201–212.

Karr L.P., Outram A.K. (2012a). Tracking changes in bone fracture morphology over time: environment, taphonomy, and the archaeological record. *International Journal of Archaeological Science* 39, 555-559.

Micozzi, M.S. (1986). Experimental study of postmortem change under field conditions: Effects of freezing, thawing and mechanical injury. *Journal of Forensic Research* 31, 953-61.

Musil R. (2005). Animal Prey. In: Pavlov I Southeast. A window Into the Gravettian Lifestyle. Brno: Academy of Sciences of the Czech Republic, Inst. of Archaeology at Brno, 190-228.

Outram A.K. (2001). A New Approach to Identifying Bone Marrow and Grease Exploitation: Why the "Indeterminate" Fragments Should Not be Ignored. *Journal of Archaeological Science* 28, 401-410.

Ritchie R.O., Kinney J.H., Kruzic J.J., Nalla R.K. (2005). A fracture mechanics and mechanistic approach to the failure of cortical bone. *Fatigue and Fracture of Engineering Materials and Structures* 28, 345–371.

Shipman P. (1981). Applications of scanning electron microscopy to taphonomic problems. In Cantwell A.E, Griffin J.B., Rothschild N.A.(Eds.) The research potential of anthropological museum collections, Annals of the New York Academy of Sciences 376, 357-386.

Svoboda J., Novák M., Sázelová S., Demek J. (2016). Pavlov I: A large Gravettian site in space and time. *Quaternary International* 406, 95-105.

Zadávající pracoviště: Katedra archeologie, Filozofická fakulta

Vedoucí práce: doc. Mgr. Sandra Sázelová, Ph.D.

Datum zadání závěrečné práce: 20.10.2020

Prohlášení

Prohlašuji, že jsem tuto disertační práci vypracovala pod vedením školitelky doc. Mgr. Sandry Sázelové, Ph.D. samostatně a uvedla jsem všechny použité prameny a literaturu. Výsledky mezioborové spolupráce v rámci řešení disertační práce jsou použity se souhlasem všech spoluautorů.

V Hradci Králové

…………………………

Soňa Boriová

Annotation

BORIOVÁ, SOŇA. *Fragmentation of osteological material in the Upper Paleolithic: Experiment and Archaeology.* Hradec Králové: Philosophical Faculty, University of Hradec Králové, 2022, 248 pp., 15 supplements. Dissertation thesis.

The presented thesis deals with bone fragmentation as one example of numerous evidence of intentional human activity related to the processing and exploitation of hunted prey at archaeological sites. The research focuses on microscopic traces on and beneath the fracture surface and the correlation of these traces with macroscopic fracture characteristics. Using two chosen microscopic methods, I was able to observe fracture surface morphology on bone fragments and the microcracking present under this surface in detail. For testing the chosen methods and the primary description of the observed traces, samples from two fragmentation experiments using dynamic impact by natural processes and intentional human activity with recent osteological material were used. The tested microscopy methods were then applied to archaeological material from the Pavlov I Gravettian site. The results of the microscopic analysis in all the observed assemblages were put into context with a macroscopic evaluation of the fragmentation. In the case of the archaeological samples, the results are also discussed in the wider context of the basic data collected in the primary analysis of the chosen areas. It has been proven that even at the microscopic level, fragmentation leaves characteristic recognisable traces. These are typical for both the type of force applied and the state of preservation of the bone which was fractured. In the presented range, the results demonstrate the interpretive potential of the observed microscopic features and thus provide a solid starting point for further research.

Keywords

bone fragmentation experiment; fracture freshness index (FFI); scanning electron microscopy (SEM); histology; Pavlov I site

Acknowledgements

I would like to genuinely thank to my supervisor doc. Mgr. Sandra Sázelová, Ph.D. for her guidance, support, time, discussions and passed experiences throughout my, not only PhD, studies. I am grateful to prof. Alan K. Outram for introducing me closely to the bone fragmentation analysis and his valuable consultations concerning not only experimental design. Thank you belongs also to Mgr. Zuzana Pokorná, Ph.D. and Ing. Filip Mika, Ph.D. for their time, advice, and creativity during the SEM analysis of the bone samples and Hege I. Hollund for discussions over the resulting SEM pictures. I am very thankful to my colleagues from the Research Centre for the Paleolithic and Paleoanthropology, Institute of Archaeology, Brno, Czech Academy of Sciences, for their great encouragement, selfless help, practical suggestions but also professional advice, especially in the final stages of the thesis preparation.

Special thank you belongs to my family, their support in doing what I love means the world to me.

Contents

List of shortcuts and terms

AI – artificial intelligence

BSM – bone surface modification

Bv – bone value (in calculation methods for mean FFI)

FFI – fragmentation freshness index

FS – fracture surface

Fs – FFI score for individual fragment (in calculation methods for mean FFI)

Fl – length of fracture surface for individual fragment (in calculation methods for mean FFI)

Flwb – fracture length for whole bone (in calculation methods for mean FFI)

Fv – fragment value (in calculation methods for mean FFI)

HTS – histological thin section

LGM – last glacial maximum

MAU – minimum number of animal units

ML – machine learning

MNE – minimum number of elements

NISP – number of identified specimens

SEM – scanning electron microscopy

List of figures

Fig. 5.3: Example of stress relief ripple marks (A) and stress resistance chattering (B) on an archaeological bison metatarsal (*Johnson 1985,* 196, Fig. 5.14). **p. 69**

Fig. 5.4: Examples of percussion marks. Percussion notch originating in the place of impact (a), percussion grooves (b, black arrows), triangular (c, red arrow) and ovoid pits (c, black arrow) also directly related to the impact. Outer conchoidal scar with flake (d) and ripple marks (e) as an example of consecutive percussion marks and microstriations (f, red arrow) with pits (f, black arrow). Scale bar 1 cm (*Vettese et al. 2020,* 9-12, Fig. 1, 3, 4, 5; modified by SB). **p. 71**

Fig. 5.5: Example of bone broken by the hammerstone on anvil technique. The bone shaft fragment displays a percussion notch (upper edge of the fragment), rebound notch (lower edge of the fragment) and the spiral fracture outline with an oblique angle (*Outram 2002,* 55, Fig. 6.8). **p. 72**

Fig. 5.6: The picture shows different stages of bovid bones by wolves as stated by *Campmas* and *Beauval* (*2008*), a) complete bone with punters, pits and grooves on both epiphyses, b) part of proximal extremity damage starting at the great trochanter, distally starting from condyles, c) the distal end disappears completely before the proximal one, d) damage to the proximal end continues, the head of the femur is not destroyed immediately because it is denser and often protected by articulation with the coaxal, e) complete removal of epiphyses, bone cylinder remains, f) furrows (close up) from cylinder chewing on the cylinder, g) final fragmentation of bone shaft (in the referred study, observed only rarely), scale bar 5 cm (*Campmas – Beauval 2008,* 173, Fig. 5; modified by SB). **p. 80**

Fig. 5.7: Typical bone surface modifications caused by carnivore gnawing, a) punctures on ventral and dorsal (smaller picture) side of the bone, b) pits (white arrows), and c) scoring on compact bone, scale bar 5mm (*Stančíková 2018,* 34-35, Fig. 10-12; modified by SB). **p. 81**

Fig. 5.8: Group of crests and ridges chewed off the bones by carnivores, scale bar 2 cm (*Binford 1981,* 59, Fig. 3.21). **p. 82**

Fig. 5.9: Microscopic picture of pits with associated striations (white arrows), characteristically originating from dynamic impact by hammerstone, magnification not stated (*Pickering – Egeland 2006*, 462, Fig. 2; modified by SB). **p. 85**

Fig. 5.10: Table summarising the criteria according to progressing moisture loss (*Johnson 1985,* 187, Tab. 5.1). **p. 89**

Fig. 5.11: Diagram showing the cross-section of a river channel in winter (upper), spring ice breakup (middle) and summer (lower) (*Thorson – Guthrie 1984,* 176, Fig. 3). **p. 91**

Fig. 6.1: Illustration of evaluated traits, a) angle of the fracture surface in relation to the outer/inner bone surface, b) outline of fracture, c) rough (upper) or smooth (lower) character of the fracture surface (*Outram 2002*, 54-55, Fig. 6.2, 6.3 6.4, 6.5, modified by SB). **p. 98**

Fig. 6.2: Schematic description of signals analysed by SEM as described in the text. The volume of the sample in interaction for specific signals is illustrated in the colour coded droplet and the size depends on sample composition and accelerating voltage (*Specimen - electron-beam interaction*; modified by SB). **p. 101**

Fig. 6.3: Example of the EDX analysis result in the histogram (upper) and supplementary table (lower). Columns in bold correspond to the peaks in the histogram, showing the composition of bone coated with manganese-oxide concretions, example from the site Stránská skála IV (*Boriová et al. 2020*, 162, Fig. 6, modified by SB, measurement of composition by R. Škoda). **p. 102**

Fig. 6.4: Sample A. The image shows the original sampled fragment (upper left), with the specific area of sampling (upper right) and the final overview image of the sample surface from SEM (lower). The red corner marks the orientation of the sample. Magnification of overview image 35× (photo Z. Pokorná and SB). **p. 103**

Fig. 6.5: Sample A. The image shows position of the cutting plane on sample observed under SEM (upper image; red line), and orientation of the profile of the same sample observed in HTS (lower image) indicated by red dashed lines. Magnification of upper image 35×; magnification of lower image 50×, scale bar 1000 μm (photo SB and Z. Pokorná). **p. 107**

Fig. 7.1: Photographic documentation from the rock-fall experiment in progress capturing the place and setting of the action (*Karr 2012*, 211, Fig. 7.4). **p. 111**

Fig. 7.62: Sample Y. Fracture cutting through the osteons without deflection (red arrows). Magnification 100×, scale bar 300 μm, polarized light (photo SB). **p. 147**

Fig. 7.63: Sample O. Diagonal (left and middle red arrow) and perpendicular (right red arrow) microfracturing. In the diagonal one, a slight deflection by concentric lamellae in the osteon can be identified. Magnification 200×, scale bar 200 μm (photo SB). **p. 148**

Fig. 7.64: Sample Z. Diagonal cracking starting in a surface depression and mouthing back to FS (red arrows). Magnification 100×, scale bar 300 μm (photo SB). **p. 148**

Fig. 7.65: Sample IOTA. More pronounced shaping of the surface profile. Magnification 50×, scale bar 1000 μm (author SB). **p. 149**

Fig. 7.66: Sample ALPHA. Straight profile line with small shifts indicated by the red arrow. Magnification 50×, scale bar 1000 μm (author SB). **p. 149**

Fig. 7.67: Sample BETA. Microfracture cutting right through the osteon indicated by the red arrow. Magnification 100×, scale bar 300 μm (author SB). **p. 150**

Fig. 7.68: Sample EPSILON. Short and thin diagonal microcracking indicated by the red arrows. Magnification 200×, scale bar 200 μm (author SB). **p. 150**

Fig. 7.69: Sample IOTA. Microfracture perpendicular to the FS indicated by the red arrows. Magnification 100×, scale bar 300 μm (author SB). **p. 150**

Fig. 7.70: Sample MI. Shaping of the FS profile in spiral fractures. Magnification 50×, scale bar 1000 μm (author SB). **p. 150**

Fig. 7.71: Sample GAMA. Wide perpendicular cracking narrowing towards the end of the crack indicated by the red arrow. Magnification 100×, scale bar 300 μm (author SB). **p. 151**

Fig. 7.72: Sample MI. Wide diagonal crack cutting through the bone microstructure, starting in surface irregularity (red arrows). Magnification 50×, scale bar 1000 μm (author SB). **p. 151**

Fig. 8.1: Position of the Pavlov I and Dolní Věstonice I sites in larger context (lower left corner) and locally under the Pavlov hills (*Svoboda – Novák – Sázelová* 2016, 33, Fig. 1; *Svoboda et al. 2016*, 96, Fig. 1, modified by SB). **p. 159**

Fig. 8.2: Pavlov I. Excavation plan from the 2013-2014 season (pale grey) with the distribution of 3D recorded finds, 2015 (dark grey on margins), and Klima's trenches from 1952-1972 (transparent blue squares). K1-K14 are units uncovered during 1952-1972 by Klíma, S1-S3 are units uncovered by Svoboda during 2013-2015 (*Svoboda – Novák – Sázelová 2016*, 34, Fig.2; *Svoboda et al. 2016*, 98, Fig. 3; modified by SB). **p. 161**

Fig. 8.3: Pavlov I, area G. Described feature with articulated skeletal parts of wolf and reindeer. Fragmented osteological material also belonging to other animal species is present, which is scattered in the area (photo M. Novák). **p. 164**

Fig. 8.4: Pavlov I, area A. Plan of the whole area A excavated in 2013-2015 (bigger plan, left) and density of 3D recorded finds from 2013-2014 (smaller plan, upper right) with area extension in 2015 (smaller plan, upper right, dark grey). The red oval represents the find of a wolf skeleton and its surrounding, red dots are recorded finds of shells, the grey areas represent hearth and charcoal concentrations (*Svoboda – Novák – Sázelová 2016*, 45, Fig. 16). **p. 165**

Fig. 8.5: Pavlov I, area A. Picture of partially complete postcranial skeleton of a wolf *in situ* most possibly belonging to the pathological skull deposited nearby (*Svoboda – Novák – Sázelová 2016*, 46, Fig. 17). **p. 166**

Fig. 8.6: Pavlov I, area SE014. Plan of the whole area with settlement unit S1and eccentrically placed hearth, pit S2, and adjacent activity zone with another hearth on the left. Units marked with a red circle/oval, hearths with grey circle. The distribution of 3D recorded finds is pictured in the upper left corner (*Svoboda – Novák – Sázelová 2016*, 43, Fig. 13, modified by SB). **p. 167**

Fig. 8.7: Pavlov I, area SE014. Eccentrically placed hearth with dense concentration of objects within settlement unit S1 (photo R. Hadacz). **p. 168**

Fig. 8.8: Pavlov I, area G. Cutmarks on fragment of a tooth (a) and caudal extremity of lumbar vertebra (b), indicated by red arrows (photo SB). **p. 171**

Fig. 8.9: Pavlov I, area G. Percussion pit of ovoid shape on the left and percussion notch with heavily corroded inner bevelling on the right are indicated by red arrows (photo SB). **p. 172**

Fig. 8.10: Pavlov I, area G. Fragment of antler bearing marks, most possibly, caused by carnivore gnawing on both sides, indicated by red arrows (photo SB). **p. 172**

Fig. 8.11: Pavlov I, area G. Silhouettes of reindeer (left) and wolf (right) showing the representation of individual skeletal elements. The percentage ranges of representation from the total highest amount of identified bones for reindeer is given on the left side of the legend; for wolf on the right side of the legend. Representation of repetitive skeletal elements (e.g. *vertebrae*, *ossa carpalia*, *ossa tarsalia*, *phalanges*) were evaluated and marked in generalised groups. The ribs were always assigned only to the mammal size category, and so are not displayed in the scheme to avoid false species-specific under/over representation of this skeletal part. Note the very specific representation in wolf, narrowed to the front paw and one lower incisor (silhouettes from *ArchéoZoo - Vectorised skeletons*; modified by SB). **p. 177**

Fig. 8.12: Pavlov I, area A. Silhouettes of reindeer (left) and wolf (right) showing the representation of individual skeletal elements. The percentage ranges of representation from the total highest amount of identified bones for reindeer is given on the left side of the legend, for wolf on the right side of the legend. Representation of repetitive skeletal elements (e.g. *vertebrae*, *ossa carpalia*, *ossa tarsalia*, *phalanges*) were evaluated and marked in generalised groups. In the case of area A, only ribs from the articulated wolf skeleton were considered, as they were easily assignable to the species. Note the high representation of antlers in reindeer and the slightly higher representation of thoracic column in wolf (silhouettes from *ArchéoZoo - Vectorised skeletons*; modified by SB). **p. 178**

Fig. 8.13: Pavlov I, area SE014. Silhouettes of reindeer (left) and wolf (right) showing the representation of individual skeletal elements. The percentage ranges of representation from the total highest amount of identified bones for reindeer is given on the left side of the legend, for wolf on the right side of the legend. The representation of repetitive skeletal elements (e.g. *vertebrae*, *ossa carpalia*, *ossa tarsalia*, *phalanges*) were evaluated and marked in generalised groups. Ribs were always assigned only to the mammal size category, and so are not displayed in the scheme to avoid false species-specific under/over representation of this skeletal part. Note the higher representation of antlers, tarsal bones, and phalanges in reindeer. A significantly higher representation can be observed in autopodial elements, tibia, caudal vertebrae and in the flat bones of wolf (silhouettes from *ArchéoZoo - Vectorised skeletons*; modified by SB). **p. 179**

Fig. 8.14: Pavlov I, area SE014. Spatial placement of fragments evaluated by FFI. The upper diagram is for reindeer bones (green triangles), the lower diagram for wolves (red dots) (*Svoboda – Novák – Sázelová 2016,* 43, Fig. 13; modified by M. Novák and SB). **p. 186**

Fig. 8.15: Sample A3. State of surface preservation in an archaeological sample. The red arrows point to areas with surface corrosion. The areas in red circles represent the original preserved structure of FS, scale bar 1000 μm (photo SB). **p. 187**

Fig. 8.16: Sample A5. Oval depression in FS with a concentration of microcracks parallel to the lamellar orientation (white arrows). Magnification 350×, scale bar 200 μm (photo SB). **p. 189**

Fig. 8.17: Sample A5. Remnant of fibre-like unit/body (white arrows) present in a surface depression. Magnification 1500×, scale bar 50 μm (photo SB). **p. 189**

Fig. 8.18: Sample A1. Parallel and subparallel lines (white arrows) present on the fracture surface. Magnification 142×, scale bar 500 μm (photo SB). **p. 189**

Fig. 8.19: Sample A9. Surface texture most probably smoothened by post-/depositional taphonomic changes. Magnification 200×, scale bar 500 μm (photo SB). **p. 190**

Fig. 8.20: Sample A9. Granularities marked by white ovals. Magnification 140×, scale bar 500 μm (photo SB). **p. 190**

Fig. 8.21: Sample A4. Transversally oriented ridges on longitudinal FS indicated by white lines. Magnification 37×, scale bar 100 μm (photo Z. Pokorná and SB). **p. 191**

Fig. 8.22: Sample A2. The white arrows point toward microfractures with variable width and course. Interaction of microfracture with most probably the Haversian canal in the white circle. Magnification 800× (left), 650× (right), scale bar 100 μm (photo SB). **p. 191**

Fig. 8.23: Sample A10. Wide microfracture with sharp edges and smooth walls (white arrows). Thinner cracks with an irregular course present in surface depression (white oval). Magnification 500×, scale bar 200 μm (photo SB). **p. 191**

Fig. 8.24: Sample A3. Microcracks with rounded and granular edges present in the surface depression. Magnification 500×, scale bar 200 μm (photo SB). **p. 191**

Fig. 8.25: Sample A5. Linear patterning of the surface clearly visible throughout the whole sample. Magnification 37×, scale bar 100 μm (photo Z. Pokorná and SB). **p. 192**

Fig. 8.26: Sample A6. Well pronounced fan-shaped pattern on the sample from helical FS (white arrows). Magnification 37×, scale bar 100 μm (photo Z. Pokorná and SB). **p. 193**

Fig. 8.27: Sample A8. Plate-like protrusion lined by cracking (white arrows). Magnification 37×, scale bar 100 μm (photo Z. Pokorná and SB). **p. 193**

Fig. 8.28: Sample A7. Series of open Haversian canals in surface depressions, microcracking most possibly related to corrosive changes (white arrows). Magnification 350×, scale bar 300 μm (photo SB). **p. 194**

Fig. 8.29: Sample A1. Shallow surface depression with different colouring (red arrow). Magnification 100×, scale bar 300 μm (photo SB). **p. 195**

Fig. 8.30: Sample A1. Colour changes most probably caused by iron staining (red circles), also filling the Haversian canals (red arrow). Magnification 100×, scale bar 300 μm (photo SB). **p. 195**

Fig. 8.31: Sample A9. Bounded dark colouring of bone avoiding the Haversian canals (left), and boundless cloud-like colouring spreading through the sample without any reference to the bone microstructure (right). Magnification 50×, scale bar 1000 μm (photo SB). **p. 195**

Fig. 8.32: Sample A4. Foggy appearance of dark coloration in polarised light. Lacunae are represented by the dots in the foggy areas (red circles). Red arrows indicate the iron colouring of the Haversian or Volkmann canals. Magnification 50×, scale bar 1000 μm (photo SB). **p. 196**

Fig. 8.33: Sample A3. Microcrack running along the Haversian canal, branching in various directions (red arrows). Magnification 100×, scale bar 300 μm (photo SB). **p. 196**

Fig. 8.34: Sample A9. Irregular FS due to the underlying bone microstructure. Magnification 50×, scale bar 1000 μm (photo SB). **p. 197**

Fig. 8.35: Sample A9. Thin and short diagonal microcracks (red arrows). Magnification 100×, scale bar 300 μm (photo SB). **p. 197**

Fig. 8.36: Sample A4. A couple of microfractures perpendicular to FS (red arrows). Magnification 100×, scale bar 300 μm (photo SB). **p. 197**

Fig. 8.37: Sample A9. Branching of open crack indicated by red arrows. Magnification 50×, scale bar 1000 μm (photo SB). **p. 198**

Fig. 8.38: Sample A2. Convex FS on sample from spiral fracture. Magnification 50×, scale bar 1000 μm (photo SB). **p. 199**

Fig. 8.39: Sample A7. Straight profile shaping with slight surface irregularities. Magnification 50×, scale bar 1000 μm (photo SB). **p. 199**

Fig. 8.40: Sample A6. Variable and shaped surface in spiral FS. Magnification 50×, scale bar 1000 μm (photo SB). **p. 200**

Fig. 8.41: Sample A7. Wide cracking and branching. Green arrows indicate cracks respecting the bone structure; red arrows indicate those that cut through the canals. Magnification 50×, scale bar 1000 μm (photo SB). **p. 200**

Fig. 8.42: Sample A6. Sinuous crack perpendicular to FS indicated by red arrows. Magnification 200×, scale bar 300 μm (photo SB). **p. 201**

Fig. 8.43: Comparison of FFI value representation in reindeer and wolf in the studied areas (*Svoboda – Novák – Sázelová 2016*, 34, Fig.2; modified by SB). **p. 203**

List of tables

List of graphs

Prologue

Human settlements are characterised by displaying traces of the presence of people. These traces have multiple forms and may be represented, for example, by hearths, dwellings, pits, activity zones, refuse zones, and other complex structures. Among these can be isolated finds indicating a settlement or another human-induced activity. These structures and materials are subjected to different influences during and after the settlement phase. The state of the preservation of every archaeological site depends on the influences involved. Therefore, each site or assemblage forms a unique situation influenced by a distinct combination of factors. Similarly, an individualised approach and a customised combination of methods for processing and gaining as much information as possible are needed. In this case, bone fragmentation was at the centre of interest. At the campsites, it can be caused accidentally or intentionally by a huge variety of taphonomic actors and activities that are both contemporary with the campsite or take place later after its disappearance (see Chapter 5). The more precisely specific fragmentation traces and patterns can be assigned to specific taphonomic agencies, the more it is possible to find out about life at the camp or the complex history of the site.

Advances in fragmentation research are of great importance, particularly in highly fragmented assemblages that contain a quantity of precisely unidentifiable fragments. Gaining information about size classes and the number and proportion of respective fragments and the fracture characteristics of individual elements in the context of other traces or the find circumstances can provide valuable information concerning the taphonomic history of the site or assemblage. However, the efficiency of the methods used should first be proven on material with known fragmentation circumstances (e.g. experimental material) or assemblages accompanied by other lines of evidence yielding information about the range of taphonomic factors and the activities that played a part.

Intentional human modification of hard animal tissues is a highly complex topic. First, bones can be modified as a by-product of dietary exploitation. Different traces, such as cut marks or percussion marks, can be observed as evidence of the effort to acquire the maximum amount of food or edible nutrients. As humans became more familiar with animal bodies and all the 'materials' they consist of, they also found a way to exploit them other than for dietary purposes. Ornaments, tools or other utilitarian objects from bone, antler or ivory represent important elements of different cultural groups/human societies from the Middle Paleolithic and form an important and remarkable field of study

(e.g. *Choyke 1997*; *Conard 2003*; *St-Pierre – Walker 2007*; *Backwell – d′Erico 2014*; *Hromadová 2016; Hutson et al. 2018a*). An association exists between hunted prey and the raw material used for tools and other object production (e.g. *Binford 1983*). Different parts of the animal skeleton possess different properties when it comes to processing, modification and use. This is caused by the variable microscopic structure of individual parts such as teeth, antlers, tusks and bones. Therefore, their response to applied force within these categories is also significantly different. However, the differences can be observed even within the categories. For example, *Haynes* (*2021*) states that the standard methods concerning bone fragmentation should be adjusted when used for mammoth bones because in the usual setting they do not reflect all the traces in the corresponding manner. However, to test such a variety of materials and the responses to different types of loading using the newly proposed methods requires intensive long-term research, which is challenging in many ways.

In this thesis, I focus on the fragmentation of medium/large-sized mammal long bones separately. In the Upper Paleolithic, medium or large-sized herbivores served mainly as a dietary source (bearing meat, containing marrow and bone fat) and as a source of raw material for certain types of tools or objects (e.g. *Rašková Zelinková 2013; Backwell – d'Errico 2014; Turner et al. 2020*). In both cases, the processing of bone includes its intentional fragmentation. In the case of tools, this was the first step of many, followed by shaping, polishing or carving the tool/object to the desired or functional condition. In dietary exploitation, the fragmentation step tended to be at the end of the operational chain after skinning, defleshing, and disarticulation of the animal carcass. Furthermore, these two processes can be mutually intermingled. As discussed later in the text, the fragmentation patterns or traces can overlap with other actors at the site, and their distinction is vital when it comes to understanding and interpreting the find situations and material.

Numerous researchers and studies have emerged working with different classification and description systems over the past decades. Some of the defined criteria are still widely used and applied today (e.g. *Morlan 1980; 1984; Villa – Mahieau 1991*) although some have proven that the outcomes of the fragmentation process under study are due, to a certain extent, because of other features than the fragmentation agent and are a result of equifinality (e.g. *Shipman 1981; Karr – Outram 2012a; Haynes – Krasinksi – Wojtal 2021*). The results of the latter reflect the differences in bone fragmentation caused

by specific bone microanatomy, variable states of preservation, and the different types of forces applied, mainly on a macroscopic level. I decided to look much closer and verify the microscopic variability and distinctiveness of the generated characteristics in individual cases. I have focused my attention on two aspects – first, the microscopic morphology and patterning of the fracture surface, and second, the abundance and behaviour of microcracking in relation to bone microanatomy.

In the analysis and description of the proposed microscopic characteristics, I draw on numerous medical, material and forensic studies. These fields provide rich literature on bone structure and properties and thorough research on bone fragmentation in standardised conditions. These studies use blocks of compact bones from specific locations and skeletal parts and work with standardised devices engaging precisely measured stress in the desired directions and positions in relation to the long bone axis. They propose different types of modelling from calculations to complete bone material modelling. On the one hand, they were able to identify the most important structures and properties responsible for the specific response of a bone to applied stress, at the level of the species, anatomic elements and specific bone portions (anterior/posterior/lateral/medial) in relation to age, sex, diseases etc. (e.g. *Ager – Balooch – Ritchie 2006; Wang 2011; Zioupos – Kirchner – Peterlik 2020*). Some of their findings are outlined in Chapters 2.2 and 2.3. On the other hand, they only rarely deal with bone as a complete element. It is important to bear in mind that the complex properties of bone as a whole (e.g. shape, cortical bone thickness, preservation state, presence of marrow in the medullary cavity, presence of the periosteum) all play an important role in the final bone response to loading (*Johnson 1985,* 161). Therefore, the above-mentioned studies may serve as a good starting point and solid base, but separate archaeological investigation/experiments are crucial in order to consider as many variables as possible (e.g. state of preservation, completeness of the fragmented bones), which significantly influence the outcomes that can be observed in archaeozoological assemblages.

Archaeological experiments with recent animal bone material are a reliable line of evidence when it comes to testing new methods and approaches. With suitable setting and material adjustment, we can eliminate the unknown variables present in the archaeological record, model observed situations or proposed technological processes and study what type of evidence they lead to and what the characteristic traits are. Since the

reaction of bone material to force depends not only on the type of acting force but also on the preservation state of the bone and the presence of other soft tissues, I decided to analyse the fracture surfaces where all these variables were known. In this case, recent animal (cattle and deer) long bones in various preservation states were fragmented and different types of dynamic forces to break the bones were implemented. The precise experimental setting and procedures are described in Chapter 7. The experimental assemblages under study provided a sample for correlation of the macroscopic method (Chapter 6.2) with the proposed microscopic characteristics. Their mutual correlation was not only tested on the experimental material but to the same extent and combination also applied to the archaeological assemblages from the Gravettian Pavlov I site (Chapter 8). In the latter, the long bones of two mammalian medium-sized species were at the centre of interest, representing different roles in the subsistence strategies of Paleolithic people. To observe the microscopic traces, two microscopic methods with different resolution abilities were applied. The gross characteristics of the fracture surface are already distinguished by different approaches in the two main categories – rough and smooth. However, the closer relationship between these two categories and the underlying bone microstructure was not described while the potential for further categorisation within the two gross categories remained to be tested. Scanning electron microscopy (SEM) was used to observe the fracture surface and its morphology and microcracking in greater detail. The transmitted light microscopy was used to visualise the cross-section perpendicular to the fracture surface, which enabled observation of the microcracking penetrating under the fracture surface. Their use was chosen based on the benefits of addressing a wide variety of archaeological analyses and the implementation of bone fracture analysis in other fields of study (more on this in Chapter 6). However, as experienced in my work, they also have some disadvantages. In addition to being financially demanding, there are specific requirements concerning sample size and preparation. Even after careful cutting, dehydrating and metal coating, the vacuum chamber pumping can take a long time or may not be successful at all. Securing the conductivity of the sample may also be difficult to establish (multiple metal coating, fastening with conducting tapes) and cause overcharging and artefacts in the final image output. The histological method is also destructive and cutting the sample is required. The preparation process is lengthy and time-consuming. A range of mistakes that can affect the final thin section can be made during the process and so can make the observation of

the given traits more difficult or even impossible. In such cases, a completely new thin section must be prepared. These methodological inconveniences are even more relevant when the analysis of unique archaeological material is the concern. In the discussion of this thesis, other methods are proposed that possibly may have fewer risks and demands when addressing this problem. However, this recommendation could only be made based on the observed consequences and the results from the currently suggested and used methods.

This dissertation thesis is organised into two parts. PART I contains the theoretical introduction and background to the topic. In the first chapter, the position of bone fragmentation within the archaeological analysis is discussed. The second chapter summarises the basic bone structure, microstructure, and biomechanical properties as relevant variables in the response of the bone to stress. In the third chapter, I discuss the influence of the bone preservation state on the fragmentation pattern and the traces observed. The fourth chapter deals with the spiral fracture phenomenon. The final chapter in this part describes the different fragmentation agents and the traces they leave behind. PART II is dedicated to experiments and the application of tested methods on archaeological material. In Chapter 6, I describe the methods and procedures, which were used equally for both types of material. Chapter 7 describes experiments with recent animal bones, their detailed setting and the results obtained. The final chapter of the thesis deals with the application of the tested method and the traces observed on the archaeological material from various areas of the Pavlov I Gravettian site in the Czech Republic.

The aim of the thesis

The thesis focuses on the fragmentation of osteological material and its recognisable morphological features on bones and their fragments. Of importance is the relevance of the traits observed in the context of archaeological sites, where different depositional and post-depositional fragmentation agencies commonly leave their marks. Human activity is not an exception and its recognition among other taphonomic factors plays a key role in the understanding and interpretation of Mid-Upper Paleolithic bone assemblages. I approached this topic through experiments with recent osteological material. The main aims of the thesis were **a)** to verify well-established microscopy methods (SEM, histology) for observation of the fracture surface and any microcracking connected to intentional human bone breakage, **b)** to correlate the perceived results with macroscopic methods of evaluation (FFI), and **c)** to test the usefulness and reliability of the mentioned approaches in the archaeological context of the archaeozoological assemblage from the Moravian Pavlov I settlement, Czech Republic.

PART I

1. Fractures and fragmentation and their position within the taphonomic analyses

Taphonomy is a broad and complex field of study previously defined by the Russian researcher *I. A. Efremov* in *1940*. It covers a huge number of agents and the modifications originating from their activity. There is a variety of biotic and abiotic taphonomic actors causing modifications and marks which can be more or less specific to their activity. The activity of the taphonomic actors is massively complex and results in a combination of traits. The more specific traits, such as gnawing marks, loading points or root imprints, can be ascribed solely to the agent. The less specific traits, such as fractures and their characteristics may be attributed to a range of taphonomic agents and, in such cases, all other traces present on bone or available from the finding context are crucial in the precise actor identification.

Hard tissue modifications and specifically bone fragmentation, have a long research tradition. The question of the actor responsible for the bone modification and breakage plays an important role in demonstrating the presence, intentional activity or the modelling of indirect evidence in early hominid behaviour, especially when other data are missing or overlapping (e.g. *Breuil 1938; 1939; Dart 1949; 1957; 1959; 1960; Brain 1969; 1976; Guthrie 1980; Binford 1981; Bunn 1981; 1989; Johnson 1985; Blumenschine 1995; Pickering et al. 2005; Smith 2015; Blasco et al. 2019; Daujeard et al. 2020*). *Breuil* (*1939*) identified spiral fractures in the assemblage from the site near Zhoukodoudian. He described the spirally fractured bones as daggers made by *Homo erectus*. *Dart*, in his works (*1957; 1959*), went even further in time and reported spirally fractured long bones by *Australopithecus africanus.* He argued that only humans can break bones in the spiral manner by the "crack-and-twist" technique (see the following paragraphs). Therefore, spiral or helical fractures and their appearance in archaeozoological assemblages may have led researchers to conclusions about human involvement, even despite a lack of other supportive evidence (e.g. *Jopling – Irvin – Beebe 1981*).

The method of fragmenting bones from the perspective of nutritional or material exploitation was already mentioned by several scholars in the 1930´s (*Breuil 1938; Weidenreich 1941; Dart 1959; Howell 1965).* By then, there was already a belief that humans break bones differently than animals and bones broken in this way possess different diagnostic patterns that are mainly observable on long bones (*Binford 1981,* 37).

Breuil (*1938*) put forward theory that humans fracture bones longitudinally, while the activity of animals led to transversal fractures. *Weidenreich* (*1941*) also later followed this opinion. The main conclusion persists until the present day, although the diagnostic features are changing, evolving and increasing in number. Human activity and distinguishing its impact was, and still is, of great importance since it could prove the earliest involvement of foragers in animal body utilisation (e.g. *Breuil 1939; Dart 1957; 1959; 1960; Thompson et al. 2019*). In 1959, *Dart* devised the so-called "crack-and-twist" technique, which was intended to stand behind the origin of the legendary and well-known term "spiral fractures". The crack-and-twist technique was widely cited and used even though the twisting itself did not play a major role in the spiral fracture emergence (e.g. *Sadek-Koros 1972; 1975*; *Binford 1978,* 152-157; *Bonnichsen 1979,* 37-53). A spiral or helical type of fracture can be more or less undoubtedly prescribed to green/fresh bone fracturing, although, it cannot solely be considered as evidence of human activity, despite some researchers might have suggested this fact (see Chapter 4; *Bonnichsen 1973, 1979; Frison 1970; Binford, 1981; Johnson 1985*, 175). Based on the conclusion that a spiral fracture is exclusive to human intentional modification, the overlap of human-carnivore activity was also omitted or mistakenly interpreted many times and played a role in the ongoing hunting-scavenging debate (e.g. *Johnson 1985,* 200; *Blumenschine 1995; Domínguez-Rodrigo 2002*). This failure to recognise the animal impact on bone fragmentation (prey-scavenging activity, other non-feeding activities such as trampling or wallowing) created a myth about a spiral fracture being a typical marker for human activity (*Binford 1981,* 41-42).

The concept of a spiral fracture was the subject of study and experimentation for decades to prove its position in demonstrating human activities. Several authors with various typologies that concerned mainly the outline of fracture emerged (e.g. *Biddick – Tomenchuk 1975; Shipman – Bolser – Davis 1981; Davis 1985; Johnson 1985; Villa – Mahieau 1991; Haynes 1983a; Marshall 1989*), with most of them based on macroscopic description. Further categorisation within the spiral shape of a fracture but on a microscopic level was made by *Shipman* (*1981*, 371-373), who described two types based on different tension failures observed under a scanning electron microscope (SEM). Type I has a smooth fracture plane emerging between the collagen bundles. Type II has the fracture plane perpendicular to the main bundle orientation, leading to a rough and stepped surface of the fracture. However, even this typology was not able to assign any

of these two types exclusively to human fragmentation. More recent studies, and experiments also focused on the occurrence of a spiral fracture in relation to different variables, such as the fragmentation factors (e.g. rockfall/human/carnivore), bone preservation conditions (frozen/dried/fresh/burned), accompanying traces, and even intuitiveness in human breaking bones (*Outram 2001*; *2002*; *Karr 2012*; *Karr – Outram 2012a*; *2012b*; *2015*; *Waterhouse 2013*; *Vettese et al. 2021*). However, as the results of these studies also showed, it became more of a subject of equifinality in fragmentation and fracture research affected by many variables (see Chapter 4).

Another method related to bone fragmentation is the analysis of percussion marks and impact or loading points assumed to be related to intentional human activity, more specifically to the marrow and bone fat exploitation in ungulates (e.g. *Blumenschine – Selvaggio 1988*). These also overlap with other similar traces such as gnawing pits, which can be observed, and are the subject of detailed analysis and material revisions participating in the extensive hunting-scavenging discussion (e.g. *Capaldo – Blumenschine 1994*; *Domínguez-Rodrigo – Barba 2006*, 170; *Blumenschine et al. 2007*; *Parkinson 2018*; *Thompson et al. 2019*). Percussion damage to the bone is the subject of intensive experimental work and modern specialised software, artificial-intelligence or machine-learning analysis (e.g. *Pickering – Egeland 2006*; *Galán et al. 2009*; *Blasco et al. 2014*; *Courtenay et al. 2019*; *Moclán - Domínguez-Rodrigo – Yravedra 2019*; *Stavrova et al. 2019*; *Vettese et al. 2020*; *Domínguez-Rodrigo et al. 2020*). The study of percussion marks is more elucidated in Chapter 5.1.3.

In addition to experiments, numerous ethnoarchaeological studies of contemporary hunter-gatherer and semi-nomadic societies in Africa or northern areas contributed to the analysis of long bone fragmentation (e.g. *Binford 1978*; *O'Connell – Hawkes – Blurton Jones 1988*; *Enloe 1993*; *Oliver 1993*; *Lupo 2001*; *Abe 2005*; *Morin 2007*; *Costamagno – David 2009*). However, these are mainly focused on hunting strategies, transport decisions, types of treatment, exploitation extent and patterns in relation to specific species or skeletal parts. The analysis of the presence and frequency of skeletal parts and the accumulations and traces left after individual processing activities also help to recognise these aspects in the archaeological record. They provide an analogy to complex situations and unlike experiments allow us to model and adapt different circumstances to study particular details.

The fragmentation topic in archaeofaunal assemblages was also approached through the analysis of fragmentation levels. Instead of focusing on specific surface modifications to bone, different ratios or indices base on standard quantification measures such as NISP, MNE, MAU or %MAU (*Lyman 1994*, 100-113) in relation to bone completeness were calculated. In their study, *Todd* and *Rapson* (*1988*, 307-325) outline several techniques with the focus on intra-site analysis, such as the percentage of complete bones, the percentage difference in the representation of proximal and distal epiphyses, the amount of shaft remaining attached to the epiphysis, and shaft fragment abundance and its relation to the frequencies of the epiphyses. *Lyman* (*1994*, 33) also notes, that an important variable in the taphonomic analysis should be the consideration of the ratio of complete unbroken bones in an assemblage. He introduces two concepts. The first is the *extent of fragmentation* represented by the ratio of incomplete bones/fragments to whole elements (total NISP) in an assemblage. The second is the *intensity of fragmentation* referring to size of the fragments studied and can be studied directly via the size of the broken bone fragments, where fragments of similar-sized bones should be compared. The second way to analyse the intensity of fragmentation is through the NISP:MNE ratio (e.g. *Richardson 1980*). The higher the ratio, the more intensive the fragmentation. However, the principle is still the same: the more of the small fragments present, the higher the intensity of fragmentation. Another combination was proposed by *Morlan* (*1994*) on an assemblage of bison bones. He put together an analysis of bone portions with the observation of volume density affecting survivorship and the percentage of bone completeness. Each of the approaches can contribute to certain aspect of analysis while other aspects can remain neglected. The combination of the named comparative techniques helps to underline various modules of bone fragmentation (e.g. *Gifford-Gonzalez 1989*; *Wolverton 2002*; *Yeshrun – Marom – Bar-Oz 2007*; *Merritt – Davis 2017*) and provides more complete information at several levels. Even though in many cases they do not necessarily lead directly to the precise process responsible for the fragmentation pattern and characteristics, these analytical procedures and their adjusted incorporation provide us with a huge body of information. They allow us to study the taphonomic history of assemblages, better define butchery practices and transport decisions, and acquire data for intra and inter-site comparison, which can be followed up by other types of more focused analyses/analytical approaches.

The importance of the discussed topic is obvious in the context of Plio-Pleistocene sites, particularly in East Africa concerning the earliest hominin ancestors, their presence, hunting capacities, and traces of their other activities in archaeofaunal material as a potential source of their subsistence strategy or as a source of raw material (see above). Since the early hominins shared the ecosystem with carnivores, a natural competition over food resources became the centre of interest. In the 1980s, this led to an exhausting hunting-scavenging debate, focused on an overlap in hominin and carnivore access to animal bodies and the traces of their activity in osteological assemblages and the importance of distinguishing between the interventions of these two has grown exponentially (*Courtenay et al. 2019*, 28). In Middle Paleolithic sites, evidence of processing or fragmenting bones for marrow extraction increases and so different, more intensive ways of carcass exploitation are suggested (e.g. *Blasco et al. 2013a*; *Speth et al. 2012*; *Marín et al. 2017*). Intensive studies and experimentation are still being undertaken to test these suggestions and attribute the observed modifications to humans (e.g. *Capaldo – Blumenschine 1994*; *Blacso et al. 2014*; *Vettese et al. 2017*; *Byers – Keith – Breslawski 2020*). This is not quite the case for the Mid-Upper Paleolithic settlements where the presence and intervention of humans are more than clear from other types of numerous evidence. To name just some of many, this is the presence of dwelling structures, hearths, workshop areas, lithic and hard animal tissue artefacts, symbolic/art objects, bones bearing different traces of exploitation activities (cutmarks, impact scars) and human burials. However, the presence of humans does not exclude the presence of other, mainly animal, actors influencing the final find situation. There is evidence that people, to some extent, interacted with wild animals around their settlements, not only in a hunter-prey relationship (e.g. *Sázelová et al. 2020*). Therefore, we can assume that traces of animal activity may be present on settlement sites and contemporary with different human activities with certain traces overlapping each other. In such cases, the ability to differentiate this overlap can aid the recognition of different activity zones or refuse zones, and the actors that are responsible for their formation. The differentiating role also holds potential for sites with multiple phases of settlement, where the individual phases stratigraphically intersect. Furthermore, the possibility to separate the later activity of various processes, whether the activity of animals on abandoned sites or post-depositional changes caused by geological or other environmental activities can help to understand the site formation process and the complex taphonomic history of finding, in our case,

osteological material. Nonetheless, it is important to bear in mind that when addressing these topics, the fragmentation analysis is only one way of looking at the evidence and its correlation with other lines of documentation from the remainder of the find material and the find context itself is necessary.

2. Bone, structure and properties

Bone represents a special type of complex living material, which (during life) undergoes continuous rebuilding and reconstruction. The bone remodelling process involves the resorption of an old bone matrix by osteoclasts and the formation of new bone tissue that emerges in the ossification process. These mechanisms are involved in fracture and fatigue microdamage reparation (e.g. *Martin – Burr – Sharkey 1998*, 181; *O´Brien et al. 2005*, 72), ageing or rebuilding of bone as a response to changing physical loading by direct mechanical stress or tension by individual muscles and tendons in specific skeletal elements (*Čihák 2001*, 74). This is typical of periosteal growth (outer bone surface) and endosteal resorption (inner bone surface), mostly in balance. Together with ageing, endosteal resorption tends to exceed periosteal growth. However, the biomechanical strength of the bone may still be preserved to a certain level because, with a growing external diameter, resistance to bending also increases (*Ortner – Turner-Walker 2003*, 21-22). On a microscopic level, the remodelling process is a multiple-phase procedure. The first phase is an *activation phase* as a reaction to the initial remodelling signal, which, for example, can be direct mechanical loading or hormone-induced changes. The following *resorption phase* represents the response of the osteoblasts to initiating signals by releasing the osteoclast precursors. Osteoclasts are focused on the places of resorption where they form characteristic Howship's lacunae. In the *reversal phase*, the osteoclasts retreat and die. The process is maintained by the so-called reversal cells (mononuclear cells of undetermined lineage), which most probably send signals that cause the transition from bone resorption to the bone formation process. In the *formation phase*, sclerostin (which prevents the initiation of bone formation) secretion by the osteocytes is inhibited through difficult signalling pathways and, therefore, bone formation by osteoblasts may play a part. The osteoblasts release a group of bone-forming proteins and osteocalcine and fill the Howship's lacunae with osteoid (organic bone matrix). The last phase is the *termination phase/quiescence* where the resorbed bone is replaced by the mineralisation of a newly deposited osteoid. The osteoblasts are differentiated either to bone lining cells or osteocytes (Fig. 2.1). All the above-mentioned steps are maintained by complex signalling pathways and hormonal signalling and many are not still fully understood (*Raggatt – Partridge 2010*, 25105-25107). The remodelling process may be further affected by other factors such as ageing, stress and diseases (e.g. *Čihák 2001*, 74; *Ager - Balooch - Ritchie 2006*, 1884-1888; *Wang 2011*, 69-78).
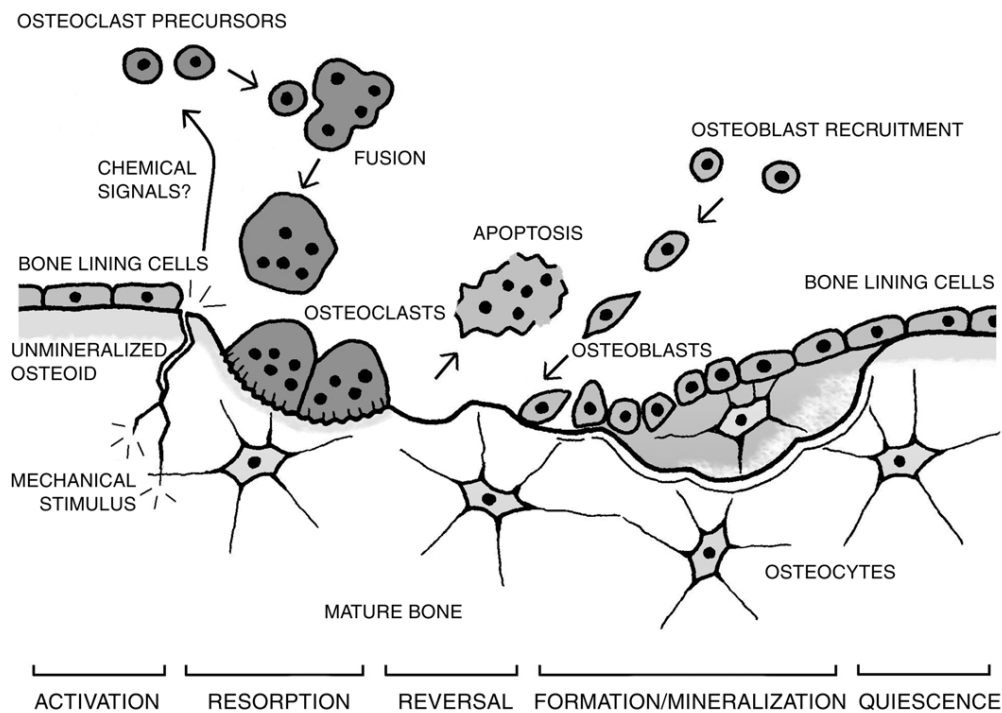
Fig. 2.1: Process of bone remodelling on a cellular level illustrated from the activation phase (left) to the termination phase/quiescence (right) (*Ortner – Turner-Walker 2003*, 23, Fig. 2-18).

In the same way that the bone changes its reaction depending on the previously stated conditions, the reaction to external loading is also variable in an altered condition according to the preservation state. To understand the principle of traces observed on the bones, the basic chemical and mechanical structure of the bone and its properties should be kept in mind. In the following chapters, I refer mainly to the mammalian long bone, its structure and properties, although in the context of information concerning these issues, in bone tissue as a material generally. Long bone is a rich source of nutrients, fat and raw material for exploitation, and therefore is an element that has been intensely focused on in the past. Considering their structure, long bones have a higher probability of preservation in archaeological contexts in comparison to flat or irregular bones with thin compacta on the surface and a large amount of spongiosa inside (e.g. skull fragments, *vertebrae*, etc.). Within the fragmentation topic, long bones are intensively being studied in archaeozoological research although knowledge from extensive medical research can also be considered (more in the following chapters).

2.1 Bone microstructure

Bone is a special type of connective tissue that provides support, protection of major organs, and movement for the whole body, and is a place of attachment for ligaments, muscles, and tendons. However, these are not the only functions of bone tissues. Bone is a dynamic and active tissue, which undergoes different processes throughout life, such as growth and remodelling according to the body's demands. Among its other functions are metabolic regulation and exchange, haematopoiesis in the bone marrow and the storage of calcium and phosphate (*Lyman 1994*, 72-73; *Rho – Kuhn-Spearing – Ziopous 1998,* 92; *Padian – Lamm 2013,* 14-15). The structure of bone can be divided into **a)** cellular components and **b)** intercellular matrix.

a) Cellular components:

i) osteocytes have a size of around 7×15 µm, are placed in *lacunae* and are not able to divide. They participate in the release of minerals from bone and thus control the physiological mechanisms responsible for the structure of the bone matrix and the calcium levels in body fluids. Together with osteoblasts, they are able to change back to osteoprogenitor cells. They do not produce a bone matrix although the residual metabolic activity is present (*Urbanová 2003*, 9).

ii) osteoblasts are specialised bone-forming cells with an average size is of 15-20 µm. Individual cells are connected through numerous protrusions and are responsible for the production of organic bone mass – osteoid and bone mineralisation, which is capable of reversible conversion to osteocytes (*Lyman 1994*, 73; *Stloukal 1999*). Osteoblasts emerge in regions of remodulation and new bone formation so are spread unevenly. Their quantity decreases with age, and they are unable to divide (*Urbanová 2003*, 8).

iii) osteoclasts are large multinuclear cells of variable shape and size with numerous protrusions. They originate from blood leukocytes and play a role in resorption processes in bone remodelling. Osteoclasts contain acid phosphatase and are able to produce extracellular collagenase, which helps them resorb the bone matrix. After their role in resorption, they become extinct or change to phagocyte cells (*Lyman 1994,* 73; *Urbanová 2003,* 10).

iv) osteoprogenitor cells are stem cells derived from mesenchyme that are stored in bone marrow and are capable of division and playing a key role in bone formation. Throughout

the phase of preosteoblast phase, they differentiate into osteoblasts (*Ortner – Turner-Walker 2003,* 11; *Urbanová 2003,* 8).

<u>v) lining cells:</u> originate by differentiation of osteoblasts and enclose the bone surface. They are responsible for the prevention of bone resorption by osteoclasts and maintain the calcium balance between bone tissue and serum (*Ortner – Turner-Walker 2003,* 13).

b) Intercellular matrix:

This is made of an organic component represented by collagen (mainly type I collagen fibrils) and non-collagen structural proteins (e.g. osteocalcine), which together constitute for approximately 20% of the matrix matter. Second are inorganic components, mainly calcium and phosphate – hydroxyapatite or fluorapatite in the form of small plate-like crystals that represent approximately 70% of the matrix matter. Finally, there is water (approximately 10%) in a solid-like form in collagen and mineral molecules and crystals, bounded to the surface of the collagen and minerals, and circulating in the cavities and canals responsible for metabolic processes (*Delmas et al. 1984,* 310-312; *Johnson 1985,* 167; *Mack 1964*; *Wilson et al. 2006,* 3722; *Wang 2011,* 55-56). The combination of these three basic components ensures flexibility (organic components, water) on the one hand and hardness and strength (inorganic components, water) on the other. The precise ratio of individual components can be influenced by species, age, sex, element structure and other factors. Simultaneously, the chemical composition of bone also influences also the resulting decomposition processes after death, so the ratio of specific components is relevant concerning the specific response of bone to different taphonomic processes, particularly fragmentation (*Agnew – Bolte IV 2012,* 221; *Evans 1973*; *Lyman 1994,* 417-423; *Karr – Outram 2012,* 202).

Together, the above-mentioned microcomponents together build and shape the basic histological bone structure. In long bones, which are the focus of interest of my activities and observations, there are two types of bone: compact/lamellar and cancellous (*Čihák 2001,* 22). Cancellous bone is a system of columns and plates called *trabeculae* that form a network of *spongiosa* that fills the epiphyses of long bones. Lamellar bone is mostly deposited in the diaphysis or the shaft of long bones and can be divided into primary and secondary bone tissue. Primary bone is composed of longitudinal vascular canals surrounded by concentric lamellae forming primary osteons. This primary type of bone tissue represents the transition from woven (typical for initial periods of growth or

bone repair) to lamellar bone types (*Currey 2002*). Other types of primary bone are also known. Laminar type of bone is typical in large land mammals, mammal-like reptilians and amphibians is laminar type, which shows various seasonal banding depending on hibernation or seasonal changes in food supply (*Enlow – Brown 1956*; *Enlow 1966*). A similar primary bone type is represented by plexiform tissue. This is characteristic for large fast-growing animals (e.g. cow, pig) but also carnivores and exceptionally can be found in primates and humans (in periods of rapid growth). This is typically due to its denser rectangular vascularisation system forming a brick-like structure (*Hillier – Bell 2007*, 251; Fig. 2.2).
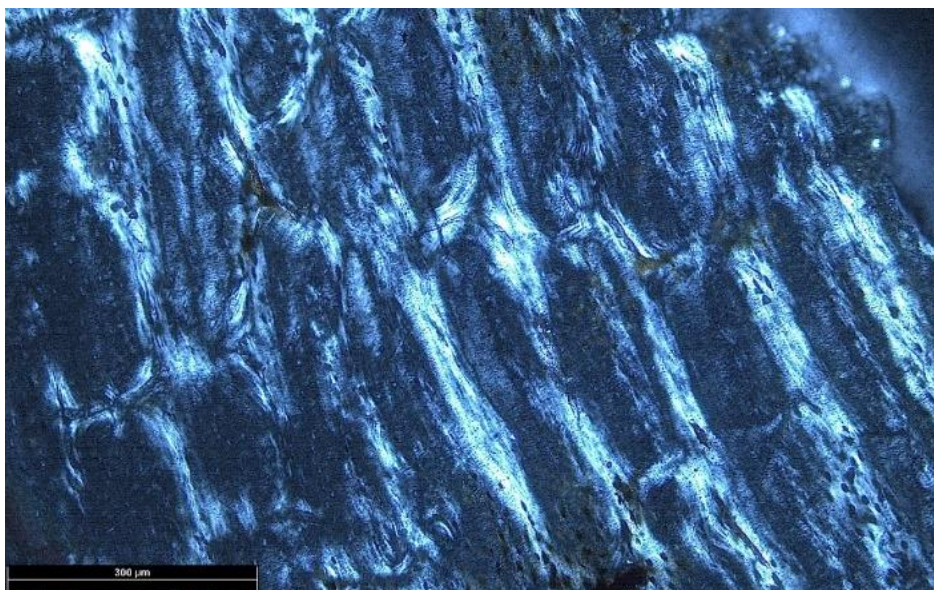
Fig. 2.2: Plexiform bone tissue in polarised light. Scale bar 300 µm (*Sázelová – Boriová – Šáliová 2021,* 131, Fig. 2; modified by SB).

By resorption of primary bone and the deposition of new lamellar tissue, secondary bone emerges where *osteon* (Haversian system) represents a rudimentary building unit. This consists of the *Haversian canal*, containing blood vessels and nerves, *concentric lamellae* of mineralised collagen fibres with embedded hydroxyapatite crystals surrounding the Haversian canal in layers, and *lacunae* (where osteocytes reside) interconnected with each other by *canaliculi*. Individual osteons communicate together through *Volkmann canals*, and the space between the osteons is filled with *interstitial lamellae*, which represent the remains of primary bone or remodelled osteons. The collagen fibres in *lamellae* have a preferred but moving orientation and vary from one layer to another. Their arrangement is commonly compared to plywood (*Weiner – Traub – Wagner 1999*, 242-244; *Hamed – Lee – Jasiuk. 2010*; *Wang 2011,* 54; Fig. 2.3).
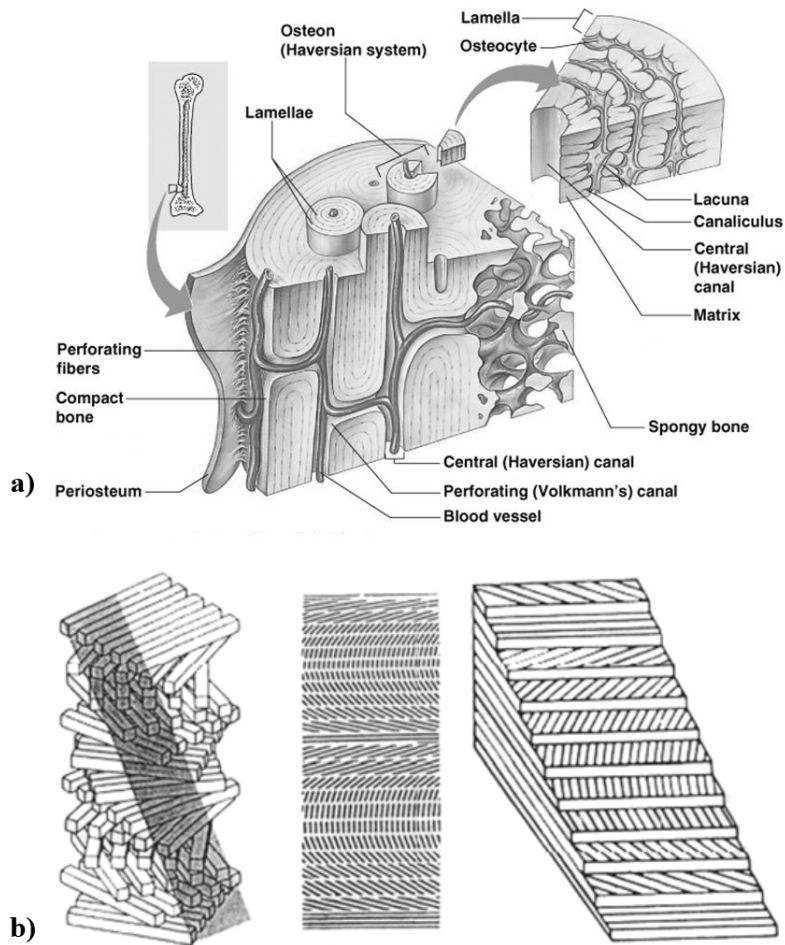
Fig. 2.3: Microscopic bone anatomy, a) illustration of individual features and their arrangement, b) schematic drawing of plywood lamellar pattern typical for lamellae arrangement (*Doblaré – García – Gómez 2004,* 1813, Fig. 2; *Hamed – Lee – Jasiuk 2010,* 137, Fig. 3; modified by SB).

In long bones, osteons are oriented longitudinally to the main bone axis. They are tubular and branching, bounded by a cement line, which represents a highly mineralised and collagen-free layer. The number of cement lines (in relation to the number of osteons in bone) and the orientation of collagen fibres in *lamellae* are important variables when it comes to the response of the bone to mechanical stress (see Chapter 2.2) (*Johnson 1985,* 166-167; *Rho – Kuhn-Spearing – Ziopous 1998,* 94; *Čihák 2001,* 21-22; *Li – Abdel-Wahab – Silberschmidt 2013,* 448).

Differences between human and animal bone on a microscopic level are apparent on both a quantitative and qualitative level, and some of the most basic ones were briefly mentioned above (e.g. *Owsley – Mires – Keith 1985*; *Cuijpers 2006*; *Hillier – Bell 2007*; *Mulhern – Ubelaker 2012*). However, the biggest qualitative differences (representation of different bone tissue types and their proportion) can be seen among different taxonomic

groups with parametrically/significantly different body types (e.g. *Martiniaková et al. 2006,* 1236-1239). There are numerous fracture studies focused on mechanical properties and the response of bone to force applied via controlled experiments with uniform settings using a wide variety of land mammal bones including humans. The results declared a predominantly uniform reaction in bones belonging to a larger group of land mammals including humans (e.g. *Hayes – Carter 1979*; *Johnson 1985,* 160; *Martin – Burr 1989*). However, there are some studies demonstrating certain differences in fracture surface morphology among species, especially under high magnification (*Wang – Mabrey – Agrawal 1998,* 1-9). This fact was kept in mind when the most suitable experimental analogy was sought for my experiments (see Chapter 7.2.1). Rather different physical and structural properties that are more related, for example, to the skeletal element and its function, rather than to a species itself, are crucial in bone reaction to fracturing force and are discussed further in the following chapters (Chapter 2.2 and 2.3).

2.2 Physical appearance and biomechanical properties

Mammalian bone is a highly complex heterogeneous composite material of various shapes. Its shape and structure are, to a large extent, given genetically although the role of physical loading in its precise final form is undisputed (*Currey 2012,* 50). Concerning the shape, long bones comprise two epiphyses made of cancellous spongy bone tissue covered in a thin cortical layer filled with bone grease. Spongy bone is arranged into structured beams that perform a specific mechanical function depending on the skeletal element and its characteristic load. The epiphyses are connected by the diaphysis made of the compact tube-shaped lamellar bone surrounding the marrow cavity. The transition between the epiphysis and diaphysis is gradual, and similarly, the characteristics facilitating the response to fracturing force (e.g. bone density) gradually change through the bone as a whole (e.g. Čihák 2001, 61; Karr 2012, 81).

Concerning bone properties, a large body of knowledge comes from material studies. Therefore, it is essential to introduce the basic terms used in this field. *Stress* is the amount of force applied to the object, in this case, bone, and is expressed as the ratio of weight to area. The implication of force to the object is called *loading*. When loading is applied, *deformation* (change in the shape) occurs in the object. The deformation of the object is measured by *strain* and is expressed as a proportion of the deformed length to the original length of the object. In general, deformation can have two distinct forms and

both also have their limits. *Elastic deformation* can be observed in objects, which after loading, recover to their original shape until their *stress/yield point* is reached. When reaching the stress point, the changes in shape are irreversible. *Plastic deformation* is present in objects whose shape is permanently changed by the application of force. The maximum the plastic deformation is called the *failure point* and represents a limit past which the object breaks/fails (*Johnson 1985,* 170; *Martin – Burr – Sharkey 1998,* 128; *Gifford-Gonzalez 2018,* 206-207). The sum of elastic and plastic deformation of an object represents its ability to absorb loading energy and resist failure and is called *toughness* (Fig. 2.4). Bone in a fresh state exhibits both elastic and viscose behaviour to deformation and is of an anisotropic nature (*Johnson 1985,* 165).
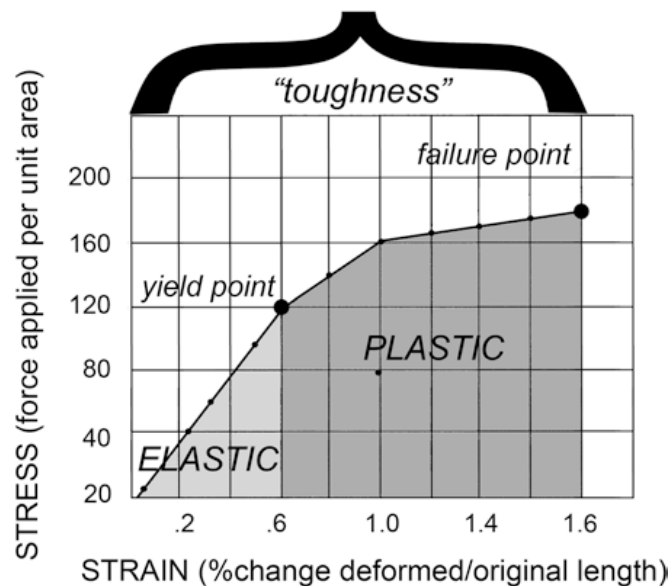
Fig. 2.4: Graph showing stress and strain linear relation in a hypothetical deformable material. Zones of plastic and elastic deformation and limit points are figured (*Gifford-Gonzalez 2018*, 207; Fig. 11.2).

Bone as a material represents an anisotropic matter, and its internal structure (and therefore, the response to stress) is based on the specific graded organisation and orientation of osteons. The anisotropy in Haversian bone is also represented by lower mineralisation of newly emerging osteons in contrast to more mineralised interstitial lamellae, which are a remnant of previously existing osteons. This difference is underlined by collagen-free cement lines binding individual osteons, which represent another heterogeneity in structure and, therefore, a place where microcracking emerges or deflects around the osteons, rather than cutting right through Haversian system (Fig. 2.5). Some studies also show that the cement line releases shear stress, reduce strain and, to a certain extent, acts as a barrier against crack growth (*O´Brien et al. 2005,* 72).
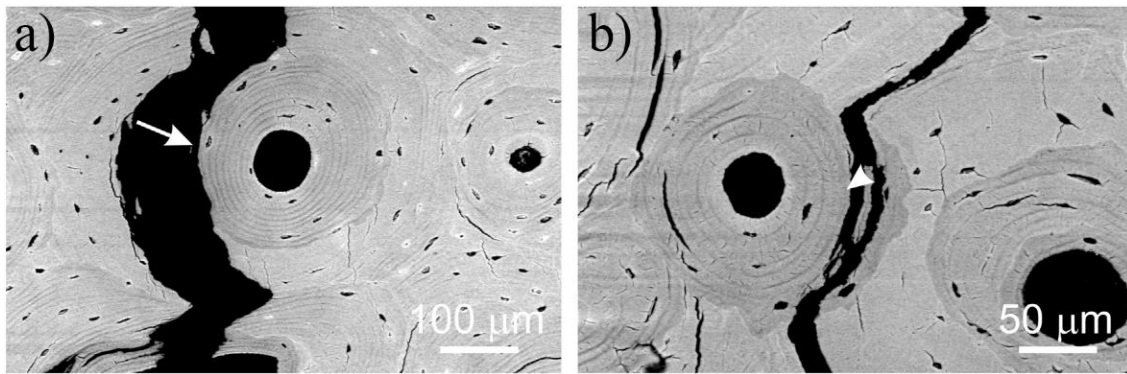
Fig. 2.5: Pictures of a bone cross-section from SEM showing deflection of microcrack by a) cement line bounding the osteon, b) lamellae in the osteon (*Tang et al. 2015,* 30, Fig. 5; modified by SB).

Another example of anisotropy can be illustrated by the fibrolamellar bone found in many large vertebrates. The complex layering of lamellar sheets, woven bone, and the net of blood vessels respond as brittle material when the load is perpendicular to the sheets but shows much higher resistance to strain when loaded along the sheets. In this way, the anisotropy of bone ensures that its elasticity is variable in different directions of applied stress, unlike in materials of an isotropic character (*Sharir – Barak – Shahar 2008,* 14; *Currey 2012,* 45; *Li – Abdel-Wahab – Silberschmidt 2013,* 448-449; *Gifford-Gonzalez 2018,* 208). The anisotropic response to stress originates in the combination of the organic and mineral compounds in osteons/*lamellae* (see Chapter 2.1; *Ascenzi – Bonnucci 1964*; *Hayes – Carter 1979*; *Herrmann – Liebowitz 1972*; *Rho – Kuhn-Spearing – Ziopous 1998*; Fig. 2.6).
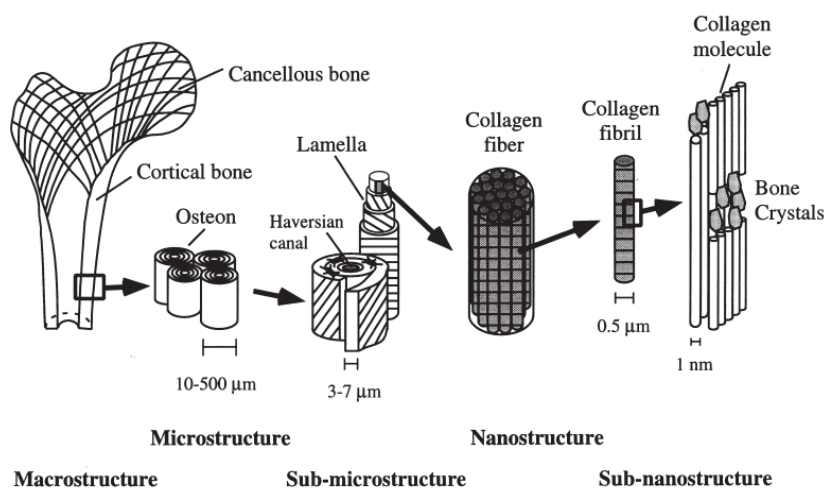
Fig. 2.6: Hierarchical graded macro to microstructural organisation of the long bone: from left cortical and cancellous bone; osteons with Haversian systems; lamellae; collagen fibre assemblies of collagen fibrils; bone mineral crystals, collagen molecules, and non-collagenous proteins (*Rho – Kuhn-Spearing – Ziopous 1998,* 93, Fig. 1).

Even though the hydroxyapatite crystals support a greater portion of the load caused by stress, its combination with collagen fibres with viscoelastic features provides much higher overall strength than each compound separately (*Currey 1964*; *Evans 1973*; *Hermann – Liebowitz 1972*; *Lyman 1994*). This so-called multiphase material has solid bonds between the matrix and the fibres, which are affected by the amount of stress applied. The deformation occurs first. The stress is absorbed, and the plastic strain in an inelastic manner is the result if the elastic limit is not exceeded. If a fracture did not occur, the bone recovers, although some irreversible changes may remain (*Bonfield – Li 1966,* 874). These changes accumulate in the bone until the elastic limit is reached, and irreversible changes occur. At that moment, the bone failure begins at a microscopic level. Microcracking tends to follow the cement lines and has a critical influence, particularly on the bone microstructure. The macroscopic level is affected after the advance of microcracking to larger cracks (*Bird – Becker 1966*; *Evans 1973*). Osteons are the basic mechanical units of bone. Their number and orientation in the bone determine to what extent the bone will be resistant to tensile or compressive force and influence the nature of fragmentation. For example, with the increasing number of osteons, also the amount of cement increases. As mentioned, it represents a weak spot where microcracks tend to propagate and so the elastic strength of the bone is reduced. Similarly, the orientation of the collagen fibres also influences the tensile and compressive strength of the bone. The higher the amount of longitudinally oriented fibres, the greater the resistance. With a decreasing angle of spiral trajectory around the osteon, the tensile strength also decreases although the compressive increased. With the growing angle of the fibres, the outcome is the reverse (*Evans 1973*). Another important variable influencing the fragmentation is the energy-absorbing capacity of a bone. The greater the ability of a bone to absorb a sudden impact, the greater the survival rate. The energy-absorbing capacity and other bone strengths are influenced by the bone properties described above, and the state of bone preservation (*Johnson 1985,* 167-169). The importance of the latter is discussed in greater detail in Chapter 3.

2.3 Bone fracture dynamics

The resistance of a bone against fracture in a living bone is due to the morphology, microstructure, cortical bone thickness, diaphysis diameter, amount, the proportion of compact and spongy bone and the presence of non-osseous tissues (*Evans 1961*; *1973*;

Johnson 1985). The different organisation of osteons characteristic to specific skeletal parts produces an element-specific response to the force applied. This explains, for example, why some skeletal parts were more suitable and preferentially used for specific tasks (e.g. antlers as soft precursors in knapping process; *Hahn 1993,* 369). These characteristics cause the response to stress within the skeletal element group or taxon group to be similar. This also applies to altered bone states. The theoretical calculations and mechanical models can take into account the anisotropic and graded nature of the compact bone material and can go as close as the cylindrical shape of the bone relating it to the tube in their calculations (e.g. *Raeisi Najafi et al. 2007,* 709; *Sharir – Barak – Shahar 2008,* 13; *Hamed – Lee – Jasiuk 2010,* 133-141). However, the complexity of shapes, compact bone thickness variability throughout the bone, and the gradual transition from the compact bone of the diaphysis to the spongious bone of the epiphysis make it impossible to precisely predict the mechanical response of the whole bone to the forces applied (e.g. *Sharir – Barak – Shahar 2008,* 16; *Currey 2012,* 50; *Li – Abdel-Wahab – Silberschmidt 2013,* 454). The importance of the overall shape and bone completeness in the resulting fracture patterns is underlined by studies proving that bones notched perpendicularly to the long bone axis have a fundamentally reduced ability to withstand the stress applied (e.g. *Nalla – Kinney – Ritchie 2003*). Evidence of this type of bone modification to reduce its resistance in the breakage process is also reported in archaeological assemblages (*Gifford-Gonzalez 2018,* 221).

Tension, compression, and shear affect the bones during daily life and can lead to the failure of a bone when it reaches its failure point. In general, a bone is more susceptible to tensile failure and is stronger in compression and shear. Unlike standardised samples in medical and physical research, intact bones are always subjected to differently mixed forces because of their variable shape (Johnson 1985, 170-172, 219). These three types of strain can be caused by three types of loading. *Static loading* is related to compression and tension and is represented by gradual loading until the failure point of the element is reached. The pressure is constant and more evenly distributed. This type of loading is typical, for example, for carnivore bone breaking (see Chapter 5.2.1). The resistance of a bone to static loading is much higher than to dynamic loading (*Čihák 2001,* 74). *Dynamic loading* mainly corresponds mainly to compressive force and represents immediate force impact exceeding the failure point. In dynamic loading, the force is applied to one point by a loading device (e.g. a hammer stone) creating a loading/impact point. This is typical

for human bone-fracturing activities. The last is the *torsional loading*, where the bone cracks under a greater twisting force than the resistance of the bone. Torsion produces tensile and shear stress and is common in bending. Torsional loading is common in injuries, and bone resistance is significantly lower than in compression or tension (*Miyasaka et al. 1991,* 3; *Turner – Wang – Burr 2001,* 376; *Hart et al. 2017,* 6). Torsion typically causes spiral fractures (as dynamic loading) but has a distinctive loading point at the interior surface of the compact bone. In addition, the final morphology can be influenced to some extent influenced by the ratio and direction of the tension and shear combined in the final stress event (*Johnson 1985,* 169-170). Another variable influencing the response of a bone to torsion is the velocity of the impact. While low-velocity impact fractures tend to be short and transversal, moderate or high-velocity impact fractures are longer, with an oblique-radial course (*Cohen et al. 2016,* 59-61). Considering the complexity of torsional fragmentation, it can be assumed that micromorphological differences on the resulting fracture surface in comparison to other processes could also be present.

The combination of compressive, tensile and shear force is represented by bending. The concave side of the bone is subjected to compression while the convex side of the bone is in tension. The shear stress affects the perpendicular cross-section. The obvious failure in long bone bending starts at the tensile (convex) side although previous local failure is present on the tensile and compressive sides (Fig. 2.7). Stress and strain are highest on the bone surface. Proceeding along the bone, the stress changes and decreases internally (*Evans 1973,* 26-27). In a living organism, failure can occur as microdamage or microcracking and is effectively subjected to bone repair processes (see Chapter 2). If the loading continues or even increases, then failure occurs, the microcracking accumulates (i.e. fatigue) and this results in breakage, also on a macrolevel. The resistance to fatigue in fresh long bones is greater in bending than in single-axis loading, with the middle-third of the diaphysis the most resistant. The damage response is also dependent on the type of skeletal element and its structural properties on a macro and microlevel. Therefore, little variability should be seen within the same type of element and taxonomic group (e.g. *Hayes – Carter 1979,* 278-280; *Johnson 1985,* 171-172; *Gifford-Gonzalez 2018,* 210-212).
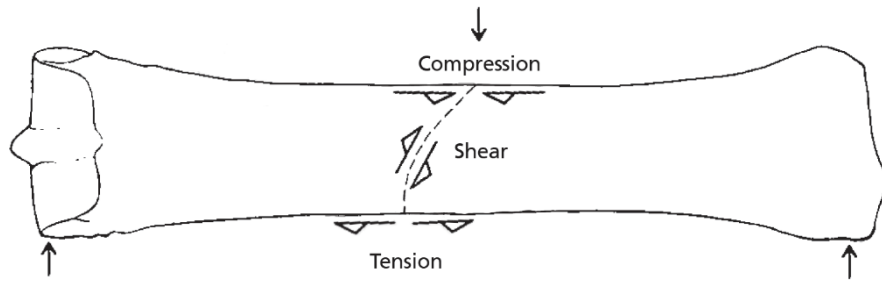
Fig. 2.7: Schematic diagram showing the combination of forces in bending. Simple beam scheme, mid-diaphysis loading with the epiphyseal ends supported (*Hutson et al. 2018a*, 85, Fig. 27; modified by SB).

In fresh bone, the natural reaction to strain is helical breakage (see Chapter 4). Force is transferred along the collagen bundles and circles around the osteons. If the stress is high enough and passes the failure point of the bone shaft, an oblique spiral fracture propagates through the cortical bone and twists around the long bone axis. The fracture starts at the point of the highest tensile strain (place of initial impact) in the outer layer of the cortical bone and moves into the bone while the stress is reduced (*Evans 1957*; *Hermann – Liebowitz 1972,* 808). The kinetic energy from dynamic loading is released by stress waves, travelling through the fracture front and generating microscopic features influencing the fracture surface morphology (*Gash 1971*). Stress waves mainly influence the compact bone of the diaphysis. The fracture terminates when meeting with another fracture front. Another termination possibility is reaching the gradual change in the bone structure approaching the epiphysis diffusing the force into the trabecular system, which has high overall resistance to stress. Therefore, in fresh bones, it is highly unlikely to observe the fracture cut through the epiphyses (*Bonnichsen 1979,* 43; *Currey 2002,* 168-172). However, if the stress is too high and the failure point in the bone is reached immediately, the bone fails to respond in its natural way (i.e. dispersing the stress into spiral fracturing), and the fracture occurs in the direction of the acting force. For example, if a disproportionate load is applied perpendicular to the long bone axis, the resulting fracture is transversal. In other words, the amount and direction of force applied by the actor and the size of the bone, respectively to the size of the animal affected, are also important in determining the final fracture morphology (*Blasco et al. 2014,* 1101; *Gifford-Gonzalez 2018,* 220).

48

2.3.1 Fracture classification systems

On a macroscopic level, the outcome of the fragmentation process is commonly described by different long bone break classification systems. These are numerous and proposed by different authors based on their research and experiences. They describe various properties such as the outline of the fracture, the characteristics of its surface, the angle relative to the outer bone surface and completeness. The outline classifications are based on basic biomedical long bone fracture shapes. These are represented by helical, transversal, and longitudinal fractures. In archaeozoology, there was a tendency to develop this classification, and many other additional shapes were described (*Johnson 1985,* 172-179; *Gifford-Gonzalez 2018,* 213-214). The basic terminology used in fracture pattern analysis was described by *Johnson* (*1985,* 172) and characterises the following terms. The *fracture surface* is a cross-section of compact bone exposed after the force was applied and the bone collapsed. *Fracture location* is the place where the collapse emerged. *Fracture front* is the leading edge of the force, and the features on the fracture surface determine its direction. *Fracture shape* is the outline of exposed compact bone and records the propagation path in a plan view taken by the fracture front. *Fracture angle* is the angle of the fracture surface to the outer cortical surface. Fracture shape is the criterion where the division and description differ between various researchers. *Johnson* (*1985,* 172) describes five fracture outlines: curved, transverse, pointed, stepped, and scalloped (Fig. 2.8).
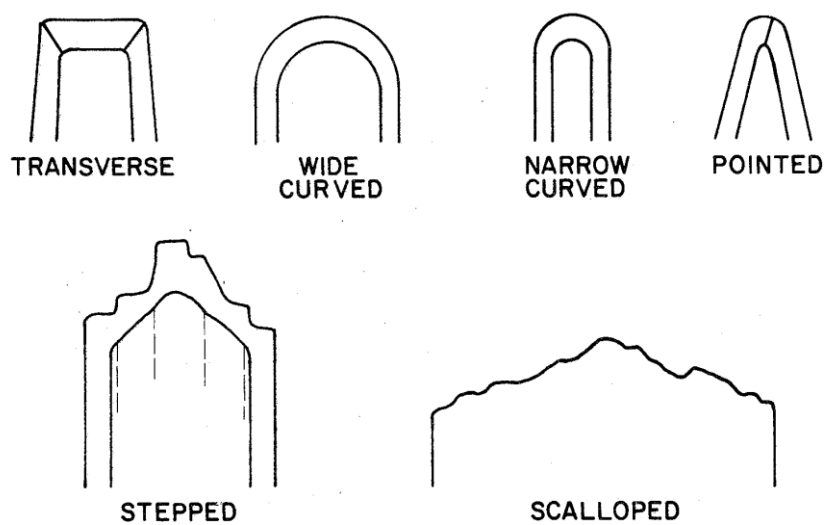
Fig. 2.8: Fracture shapes according to *Johnson* (*1985,* 177, Fig. 5.5; modified by SB).

Marshall (*1989*) presented a broader categorisation of a total of eight types of fracture shapes. The proposed categorisation is based on earlier typology by *Shipman, Bolser* and *Davis* (*1981,* 260) with the addition of the longitudinal type. These include stepped, teeth-saw, V-shaped, chipped, transversal smooth, transversal rough, spiral, and longitudinal outlines (Fig. 2.9).
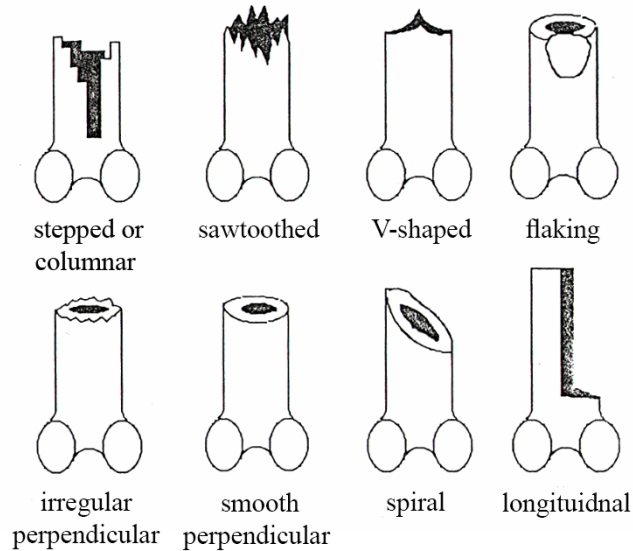
Fig. 2.9: Fracture shapes according to *Marshall* (*1989,* 14, Fig. 1; modified by SB).

With more simple division came *Villa* and *Mahieau* (*1991*) who defined a transverse shape to the long bone axis, curved/V-shape, and intermediate shape (diagonal to the long bone axis, stepped). Considering the angle, smoothness, roughness, and colour of the surface, significantly fewer options are available and used. Angle is being described as right or oblique (acute/obtuse). Surface has two main characteristics, smooth and rough although some authors distinguish between jagged and stepped morphology. These two traits were first proposed by *Morlan* (*1980*, 48-49) and were further adapted and used (mostly in combination) by others (e.g. *Haynes 1983a*; *Davis 1985; Villa – Mahieau 1991*; *Outram 1998*; *2001*). These criteria mainly serve to distinguish freshly fractured bone from dry or mineralised bone fragmentation. Right angle, rough surface and the different colours of the fracture mainly emerges on bones fractured in a heavily altered, mineralised, or dry state. On the other hand, fractures with a smooth surface, an oblique angle to the cortical surface, and the same colour are typical for bones fractured in a fresh state (Fig. 2.10, and Fig. 6.1c concerning colour differences). Another criterion used is the completeness of the circumference of the long bone cylinder with categories with approximately 20%, 50% and 100% completeness of the element of interest (e.g. *Bunn*

1989; *Villa – Mahieau 1991*). The methodological approach combining fragmentation levels (e.g. *Todd – Rapson 1988*; *Gifford-Gonzalez 1989*; *Lyman 1994*; *Morlan 1994*) and fracture patterns using the fracture freshness index (FFI) was developed by *A. K. Outram* (*2001*) to closely define the level, extent, and type of fat exploitation in assemblages where this type of treatment is assumed. In this way, small bone fragments reported as unidentifiable, also contain valuable information about the subsistence strategy or the resource pressure in the studied society. Different classification systems variably combine fracture characteristics to understand the fragmentation process and the history of bone assemblages. However, as described in Chapters 2.2 and 2.3 and later discussed in Chapter 3, these characteristics are to a large extent dependent on the bone structure and state of preservation. Only in combination with contextual information obtained from. other bone surface modifications can we get closer to the specific actor responsible for the fragmentation

Fig. 2.10: Rough and right-angled surface of the fracture surface with a predominantly transversal course in the upper picture (wolf metapodial, area G, Pavlov I) and a smooth fracture surface with an oblique angle and spiral outline in the lower picture (medium-sized mammal femur, area G, Pavlov I) (photo SB).

There are plenty of studies describing the characteristics of bone fragmentation on a microscopic level although these are mainly related to material and are biomechanical, medical, or forensic (e.g. *Alunni-Perret et al. 2005,* 796-801; *Lynn – Fairgrieve 2009,* 793-797). In their experiments, the authors work mostly with standardised specimens whose in their reactions do not fully correspond with whole bone response to stress (see in Chapter 2.2 and previous paragraphs in this chapter) or they analyse traumatic fractures

caused mainly by various instruments. The use of microscopic methods to address the fragmentation issue in the archaeological context was implied, for example by *Shipman* (*1981,* 372). She described two types of helical fractures based on different tension failures observed under a scanning electron microscope (SEM). Type I is the result of horizontal tension failure and causes the smooth fracture plane to emerge between the collagen bundles. It should be characteristic for all types of actors able to develop torsion resulting in the separation of adjacent bundles of collagen fibres, i.e. carnivores, weathering, trampling or humans. Type II is the outcome of spiral tension failure and has the fracture plane perpendicular to the main bundle orientation, leading to a rough and stepped surface of fracture (Fig. 2.11). This is the outcome of torsional force strong enough '*to overcome the structural strength of bone*' (*Shipman 1981,* 372). The more passive fragmentation actors, such as weathering and trampling, were not taken into account for Type II although its typicality and proportion to Type I in carnivore or human-affected assemblages were not stated.
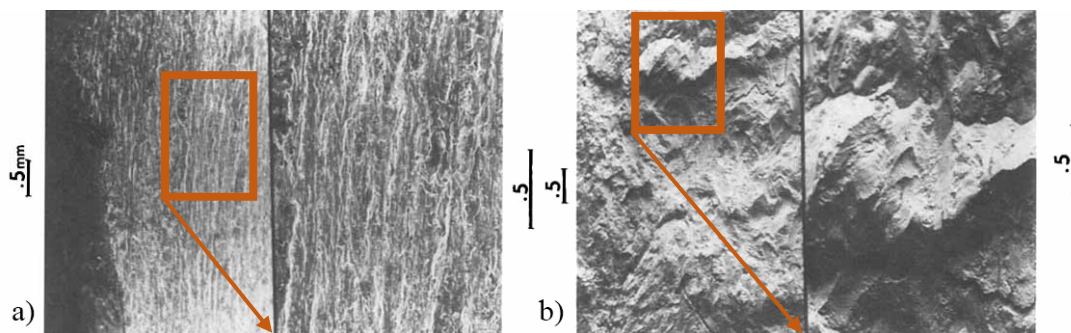
Fig. 2.11: SEM pictures of the two types of spiral fractures, a) type I fracture from weathering on an antelope tibia. Parallel patterning captured on the left, higher magnification showing the laminated structure and vascular canals on the right, b) type II fracture on an antelope tibia induced by torsion. The stepped character of the surface on the left, the intersection of the fracture front with lamellae on the right. Scale bars 5mm (*Shipman 1981,* 373, Fig.6; modified by SB).

Unfortunately, works concerning microscopic features of fragmentation processes in archaeological contexts are very rare. Despite the huge number of experiments and studies carried out since the 1970s and the great advancement and development of microscopic techniques used, particularly in archaeology, none of them systematically deals with micromorphology of fracture surfaces or the role and form of microcracking in specific fragmentation activities and/or conditions.

3. Influence of bone preservation state

The biomechanical properties and reaction of bone in a fresh state to applied stress were discussed in the previous chapters. The fresh bone holds a substantial part of its moisture that has a key role in changing its properties and so responds to the stress applied. Furthermore, in fresh bone, the collagen and within-bone nutrients are preserved; some greasiness may be also present (see Chapter 2.2). However, during the taphonomic history, the bone can undergo fragmentation in various states of gradual decomposition and fossilisation. These are processes where a significant amount of moisture can be lost. After losing a notable part of the moisture, while the preserved marrow is still edible, the bone is characterised as dry. Mineralised bone has lost the predominant part of its moisture and energy-absorbing capacity. It lacks marrow and its microscopic structure may be changed by fossilisation (*Johnson 1985,* 172). These states may be reached by different processes but lead to one common result: elasticity reduction. At a macroscopic level, this change may be illustrated by emerging split-line cracking, commonly observed in the weathering process (see Chapter 5.2.3). This phenomenon is caused by the collapse and shortage of collagen fibrils to shorter segments. These changes facilitate the characteristics of the breakage process such as the outline, surface texture or angle of the fracture. The fracture has a greater tendency to jump from one fibril to another through these segments and results in more transverse breakage patterns with rough or jagged surfaces. A condition such as this allows not only breakage transversal to the long bone axis but also penetration of the fracture through the epiphyses (*Johnson 1985,* 176; *Marean et al. 2000,* 208; *Gifford-Gonzalez 2018,* 214-215). Nevertheless, if the state of the bone is modified even further (fossilised), the fragmentation morphology is given by the altered mineral structure rather than the original microanatomy and may show a greater variability of fracture outlines (longitudinal, transverse), with the spiral fracture outline being very rare. In general, the angle of the fracture surface tends to be right-angled, and the character of the surface is rough, jagged, or stepped. The character of the surface was evaluated in forensic experiments as most reliably reflecting the changes in moisture content, and therefore collagen preservation (*Wieberg – Wescott 2008,* 6). In mineralised bones, the notably contrasting colour difference between the fracture surface (FS) and the rest of the bone surface is also an indicative trait. The intensity of the mentioned features is dependent on the actual amount and rate of moisture lost and

collagen degradation, and alternatively on the level of fossilisation (e.g. *Morlan 1984,* 164-165; *Johnson 1985,* 178; *Gifford-Gonzalez 2018,* 219).

Moisture loss and collagen degradation (i.e. drying) can be a result of natural processes such as weathering. This process is greatly influenced by the actual environmental conditions from which the amount and rate of diagenetic change are also dependent. According to the study by *Wieberg* and *Wescott* (*2008*), the most significant moisture loss occurs in the first two months after death, then the drying slows down and can continue for another five or more months depending on the environmental conditions. The fracture characteristics changed from a smooth surface, oblique angles and mostly curved or V-shaped outlines in bones fractured near death to a jagged surface, right angles and fewer curved or V-shaped outlines predominantly observed at the time of at least five months after death. They found that there is a significant correlation between moisture loss and fracture characteristics, where moisture loss determines collagen preservation influencing the actual bone response to stress. Closer weathering fragmentation traces and patterns were described in Chapter 5.2.3.

3.1 Freezing

Freezing is one of the extreme environmental processes altering bone, its properties and its response to stress. It may be a natural part of weathering in cold environments or a common phenomenon in areas where soils freeze and thaw in cycles or are permanently frozen (e.g. permafrost). Cryoturbation influences the deposition of the sediment, introducing different formations (e.g. frost heaves, wedges, clefts, potholes) that may significantly warp and mix cultural layers, and naturally within these processes notably fragment the bones contained in them. Freezing can also be taken advantage of to store bone for delayed consumption or use. In experimental practice, it represents an artificial state since the bones are commonly stored in refrigerators or freezers (e.g. *Bonnichsen 1979*; *Morlan 1984*; *Haynes 1981*; *Karr – Outram 2012a*; *2012b*; *2015*; *Grunwald 2016*). Therefore, in the evaluation process and interpretation of the experimental results, it is necessary to know what changes may be caused by this treatment and to take them into account (e.g. *Karr – Outram 2015*).

The temperature, time of exposure to the temperature and possible thawing-freezing cycles influence the final amount of moisture lost and, therefore, the response to the force applied (*Johnson 1985,* 188). In general, freezing significantly slows down the

degradation process. It was observed that bones frozen for a short time (days to weeks) possess the same fracture characteristic and FFI score as fresh bones, sometimes even better pronounced with lower index values (e.g. *Karr – Outram 2012a,* 557; *Outram 2001,* 406; *2002,* 57). The principle in such a reaction may be in the solidification of water and lipids contained in bone, causing improved fresh fracture characteristics. As *Karr* and *Outram* stated in their study, these changes appear to '*facilitate flaked bone toolmaking, and may have significant implications for understanding human cultural activities in the archaeological past*' (*Karr – Outram 2012a,* 558).

Nevertheless, besides the loss of moisture, freezing also causes the formation, growth and conversion of crystals both in bone and the surrounding soft tissues (periosteum, muscles, marrow). This process, especially when repeated (e.g. in the cyclical freezing and thawing), may cause certain damage to the bone microstructure (e.g. *Tersigni 2007,* 19). In bones frozen for longer periods (several weeks to months), the presence of dry fracture characteristics increases as the slowed degradation has the time to progress. At the same time, as the decomposition slowly proceeds, the bone fats and marrow may remain edible, even after more than one year. The difference in the relation between the rate of bone degradation and the FFI value over time among frozen and heated bones is illustrated in Fig. 3.1. The process of thawing after long-term freezing is likely to cause additional microcracking and is assumed to produce an even more pronounced shift toward dry fractures (*Outram 2002,* 60; *Karr – Outram 2012a,* 557-558). In her study, *Grunwald* (*2016*) describes, that the still frozen fragmented bones have a tendency to fragment across the diaphysis, producing fragments with a greater width than length. On the other hand, thawed bone fracturing imitates the fresh fracture outlines, producing long and thin fragments that copy the dominant collagen bundle orientation. To differentiate it from the bone fragmented in fresh state, the higher variability of fracture outlines, right angles, and rough surfaces present in bones fragmented in the thawed state may serve as distinctive traces (*Grunwald 2016,* 364). The processes described are hugely relevant, especially when dealing with archaeozoological material recovered from long-term/periglacial or permanently frozen environments. These also undergo the decomposition process of freezing, thawing, and drying – many times in multiple cycles – and influence the fracture morphology (*Johnson 1985,* 189). Some authors argue that the frozen environment may retain fresh fracture characteristics even in bones dated to the Pleistocene (e.g. *Bonnichsen 1982*; *Haynes 2017*), although recent

experiments showed that slowed decomposition already influences the fracture morphology after a few months (*Outram 2001*; *2002*; *Karr – Outram 2012a*). Whether the freezing period or thawing of the bone influences the final fracture morphology more significantly, is not clear. The interaction of these two processes in different settings remains to be tested to better understand the final fracture characteristics and to move one step closer to the interpretation of these traces in archaeological assemblages.
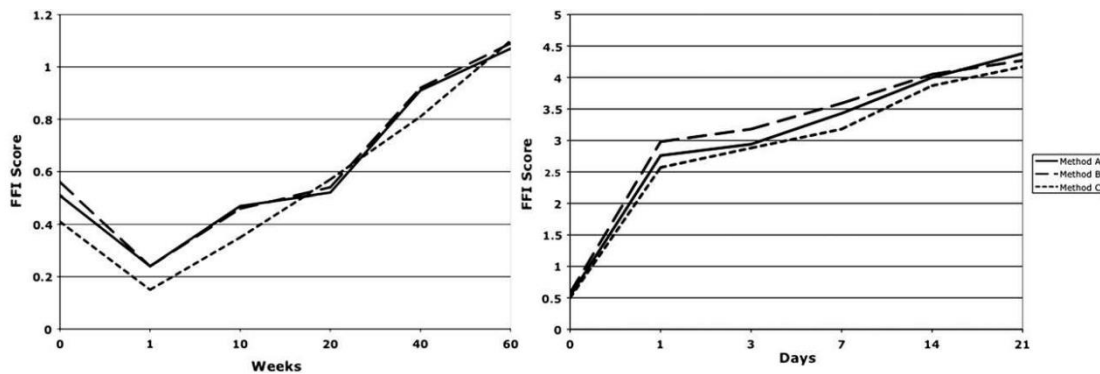
Fig. 3.1: The graphs show different trends in FFI development during the process of freezing (left) and hot dry conditions (right). The changes in the index value introduced by freezing are in comparison to heating very slow and small, with a decreasing tendency at the beginning of the process. Method A/B/C is for three different methods of FFI calculation, for more, see Chapter 6.1 (*Karr – Outram 2012a,* 557, Fig.1 and 2; modified by SB).

3.2 Heating

Another extreme process that significantly changes the rate and nature of degradation compared to natural temperate weathering is drying the bones by heating. Several approaches were applied when experimentally testing the heating effect. These were heating over/in fire, before or after breakage, radiant heating by placing the bones near the fire or a heating element, or heating in an oven by dry air at different temperatures for different time periods. These approaches help to model the extreme conditions opposing freezing and provide a starting point for a better understanding of the degradation processes occurring in hot and dry environments (e.g. *Cáceres et al. 2002*; *Outram 2001*; *2002*; *Karr – Outram 2012a*). The heating generally causes a loss of moisture and fats contained in the bone and significantly accelerates the process of drying and decomposition. Heating (or eventually heating and cooling, e.g. *Outram 2002*) reduces the elasticity of the bone by the physical decomposition of collagen and improves the efficiency of bone breakage. The fractures originating on heated bones are morphologically similar to the fresh ones depending on the level of alteration. When

proceeding with the drying of a bone, there is an increase of mixed and right angles and rough or jagged fracture edges (Fig. 3.2). The proportion of small fragments (around 2 cm) in heated bones is greater in comparison to fresh ones while fragment quantity and dispersion also increase (*Cáceres et al. 2002*, 474-477; *Blasco et al. 2014*, 1086). The phenomenon is a result of elasticity reduction by moisture loss and collagen degradation. These changes appear gradually.

Fig. 3.2: Fracture morphology of bone broken after 5 hours of heating in an oven at approximately 100˚C. The bone displays a mixture of angles and texture types; the spiral outline of the fracture is not present. Scale bar 10 cm (*Outram 2001*, 406, Fig. 5).

In his experiments, *Outram* (*2001*; *2002*) describes a series of oven and radiant bone heating. While the short-term oven (1 hour) and the radiant (4-6 minutes) heating had only a mild effect on the final fracture morphology and the growth of the FFI value (around 2), prolonged treatment in the oven (5 and 43 hours) generated both a predominance of the fresh fracture features and a significant increase in the FFI value (3 to 5). The outer layer of the bone is the first and the most affected, while the inner layer of the bone and the tissues remain intact. If the heating conditions are mild or the bone is exposed to them for short time, it typically shows a low grade of burning and gradual melting of the marrow (*Blasco – Fernández Peris 2012*, 279). The change in bones placed in hot and dry environments is much more rapid than in a frozen one (Fig. 3.1). *Karr* and *Outram* (*2012a*; *2015*) observed that the FFI increases significantly even after one day in a hot (40˚C) and dry environment to values close to 3. After 21 days, the bones scored more than 4 (*Karr – Outram 2012a*, 557). This rapid degradation suggests that in sites where hot and dry environments are predicted, there is a very short time span after death (1-3 days) in which the bones could have been broken displaying fresh characteristics. Even minor seasonal changes in the environment may have a considerable impact on the fracture morphology. Therefore, in colder regions the fresh fractures associated with possible human activity may be overestimated, while in warm regions the rapid shift in fracture morphology may cause underestimation. Knowledge of the environment and the

season of death should be considered when interpreting observed fragmentation patterns and subsistence strategies (*Karr – Outram 2012a,* 558-559)*. Further importance lies in contexts where marrow exploitation is assumed. It was shown that the mild heating treatment may facilitate this process by melting the outside part, making the extraction of marrow much easier and more effective (*Outram 2002,* 59). Heating treatment prior to bone exploitation was also observed in ethnographic contexts usually in cold environmental conditions (e.g. *Bonnichsen 1973*; *Binford 1978*; *1981*; *Gifford-Gonzalez 1989*; *Kent 1993*; *Oliver 1993*; *Outram 1998*; *2001*).

3.3 Boiling

Boiling is another thermal process of bone alteration in which a bone is heated at a constant temperature by liquid. Nevertheless, its effect on bone fragmentation patterns has not yet been examined in depth. In her experiments, *Richter* (*1986*) showed that fish bone collagen begins to already denaturise after 30 minutes at 60˚C and reported complete denaturation after 30 minutes in boiling water. The results were the same for bones with and without soft tissues. Nevertheless, she points out that the rate of denaturation may be different for mammalian bones, where collagen is, to a certain extent, more protected (*Richter 1986,* 479-480). Indeed, a study examining the thermal denaturation of bovine bone collagen showed that the process already starts at temperatures around 50 °C and proceeds in multiple steps. However, conformational and mechanical changes that lead to a loss of collagen integrity are present up at the temperatures between 230-290°C. Moreover, the rate of change was variable for different skeletal parts (*Lambri et al. 2018,* 10). The physicochemical changes ongoing in bone during boiling are very similar to depositional diagenesis. The main shared traits are loss of protein, increased crystallinity and porosity. However, in the case of boiling, a very long period (over 30 hours) is required to induce these changes. The shorter boiling times (1-9 hours) were reported to have none or very little effect. In boiled bones, a disrupted mineral-organic connection may be responsible for lowered mechanical strength, and the increased porosity provides a larger surface for dissolution processes. This makes the boiled bone more prone to further diagenetic changes or mineral alteration occurring after deposition (*Roberts et al. 2002,* 488-492).

The consequences are similar in the fragmentation process. The shorter boiling times (respectively roasting or baking) are not able to introduce considerable changes into

the fracture morphology that allow a clear distinction from fresh bones. The outline pattern is mainly described as a mix of spiral and longitudinal fractures, the transverse ones being rare and in the case of prolonged treatment. The surface remains mainly smooth. Rough and jagged surfaces, together with an increasing proportion of right-angled surfaces, were observed again in bones boiled for longer periods (*Alhaique 1997,* 51; *Outram 2002,* 58). According to *Outram's* observations (*2002*), boiled bones were more difficult to break in comparison to fresh bones. With an increased boiling time, the effort needed to break the bone grew, similar to the FFI value. After an hour of boiling, an almost complete loss of the marrow was observed (*Outram 2002,* 58). Since the changes in fracture morphology are mostly induced by loss of moisture and fat, which occur more rapidly than the denaturation of collagen and crystallisation, they are largely reminiscent of fracture patterns observed in dry bones (*Gifford-Gonzalez 1989,* 199). Nevertheless, the intensity of the characteristics largely depends on the boiling time or the presence of soft tissues. The shorter the treatment, the less clear the distinction from freshly fragmented bones (*Alhaique 1997,* 54).

The same relationship and influence on fracture morphology were described in other cooking techniques such as roasting or baking, where one of the most important variables is the presence of meat/soft tissues. Due to the presence of soft tissue, and the generally shorter time of this culinary treatment, the change in fracture morphology tends to be even less pronounced. The colour changes on the surface were also considered in the case of meatless bones. However, these bones were most likely exposed to roasting/baking for only a short period of time (since the prolonged heating causes a loss of marrow), which did not affect the colour or the fracture morphology (*Kent 1993,* 342-343; *Alhaique 1997,* 54; *Roberts 2002,* 486).

The processes described above represented the degradation of components responsible for bone elasticity, mainly by physical force, which causes a loss of moisture and collagen degradation. However, also the deposition of bones in wet/submerged conditions considerably changes its properties (e.g. *Hedges – Millard 1995*; *Nielsen-Marsch et al. 2000*). In comparison to the influence of extremely arid and hot conditions, how such an environment may change the original biomechanical properties of bone, and how the degradation process influences the final fracture morphology, remains to be tested.

4. The spiral fracture phenomenon and its relevance to the topic

The concept of a spiral fracture is mostly related to long bones in land mammals. Long bones were usually the primary interest of human or animal agents, are largely preserved in archaeological collections, were the object of interest and concern, and make the most from available research data (e.g. *Johnson 1985*, 158). Spiral or helical-shaped fractures can originate from a variety of forces (tensile, compressive, shear) of the various natures (dynamic, static, torsional) applied. However, the structure, biomechanical and physical properties of fresh bone appear to be crucial in a specific response to applied force, more than intentional human activity (see Chapters 2.2 and 2.3; *Johnson 1985*, 157-160).

The spiral fracture in long bone has helical morphology, circles around the diaphysis, and curves through a set of planes (*Johnson 1985*, 157). In the case of dynamic loading of an intact bone, multiple fracture fronts can occur and travel helically from the loading point radially around the long bone axis at a 45˚ angle. This is an outcome of tensile-shear bone failure (Fig. 4.1). The characteristic helical or spiral shape is conditioned by the cylindrical shape and hollow bone structure. From the diaphysis to the epiphysis, a gradual change in structure, porosity, composition and shape causes the helical fracture to scatter and does not reach the epiphyseal ends (*Johnson 1985*, 171; *Karr 2012*, 86).

Fig. 4.1: Freshly fractured humerus of domestic cattle. The point of impact is visible in approximately the middle of the shaft; helical fracture lines spread towards the epiphyses (*Outram 2001*, 404; Fig.3).

Both static and dynamic loading in a fresh bone can lead to the final spiral morphology of the fracture and humans are not the only agent who can apply this kind of forces. However, other traces are emerging, which allow us to distinguish between the techniques that were applied and move a step closer to the agent of fragmentation. Some

of the most important traces are presence, the position or shape of the loading point, and gnaw marks. For example, *Haynes* (*1983a*) describes the possibility of spiral fracturing of long bone shafts by large carnivores in the consumption process. On the other hand, he also states that this kind of modification, especially in larger bones, is rare due to the specific way of handling/the operational chain (see Chapter 5.2.1). In such cases, the epiphyses are already missing most of the time. The remaining shaft can bear spiralling cracks, which are underlined by weathering or can easily fail in animal trampling (*Haynes 1983a,* 104-106). However, the coexistence of carnivore markings and fractures indicating fragmentation in a fresh state suggests a more complex taphonomic history of the fragment than a simple and clear sequence of events (*Johnson 1985,* 192-193).

Moreover, torsional loading or twisting can also cause the emergence of spiral fractures. *Dart* (*1959*; *1960*) and *Sadek-Koros* (*1972*; *1975*) described the so-called crack-and-twist method of bone breakage, which was meant to prove the human intervention behind the bone fragmentation in the assemblages they observed. Unfortunately, in their experiments, they did not manage to meet the criterion of fresh bones. Furthermore, the actual breaking was governed by hammerstone, and the torsional move served only to separate the fragments held together by the periosteum present on the bone. In the case of torsional loading in action, some authors refer to a certain trait for recognition from the dynamic bone loading. The position of the loading point in torsion is on the inner compact bone surface while the dynamic loading point lies on the outer surface of the compact bone. The force is then analogically directed outward or inward to the bone. But again, the differentiation trait is not directly the fracture and its characteristics, and when the loading point or other distinguishing marks are missing, the origin of the breakage may still be questioned (see Chapter 2.3; *Johnson 1985,* 178).

Some authors refer to the presence of "green-bone" fractures (a substitute term for a spiral fracture of fresh bone without specific reference to human activity) in bones, which were not truly fresh when broken. The state of preservation plays a key role. In some depositional conditions, such as waterlogged and anaerobic environments, bones (but also other tissues) can preserve their fresh properties for a considerably long time. This leads to post-depositional fragmentation resulting in spiral breaks, for example, due to sediment pressure or heavy technique movement on the site. This is not the helical outline itself, but other accompanying traits such as loading points, impact scars or

staining on bones that are the decisive factor for intentional post-mortem human intervention (*Haynes 2017,* 176-178; *Haynes – Krasinksi – Wojtal 2021,* 1001).

Similarly, there is a need to be cautious about a helical type of fracture in the complex context of the archaeological find situation, since helical fracturing can be a relic of ante/peri-mortem injury, especially in large mammals, and result in their death before the healing process started or could be visible on the bone (*Haynes 2017,* 176; *Haynes – Klimowicz 2015,* 136; *Haynes – Krasinksi – Wojtal 2021,* 1008-1009; Fig. 4.2).

Fig. 4.2: Femur of adult African elephant fractured while alive. The individual died before the healing process began. Helical outline present on fitting fragments (*Haynes – Krasinksi – Wojtal 2021;* Fig. 34; modified by SB).

Intensive actualistic studies by various authors emerging as early as the 1970s show that humans are not the only taphonomic factor causing a spiral fracture. Many others, such as carnivores or herbivores (*Richardson 1980*; *Brain 1981*; *Haynes 1983a*), water transport in freezing and thawing rivers (*Thorson – Guthrie 1984*) or other weathering factors (e.g. *Behrensmeyer 1975*) must be considered (more in Chapter 5.2.3).

Johnson (*1985,* 158) argues that the controversy of a spiral fracture occurring in fresh bone and its origin in an archaeological context was caused by a lack of understanding the recognition of the real spiral fracture characteristics from morphologically similar, but in essence, different diagonal fractures as a result of the horizontal tension failure of the bone in altered states (*Karr 2012*, 87). The general deficiency of the focus on bone as a material, its properties in fresh and differently altered states, and how it responded to the force applied gave rise to misunderstandings, misleading interpretations and bias in archaeological literature concerning different fragmentation factors (e.g. *Hill 1976*; *Dart 1957*; *1960*; *Binford 1981*; *Myers – Voorhies – Corner 1980*; *Haynes 1981*; *1983*; *2000*; *Gifford 1981*). *Shipman* (*1981,* 371-373) provided a useful description and additional criteria for the characterisation of these two, shape overlapping, fracture types based on observing the relationship between the fracture

plane and the orientation of the collagen bundle under a scanning electron microscope (see Chapter 1). Other additional marks, characterising a spiral fracture on fresh bone were stated by *Morlan* (*1980,* 30-66) including the angle of the fracture surface, the surface smoothness and the colour of the fracture in comparison to the rest of the bone. His work, and the criteria he used, were later developed also by other authors (e.g. *Villa – Mahieau 1991*; *Outram 1998*; *2001*). There is still more experimental research elucidating the causes of spiral fracture pattern emergence. A multidimensional approach in fracture analysis, taking into account many other traces, such as gnawing or percussion scars, represents how to deal with this complex, but for the archaeological record, very important trace recognition and interpretation.

To conclude with *Johnson's* words '*The spiral pattern indicates bone breakage in a fresh state. It does not necessarily indicate the agency involved, which must be determined from the preserved exposed compact bone surface and fracture features. Nor does a spiral pattern indicate that the bone was used as a tool, as misunderstood…*' (*Johnson 1985,* 75).

5. Specific fragmentation agents

As it was mentioned earlier, archaeozoological assemblage and its condition are a result of the action of multiple taphonomic factors together with post-depositional processes. In the following chapters, agents causing fragmentation in osteological material are discussed. Typical traces of modification are outlined for each factor. Nevertheless, more attention is focused on how their activity may lead, or be related, to fragmentation, and what are the characteristic traces left behind. Examples of experimental studies and their results concerning individual taphonomic agents and characteristic traces are referred to.

5.1 Human bone fragmentation

Different traces specific to human-derived modification are well known and described. These may be left behind as traces of activities related to dietary exploitation, such as different marks left after butchering (*Binford 1981*; *Lyman 1994,* 294-353; *Fernández-Jalvo – Andrews 2016,* 25-30, 201). Not only meat was subjected to exploitation interest. Marrow and grease have a high caloric value and so were vitally important, especially in societies depending on animal resource or their products (e.g. hunter-gatherer societies). Nutritional and other utilitarian functions of fat are known from traditional societies, such as waterproofing of skins, treating bowstrings (*Binford 1978,* 24), and fuel for light (*Burch 1972,* 362) and may also be relevant to societies in the past (e.g. *Outram 1998*; *1999*; *2005*; *Karr – Outram – Hannus 2010*; *Karr et al. 2015*). One of the most typical traces left after butchering is cut marks. Their position on the animal body is dependent on the activity from which they originate. Marks from skinning typically encircle distal ends of limb bones such as *tibiae*, *metapodia* and *phalanges*. They may also be present on the skull, e.g. the lower jaw or around the base of antlers and horns. Filleting marks mainly appear along the long bone axis from cutting the meat off the bone. Dismemberment cut marks mainly originate from disarticulation and are associated with articular surfaces or parts where the major tendons and ligaments hold and strengthen the joints (*Binford 1981,* 98-107). Other marks also related to butchering practice are chop marks caused by using a heavy tool such as a hatchet or axe (*Olsen 1988c,* 349; *Shipman 1981,* 366; *Okaluk – Greenfield 2022*). These represent a type of percussion mark and are generally described as V-shaped impacts with fractures and splinters. However, they can vary significantly in their shape and form depending on the

effector and have not yet been systematically categorised. The chopping technique was also identified at Lower Paleolithic sites, but these traces are more relevant to earlier periods such as the Chalcolithic, Bronze or Iron Age where there is a significant change in butchering practices (*Horwitz – Monchot 2002,* 50; *Okaluk – Greenfield 2022,* 2). Nevertheless, similar traces can also result from batting the bone against the edge of a hard object, such as an anvil (*Blasco et al. 2014,* 1093). Another manifestation of dietary exploitation, similar to carnivores, are chewing traces. These represent the most direct processing of the bone by humans without the need to use any other tool and can typically be found on skeletal elements suitable for such treatment. These are bones of small-sized animals such as rabbits or birds, or certain bone types independent of animal size, e.g. ribs (*Blasco – Fernández Peris 2012,* 269; *Blasco et al. 2014*, 1085). Typical damage caused by human gnawing is shown by bent or smashed ends, crenulated edges, complemented by shallow linear marks, punctures and peeling. There can be a qualitative overlap between gnawing marks caused by humans and carnivores although the quantitative proportions are significantly higher in favour of carnivores (*White 1992,* 140; *Fernández-Jalvo – Andrews 2011,* 121; *Stančíková 2018,* 36-37).

Other reasons leading to bone modification by humans may be utilitarian or symbolic. Modification may serve for practical adjustment (e.g. handle grooving, perforations for threading of objects, tool manufacture), a form of decoration (e.g. grooves, lines, pits but also complete figural engravings) or the capture of information (e.g. a possible map on a tusk from Pavlov I) (e.g. *Hromadová 2016*; *Svoboda 2017*; *Sázelová et al. 2021*). Different techniques such as chipping, drilling and carving but also fragmentation and breakage may be engaged and combined to shape the bone into the desired form (e.g. *Rašková Zelinková 2013*; *Hutson et al. 2018a).*

'*Hominid modification of bones is a dynamic process of bone reduction involving the interaction of technology and biomechanics that is documented in the final morphology of the bone. This reduction process reflects a cognition to behaviour to product sequence that creates a pattern or standardization that can be deduced through the bone refuse recovered from a locality. The issue being raised is whether or not the patterns produced by hominid modification of bones can be distinguished from those patterns produced by natural agents' modification and if they can, then what are the distinguishing criteria that researchers can use to segregate the agencies and reliably identify hominid modification*' (*Johnson 1985,* 191). In this way *Johnson* (*1985*)

described the topic of hominin-induced changes in bone and introduced dynamic loading as a characteristic of human-induced fragmentation.

5.1.1 Dynamic percussion techniques

Dynamic percussive force is the characteristic and most common human strategy to break the long bone and open the diaphysis and is mostly focused on one loading/impact point. In the "hammerstone on anvil" technique, the force is focused on impacting one point by acting in one direction and is called passive percussion, because the bone lies passively and the active part is taken by the moving tool (*Blasco et al. 2014,* 1086; *Moclán - Domínguez-Rodrigo – Yravedra 2019,* 4664). The bone can be placed on a hard anvil. In relation to the size of the anvil and bone, the mutual position can be variable, with the epiphyses touching the anvil and the diaphysis not being directly supported, or the diaphysis lying directly on the anvil. In addition, the vertical position of the bone with one epiphysis supported by the anvil, or the support of one epiphysis by the anvil and hitting the opposite one with a hammerstone can be employed (Fig. 5.1). The bone is impacted by the hammerstone, which is usually a stone used to break the bone and can be a pebble or a manufactured tool with rounded or sharp edges. However, a hammerstone can also be in the form of other hard materials, such as wood or other bone (*Vettese et al. 2020*). This type of impact combines compressive, tensile, and shearing failure which usually leads to spiral fractures in fresh long bones (see Chapter 4; *Morlan 1980*; *Johnson 1985,* 192). From the point of impact, several fracture fronts expand and travel through the bone radially until they interact with other fracture fronts, terminate or are diverted by the epiphyses. The fracture edges of the diaphysis fragments are curved with a fine surface and form an acute or obtuse angle with the cortical surface of the bone. The fragments loosening from the bone element are mostly longer than wide, which is caused by longitudinally arranged collagen bundles (*Bonnichsen 1979*; *Morlan 1980*; *Johnson 1985*). Although the "hammerstone on anvil" technique is the most frequently studied and used in experiments it is not the only one.
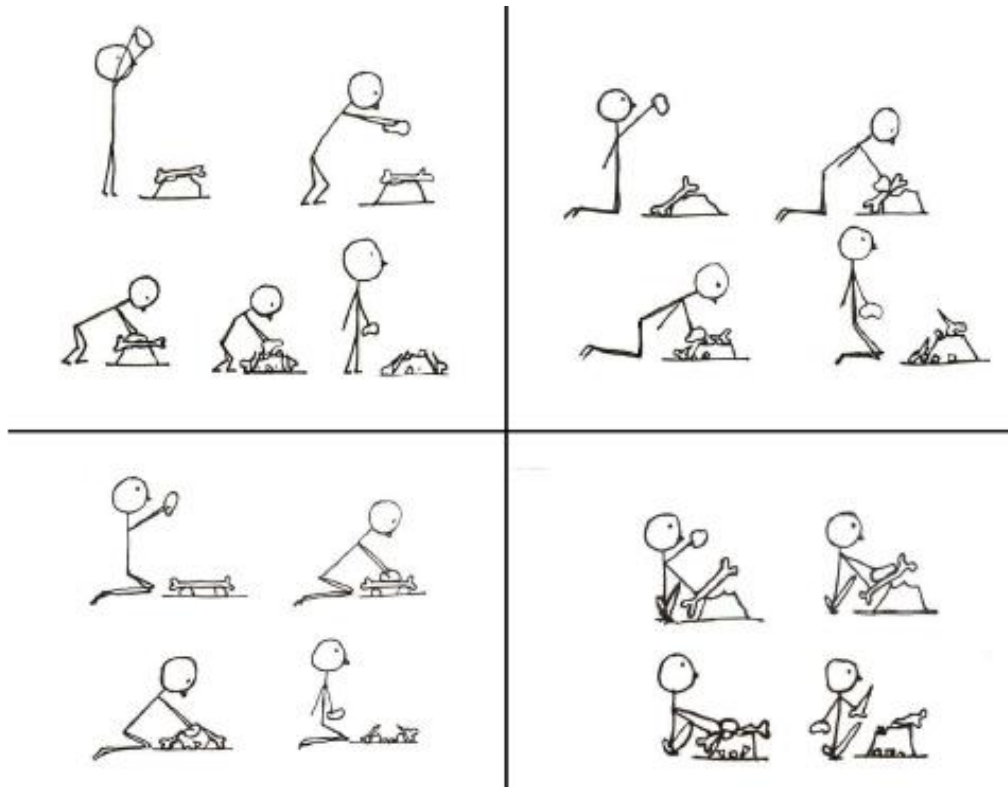
Fig. 5.1: Scheme of different positions the experimenter may take while using the "hammerstone to anvil" technique to break bones (*Vettese 2019,* 155, Fig. 9; modified by SB).

The batting technique uses the bone as a tool and is therefore categorised as an active percussion technique (*Blasco et al. 2014,* 1086). There are also various ways in which this technique can be performed. The bone can be held in the hands at one epiphyseal end, batting the other against the floor, anvil or another hard surface or batting with the diaphysis against the prominent surface. Alternatively, both epiphyses can be held in the hands and the diaphysis struck against the edge of the protruding object/surface (Fig. 5.2). This technique is one of the easiest ways of bone breakage since it does not require any other tool (*Noe-Nygaard 1977*; *Peretto et al. 1996*; *Vettese et al. 2020*). According to *Blasco et al.* (*2014*), this technique also requires less time for actual bone breakage and produces fewer bone fragments. These fragments also tend to be longer than fragments emerging in hammerstone breakage and more complete in circumference. The results of experimental work also describe other systematic differences when compared to a hammerstone broken assemblage, such as a different proportion and morphology of the various percussion marks or their different spatial distribution. However, they report a certain level of overlap in traces similar to carnivore tooth marks, advising a cautionary approach (*Galán et al. 2009,* 783; *Blasco et al. 2014,* 1102).
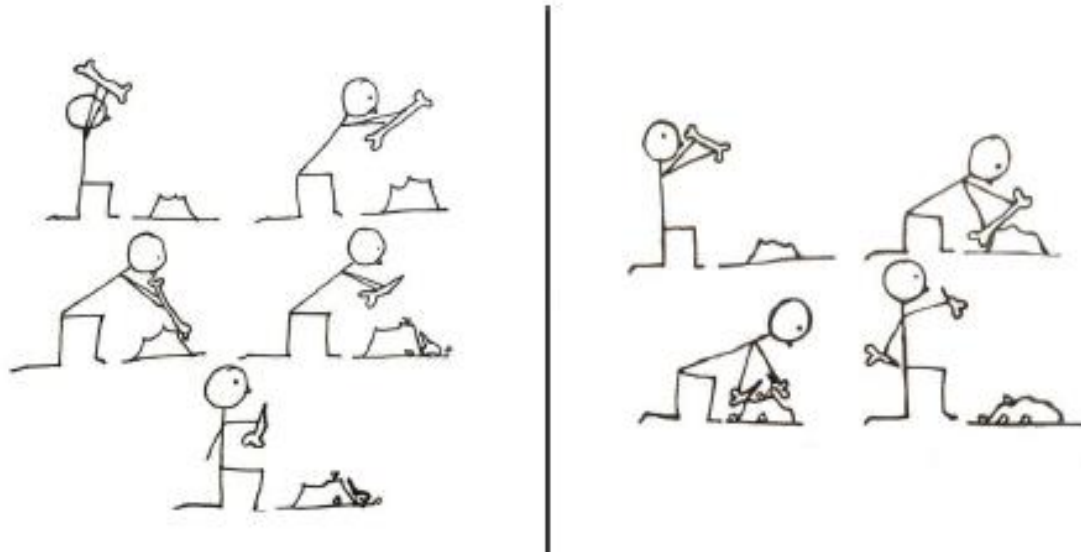
Fig. 5.2: Scheme of different positions the experimenter may take while using the batting technique to break bones. Bone held by the diaphysis on the left or the bone held by both epiphyses on the right (*Vettese 2019,* 155, Fig. 9; modified by SB).

I described the two major techniques used in experimental activities but also reported in contemporary hunter-gatherer societies (e.g. *Binford 1981*; *Oliver 1993*). Nevertheless, it is important to remember that they do not have to be applied exclusively. A hybrid operational chain comes to mind since the fragmentation process (e.g. for marrow extraction) mostly requires multiple impacts on the bone to break the thick compact layer and open the marrow cavity. The initial stages may be performed using other techniques than the final ones. Moreover, after the first breakage, other types of loading less specific for human fragmentation such as torsion, can be employed (*Blasco et al. 2014,* 1102; *Vettese et al. 2020,* 7). The final technique or combination of techniques used is dependent on multiple variables. Not only is the shape and state of the bone relevant but also the sociocultural background, skills and customs or current availability could have played a role and influenced the final choice (*Blasco et al. 2013b*; *Vettese et al. 2017*; *2021*).

5.1.2 Fracture surface and fracture plane

Dynamic loading of fresh long bones also produces typical fracture surface features. Under the SEM examination, the texture of the fracture surface in dynamically broken fresh long bones may have two forms depending on the amount of force applied leading to either spiral or horizontal tension failure (see Chapter 2.3.1; *Shipman 1981,* 371-373). Further, two stress relief features are described, which typically emerge from

dynamic loading and show the direction of the fracture front propagation from the point of impact. *Hackle* or *ripple marks* are interrupted curved grooves and ridges (Fig. 5.3a). *Ribs* are mainly continuous semi-circular, arched and form depressions on the original fracture surface. Their presence is diagnostic for the dynamic loading; however, their absence cannot exclude its action (*Gash 1971*; *Johnson 1985*; *Pickering – Egeland 2006*). *Chattering* is characteristic of pronounced peaks and valleys close together (Fig. 5.3b). This feature is a result of resistance in the bone microstructure or changing bone morphology. *Stepping* is a result of encountering the split line, which interrupts the flow of force and stepped or jagged morphology of the fracture edge emerges. Chattering and stepping are considered to be contrary to the ripple marks and ribs as resistance features (*Johnson 1985,* 197).

In the sense of differentiating the actor according to the surface appearance, a macroscopic description of the overall surface character is mainly used (see Chapter 2.3.1). Since the assumption is that humans fragmented bones in a fresh or slightly altered state, mainly for nutritional purposes, the smooth fracture surface is most often referred to in human fragmented assemblages.
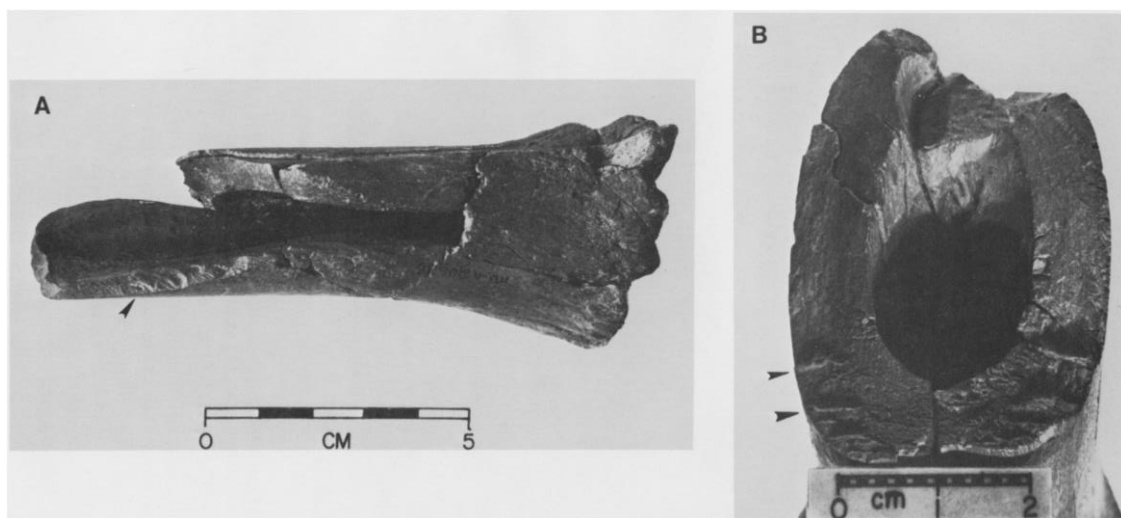
Fig. 5.3: Example of stress relief ripple marks (A) and stress resistance chattering (B) on an archaeological bison metatarsal (*Johnson 1985,* 196, Fig. 5.14).

The fracture planes were usually studied according to their outlines (see Chapter 2.3.1) and the relation to bone preservation (see chapter 3) relying on the qualitative descriptive system (e.g. *Villa – Mahieau 1991*). More recent studies approached this trait through quantitative evaluation by measuring the angles between the fracture surface and the cortical bone surface (*Alcántara García et al. 2006*; *Coil – Tappen – Yezzi-Woodley*

2017). These provided results differentiating between human and carnivore activity (and therefore static vs. dynamic loading) based on the measurements of the fracture surface angle in the context of other diagnostic traits and contextual information. However, their results are ambivalent to a certain point, since they both use different animal taxa and report a strong dependency on a specific skeletal part. Therefore, their application to archaeological assemblages on their own is limited (*Alcántara García et al. 2006,* 43; *Coil – Tappen – Yezzi-Woodley 2017,* 914).

5.1.3 Percussion marks

Besides the characteristic fracture outlines and fracture surface macro-morphology, a group of other diagnostic traces such as percussion pits, notches, scars and flakes emerges (e.g. *Capaldo – Blumenschine 1994; Pickering – Egeland 2006*; *Galán et al. 2009*; *Blasco et al. 2014*). These traces can generally be called as percussion marks (*Vettese et al. 2020*). Percussion marks represent accompanying traces emerging during the process of percussive bone fragmentation. Their position and spatial distribution vary according to the technique used and the final form/type also depends on the type of affected bone (compacta/spongiosa) or the presence of the periosteum. The skills of the actor (in this case, human) and the tool or technique employed in this process also significantly influence the outcome (*Vettese et al. 2020,* 7-8). Numerous studies approached this topic through extensive experimental research and employed various methods of evaluation. They described a huge variety of traces emerging in the fragmentation process that were more or less specific to the actor and the effector employed. However, they also report several overlaps in traces left by various actors/effectors, and a multiplicity in traces left by one type of tool or activity (*Haynes 1982*; *Galán et al. 2009*; *Organista et al. 2016*; *Moclán - Domínguez-Rodrigo – Yravedra 2019*). A certain ambivalence is, according to *Vettese et al.* (*2020,* 8), introduced into the topic by the nonuniform terminology used to describe these traces in works by various authors in different languages. These authors propose a new nomenclature based on a description system for a more reliable comparison of different studies. To briefly summarise the different types of percussion marks, I will use the proposed categorisation. Three main groups of traces can be described. First are *percussion marks sensu stricto*. These result directly from the impact and include adhering flakes, crushing marks, flakes, percussion notches, and percussion pits and grooves. In the second group are *traces*

subsequent to bone breakage, which are related to the spread of force from the point of impact further into the bone. These are fractures and cracks, ripple marks, peeling and pseudo-notches. In the third category are *striations related to the percussion marks*. These include scraping marks left after periosteum removal or microstriations and striations caused by scrubbing the bone against the anvil or percussor. Examples of the listed marks can be seen in Fig. 5.4 (*Vettese et al. 2020,* 8-14).

These represent a broad problem of which a detailed description is beyond the scope of this thesis. Moreover, since the percussion marks were not subjected to closer observation and description in my study, I will not be discussing them in greater detail. For a more comprehensive description of the individual types of percussion marks, their categorisation and the characteristic context of their emergence, I refer the reader to the following studies (e.g. *Blumenschine – Selvaggio 1988*; *Capaldo – Blumenschine 1994*; *Pickering – Egeland 2006*; *Galán et al. 2009*; *Blasco et al. 2014*; *Moclán - Domínguez-Rodrigo – Yravedra 2019*; *Vettese et al. 2020*).
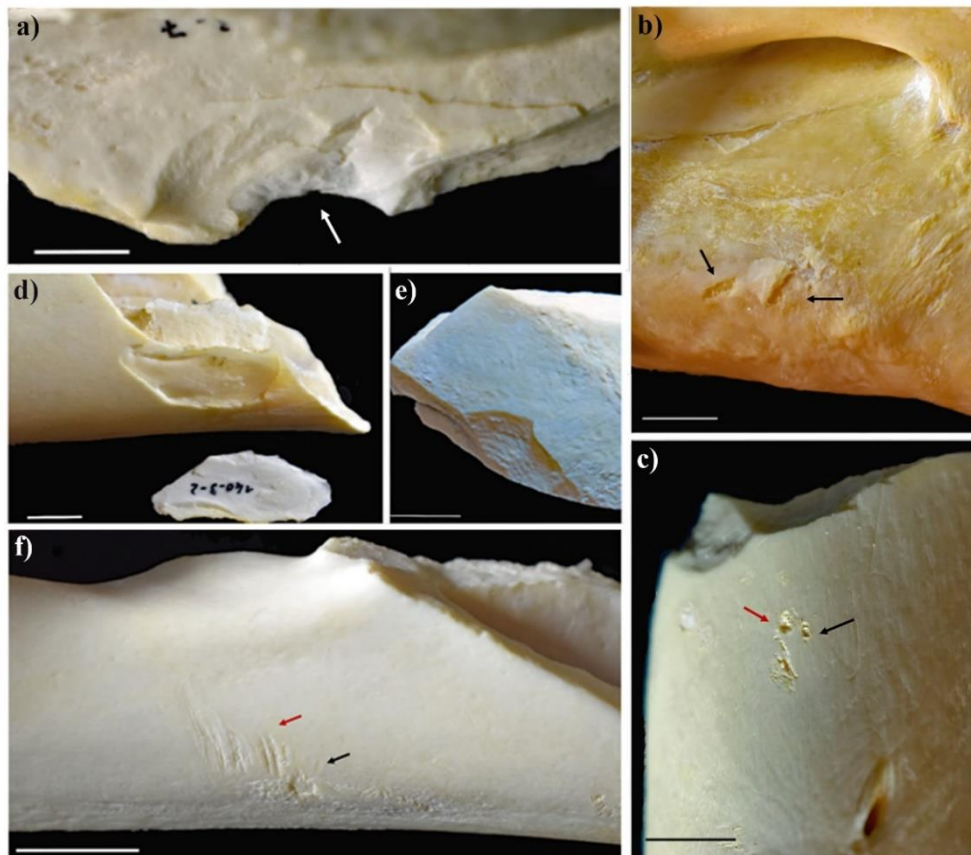
Fig. 5.4: Examples of percussion marks. Percussion notch originating in the place of impact (a), percussion grooves (b, black arrows), triangular (c, red arrow) and ovoid pits (c, black arrow) also directly related to the impact. Outer conchoidal scar with flake (d) and ripple marks (e) as an example of consecutive percussion marks and microstriations (f, red arrow) with pits (f, black arrow). Scale bar 1 cm (*Vettese et al. 2020,* 9-12, Fig. 1, 3, 4, 5; modified by SB).

In the "hammerstone on anvil" technique, also used in one of the experiments reported in this thesis, the point of impact for breaking the bone can be placed to the mid-diaphysis or closer to one of the epiphyses. The bone may be, for better efficiency of the blow, placed on one anvil in the middle or on two anvils placed under the epiphyseal ends (*Johnson 1985,* 192). After impacting the bone with a hammerstone, two percussion notches may emerge. One is in the place of percussion; the second may emerge at the opposite side of the bone as a force rebound from the anvil. The rebound notches tend to be smaller than percussion notches in the loading position as the rebound force is weaker than the initial force (*Capaldo – Blumenschine 1994,* 742; Fig. 5.5). These loading points have the form of circular depressions caused by local compression of the bone in the place where the loading device hits and regularly results in bone flakes/cones or pieces of crushed bone. Loosened bone flakes leave negative flake scars on the outer surface of the compact bone at the impact point (*Johnson 1985,* 194). These represent the percussion marks *sensu stricto*. Traces after bone fragmentation may be represented by stress relief and resistance marks as described in Chapter 5.1.2, and different fracture outlines depending on the state of the bone and the amount of force applied also appear (see Chapter 2.3.1). Finally, as the use of at least two tools is involved (anvil and hammerstone), the striations resulting from their mutual interaction with the bone are common.

Fig. 5.5: Example of bone broken by the hammerstone on anvil technique. The bone shaft fragment displays a percussion notch (upper edge of the fragment), rebound notch (lower edge of the fragment) and the spiral fracture outline with an oblique angle (*Outram 2002,* 55, Fig. 6.8).

Many experimental studies concerning the topic of human bone fragmentation were conducted and multiple mechanisms and traits were also described and explained in ethno-archaeological contexts. However, the main question regarding the distinguishing possibilities of specific traits to identify the fragmentation agent is still the subject of research today. In the conclusion to this chapter, I provide an overview of the most

relevant experimental studies concerning human bone fragmentation in the context of other variables published in the last 20 years (Tab. 5.1). Most of the studies consider the hammerstone on anvil fragmentation technique and observe the emerging traces. These are mainly percussion marks, their characteristics, abundance, proportions in relation to different skeletal parts, animal species or types of force (dynamic vs. static) to differentiate humans from carnivores. Other traces studied include fracture outline, fracture edge texture and fracture angle. These can be combined in the calculation of indices (e.g. FFI) or complemented by other parameters such as standard archaeozoological measures (NISP, MNE, MNI and their mutual ratios), fragment counts and measurements, bone circumference completeness, cortical wall thickness, and the proportions of parts of the epiphysis and diaphysis that were preserved dependent on bone density. These are often examined on bones in different states of preservation to model and study the level and pace of the degradation processes in different environments and the influence on bone response to fragmentation agents. The main results, together with basic information on the aim of the study, the material, studied traces and used methods are available in the following table (Tab. 5.1).

Of considerable significance in recent years is the increased use of modern software, computational methods, and artificial intelligence in the analysis of bone surface modifications (BSM) also related to fragmentation processes. However, the absence of any kind of microscopy-based methods and approaches implied in the study of traces left by fragmentation can be noticed. The results of the listed studies provide different diagnostic traces with their reliability depending on a large amount of other contextual information. A holistic approach and the use of a multi-variable analytical process combining different types of direct and indirect evidence is strongly recommended and encouraged to achieve the most accurate interpretations and explanations.

Study	Aim/Focus	Material	Studied traces	Methods	Results
Outram 2001; 2002	hammerstone percussion in different states of preservation	cattle	fracture outline; fracture edge texture; fracture angle; steps and columns; percussion marks	*Morlan 1984*; *Johnson 1985*; *Villa – Mahieau 1991*; FFI; Pearson´s correlation coefficient	construction of valid fracture freshness index (FFI) distinguishing fracture patterns on fresh, mildly and heavily altered bones; the index is sensitive to pre-fracture bone treatment
Alcántara García et al. 2006	carnivores (hyenas) vs. humans (hammerstone)	cattle, pig, sheep	angle of the fracture surface	*Capaldo – Blumenschine 1994*	angles between 80˚ and 110˚ are caused by static loading (carnivores); angles <80˚ and >110˚ result from dynamic loading (hammerstone)
Pickering – Egeland 2006	patterns of hammerstone percussion	white-tailed deer	percussion mark types; frequencies and distribution	*Turner 1983*; *Blumenschine – Selvaggio 1988*; *1991*; *Villa – Mahieau 1991*; *White 1992*; *Capaldo – Blumenschine 1994*	in humeri more spiral and oblique-angled fractures than in radii which have mostly right-angled and longitudinal fractures; processing intensity strongly influenced by the skeletal part; the most common type of percussion mark is pitting; frequencies of percussion marks are related to the character of the tool surface; the negative correlation between the number of blows and the number of resulting percussion marks
Galán et al. 2009	modified vs. non-modified hammerstone	cattle, goat	percussion marks; notches;impact flakes	*Capaldo – Blumenschine 1994*; statistical evaluation of frequencies and distribution (one-way ANOVA procedure)	higher frequencies of pit/scores with microstriations left by the modified tool; absence of microstriations in significant part of the percussion marks caused by a non-modified hammerstone (overlap with carnivores); the prevalence of single notches using both types of tools when compared to static loading by carnivores; metric data for notches and flakes in small animals is ambiguous
De Juana – Domínguez-Rodrigo 2011	hammerstone percussion of horse vs. cattle bones	horse	NISP/MNE; percussion notches and marks; impact flakes; angle range of breakage planes	*Capaldo – Blumenschine 1994*; *Blumenschine 1995*; *Pickering – Egeland 2006*; *Domínguez-Rodrigo – Barba – Egeland. 2007*; *Galán et al. 2009*; multivariate statistical analysis	more complex notch types in equine bones; notch shape and size in equine bones alone unreliable and overlapping with several actors/effectors; impact flake proportions identical in both horse and cattle bones; horse bones produce more right angles than cattle bones with the same effector, overlapping with static loading in cattle bones

Study	Aim/Focus	Material	Studied traces	Methods	Results
Karr – Outram 2012a	hammerstone percussion in altered states of preservation	cattle, horse	fracture outline; fracture edge texture; fracture angle	*Outram 1998; 2001*; FFI	slower degradation of bones in the frozen state, the response to fragmentation in the frozen state very similar to fresh bones, differences in FFI values visible after a longer period of freezing; rapid degradation of bone in hot and dry environments leading to higher FFI score and reduced fresh fracture characteristics even after a short period of heating/drying
Karr – Outram 2012b	dynamic impact by rockfall and bone fragments identification and survivorship	cattle	fragment counts and proportions in relation to bone density and bone preservation state	proportions and completeness of epiphyseal and diaphysis parts of bones	greater bone density leads to an increased probability of heavy fragmentation in rockfall events (contradictory to density-mediated attrition)
Almeida – Saladié Balleste 2014	modified vs. non-modified hammerstone percussion in fresh, frozen, boiled and thawed bones	cattle	metric analysis of impact flakes	*Pickering – Egeland 2006; Galán et al. 2009*	modified hammerstones produce longer and narrower impact flakes if compared to non-modified hammerstones; most impact flakes from fresh bones; the existence of overlaps in cow impact flake dimensions, even despite the different conditions prior to fragmentation
Blasco et al. 2014	batting vs. hammerstone on an anvil	cattle	completeness of fragments; outline; angle and surface of fracture surface; percussion marks	*Villa – Mahieau 1991; Capaldo – Blumenschine 1994; Pickering – Egeland 2006*; non-parametric statistical tests; multivariate analysis; multiple factor analysis	distinctive placement of notches and proportion of different types (double in batting vs. single and opposing in hammerstone); in hammerstone technique, a larger proportion of spiral and longitudinal fractures
Karr – Outram 2015	hammerstone percussion in different states of preservation (modelling of environmental conditions)	cattle, horse	fracture outline; fracture edge texture; fracture angle	*Outram 2001; 2002; Karr – Outram 2012a*	evidence of bone degradation rate and its influence on the response of bone to fragmentation; underlining the state of bone preservation as a significant variable, which attention should be paid to in experimental practice and interpretation processes

Study	Aim/Focus	Material	Studied traces	Methods	Results
Grunwald 2016	hammerstone percussion of frozen and thawed bones	cattle	cortical wall thickness index; fragment size (length-to-width ratio); FFI	*Järvinen et al. 1998*; *Outram 2002*; analysis of variance by ANOVA	thawing process is more crucial in fracture pattern changes than the duration of freezing; fragments from frozen bones are wider, frozen bone fracturing laterally across the diaphysis; fragments from thawed bones are longer, the fracturing pattern variability greater than in frozen bones, showing helical outlines, but rough surfaces and right angles
Coil – Tappen - Yezzi-Woodley 2017	carnivores (hyenas) vs. humans (hammerstone)	elk	angle of the fracture surface; fracture outline	*Villa – Mahieu 1991*; *Pickering et al. 2005*; *Alcántara García et al. 2006;* statistical permutation tests	underline the importance of the fracture plane, skeletal element and limb portion; carnivores cause more oblique angles (further from 90˚) on oblique fracture planes than hammerstone
Merritt – Davis 2017	hammerstone percussion and long bone fragment diagnostic properties and identifiability	goat	shaft circumference completeness; specimen size; calculation of standard archaeozoological measures; epiphysis-to-shaft ratio	*Bunn 1983*; *Lyman 1994*; identifiability categories 1-5; Mann-Whitney U-Test; Chi-squared test	the smaller the fragment, the less identifiable to the specific category; the circumference completeness positively correlates with the identifiability to the skeletal element or at least bone portion; missing epiphyses underestimate MNE and MNI and can lead to underrepresentation of butchery practices
Moclán – Domínguez-Rodrigo 2018	hammerstone percussion and surface modification frequencies	red deer	cut marks; percussion mark types and frequencies;	*Pickering – Egeland 2006*; *Domínguez-Rodrigo et al. 2009*; *Galán et al. 2009*; MonteCarlo method and multinomial test; Chi-square test; correspondence analysis	the percentual abundance of cut and percussion marks does not depend on the intensity of green bone breakage; fracture of long bones is dependent on the anatomical element and position in relation to the anvil surface; percussion notches characteristics in medium-sized animals correspond to those previously identified in large and small-sized animals and can be distinguished from the batting technique and carnivore agency
Moclán - Domínguez-Rodrigo – Yravedra 2019	carnivores (captive wolves and hyenas) vs. humans (hammerstone)	pig, red deer	angle and outline of fracture planes; presence of percussion notches	*Villa – Mahieau 1991*; *Alcántara García et al. 2006*; *Pickering – Egeland 2006*; statistical analysis by uni and bi-variate analysis and machine learning	significantly higher proportion of oblique fracture planes in hammerstone assemblages compared to carnivores; ability to differentiate wolves and hyenas through fracture planes; higher frequency of double notch types in wolves than in hammerstone (large sample needed)

Study	Aim/Focus	Material	Studied traces	Methods	Results
Vettese et al. 2021	intuitiveness in the process of human bone breakage	cattle	fragment measurements; measurements and spatial distribution of percussion marks;	ArcGIS "optimized hot spot" analysis; *Stavrova et al. 2019*; Spearman´s Rho; Wilcoxon test; Efficiency index	similar distribution of percussion marks despite different breakage routines; identification of "hot spot" areas considered as intuitive areas; the main influence in the location of percussion marks has bone anatomy in the case of *humeri*, *radio-ulnae* and *tibiae* and the experimenters' behaviour in the case of *femora*; underlining the importance of gestures in the bone breakage process

Tab. 5.1: Summary of experimental studies from the last two decades examining human bone fragmentation and characteristic techniques. The studies mostly focus on the description end evaluation of characteristic traits originating from the fragmentation process, their change with different kinds of bone degradation/alteration, and a comparison with similar traces left by other fragmentation agents, processes or techniques. Ordered chronologically (author SB).

5.2 Nonhuman/natural bone fragmentation

Not only human-induced activities can lead to the fragmentation of bone material. Among other actors causing this kind of modification, I will discuss the activity of carnivores as another example of intentional bone breakers. Following this will be examples of activities where fragments originate unintentionally, such as trampling by large animals, and via post-depositional circumstances such as sediment pressure/movement, weathering and water transport.

5.2.1 Carnivores

5.2.1.1 Accumulative tendencies

Carnivores as taphonomic agents influence the osteological material in two key ways. The first involves the specific spatial distribution of archaeofaunal remains and the creation of accumulations. The accumulation sites can have different functions such as dens, breeding dens, prey depots, hunting places and feeding shelters (*Palomares et al. 2022*, 3). The accumulative tendency and its characteristics are mainly discussed in the case of hyenas. Similar to other large carnivore species, hyenas overlap in inhabited ecosystems and hunted prey with humans in Plio-Pleistocene Africa and Eurasia. Their activities affecting the bones are discussed as a part of early hominin subsistence strategies and the hunting-scavenging debate (e.g. *Capaldo 1997*; *Pickering 2002*; *Pickering – Clarke – Moggi-Cecchi 2004*). There are studies offering a variability of criteria for human/hyena accumulation distinction (e.g. *Cruz-Uribe 1991,* 475; *Lam 1992,* 401) including, for example, carnivore-ungulate MNI ratios, bone surface modifications and the relative intactness of limb bones (*Pickering 2002,* 135). Again, the importance of a multivariate holistic approach considering multiple lines of evidence is emphasised. The accumulative tendencies can also be observed in other carnivore families such as felids (e.g. *De Ruiter – Berger 2000*; *Sauqué et al. 2014*; *Arriaza et al. 2016*; *Rodríguez-Hidalgo et al. 2020*) or canids (e.g. *Krajcarz – Krajcarz 2012*; *Lord et al. 2007*; *Morley et al. 2019*; *Palomares et al. 2022*).

Concerning accumulative and transport behaviour regarding the bones of carnivore prey, the analogical frameworks are built on assemblages from wild and also captive animals. Multiple authors have already raised cautionary notes about the use of captive vs. wild animals to model past situations, underlining the importance of other environmental variables playing a key role in animal behaviour (e.g. *Gidna – Yravedra –*

Domínguez-Rodrigo 2013; *Sala – Arsuaga – Haynes 2014*; *Palomares et al. 2022*). The topical studies showed a significantly higher intensity of bone modification in captive animals of the same species than in wild ones. Their results show that not only spatial distribution and accumulations of skeletal remains but also studies addressing the frequencies of different modifications on individual skeletal elements may be burdened with this error. A different situation occurs when it is strictly the traces left by the effector and their individual characteristics, such as measurements, that are the point of interest. Here, the morphology and function of the jaws and teeth play a key role rather than the behavioural and ecological adaptation of the species to certain environments (*Coil – Tappen - Yezzi-Woodley 2017,* 903).

5.2.1.2 Consumption operational techniques and related bone surface modifications (BSM)

Another way of carnivore bone modification is represented by a group of characteristic bone surface modifications and fragmentation patterns. These are related to the direct exploitation of bones as resource of fats and nutrients and so represent the result of intentional bone modification. There are multiple ways in which carnivores operate when trying to open a bone (*Binford 1981,* 51; *Haynes 1981*). They characteristically use static loading, which is described as a '*constant compressive pressure technique that generally employs an even distribution of force*' (*Johnson 1985,* 192). The pressure acts from two opposing directions and gradually increases until it reaches the point of structural failure. The use of static loading to access the in-bone nutrients is one of the most remarkable differences, when comparing human and carnivore-induced fragmentation (*Gifford-Gonzalez 2018,* 211). However, both forces may lead to the emergence of spiral fractures, and therefore close study of other, mainly surface, traces accompanying fragmentation activity is crucial (*Johnson 1985,* 193).

In the most frequently employed strategy, carnivores break bones primarily from the epiphyseal ends. These are soft and spongy and prone to modifications such as gnawing pits, scratching or chewing of the protruding parts. When the epiphyses are chewed away and once the bone shaft is obtained, the animal tries to either lick the marrow out with its tongue and canines or (more effectively) break the shaft with a vice-like grip with strong cheek teeth (*Binford 1981,* 51; *Johnson 1985*, 182, 192; *Gifford-Gonzalez 2018,* 211; Fig. 5.6). After partial or complete removal of the epiphyses, the

diaphysis is weakened and its mechanical properties change. It can collapse from the static pressure applied by the carnivores' jaws resulting mainly in longitudinal rectilinear bone fragments following the main collagen bundle orientation (*Johnson 1985,* 192). In the second strategy, the carnivores aim directly at the diaphysis, mainly in the case of cached or scavenged bones. The final fracture morphology depends on the actual state of the bone and can easily result in a spiral fracture (*Haynes 1980*; *1981*; *1983a*). In such a case, this pattern of fragmentation and its results could be easily mistaken for human activities. However, this operational chain reported by *Haynes* (*1981*) is an occasional and not characteristic one; moreover, the experimental setting in which it was observed is loaded by the discrepancies closely referred to by *Johnson* (*1985*, 192).

Fig. 5.6: The picture shows different stages of bovid bones by wolves as stated by *Campmas* and *Beauval* (*2008*), a) complete bone with punters, pits and grooves on both epiphyses, b) part of proximal extremity damage starting at the great trochanter, distally starting from condyles, c) the distal end disappears completely before the proximal one, d) damage to the proximal end continues, the head of the femur is not destroyed immediately because it is denser and often protected by articulation with the coaxal, e) complete removal of epiphyses, bone cylinder remains, f) furrows (close up) from cylinder chewing on the cylinder, g) final fragmentation of bone shaft (in the referred study, observed only rarely), scale bar 5 cm (*Campmas – Beauval 2008,* 173, Fig. 5; modified by SB).

The epiphyses and diaphyseal fragments that emerge from whatever breakage technique usually bear various surface modifications that represent traces after gnawing, such as punctures, pits, scores and furrows. Punctures are traces after the sharp teeth of carnivores, better pronounced and mostly observed in the part of the bone with a thinner compact bone and more spongious bone. Their depth and size are given by bone resistance and carnivore size/strength. Pits can be described as shallow punctures, mostly observed in places with more resistant bone and mainly found in larger groups. Scores are U-shaped channels, at least four times longer than wide in their measurements and are typically

observed perpendicular to the long bone axis on long bone shafts. Furrows are in shape similar to scores, approximately 2-4 cm long and up to 4 mm wide. Contrary to scores, are typically present on the epiphyseal ends with a large amount of spongious bone and represent the most frequent type of BSM by carnivores (*Haynes 1980,* 344-348; *Binford 1981,* 44-48; Fig. 5.7). Their absence may exclude carnivores from the list of potential breakage actors although their presence does not necessarily indicate their exclusive access to the bones and may reflect more complex taphonomic history. If the bone is too thick/resistant, the animal uses so-called channelling (biting the bone starting at the 'cylinder crown' and proceeding through its longitudinal axis). This process is unique to carnivores (*Binford 1981,* 51).
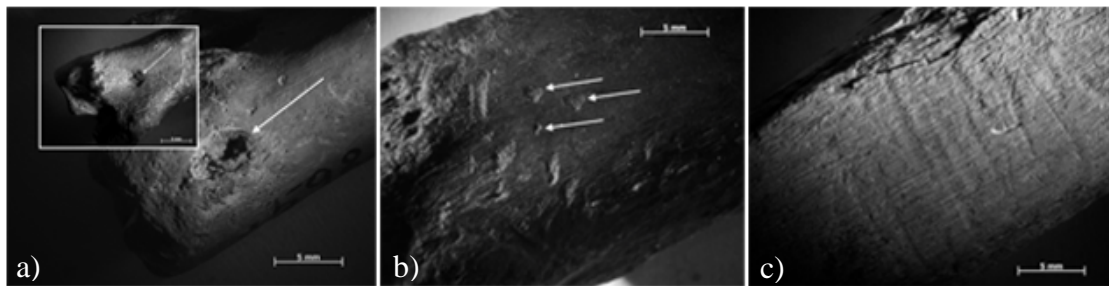
Fig. 5.7: Typical bone surface modifications caused by carnivore gnawing, a) punctures on ventral and dorsal (smaller picture) side of the bone, b) pits (white arrows), and c) scoring on compact bone, scale bar 5mm (*Stančíková 2018,* 34-35, Fig. 10-12; modified by SB).

Another way of accessing the bone marrow is the distortion and removal of the bone splinter. The result of this activity is largely observed in archaeological assemblages, and the resulting fragments/splinters are commonly mistaken for human activity (*Binford 1981,* 51). Another type of modification is "chipping back" on the edge. By chewing on the edge of a broken bone, and using the strong carnassial teeth, vice-like pressure results – mainly in dense compact bones, in the removal of small chips. This type of modification was regularly mistaken with microretouching of bone tools (*Breuil 1938*; *Dart 1960*; *De Lumley 1969*; *Freeman 1978*; *Binford 1981,* 51). However, the typical scoring caused by slipping teeth on the outer bone surface just below the chipped edge can serve as a lead to the correct interpretation. In addition, random chipping and flaking, distinguishable from systematic technological flaking employed by humans, can be present in carnivore-damaged bones (*Johnson 1985,* 197).

The surface modifications described are mainly observed on larger fragments (larger than 4 cm), and the smaller ones are commonly consumed and excreted in scatters, and if recovered may bear traces of stomach acid erosion (*Binford 1981,* 60; *Villa et al.*

2004, 705). The length and width, and the shaft circumference completeness may also serve in combination with other traits as discriminant features. The proportion of fragments representing less than 1/4 of the original length of the shaft will be significantly lower in carnivore-modified assemblages than in those modified by humans. Shaft fragments with more complete circumference are interpreted as typically originating from carnivore activity, whereas fragments retaining less than 50% of their original circumference were mainly ascribed to human activity (*Bunn 1983*; *Villa – Mahieau 1991*; *Villa et al. 2004*; *Merit – Davis 2017*). Considering the splinters emerging from carnivore feeding activities, the uniqueness of a spiral fracture as a result of human activity comes into question (see Chapter 4). In *Binford's* (*1978,* 262-265) controlled dog feeding, almost half the bones (44%) were broken by dogs resulting in a helical fracture, also present in caribou leftovers from a wolf hunt (*Binford 1981,* 57). Similar observations were made by several other authors (*Buckland 1823*; *Zapfe 1939*; *Bonnichsen 1973*; *Hill 1976*; *Haynes 1978a*; *1978b*; *1980*). *Binford* (*1981,* 60) points out another carnivore-characteristic feature. Fragments are long, triangular in cross-section with pointed ends, originating from chewing on bone tuberosities or protrusions such as the tibial crest, femoral *linea aspera* or the supracondylar ridge of the humerus (Fig. 5.8). According to *Binford's* observations (*1981,* 60), these emerge exclusively in accumulations and were not identified in percussion-fractured assemblages.

Fig. 5.8: Group of crests and ridges chewed off the bones by carnivores, scale bar 2 cm (*Binford 1981,* 59, Fig. 3.21).

5.2.1.3 BSM characteristics in the context of fragmentation

In the previous chapter (Chapter 5.1.2), I discussed the use of fracture characteristics, such as the angle of the outline of the fracture or the surface texture to differentiate the fragmentation agents. Previous studies showed that carnivore breakage (static loading) leads to more right-angled fracture planes, whereas hammerstone breakage (dynamic loading) leads to more acute and obtuse angles (*Bunn 1983*; *Capaldo – Blumenschine 1994*). One of the more recent approaches (e.g. *Alcántara Garcia et al. 2006*) quantified the angles and identified the intervals for angles originating from static (80˚-110˚) and dynamic (<80˚ and >110˚) forces applied. However, some of the following experimental studies (e.g. *De Juana – Domínguez-Rodrigo 2011*), did not confirm these results and underlined the complexity of bone breakage as a taphonomic trace. Further study by *Coil – Tappen – Yezzi-Woodley* (2017) reports a closer relation and dependence of the final fracture angles on a specific skeletal element, skeletal region and break plane (transversal/longitudinal/oblique) (*Coil – Tappen – Yezzi-Woodley 2017,* 914). Their results are consistent with those observed by *Alcántara Garcia et al. 2006*. The most recent study by *Moclán – Domínguez-Rodrigo – Yravedra* (*2019*) dealing with fracture angles and planes also reports equifinality in the interpretation of fracture angles although raises interesting differences in fracture outline frequencies. They observed that the frequency of oblique fracture was significantly higher than longitudinal and transversal fractures in hammerstone broken assemblage, while in carnivore broken assemblages the frequency of oblique and longitudinal fractures is similar. They introduced a ratio describing this phenomenon. In hammerstone broken assemblages, the ratio always scored below 1, whereas in the case of carnivore broken assemblages, values equal to 1 or higher were observed. Their observations are also consistent with results reported on different animal size categories (*Moclán – Domínguez-Rodrigo – Yravedra 2019,* 4671). Although these studies quantified the differences in precisely given experimental settings, they were unable to provide reliable unambiguous distinctive traits between human and carnivore broken assemblages easily applicable to archaeological material. They underscore the importance of contextual and background information, and the use of other accompanying traces to reliably identify the fragmentation agent.

The similarity between humans and carnivores in other traces left behind in the fragmentation process was already reported in 1982 by *G. Haynes*. He notes that the large notches on the edge of fragments chewed by carnivores are similar to the notches

emerging in the place of impact by dynamic loading (*Johnson 1985,* 200). The topic was thoroughly examined by *Capaldo* and *Blumenschine* (*1994*), following the frequencies and morphology of notches made by carnivore static loading and hammerstone dynamic loading. They recorded significant differences in both the observed traces in their work. The frequency of normal notched specimens was significantly higher in hammerstone fragmented assemblages, complete notches prevailed in carnivore fragmented assemblages, while a high proportion of incipient notches was described for hammerstone broken assemblages. The width-to-maximum depth of notch ratio describing the shape is also different for the two compared actors. Hammerstone-made percussion notches are broader and shallower and have more obtuse release angles, while carnivore tooth notches are close to a semi-circular plan shape with an almost perpendicular release angle (see also *Blumenschine – Selvaggio 1991*). Nevertheless, they also state a list of variables that most probably greatly influence the observed differences such as element type, cortical thickness and the type of force used and call for further experimental work to confirm the accuracy and usefulness of their results. Their work was further developed by other authors (e.g. *Pickering – Egeland 2006*; *Galán et al. 2009*; *Moclán – Domínguez-Rodrigo 2018*), and more detailed information on their work can be found in Tab. 5.1.

Among other overlapping surface modifications are pits and their associated characteristics. These can originate from carnivore gnawing or as a type of percussion mark left after hammerstone impact (see Chapter 5.1.3). In the case of hammerstone percussion origin, they were reported to be typically associated with microstriations resulting from slippage of the stone during the impact event (*Blumenschine – Selvaggio 1988,* 763; *Pickering – Egeland 2006,* 462; Fig. 5.9). A more recent study by *Galán et al.* (*2009*) on the effects of modified and unmodified hammerstones reported a significant abundance of pits without associated microstriations in bones fragmented by non-modified cobble. Further, the mean values of the pit measurements overlapped with the pits originating from gnawing by medium-sized carnivore (e.g. hyena) (*Galán et al. 2009,* 782). Similar results are also reported from studies examining different marrow extraction techniques. No microstriations associated with surface percussion marks were observed in the case of the batting technique (see Chapter 5.1.1), clearly differentiating the traces from carnivore-induced pits (*Blasco et al. 2014,* 1102). Both these results point to the equifinality that remains to certain degree when it comes to the differentiation of carnivore bone modification and may lead to an incorrect description of the dual pattern

(hominin-carnivore), even in cases where only human activity is responsible for the damage observed.
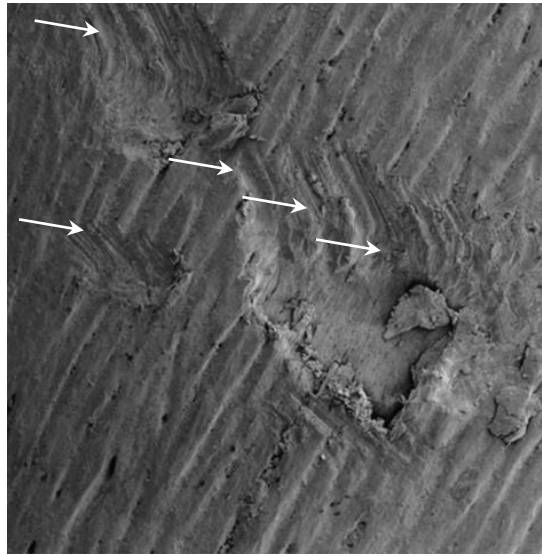
Fig. 5.9: Microscopic picture of pits with associated striations (white arrows), characteristically originating from dynamic impact by hammerstone, magnification not stated (*Pickering – Egeland 2006*, 462, Fig. 2; modified by SB).

Concerning the fact that archaeofaunal assemblages may be approached in their taphonomic history by a variety of modifiers in different time periods, the frequencies of tooth marking on bones and their fragments have been studied. Several authors report that the frequency of tooth marks on specific bone fragments may be distinctive for the primary access of humans or carnivores to the bone. For example, in his experimental works, *Blumenschine* found that assemblages primarily accessed by hyenas have a significantly higher percentage of tooth-marked midshaft fragments than those accessed secondary, defleshed, and demarrowed by humans (*Blumenschine 1986*; *1988*; *1995*). On the contrary, more recent studies by *Organista et al.* (*2016*) showed the opposite pattern in assemblages modified by lions. In models with primary lion access, the frequencies of tooth-marked mid-shafts were significantly lower. Further, the frequencies depended on the anatomical part, unlike in hyenas, which do not discriminate according to the skeletal types (*Organista et al. 2016,* 74-75). Their results again proved, that for a better understanding of observed traces, not only the differences between humans and carnivores in general but also the differences within the order of carnivora must be described and understood.

Research dealing with carnivore damage to animal remains and its overlap with human activities is usually focused on medium to large-sized carnivores such as hyenas, wolves, lions and leopards. Besides sharing the same environment and very often the

hunted prey, we share (with exaggeration) specific behavioural patterns in killing, transporting and processing the prey (*Palomares et al. 2022,* 1). As I attempted to demonstrate in previous paragraphs, the identification of the actor responsible for bone modification requires more than an understanding of the basic differences between traces left after humans and carnivores in general. The individual species/families differ significantly, not only in the teeth morphology and function of the masticatory apparatus but also in the extent and manner of prey consumption, exploitation and operational chain. Therefore, the presence, level and pattern of fragmentation may vary. The distinction of these specific patterns should help to accurately describe the origin and taphonomic history of studied assemblages (e.g. *Ferretti 2007*; *Tseng – Binder 2010*; *Domínguez-Rodrigo et al. 2012*; *Palomares et al. 2022*). Significantly less attention is paid in archaeological literature to ursids as bone modifiers. Nevertheless, forensic literature provides rich body of knowledge. Considering bone modification, bears leave traces of a similar nature to other carnivores, or in individual cases, even hominins (e.g. *Rosell et al. 2019,* 67; *Udoni – Pokines – Moore 2021*; *Indra et al. 2022,* 8). The level of bone damage caused by bears is described as slight to moderate, including pits, punctures, furrows and peeling. Major damage can be observed in flat bones, *vertebrae*, *costae*, bones from juvenile animals and fragile elements from small and medium-sized animals. However, the overall level of modification is dependent on the actual nutritional requirements and source availability (*Haynes 1983a*; *1983b*; *Carson – Stefan – Powell 2000,* 523; *Saladié et al. 2013; Indra et al. 2022,* 8). Long bones are typically not fragmented, but if so, only the epiphyseal ends are typically removed, and the bone shafts tend to remain unbroken in one piece. Fragmentation was mainly observed in elements of the axial skeleton compared to canids, who primarily attack the extremities (e.g. *Carson – Stefan – Powell 2000*, 519; *Sala – Arsuaga 2013,* 1394; *Arilla et al. 2014,* 1). The tendency to accumulate or transport the whole carcasses or their larger parts in general may be present; however, it has not been described in their dens to date (e.g. *Arilla et al. 2014,* 14; *Indra et al. 2022,* 8).

Some of the most recent experimental studies focused on the comparison of human and carnivore-induced fragmentation and its traces can be found in Tab. 5.1, where details about the experimental setting, methods and material used, observed traces, and the main results can be found.

5.2.2 Trampling

Trampling represents an activity that is not related to consumption and is typically assigned to medium to large-sized, hoofed animals although humans and large carnivores can also be responsible for this kind of modification. Usually, it is not intentional and appears in areas with increased movement of animals/humans and the parallel presence of osteological material on or just below the surface. An example is the increased movement around water sources (e.g. *Gifford 1977*; *Reynard 2014*), in enclosed areas such as caves or rock shelters (e.g. *Klein 1975*; *Reynard – Henshilwood 2018*), but potentially also campsites where the character of their function could represent areas where trampling took place. However, there are also cases of intentionally trampled bones being reported. A specific example is elephants, who were observed coming to the sites of death of their own species, playing with the bones, kicking, wallowing, tumbling, rocking and displacing them (e.g. *Coe 1978,* 76-79; *McComb – Baker – Moss 2006,* 28; *Haynes – Krasinksi – Wojtal 2020,* 2-3). Such activities could, besides other modifications, easily lead to the fragmentation of bone elements. Nevertheless, the final morphology of the fragment then largely depends on the actual state of bone preservation (*Myers – Voorhies – Corner 1980,* 487; *Binford 1981,* 80).

Modifications typically caused by trampling are multiple. The dislocation and reorientation of bones in both the horizontal and vertical axes are commonly observed. The authors describe the dislocation of skeletal elements over hundreds of meters, the plunging of bones into the sediment at steep angles as a result of pushing the bone into the soft substrate (e.g. *Fiorillo 1984*; *Gifford-Gonzalez et al. 1985*; *Rozada – Allain – Tournepiche 2018*; *Haynes – Krasinksi – Wojtal 2020*). Abrasive modifications are also very common, represented by rounded edges and smoothed or polished surface (e.g. *Reynard 2014,* 160). Another category includes bone surface modifications of a linear and non-linear character. The linear ones are surface striations, scratches, grazes, lines, or grooves and are often reported as a pseudo-cutmarks (e.g. *Fiorillo 1984*; *Behrensmeyer – Gordon – Yanagi 1986*; *Olsen – Shipman 1988*; *Domínguez-Rodrigo et al. 2009*; *Courtenay et al. 2019*). The criteria for distinguishing them from actual cut marks are numerous, for example, a U-shaped cross-section with a flat bottom, lack of distribution and placement pattern (random distribution), parallel and subparallel orientation and mutual overlap, and a shallower morphology without internal microstriations, association with polishing, etc. (e.g. *Olsen – Shipman 1988,* 550-552). Nevertheless, as the revision

of some of the originally proposed traces showed, their interpretational reliability may depend on the actual experimental setting, environmental conditions, and bone preservation state (*Domínguez-Rodrigo et al. 2009,* 2653-2654; *Pineda et al. 2014*, 85, 91). The nonlinear trampling marks are represented by pits, which tend to be much smaller and shallower than pits originating from carnivore gnawing, and more superficial, irregular, and randomly scattered than pits resulting from percussion impact (*Reynard 2014*, 160; *Fernández-Jalvo – Andrews 2016*, 109; *Reynard – Henhilswood 2018*, 4).

In the 1960s and 1970s, various authors pointed out the important role of trampling in the fragmentation of osteological assemblages (*Brain 1967*; *Gifford 1977*). There is an agreement among researchers that trampling cannot cause sufficient impact to break the fresh and complete long bone element of a medium or large-sized mammal. However, in slightly weathered conditions (Stage 1 and 2 according to *Behrensmeyer 1978*), or other altered states when the mechanical property of bone is changed (e.g. missing epiphyses, degreased), the incidence of spiral fracturing from trampling is undeniable (e.g. *Fiorillo 1984*, 65). This fact was also reflected in *Shipman's* spiral fracture typology (see Chapter 4; *Shipman 1981*, 372). In the case of bones from large mammals such as bison or moose, the frequency of spiral fracturing is reported as very low (around 5% according to *Haynes 1983a*). In the case of medium-sized mammals such as deer, horses or caribou, the incidence increases significantly (*Myers – Voorhies – Corner 1980*, 487-488; *Binford 1981*, 80; *Haynes 1983a*, 112). Considering trampling damage on the bones of extra-large sized mammals such as mammoths or rhinoceroses, *Haynes, Krasinksi* and *Wojtal* (*2020*) report that long bone fractures from elephant trampling usually show a mixture of dry and fresh bone fracture characteristics (*Haynes – Krasinksi – Wojtal 2020,* 3). However, in their experiments with static loading corresponding to trampling damage to fresh elephant bones, no spiral fractures were produced. The overlap with human-induced activities was detected in other traces resulting from trampling, and more typical for dynamic impact, such as an abundance of pseudo-notches and pseudo-cone flakes (*Haynes – Krasinksi – Wojtal 2020*, 12).

5.2.3 Geological processes

A wide variety of geological and natural processes can lead to bone breakage. In the following text, I paid focus on the processes most reported in the literature concerning bone fragmentation and its traces.

Weathering represents a group of complex physical and chemical processes that separate and destroy the organic and inorganic bone components. It significantly affects the state of the bone, its properties and, therefore, the fracturing response (*Behrensmeyer 1978,* 153; *Johnson 1985,* 184). Bones can weather both on the surface and when buried in soil (*Behrensmeyer 1978*; *White – Hannus 1983*). *Behrensmeyer* (*1978*) describes various weathering stages (0-5), which are characterised by macroscopic changes such as surface exfoliation, transverse and longitudinal cracking penetrating the cortical bone and complete bone disintegration (*Behrensmeyer 1978,* 151). Split-line cracks originate between the collagen bundles and are parallel to the long bone axis (*Ruangwit 1967*; *Tappen 1969*; *Tappen – Peske 1970*). Their existence also influences the propagation of stress in the bone, and, therefore, the final morphology of the fracture. They cause so-called split-line interference (*Johnson 1985*, 184). This means that the proceeding fracture front slightly jumps each time it encounters the split-line crack, resulting in an irregular, stepped fracture edge (*Johnson 1985,* 184, Fig. 5.9). The microcracking originating from moisture loss and exfoliation in weathering also influences how the bone responds to force. According to *Behrensmeyer* (*1978*), stages 0-2 are of greater importance when dealing with the possible cultural interpretation of bone breakage where according to criteria summed up by *Johnson* (*1985*, 185-187), different characteristics of fresh bone fracturing, such as a helical fracture, presence of the impact point or edible marrow, can be present. As the moisture loss progresses toward the dry or even mineralised bone, the characteristics change (no edible marrow, no impact point, horizontal tension failure) (*Johnson 1985,* 187; Fig. 5.10).

Moisture Loss Model: Proposed Phases and Characters

Fresh	Dry					Mineralized	
Phase 0	Phase 1	Phase 2	Phase 3	Phase 4	Phase 5	Initial mineral replacement	Advanced replacement
1. High-level moisture content	Initial moisture loss	Low-level moisture	Low-level to advanced moisture loss	Advanced moisture loss	Advanced moisture loss		
2. No desiccation features	Split lines may begin to form without interference	Split lines begin to form and cause interference	Split line interference	Split line interference	Split line interference		
3. Marrow fresh	Marrow unsoured; edible	Marrow still unsoured; edible	Marrow soured; unedible	Marrow decay	No marrow		
4. Impact point	Impact point	Impact point	Probably no impact point	No impact point	No impact point		
5. Helical fracture	Helical fracture	May be combination of helical and horizontal tension failure	Mainly horizontal tension failure	Horizontal tension failure	Horizontal tension failure		
← Weathering Stage 0 →		← Weathering Stage 1 →		← Weathering Stage 2 →			

Fig. 5.10: Table summarising the criteria according to progressing moisture loss (*Johnson 1985,* 187, Tab. 5.1).

The characteristics were assigned into six phases. Phase 0 refers to fresh bone from a just-killed animal. Phase 1 is a couple of hours/days old bone losing moisture, where the split-line crack can start to occur but mostly on a microscopic level and does not cause the split-line interference. Phase 2 is a transitional phase where the moisture loss reaches the critical level and the response to force changes from a helical or spiral fracture to horizontal tension failure. In phase 2, the split-line cracking is more obvious and causes split-line interference. In phase 3, the marrow becomes inedible. For phases 2 to 5, the empirical data for the timeframe are missing (*Johnson 1985,* 188). The changes described lead to more common transverse fractures and an altered fracture surface, which is exposed during the weathering process (*Gifford-Gonzalez 2018,* 16).

Water is undoubtedly a significant taphonomic agent, influencing bone preservation and introducing a wide variety of modifications. Different alluvial, colluvial and fluvial processes may cause significant chemical and physical alterations to the bone. From the physical alterations, traces such as polishing, rounding and abrasion are the most typical changes observed on bones from ponds, lakes, rivers, shores and groundwater-affected situations (e.g. *Hedges – Millard 1995*; *Haglund – Sorg 2002*; *Fernández-Jalvo – Andrews 2016*; *Bertoglio et al. 2021*). In the case of cold environments, the influence of groundwater is closely related to freezing or freezing-thawing cycles, as described in Chapter 3.1. Further, I discuss a specific case of fluvial bone alternation, reported in the literature as one of the geological/natural dynamic processes commonly causing bone fragmentation. The seasonal river ice break-up represents another natural process possibly causing bone breakage (*Haynes 1981*; *Thorson – Guthrie 1984*; *Johnson 1985*; *Haynes – Krasinksi – Wojtal 2021*). In winter, the ice on a river can reach a thickness of hundreds of centimetres. In spring, the thawing ice breaks up and together with entrained sediment has the power to break and modify the shore boulders of cobbles in the river channel. This process is typically very strong and unorganized and can cause significant modifications to sediment and rock material in the river channel and its immediate vicinity (*Thorson – Guthrie 1984,* 174; *Haynes – Krasinksi – Wojtal 2021*, 1012; Fig. 5.11).
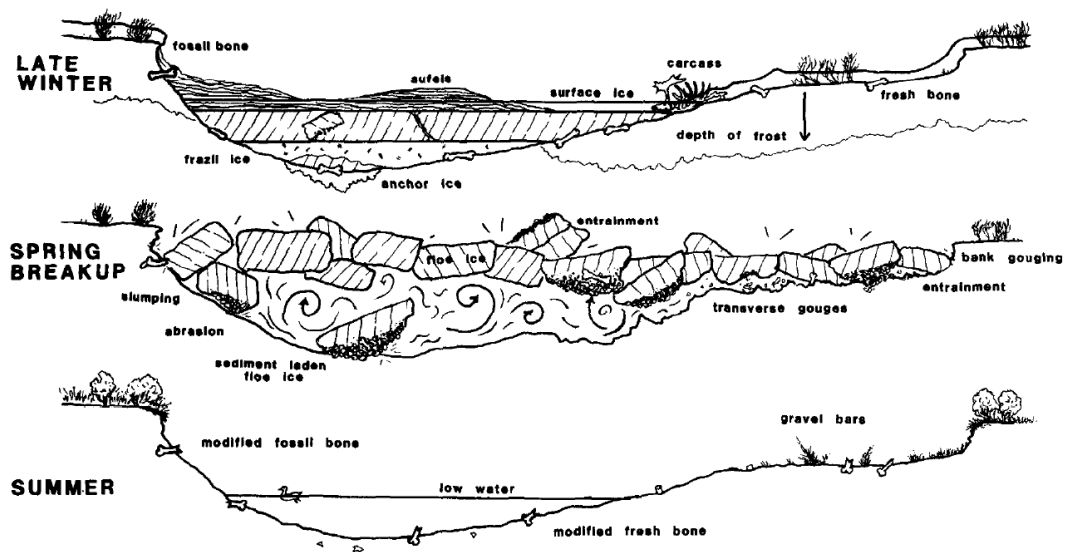
Fig. 5.11: Diagram showing the cross-section of a river channel in winter (upper), spring ice breakup (middle) and summer (lower) (*Thorson – Guthrie 1984,* 176, Fig. 3).

Bones in variable preservation states can enter the river system by any mechanism and the time of the year by any sediment entrainment or movement. After entering the system, the bones are exposed to forces of variable strength and direction. Compression, shear and tension can occur when encountering ice floes in the stream. A wide variety of modifications can occur during this process, transporting the bone to significant distances. A variety of breakage patterns was observed by experimental modelling of the ice break-up process (*Thorson – Guthrie 1984*). The spiral fractures were mainly common in large fresh and old bones and were usually introduced by shear (dragging) and compression (dropping the bone embedded in ice) stress. Longitudinal fractures occurred in all states of bone preservation, mainly during the interlayer shear by batting the exposed bone against the bottom or shore. Transversal fracturing was the most prevalent in fossil bones (*Thorson – Guthrie 1984,* 184). However, the moving ice floes and water can also introduce other modifications, such as flaking from compressive impact, individual scratches, or a series of parallel and subparallel striations. Further, polished, or abraded surfaces on bones resulting from this process were described (*Bonnichsen – Will 1980,* 9; *Morlan 1980,* 35; *Thorson – Guthrie 1984,* 185-186). The described traces may, to a large extent, be mistaken for intentional human activity. It is important to keep the possible intervention of a similar process in mind, especially in the case of sites where these processes are relevant and assumed. Modelling of ice break-up modifications by experiments is demanding due to the extremely high number of input variables that

91

mutually interact in unpredictable ways. The actual data concerning fragmentation by this process are scarce and mainly at the level of hypotheses, and further research by experiments and observations from natural contexts is essential for better understanding (*Thorson – Guthrie 1984,* 177; *Haynes – Krasinksi – Wojtal 2021,* 1012).

Another natural process that causes, in addition to other modifications, bone fragmentation is a type of sediment movement called debris flow. This is '*the fast downslope movement of watery slurries of sediments, rocks, and entrained material such as bones, usually following heavy rains or rapid snowmelt* ' (*Haynes – Krasinksi – Wojtal 2021,* 1012). This process can influence undisturbed isolated bone accumulations or entire situations (e.g. *Roebroeks et al. 2018*; *Soledad Domingo et al. 2017).* All the material contained in the debris flow is rolling and tumbling and the individual objects may be smashed against each other. This action gives rise to different accumulations and redistribution of bones or causes variable bone surface modifications such as scratching or striations. It may also significantly splinter and fracture the bone by the pressure, movement or when encountering other objects present in the flow, especially in a slightly or more progressively weathered state. A good example of such activity is landslides, emerging before or after the formation of an archaeological situation. These can significantly influence the original landscape and the already existing archaeological sites (*Svoboda et al. 2019,* 4-5).

As I directly used material originating from a rockfall experiment, I should briefly mention this natural process, which represents a direct dynamic impact by randomly falling rocks. Concerning fragmentation, a similar result of this process with intentionally fractured bones by humans was previously reported in the 1980s (e.g. *Dixon 1984*; *Agenbroad 1989*). Understanding the differences in fragmentation patterns and traces caused by these two dynamic processes is particularly relevant, especially in the case of bone assemblages originating from the corresponding environments (i.e. cave, rock shelter). The experiments conducted by *Karr* (*Karr 2012*; *Karr – Outram 2012b*) revealed that the rockfall process can truly produce fragmentation patterns showing spiral fractures and produce flakes, that to a large extent depend on the state of bone preservation. However, these pseudo-flakes are morphologically distinguishable from those originating from intentional human intervention. The rockfall breaks the part of the bone with higher density (i.e. the diaphysis) the most, while the epiphyses resist fragmentation. In this way, the process artificially accelerates the attrition of dense fragments, which are usually

reported to have the highest survivorship in most archaeological contexts. Therefore, bone fragmentation caused by falling rocks can significantly intervene and should be carefully considered when dealing with bone density-mediated attrition in environments where rockfall could be expected (*Karr 2012,* 252-254; *Karr – Outram 2012b,* 3448-3449).

PART II

6. Introduction to analytical methods

Several macroscopic and imaging methods were used for the basic description of the bone assemblages (see Chapter 6.1). These methods are commonly used in the description of archaeological bone collections. In my case, they were used to control the known data in experimental assemblages, and their main use was implied in processing the archaeological assemblages from the Pavlov I site.

I decided to imply three specific methods, to investigate the above-described phenomena and the state of bones originating from the fragmentation process. The first method is a macroscopic observation by the naked eye. This helps to evaluate the character of bone fragmentation in the assemblage based on a simple scoring of the chosen criteria and the calculation of the final index (see Chapter 6.2). The other two methods are microscopic, both of which are widely and regularly used in archaeology and anthropology and provide a solid interpretational background in a huge variety of material analyses (bone, stone, ceramics, etc.). The selected microscopic methods have particularly proven their efficiency in studying bone fracture and fragmentation mechanics in medical or material studies (e.g. *Piekarski 1970*; *Braidotti 2000*; *Hiller et al. 2003*; *Nalla – Kinney – Ritchie 2003*; *Ritchie et al. 2005*; *Li – Abdel-Wahab – Silberschmidt 2013*; *Zhang et al. 2013*). Therefore, I decided to imply these methods to also address the archaeological questions set. The principles of the three chosen methods and the pros and cons will be described in the following chapters (Chapter 6.2 to 6.4).

The three methods were applied to both experimental and archaeological material. The macroscopic method in experimental material was used to cross-check the outcome and evaluation system of experimental fracturing with the published data and the values for the specific states of preservation in bones. The influence of the presence of periosteum during the fragmentation process on fracture surfaces and other traits, such as the incidence of impact points and the number of the resulting fragments, was also observed. The observed FFI scores were then compared with results from microscopic analysis and their mutual correlation was discussed. Samples representing each experimental setting (state of preservation, type of force used, presence of periosteum) and the type of fracture (longitudinal, helical, transversal) were chosen for microscopic analysis. The samples first underwent SEM analysis, and the last method applied was the preparation and analysis of histological thin sections. The order of this was chosen from the non-destructive treatment to the most destructive and irreversible type of treatment

involved in the preparation process. This ensured that minimal destructive sampling took place and that the same sample was observed by both microscopic methods. The same protocol procedure was adhered in the archaeological material analysis, where here the most important role was played by the FFI calculation and observing the obtained values in the context of other specific information such as the type of skeletal element, species determination, spatial distribution of bones, etc. The microscopic methods were applied to significantly lower number of fragments chosen according to the FFI score. The main aim of this part of the thesis was to a) verify if the observed patterns from the experimental work can also be identified in archaeological bones, b) if the correlation of FFI with microscopic traits is also present in the archaeological samples, and c) how depositional and post-depositional conditions may interfere. Based on the observations described, the potential and benefit of the microscopic methods in addressing this specific issue in archaeozoological material are discussed.

The following text is organised into chapters addressing the methods used (Chapter 6), the specific experiments and results (Chapter 7) and then an analysis of the archaeological material and the application of the methods chosen (Chapter 8). Each thematic unit (experimental and archaeological) and the results are discussed directly at the end of the relevant section to maintain a fluent topical relation and connection.

6.1 Methods for the basic material description

For anatomical and taxonomical identification of the osteological material standard manuals, atlases and supplementary publications (*Schmid 1972*; *Hilson 1992*; *2005*; *Ziegler 2001*; *France 2009*), 3D digital models (*Niven et al. 2009*), atlases and reference collections available online (*ArchéoZoo*; *Laetoli Production*) and a comparative collection of the Research Centre for Paleolithic and Paleoanthropology in Dolní Věstonice were used. Information on weathering and taphonomic changes was collected according to standard manuals and widely used publications (*Behrensmeyer 1978*; *Binford 1981*; *Lyman 1994*; *Fernández-Jalvo – Andrews 2016*). Root etching was evaluated by a 6-stage scale designed by S. Sázelová. In stage 0 no traces of root imprints are present, stage 1 is typical by the fine traces of the roots covering a small area of the evaluated bone/fragment. In stage 2, the imprints are deeper/more pronounced and cover a major part of the bone/fragment and in stage 3 besides the imprints, tunnelling of the bone surface is also present. In stage 4, the bone displays surface corrosion, tunneling and

peeling induced by root system activity. The final stage 5 is, in comparison to stage 4, distinguished by the presence of the root remnants. Age was estimated according to *Takken Beijersbergen* and *Hufthammer* (*2012*) in the case of reindeer and *Harris* (*1978*) in the case of fox. For quantification and calculation of the elementary quantitative characteristics, I used units and methods identified by *Lyman* (*1994*) and *Kyselý* (*2004*). The following units were used. **NISP** (number of identified specimens) represents the overall number of identified bones/teeth/their fragments. In other words, it could be identified as a number of osteological finds (*Kyselý 2004*, 282). Unit **MNE** (minimum number of a particular skeletal element) represents the number of bones/teeth/their fragments belonging to one specific skeletal/anatomical unit. The **NISP:MNE** ratio is one of the basic methods for evaluating the fragmentation level of specific skeletal parts (*Lyman 1994*, 102). **MNI** (minimum number of individual animals) is calculated as the most represented anatomical part of specific species in an assemblage reduced according to its abundance in the complete skeleton of one individual. In the process of calculating variables such as intraspecies body size variability, sexual dimorphism or age-related changes may or may not be considered. The **MAU** (minimum number of animal units) unit describes the resistance and durability of specific skeletal parts, or whether and in what intensity the animals were butchered, and their parts transported by humans. It can also be described as MNI for every skeletal part (*Lyman 1994*, 100-105; *Binford – Bertram 1977*, 77-153). For photographic documentation I used a Nikon D5300 camera with different objectives. The microphotographs were taken on a Nikon SMZ1500 stereomicroscope with a Nikon D7000 camera, and DCam Capture and NIS-Elements software were used to document and calibrate the image data. These methods were used for the basic description of the observed experimental and archaeological assemblages. The methods used for detailed fragmentation analysis are described in the following Chapters (Chapter 6 and 8.3).

6.2 Fragmentation Freshness Index (FFI)

The Fragmentation Freshness Index (FFI) is a method developed and tested on the faunal experimental material and archaeozoological collections from the Holocene period. It was originally invented to investigate the level of bone marrow extraction (*Outram 1998*; *1999*; *2001*; *2002*). However, it also proved to be effective in addressing other activities concerning the fragmentation of bones originating from archaeological

contexts (e.g. *Karr 2012*; *Li 2018*). This method (*Outram 1998*; *2001*) is the most suitable for an average description of the fragmentation character of the whole assemblages – not to reveal the cause of fragmentation of individual bone fragments. It was designed to be quick and functional, in comparison to other approaches concerning, for example, the size of the fragments that make the analytical process lengthy and time-consuming (e.g. *Lyman – O´Brien 1987*; *Villa – Mahieau 1991*). It is based on a macroscopic description of three fracture surface characteristics detected on long bone diaphysis and their fragments. The chosen criteria are mainly based on previous suggestions of other authors (*Morlan 1984*; *Johnson 1985*; *Marshall 1989*; *Villa – Mahieau 1991*), such as a) angle, b) surface texture, and c) outline of the fracture surface (Fig. 6.1).

Fig. 6.1: Illustration of evaluated traits, a) angle of the fracture surface in relation to the outer/inner bone surface, b) outline of fracture, c) rough (upper) or smooth (lower) character of the fracture surface (*Outram 2002*, 54-55, Fig. 6.2, 6.3 6.4, 6.5, modified by SB).

Although their form varies, three distinctive forms are described in each criterion and scored from 0 to 2. Zero is assigned to specimens showing signs of fresh fractured bone, 1 to the specimens with mixed traits and 2 to specimens manifesting non-fresh/dry fragmentation. A more detailed description of the scoring criteria is shown in Table 6.1. The FFI score for each fragment (Fs) is calculated by summing the individual trait scores. The final FFI for the assemblage as a whole is the sum of the values of the individual fragments divided by the number of scored fragments (set score= (Fs1+Fs2+Fs3+…)/number of evaluated fragments) and ranges from 0 to 6. This equation considers each fragment equally independent of the size or length of the fracture surfaces. Lower average values (under 2) indicate fresh fracturing of the assemblage, and higher values (above 4) imply the opposite. An average FFI score of around 3 may be the result of a wider range of fragmentation activities and conditions. However, along with other indicators of fragmentation activity, it is possible to eliminate the rank of plausible explanations. The author emphasises that despite its efficiency in certain aspects (mostly

low time consumption), this index cannot be used separately to make an overall interpretation, and the consideration of other factors such as skeletal part abundance, their spatial distribution, presence of other taphonomic actors and their traces is essential for the final explanation of the assemblage fragmentation pattern (*Outram 2001*, 407).

In the individual experimental sets, the mean value obtained by *Outram's* method was complemented by other mean value calculations proposed by *Karr* and *Outram* (*2015*, 207-208), which emphasised various aspects of experimental sets such as the number of fragments or the length of fracture surfaces. The first method (Method A) measures the length of the fracture surface (Fl) and the FFI score (Fs) for each fragment. By their multiplication, the mean fragment value (Fv=Fl×Fs) is obtained. Dividing the sum of fragment values by the fracture length for the whole bone (Flwb), the mean bone value (Bv=Fv1 + Fv2 + Fv3…)/Flwb) is obtained. The score for the whole experimental set is then expressed as the sum of the bone values divided by the total number of bones in set (set score= (Bv1+Bv2+Bv3+…)/number of bones in the set). This method weights each bone equally, regardless of the differences in fracture length between individual bones. The second method (method B) provides one length-weighted average by summing the fragment values and dividing them by the total fracture length for all the fragments in the set (Flws). The set score is equal to (Fv1+Fv2+Fv3+…)/Flws. This method considers the total length of fracture surfaces in the experimental set. Therefore, fragments with a greater length of fracture surfaces weigh more on average than bones with a shorter length of fracture surfaces. If obtaining same or similar values by various methods outlined above, the methodological error can be excluded and it can be assumed that the result reflects the real changes in fracture morphology influenced by the environmental setting or bone preservation (*Karr – Outram 2015*, 207).

Score	Angle of fracture surface	Fracture surface texture	Fracture surface outline
0	no more than 10% perpendicular to bone surface	entirely smooth	mainly helical breaks
1	between 10% and 50% perpendicular to bone surface	some roughness present, but mainly smooth	mixture of outlines
2	more than 50% perpendicular to bone surface	mainly rough	absence of helical outlines

Table 6.1: Summary of scoring criteria for individual traits relevant in the FFI calculation (*Outram 2001*, 406; table by SB).

6.2.1 Sample treatment for FFI

No previous preparation or special treatment of samples in this thesis was needed for the FFI calculation (*Outram 1998*; *2001*). In the experimental material, all long bone fragments ≥4cm were evaluated and the average FFI was calculated for individual experimental sets. In the archaeological assemblage, mainly taxonomically identifiable long bones and fragments ≥2cm were assessed. Again, the average values for specific taxa and contexts were calculated and set into the context (for further information, see Chapter 7.1.4, 7.2.4 and 8.3).

6.3 Scanning electron microscopy (SEM)

Scanning electron microscopy has been intensively used for almost 50 years in the examination of different materials and artefacts in archaeology, and bones are no exception (*Shah – Rucsák – Palmquist 2019*, 1). The first archaeological papers using SEM date back to the late 1960s (*Brothwell 1969*; *Pilcher 1968*). By the late 1980s, its potential in addressing the archaeological issues was fully recognised (*Olsen 1988a*; *1988b*). Since then, it undergone significant technological development and advancement. The adoption of this microscopy technique in common analytical practice was significantly delayed in many fields, similarly to archaeology. However, today SEM technology is widely and commonly used (e.g. *Charlier et al. 2010*; *Bendrey 2011; Vergès – Morales 2014*; *Gonzáles Carretero – Wollstonecroft – Fuller 2017*; *Keenan – Egel 2017*; *Turco et al. 2017*; *Þórhallsdóttir et al. 2019*; *Bello – Galway-Witham 2019*; *Seetha – Velraj 2019*; *Boriová et al. 2020*). SEM allows detailed imaging in within significant magnification range (depending on the specific microscope from 5× up to 200,000×) and has an approximately 300 times greater depth of field when compared to visible light microscopy. It is not only surface topography but also compositional or structural information that can be obtained by this type of analysis (*Frahm 2014*, 6487; *Olsen 1988a*, 358; Fig. 6.2).

In SEM, information is acquired from the interaction of electrons, which are emitted by an electron gun in the microscope, with the surface of observed samples. The high-energy beam of electrons is directed by a system of coils/lenses and apertures. The samples of interest are placed in a vacuum to avoid the interaction of electrons with air molecules.
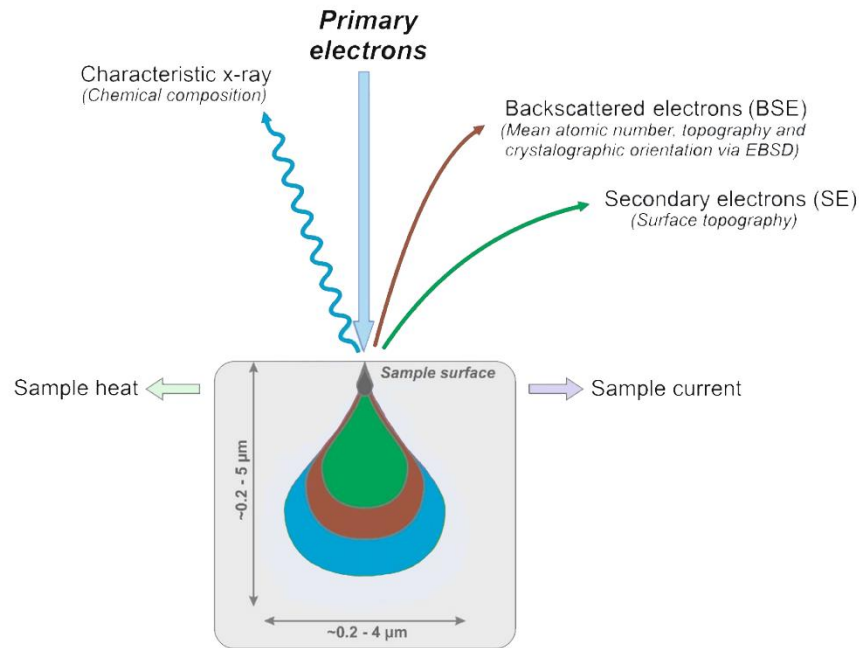
Fig. 6.2: Schematic description of signals analysed by SEM as described in the text. The volume of the sample in interaction for specific signals is illustrated in the colour coded droplet and the size depends on sample composition and accelerating voltage (*Specimen - electron-beam interaction*; modified by SB).

In case of organic samples, a thin layer of metal coating is used to secure the conductivity of the studied sample (*Ponting 2004*, 166). After the interaction of the electrons with the sample, a variety of signals for imaging or compositional analysis are produced. Imaging is secured by secondary (SEs) and backscattered electrons (BSEs). Secondary electrons are a result of inelastic interactions between the electron beam and the sample surface and provide a detailed high-resolution black and white image. This signal is the most suitable for imaging microstructure, textures, surfaces and their modifications. Backscattered electrons have higher energies than secondary electrons and are affected by the atomic number of the collided atom and come from the deeper layers of the sample. BSEs result from elastic collisions of electrons with atoms, which change the trajectory of the electrons. The image made by backscattered electrons distinguishes areas of different composition within the sample. The higher the contrast in atomic number, the higher the contrast reflected on the image although the differences in composition displayed by SEM are only relative (unlike in the EDX analysis, see below). This method is ideal for inorganic material analysis (metal, glass, pottery, etc.) and is widely used in the reconstruction of technologies, material composition and production processes in past societies. The compositional analysis (EDX) is provided by an x-ray signal originating from the excitation of atoms. The wavelength and energy of the x-ray

101

signal depend on the specific element from which they are emitted. The signal is measured by a spectrometer and displayed in the form of a histogram with different energy peaks for specific elements and is optionally supplemented by tables with individual values (*Ponting 2004*, 166-169; *Frahm 2014*, 6488; Fig. 6.3). I used the secondary electron imaging to observe the fracture surface in detail and see if any systematic differences in its morphology can be defined dependent on the state of bone preservation when fragmented.
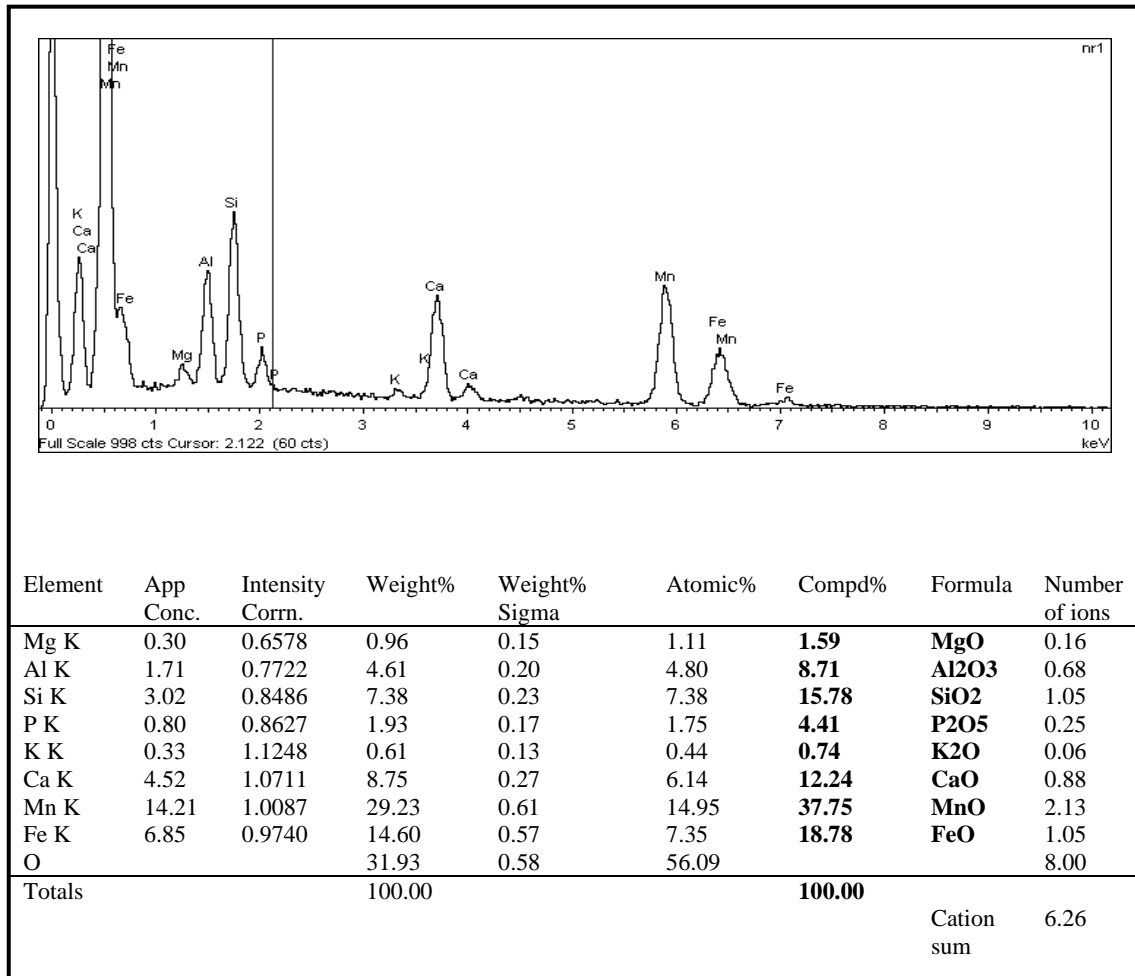
Element	App Conc.	Intensity Corrn.	Weight%	Weight% Sigma	Atomic%	Compd%	Formula	Number of ions
Mg K	0.30	0.6578	0.96	0.15	1.11	**1.59**	**MgO**	0.16
Al K	1.71	0.7722	4.61	0.20	4.80	**8.71**	**Al2O3**	0.68
Si K	3.02	0.8486	7.38	0.23	7.38	**15.78**	**SiO2**	1.05
P K	0.80	0.8627	1.93	0.17	1.75	**4.41**	**P2O5**	0.25
K K	0.33	1.1248	0.61	0.13	0.44	**0.74**	**K2O**	0.06
Ca K	4.52	1.0711	8.75	0.27	6.14	**12.24**	**CaO**	0.88
Mn K	14.21	1.0087	29.23	0.61	14.95	**37.75**	**MnO**	2.13
Fe K	6.85	0.9740	14.60	0.57	7.35	**18.78**	**FeO**	1.05
O			31.93	0.58	56.09			8.00
Totals			100.00			**100.00**		
							Cation sum	6.26

Fig. 6.3: Example of the EDX analysis result in the histogram (upper) and supplementary table (lower). Columns in bold correspond to the peaks in the histogram, showing the composition of bone coated with manganese-oxide concretions, example from the site Stránská skála IV (*Boriová et al. 2020*, 162, Fig. 6, modified by SB, measurement of composition by R. Škoda).

6.3.1 Sample treatment for SEM

Small fragments, approximately 1×1cm, were cut out of the fracture surface that reflected my interest (Fig. 6.4). The samples were cut out by using a Proxxon FBS 240/E hand precision drill/grinder with a diamond cutting disc. The same disc was used for all the samples with airflow and ethyl alcohol cleaning applied in between individual cutting sessions. Since the samples were not subjected to any kind of biomolecular analysis,

tracing of intersample contamination was irrelevant in this case. The fragments were properly marked to prevent confusion in further treatment and analytical processes and the system of marking is simple without coding (also described in corresponding tables summarising the samples e.g. Tab. 7.1; 7.4; 8.5). At this stage, the fragments went through an alcohol dehydration row (70%, 90%, 96% and 99.8% for 30 minutes in each).
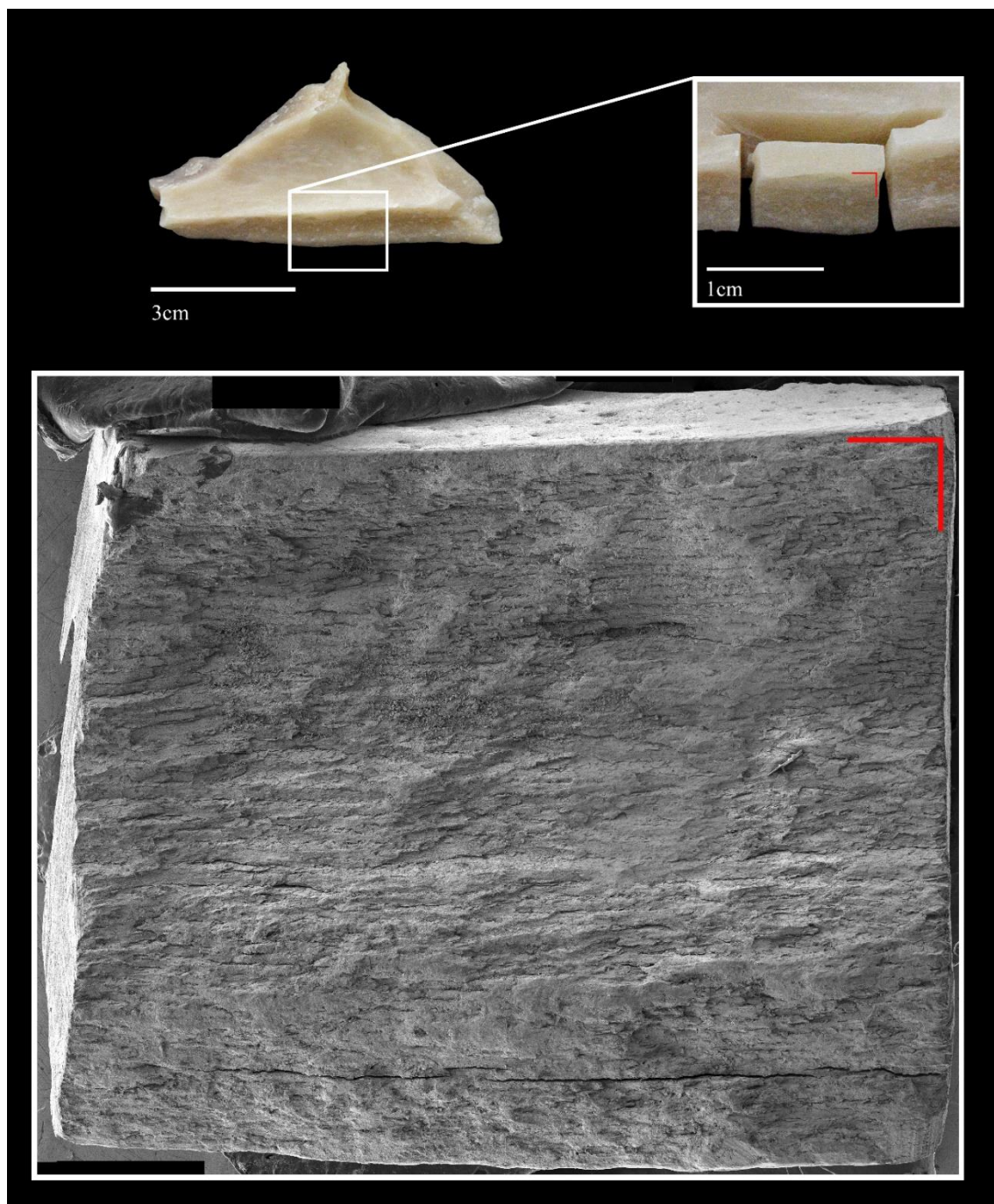
Fig. 6.4: Sample A. The image shows the original sampled fragment (upper left), with the specific area of sampling (upper right) and the final overview image of the sample surface from SEM (lower). The red corner marks the orientation of the sample. Magnification of overview image 35× (photo Z. Pokorná and SB).

The subsequent treatment, observation and documentation took place at the Institute of Scientific Instruments, The Czech Academy of Sciences. Before placement in the electron microscope, the samples were coated with chromium (a layer of 55nm) or chromium and gold (a layer of 20nm of both) by magnetron sputtering. I used JEOL JSM 6700F and MAGELLAN 400 scanning electron microscopes with an Everhart-Thornley detector at 5 keV. Overview images at 35-39× magnification (2.85-2.56 µm/px) were analysed and the detail of microcracks and surface irregularities were taken at higher magnifications (from 70× up to 6500×). Magnification in individual images always presents part of the scale bar in the image itself or is stated in the picture title (see Chapter 7.1.5, 7.2.5 and 8.3.2). The images illustrating all the observed and described morphological changes are always present in the respective chapters. The database/catalogue of all overview sample images is a rich source of data which will be subjected to further analysis and publication of the results. Therefore, this catalogue is not included in the thesis or the supplementary material although it is available upon request from the author of the thesis.

6.4 Histological thin sections (HTS)

Optical microscopy represents another much less expensive but in respects, limited (e.g. resolution abilities) way of observing different materials on the microlevel. There are different types of optical microscopic methods: a *stereomicroscope* allows one to observe objects and their details in magnifications up to 100× and uses mostly incident light reflected from the sample surface. However, some instruments can also use light transmitted by bulbs or mirrors underneath the observed object. The stereomicroscope is most suitable for observation of 3D objects, their details and surface topography. The resolution in these microscopes is inversely correlated with the depth of field and working distance, and therefore brings certain limitations when it comes to an overview examination of a whole sample or larger sample areas. Another type of microscopy is *light microscopy*, commonly referred to as optical microscopy. This is where a light transmitted through a system of lenses and the sample itself enables to observe magnification as high as 1000× with resolution limit of around 0.2 µm.

Different contrast imaging methods (e.g. dark field, polarised light, phase contrast, inferential contrasts and fluorescence) are available to serve the specific needs of sample observation or analysis. The overall resolution abilities are given by visible light

wavelength (380-700nm) and represent the main limitation of light microscopy. This is where electron microscopy allows us to go further in detail imaging and analysis (see Chapter 6.3). However, numerous advantages of light microscopy cannot be omitted. A large variety of samples can be examined and observed (whole, sectioned, live, dead, wet dry, moving, etc.) by various imaging techniques providing specific information about the structure, anatomy, composition and other features of the studied sample. The image can be observed live or captured by high-quality camera systems, which are described and analysed in special customised software. In comparison to others (e.g. electron microscopy), the microscopes and accessories are much less expensive and less demanding on working conditions (e.g. vacuum) and skills (*Evennett – Hammond 2005, 37-41*).

In archaeology and anthropology, different materials are observed by optical microscopy, and extensive interest is dedicated to hard animal and human tissues from various time periods. The preparation of a thin section enables to observe the inner microstructure of these tissues (bone, tooth, antler, ivory) and traces after the processes that affect them in transmitted light. Analytical methods are numerous and are represented by metric and non-metric/qualitative approaches, most of which originated for forensic purposes but show great potential in addressing archaeological issues. As just some of many, I can mention methods for human/animal bone separation (e.g. *Rämsch – Zerndt 1963*; *Cattaneo et al. 1999*; *2009*; *Mulhern – Ubelaker 2001*; *2012*; *Urbanová – Novotný 2005*; *Cummaudo et al. 2019*), species determination (e.g. *Hidaka et al. 1998*; *Martiniaková et al. 2006*; *2007*; *Sawada et al. 2010*; *2014*; *Padian – Lamm 2013*; *Zhang et al. 2018*), age at death or age-related changes in structure, sex or inter-individual recognition (e.g. *Bouvier – Ubelaker 1977*; *Eriksen 1991*; *Thomas et al. 2000*; *Crowder – Stout eds. 2012*), seasonality (e.g. *Smith – Reid – Sirianni 2006*; *Nývltová-Fišáková 2007*; *2013*; *Dean 2017*), unspecific stress events (e.g. *Dirks et al. 2002*; *Hupková et al. 2016*; *Lorentz et al. 2019*), pathological changes (*Bancroft – Stevens – Turner 1996*) and in my case, most importantly taphonomical changes and processes (e.g. *Jans et al. 2002*; *Turner-Walker – Jans 2008*; *Hollund et al. 2011*; *Hollund – Blank – Sjogren 2018*; *Bell 2012*; *Huisman et al. 2017*; *Brönnimann et al. 2018*). This method proved to be a useful tool, when addressing taphonomical issues. Different studies focused their attention, for example, on the microstructure of burnt bones and were able to describe systematic changes in this and their relation to well-known and widely used macroscopic methods

of study (*Hanson – Cain 2007*; *Végh et al. 2021*). Another example is biodegradation and microbial attack on hard tissues as an indicator for post-depositional in situ environment and burial conditions (*Jans 2005*; *Hollund et al. 2012*; *2015*; *Caruso et al. 2020*; *Lemmers et al. 2020*), which has been a major subject of interest in taphonomic studies in recent years. A more extensive literature review concerning the use of histological methods addressing archaeological and anthropological issues can be found, for example, in the monography by *Crowder* and *Stout eds. (2012)* and a recent article focused on the histology of Upper Paleolithic osteological material by *Sázelová, Boriová* and *Šáliová (2021)*.

Microcracking is also one of the observed aspects and according to its range, course and interaction with basic tissue building microstructures can be characteristic for different types of taphonomic origin (e.g. *Ritchie et al. 2005*; *Hanson – Cain 2007*). Since every fracture begins as a microfracture and then spreads further, I assumed that some specific markers in microfracture emergence and course could be identified. The differences might be dependent on the state of bone preservation, or the type of force applied to the bone element in the fragmentation process.

6.4.1 Sample treatment for HTS

The samples which underwent SEM analysis were further used for histological thin section preparation. This analytical protocol ensured that I observe the same part of the surface scanned by electron microscopy (Fig. 6.5). The preparation process followed the standard steps and rules (e.g. *Sázelová – Boriová – Šáliová 2021*). Only a slight difference was made in the initial steps as the samples were already dehydrated before SEM, this phase could be omitted in the preparation treatment. Dry and dehydrated samples were embedded in two-component epoxy resin (Araldite 2020) and placed in a vacuum to ensure good penetration of the samples (vacuum pump: CitoVac, Struers). After hardening, they were cut perpendicular to the fracture surface by a saw machine with a diamond plate (Accutom 100, Struers), ground and polished by hand on grinding papers and polishing cloths (roughness 500-4000 #FEPA). The sample was then mounted on the slide-glass, cut for the second time, and again ground and polished to the final thickness between 49-118 µm measured with a digital micrometre (Mitutoyo, High Accuracy digital micrometre). The final thickness is always adapted to optimise the visibility and definiteness of the observed traces on the one hand and to preserve the major

or most important part of the thin section on the other. The thickness of individual sections is always stated where necessary (in the appropriate chapter/image/image capture). The final sections were not covered with glass, in the case of further thinning or if an additional analysis was needed or performed. The prepared sections were observed and documented by a Leica DM2500 LED optical microscope with a Leica DMC 6200 microscope camera. The samples were observed in both transmitted and polarised light. The propagation of microcracking in relation to actual internal bone microanatomy and its influence on fracture surface morphology was studied at the level of osteons and interstitial matrix at the most used overall magnification of $50\times$ (resolution 1.17 µm/1px). The details were studied and captured mainly at $100\times$ (resolution 0.59 µm/1px) and $200\times$ (resolution 0.29 µm/1px) overall magnification. The images were captured in the Leica LAS X software and then edited in Adobe Photoshop CS4. The images illustrating all the observed and described morphological changes are always present in the respective chapters. The database/catalogue of all fracture surface profile images, similar to the data collected by SEM, represents a data source which will be subjected to further analysis and publication of the results. Therefore, this catalogue is not directly included in the thesis nor its supplementary material although it is available upon request from the author of the thesis.
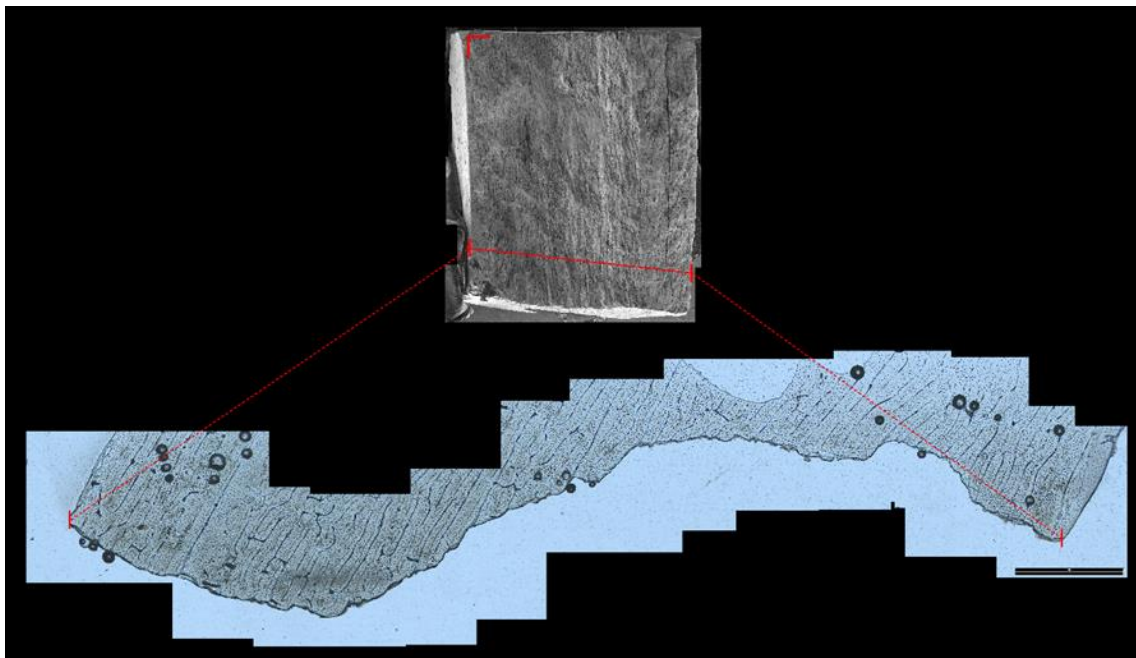
Fig. 6.5: Sample A. The image shows position of the cutting plane on sample observed under SEM (upper image; red line), and orientation of the profile of the same sample observed in HTS (lower image) indicated by red dashed lines. Magnification of upper image $35\times$; magnification of lower image $50\times$, scale bar 1000 µm (photo SB and Z. Pokorná).

7. Experiments and experimental results

Experimentally fragmented bones used to verify the chosen analytical and imaging methods originate from two different experiments. These are represented by an experiment conducted by colleagues from the University of Exeter, modelling unintentional geological/environmental activity (rockfall) and an experiment performed at the Centre for Paleolithic and Paleoanthropology, Institute of Archaeology, Brno (IAB) imitating intentional human activity (hammer stone and anvil) designed for the purpose of this thesis. The experiment at IAB followed up on the results and conclusions observed in the rockfall experiment material. The rockfall experiment presents the result of dynamic force acting, however, of a different nature than human. Therefore, I decided to directly engage human acting force and simulate intentional human fragmentation in my own experiment. The three basic states of preservation (fresh, dry and frozen) were given by the rockfall experiment material, where the differences between them could be observed. A description of these differences might be important when looking for the effector responsible for specific fracture patterns/traits. To see if other forms of dynamic impact (deliberate human activity) influence the fragmentation differently in the same state of preservation, I decided to compare the sets of bones fragmented in the fresh state. Bones as a source of food/nutrients/raw material were most probably exploited fresh (fresh and edible nutrients/fats, the best chipping behaviour), so I decided to further study this kind of preservation. The impact of the presence or absence of periosteum was previously demonstrated in rockfall experiments in the aspects of accelerated moisture loss and thus more severe effect of environmental conditions on the fragmentation pattern (*Karr 2012*, 131). Other experimental studies also refer to the relevance of the presence of periosteum due to the moderate cushion it may provide and the significantly higher slippage of the bone surface in the fragmentation process (e.g. *Pickering – Egeland 2006*, 467; *Blasco et al. 2014*, 1086). The most visible differences in periosted and de-periosted bones were observed in altered bone states although in fresh bones the FFI showed the reverse effect. The values were higher for bone without periosteum. The presence of periosteum on bone during fragmentation provides a small cushion to the force applied although a more significant effect is in holding the bone together in one piece after the initial blows, thus requiring more blows for actual fragmentation of the bone and a longer time to open the marrow cavity. The initial blows can introduce first cracking or microcracking, which potentially could be followed by other blows, and influence how

differently the force travels or spreads out through the bone. To examine this assumption, the experimental set was divided into two parts: one with periosteum present on bone, and the second with periosteum missing.

Summing up the introduction into the background behind the experimental designs and their relation, the main aims of experimental material analysis were as follows: **a)** to test the hypothesis that the traces caused by fragmentation on the resulting fracture surface are influenced by the state of bone preservation, and are distinctive at the micro level, **b)** to observe whether the different types of dynamic loading leave behind different microscopically identifiable marks on bone fracture surfaces or microcracking, **c)** to test the hypothesis that the presence of periosteum has an impact on fracture surface morphology and bone microcracking patterns, and **d)** to study the differences in general macroscopic fracture morphology, the number of resulting fragments and the incidence of percussion marks in bones fragmented with and without periosteum. These points were tested and studied with respect to the application of the results obtained on archaeozoological material from the Pavlov I site. A more detailed description of both experiments can be found in the following chapters (7.1 and 7.2).

7.1 Experimental assemblage from the rock-fall experiment (University of Exeter)

This experiment was designed and conducted at the University of Exeter (United Kingdom) by L. Karr and A. Outram in 2010. The experiment aimed to test rockfall as a taphonomic factor forming bone fragments/pseudo-flakes similar to cultural bone modification. For my purposes, fragments resulting from these experiments were revised for the FFI calculation, the qualitative description of fragmentation traces, and a selection of samples for testing the chosen detailed microscopic analytic methods. A possible comparison of results between intentional and unintentional dynamic force acting may be observed, simultaneously a wider range of bone preservation states such as freezing and drying of bones was provided to enlarge the dataset collected from my own experiment (Chapter 7.2.). The basic information concerning material, environmental and experimental setting necessary for this thesis are summarised in the following chapters (Chapter 7.1.1 to 7.1.3). For more detailed information and original results of this experiment, see the work of *Karr* (*2012*) and *Karr – Outram* (*2012a*; *2012b*; *2015*).

7.1.1 Material

Long limb bones (*humerus*, *radio-ulna*, *femur*, and *tibia*; left and right elements) of domestic cattle (*Bos taurus*) obtained from local butchers (from Exeter, UK) were used for this experiment. The age of the individuals varied from 18 to 36 months. All the bones used were refrigerated immediately after the death of the animal for two weeks while still retaining the meat. The soft tissues removal took place before the fragmentation in the case of fresh bones. For the frozen and dried bones, the removal took place before the alteration of the bone state began (*Karr 2012*, 205).

7.1.2 Environmental setting

The bones were modified to six different stages of preservation. These included: a) fresh bones cleaned from soft tissues, b) fresh bones with the periosteum and some soft tissues intact, c) bones frozen bones at -20°C for 15 days cleaned from soft tissues, d) bones frozen at -20°C for 15 days with the periosteum and soft tissues intact, e) bones dried at 20°C for 40 hours cleaned from soft tissues and f) bones dried at 20°C for 20 days with the periosteum and some soft tissues intact. These were designed to reflect a greater variety of possible environmental conditions and states of bone preservation (*Karr 2012*, 205-207).

7.1.3 Experimental procedure

For each state of preservation, eight complete bones were placed in an area paved with asphalt. The rocks of different sizes (13-37 cm) and weights (2-12 kg) were then released individually from a height of 2.75 m onto the pile of bones. In total, 150 rock-falls were carried out, and since the material tended to drift away from the impact area, it was randomly relocated a few times during the experiment to the centre of the impact area. Tarpaulin and an adjacent wall were used to secure the highest possible recovery of the fragments originating from the experiment (Fig. 7.1). After collection of the fragmented osteological material, the larger fragments and epiphyses were cleaned from the remaining tissues and fat by boiling in a sodium hydroxide solution (NaOH). They were then left to dry along with the rest of the recovered material before further analysis (*Karr 2012*, 208-211).

Fig. 7.1: Photographic documentation from the rock-fall experiment in progress capturing the place and setting of the action (*Karr 2012*, 211, Fig. 7.4).

7.1.4 Macroscopic observation

In this section, the results are reported according to the above-described six different states of preservation (see Chapter 7.1.2). The FFI score calculation method was used according to the collected data with over 990 bone fragments observed and evaluated. The methods calculating with the length of the fracture surfaces were omitted because of the unavailability of this variable. The final numbers of the resulting analysed fragments may differ from those reported in *Karr* (*2012,* 211-237). This discrepancy may be caused by the manipulation of experimental material for different educational purposes (workshops or lectures) in the time between the experiment and my analysis (9 years). All the available material assignable to individual experimental settings with specific conditions stored at the University of Exeter was subjected to observation (Fig. 7.2). The FFI values and measurements of the individual fragments analysed can be found in the supplementary material (Supplement 1-6). The proportional representation of the FFI values in individual states of preservation is summarised in Graph 1. In most cases, the assignment of the described fragments to a specific skeletal part was not possible since the groups of bones were fragmented and further stored together.

Fig. 7.2: Nature of the analysed material from the rockfall experiment. The material in the picture represents diaphysis fragments from one experimental run for one of the six settings: in this picture, specifically frozen bones without soft tissues. Larger fragments showing predominant fracture morphology, smaller fragments mainly under 4 cm accumulated in the upper left corner (photo SB).

7.1.4.1 Fresh bones cleaned from soft tissues

Together 16 long bones (5 *femora*, 5 *tibiae*, 3 *humeri*, 3 *radio-ulnae*) were fragmented in two experimental runs with the same setting and state of preservation. For the fracture freshness index, altogether 150 diaphysis fragments ≥ 4 cm were evaluated (Supplement 1). The mean FFI value for both experimental runs is **3.2**, and the most represented value (modus) of the index is **2**.

7.1.4.2 Fresh bones with the periosteum and some soft tissues intact

Again, 16 long bones (6 *femora*, 6 *tibiae*, 2 *humeri*, 2 *radio-ulnae*) were fragmented by rockfall in two experimental runs in an identical setting and state of preservation. The periosteum and a small amount of soft tissue were left intact on the bones during the experiment. The mean FFI was calculated for 150 diaphysis fragments ≥ 4 cm (Supplement 2). The mean FFI value is **2.5**, and the modus value is **2**.

7.1.4.3 Bones frozen at -20 °C for 15 days cleaned from soft tissues

Altogether, 16 long bones (4 *femora*, 5 *tibiae*, 3 *humeri*, 4 *radio-ulnae*) were fragmented in two experimental runs. The bones were subjected to fragmentation in the frozen state, and the soft tissues were removed prior to the freezing cycle. In total, 126 diaphysis fragments ≥ 4 cm were evaluated for the FFI calculation (Supplement 3). The mean value is **3.8**, and the modus value is **4**.

7.1.4.4 Bones frozen at -20°C for 15 days with the periosteum and soft tissues intact

In this setting, 16 long bones (5 *femora*, 5 *tibiae*, 3 *humeri*, 3 *radio-ulnae*) were fragmented by rockfall in two experimental runs. The identical setting and state of preservation were ensured in both runs. The bones were removed from the freezer immediately before the experiment. In total, 139 diaphysis fragments ≥.4 cm were evaluated (Supplement 4). The mean FFI value is **1.7**, and the modus value is **1**.

7.1.4.5 Bones dried at 20 °C for 40 hours cleaned from soft tissues

Again, 16 long bones (6 *femora*, 6 *tibiae*, 2 *humeri*, 2 *radio-ulnae*) were fragmented by rockfall in two experimental runs in an identical setting and state of preservation. The periosteum and a small amount of soft tissue were left intact on the bones during the experiment. The mean FFI was calculated for 219 diaphysis fragments ≥ 4 cm (Supplement 5). The mean FFI value is **4.4**, and the modus value is **6**.

7.1.4.6 Bones dried at 20 °C for 20 days with the periosteum and some soft tissues intact

Together, 16 long bones (8 *femora*, 6 *tibiae*, 1 *humerus*, 1 *radio-ulnae*) were fragmented in two experimental runs in the same setting and preservation state. For the fracture freshness index, altogether 207 diaphysis fragments ≥ 4 cm were evaluated (Supplement 6). The mean FFI value for both experimental runs is **3.9**, and the modus value is **4**.
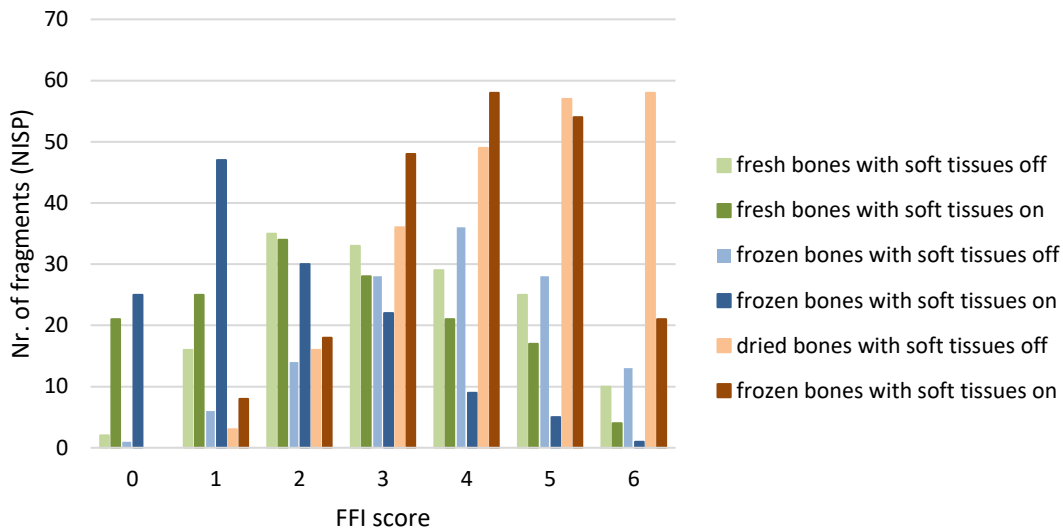
Graph 7.1: Proportion of FFI scores in individual preservation groups. The lower score is abundant in fresh and frozen samples, whereas higher scores can be observed in the dried bones. Some influence of periosteum presence is visible although the observed differences are ambivalent (author SB).

7.1.5 SEM analysis

For a description of the differences, I focus only on the individual states of bone preservation. Each state of preservation is represented by 4 samples. These combine imaging of longitudinal and helical fracture surface (FS) images in the case of fresh and frozen bones and longitudinal and transverse FS in dried bones (Tab. 7.1). As mentioned above, since the bones were fragmented in mixed groups (see Chapter 7.1.4.1 - 7.1.4.6), the assignment to the skeletal element was not possible. The influence of the presence of soft tissues/periosteum was not referred to due to the low number of samples for each state of preservation and type of fracture. This variable was observed in greater detail in the following experiments (Chapter 7.2). A summary of the main features observed by electron microscopy can be found in Tab. 7.2 at page 128.

Sample	State of preservation	Fracture surface (FS)	Histological section thickness
A	dried with tissues on	longitudinal	50 μm
B	fresh with tissues on	longitudinal	64 μm
C	frozen with tissues off	longitudinal	64 μm
D	frozen with tissues on	longitudinal	60 μm
E	frozen with tissues on	spiral	68 μm
F	dried with tissues on	transversal/oblique	69 μm
G	dried with tissues off	longitudinal	59 μm
J	dried with tissues off	transversal	98 μm
K	fresh with tissues on	spiral	80 μm
L	fresh with tissues off	longitudinal	66 μm
M	frozen with tissues off	spiral	50 μm
N	fresh with tissues off	spiral	75 μm

Tab. 7.1: List of samples from the rockfall experiment subjected to SEM and histological treatment and analysis. Designation of the sample (simple without coding), state of preservation, type of observed fracture surface and thickness of the section are listed. The presence of soft tissues is stated although it was not considered in the evaluation (author SB).

7.1.5.1 Fresh bones

The observation under SEM allowed the description of several surface characteristics and features occurring in fresh samples. The surface of the samples has a uniform character in both types of FS. The surface is smooth and has no massive morphological irregularities. This smooth surface is also characteristic of the linear patterning occurring in all samples for the major part of the surface. This linear pattern is most probably given by the microstructure of the underlying bone. A slightly more expressed surface morphology was partially observed in sample B. In samples from longitudinal FS (samples B and L), small singular areas with granular character were present. In samples from helical FS, a fan-shaped pattern was described. This is characteristic of not corresponding with the underlying bone microstructure and arcuate ridges. In sample K, this pattern is highly pronounced (Fig. 7.3) although in sample N, only moderate indications of this pattern in a small area are apparent. A significant plate-like formation was present in sample N (helical FS), and to a much lesser extent it was also identified in sample K (Fig. 7.4). This type of laminar breakage was not observed in samples from longitudinal FS.

Microcracking was present in all the samples analysed. Except for laminar plate-shaped protrusions, the cracks generally respected the lamellar microstructure of bone (Fig. 7.5). These usually occurred along the osteons, cutting the wall of the Haversian canal (Fig. 7.6) with a possible bifurcation at the end. Cracking varies from tiny cracks to longer and wider cracks. The edges of the cracks are more or less smooth, without

significant fibrillary projections or granularities (Fig. 7.5). In general, more pronounced microcracking was observed in longitudinal FS.
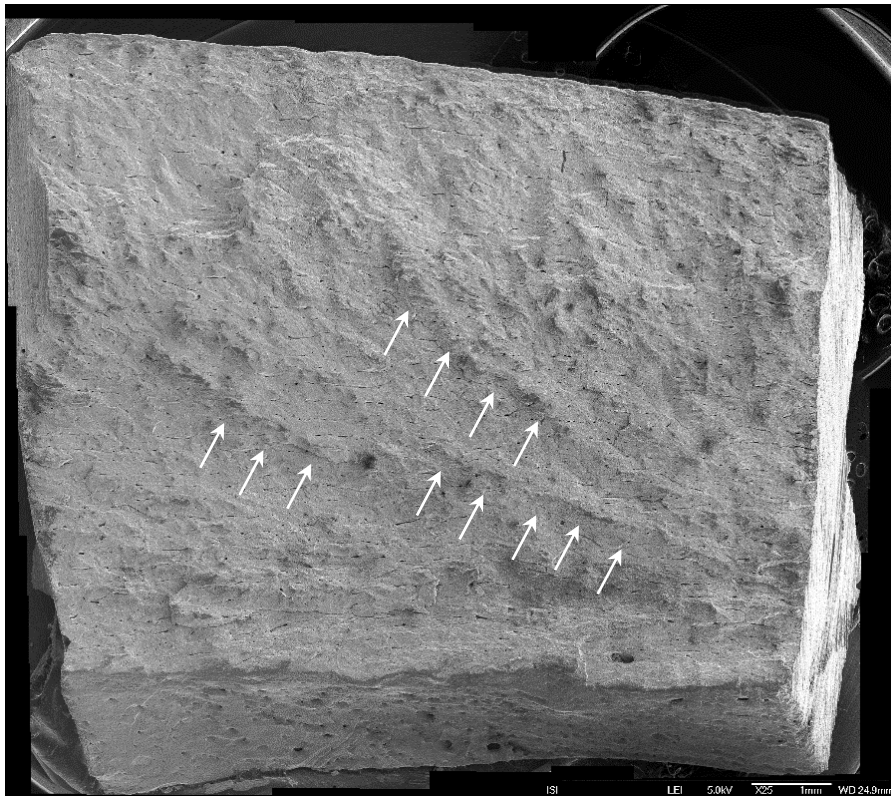
Fig. 7.3: Sample K. Freshly fragmented bone, helical FS showing a fan shaped pattern (white arrows). Magnification 25×, scale bar 1 mm (photo Z. Pokorná and SB).
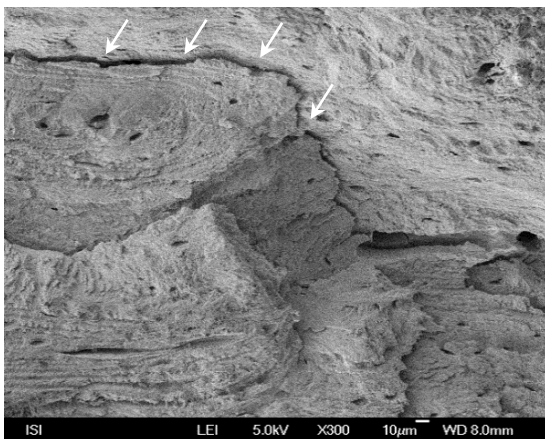
Fig. 7.4: Sample K. Crack lining the plate-like protrusion (white arrows). The laminar structure of the bone is visible. Magnification 300×, scale bar 10 μm (photo SB).
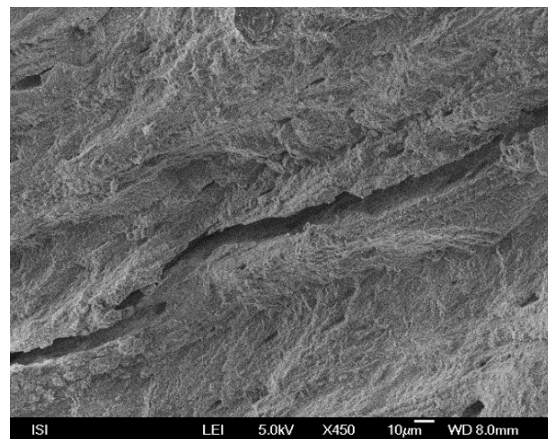
Fig. 7.5: Sample N. Microfracture respecting the longitudinal lamellar bone structure. The edges are smooth. Magnification 450×, scale bar 10 μm (photo SB).
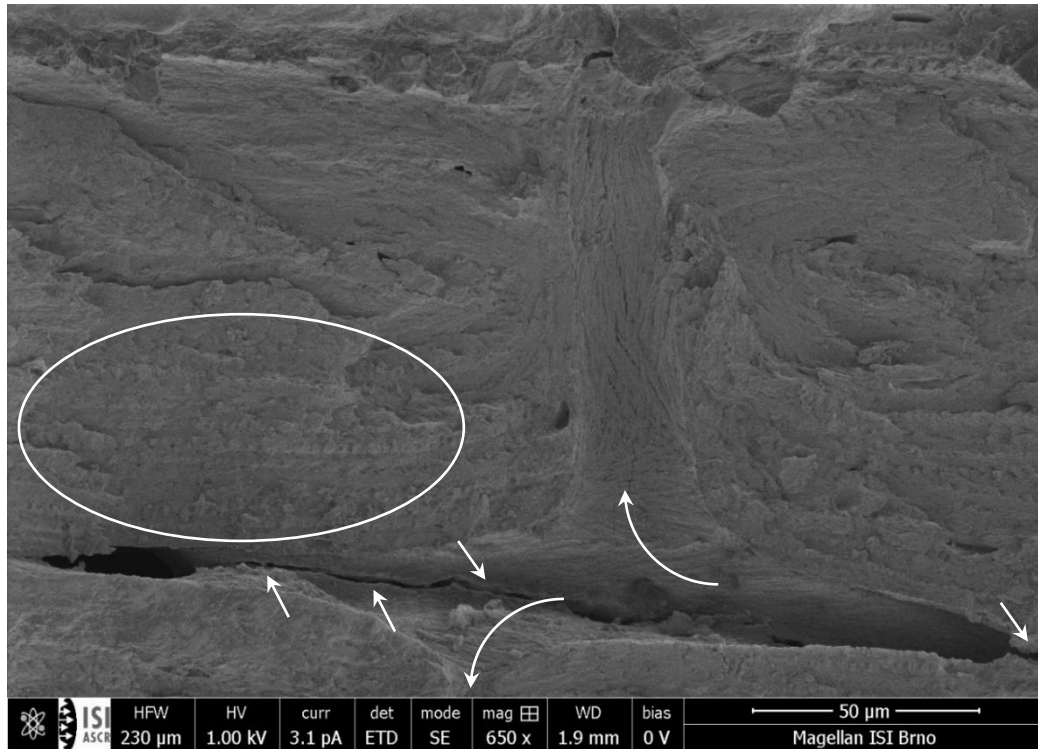
Fig. 7.6: Sample B. Microcrack cutting the wall of Haversian canal (white straight arrows); the lamellar structure of bone is visible (white circle). The Volkmann canals connecting individual osteons present on the cross-section (white angled arrows). Magnification 650×, scale bar 50 μm (photo SB).

7.1.5.2 Frozen bones

Very similar morphology to the fresh samples was observed in the samples from the frozen bones. In general, the surface of the samples was smooth; only sample E showed a more pronounced morphology. Considering the surface pattern, the longitudinal FS showed typically linear or columnar patterning (Fig. 7.7) respecting the microstructural bone characteristics. In helical FS, this trend was also observed but not uniformly spread throughout the whole observed surface as previously. The fan-shaped pattern on FS was observed in sample E (Fig. 7.8), representing a helical fracture although in sample M only very mild signs of this pattern were identified (also helical FS). On the contrary, in sample D, another pattern was present that did not respect the bone microstructure. This is strongly reminiscent of the fan-shaped pattern more typically observed in helical fractures although the ridges are much less pronounced and have a more diagonal course (Fig. 7.7). Plate-like protrusions organised transversally to the longitudinal patterning were rare and only on a small part of sample E (Fig. 7.8); similarly, the granularity of the surface was only present in sample D. Three types of microcracking were observed and described. The first was cracking that respected the laminar structure of the bone with longitudinal course and was mainly present on the

osteon walls connecting the individual Haversian canals (Fig. 7.9). The second type was lining the plate-like protrusion in sample E. The third type of cracking was irregular and reticulate, obviously not respecting the underlying bone microstructure (Fig. 7.10).
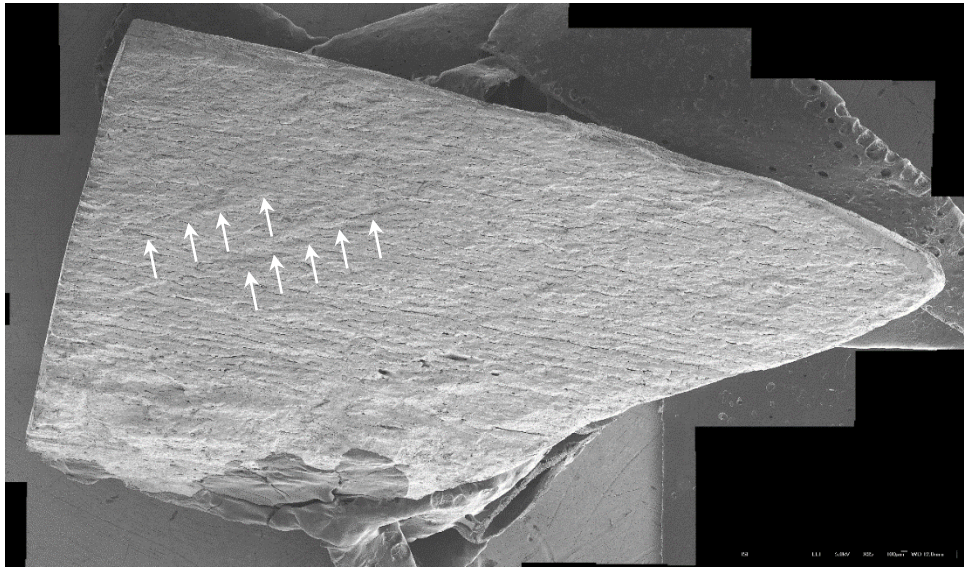
Fig. 7.7: Sample D. Linear pattern typically observed in longitudinal FS in both the fresh and frozen samples. Diagonal ridges indicated by white arrows. Magnification 35×, scale bar 100 μm (photo Z. Pokorná and SB).
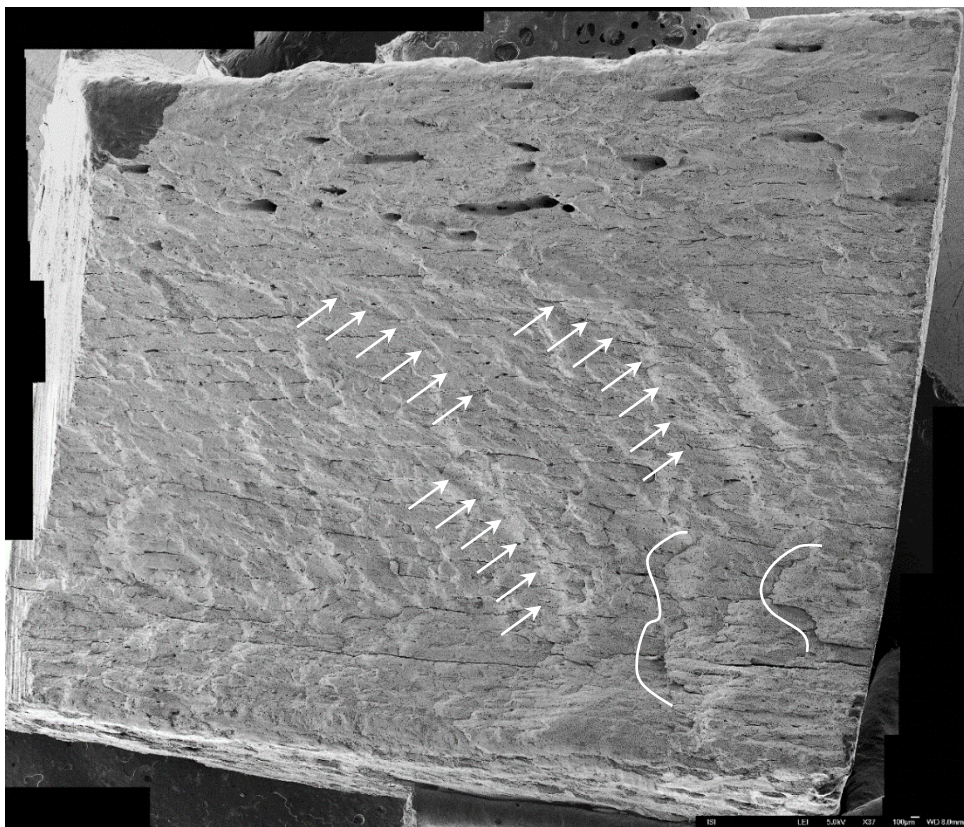
Fig. 7.8: Sample E. Fan-shaped ridges mainly observed in helical fracture types indicated by white arrows; plate-like protrusions underlined by white lines. Magnification 35×, scale bar 100 μm (photo Z. Pokorná and SB).
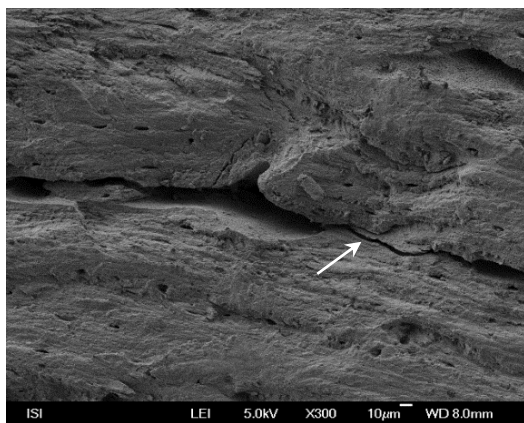
Fig. 7.9: Sample D. Longitudinal cracking (white arrow) related to the course of osteons and Haversian canals respecting the lamellar structure. Magnification 300×, scale bar 10 µm (photo SB).
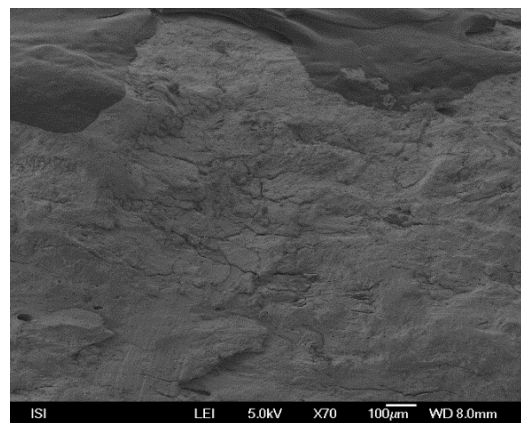
Fig. 7.10: Sample D. Third type of microcracking observed in frozen the samples. The irregular course probably not related to the bone microstructure. Magnification 70×, scale bar 100 µm (photo SB).

7.1.5.3 Dried bones

Again, various surface characteristics and features occurring in dried samples were identified. The character of the observed surface was generally rough with granular areas (Fig. 7.11). These granular areas were more abundant in the longitudinal samples (A and G) than in the transversal samples (G and J). The patterning of the surface was dependent on the type of FS. In the longitudinal samples, linear patterning of the surface was present, most probably due to the osteonal or laminar arrangement (Fig. 7.12). However, in the transversal fractures, the surface is highly irregular and does not appear to respect the underlying microstructure. Moreover, in the longitudinal FS, transversal ridges creating a stepped character were identified. Laminar breakage was present in samples F and G, forming plate-shaped protrusions (Fig. 7.13). Microcracking was observed in all four samples. In the longitudinal FS, the cracks run along the longitudinal course of patterning, whereas in the transversal FS they tend to line the surface irregularities (Fig. 7.14). The range of microfractures varies significantly, from wide cracks running almost through the whole sample (Fig. 7.12) to fine and short microcracking spreading in numerous directions in a cobweb-like manner. Their course in relation to the microstructure is also ambivalent. This variance may be due to the different origins of the cracking (fragmentation process vs. drying/weathering of the specimen).
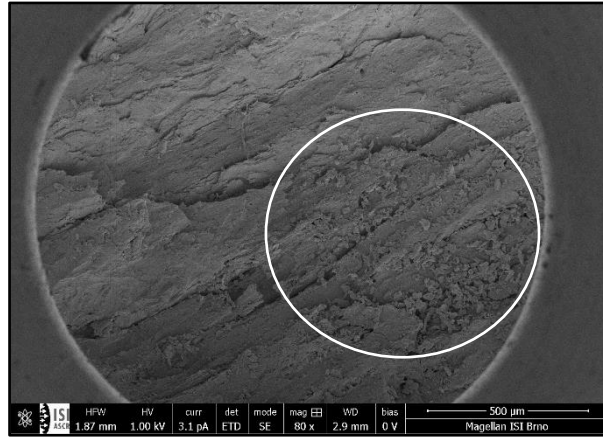
Fig. 7.11: Sample A. Closer caption of granular area (white circle). Magnification 80×, scale bar 500 μm (photo SB).
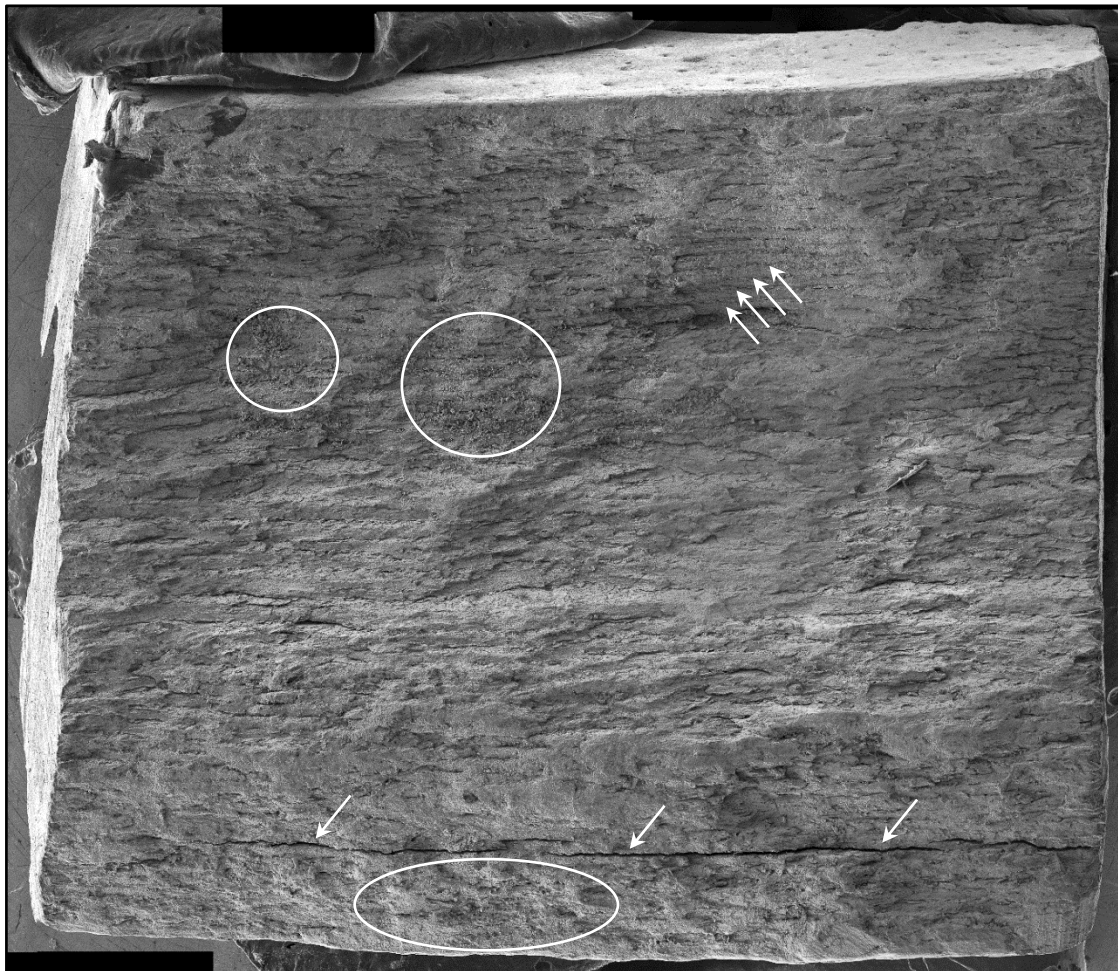
Fig. 7.12: Sample A. Overview image of longitudinal FS in bone dried for 20 days with soft tissues present. Despite the rough surface, the linear patterning typical for longitudinal FS is visible (white arrows in the upper part of the picture). Multiple granular areas are present (white circles and oval). Large linear crack, most probably resulting from additional drying/weathering process (white arrows in lower part of picture). Magnification 35× (photo Z. Pokorná and SB).
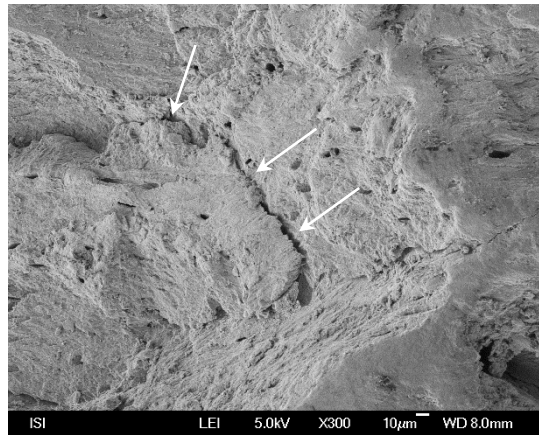
Fig. 7.13: Sample F. Closer caption of plate-shaped protrusion (white arrows). Magnification 300×, scale bar 10 µm (photo SB).
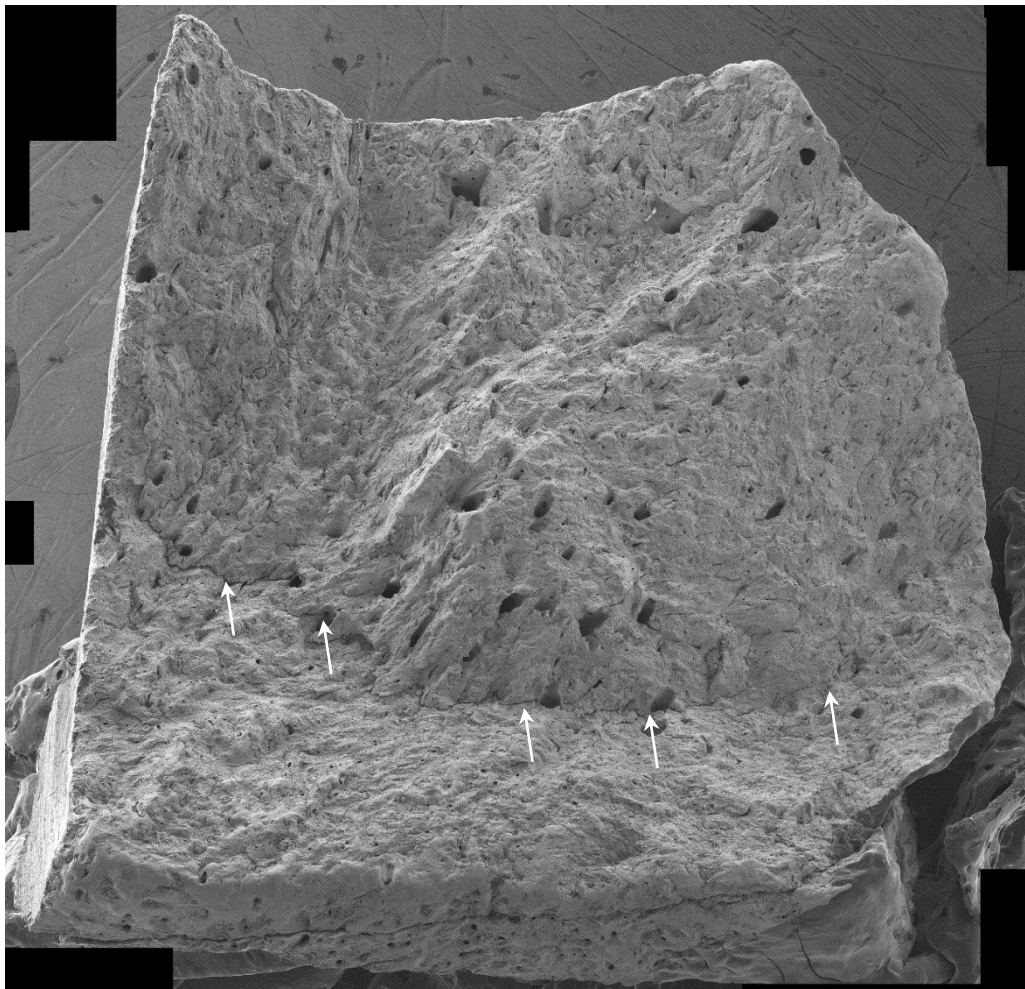
Fig. 7.14: Sample J. Overview image of transversal FS in bone dried for 40 hours without soft tissues. Irregular and significantly rough surface visible. Microcracking lining the surface irregularities indicated by white arrows. Magnification 35× (photo Z. Pokorná and SB).

7.1.6. HTS analysis

The samples analysed by SEM were subsequently used to prepare the histological thin sections. In all the samples, the cutting plane was perpendicular to the FS so I could observe possible microcracking penetrating under the FS, or how deep it penetrated when lining the surface irregularities. Moreover, it allowed me to observe the morphology of the fracture surface profile and its interaction with bone microanatomy in detail. Transmitted and polarised light techniques were used. The final thicknesses of the sections are stated in Table 9. The summary of the main features observed on histological thin sections can be found again in Tab. 7.2 at page 128.

7.1.6.1 Fresh bones

In samples from the longitudinal FS, I observed a generally uniform surface profile, with minimum significant elevations or depressions (Fig. 7.15). The surface irregularities were only mild. Deflection of the fracture front was observed mainly by longitudinal lamellae or encountering the Haversian canal (Fig. 7.16) although deflection by osteons was not observed. In contrast, when interacting with the osteon, the cracking always went right through (Fig. 7.17). Microcracking was present in two forms. Fractures lining the surface irregularities, penetrating into a variable distance (Fig. 7.18), and thin and short microfractures perpendicular to FS (Fig. 7.19).

In the helical FS, the line of the profile was generally uniform with no significant stepping. Only individual sections were more shaped (Fig. 7.20). No deflection of the fracture front was observed by the basic structural units. The microcracking appeared under the surface irregularities, starting at one side of the irregularity but not reaching the other, similar to samples from the longitudinal FS. Alternatively, the fractures emerged in surface depressions and took an almost parallel course to FS. In the latter case, the cracks were almost all directed in the same way (Fig. 7.21). A few cracks perpendicular to the FS were also observed (sample N).
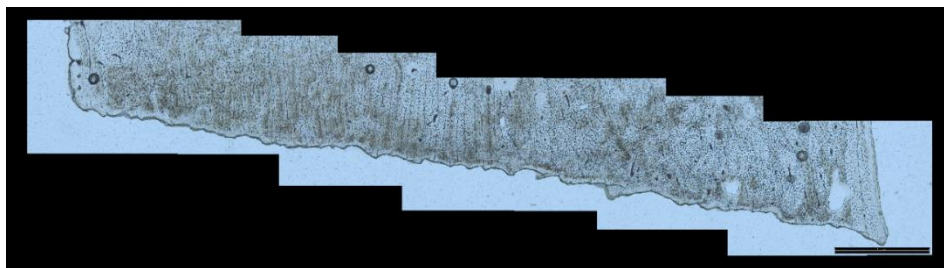
Fig. 7.15: Sample B. Profile of the longitudinal fracture surface in a freshly fragmented sample. Magnification 50×, scale bar 1000 μm (photo SB).
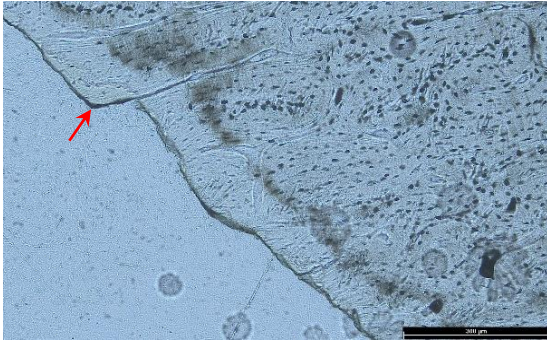
Fig. 7.16: Sample L. Deflection of the fracture by longitudinally arranged lamellae (red arrow); in this case, facilitated by the Haversian canal. Magnification 100×, scale bar 300 µm (photo SB).
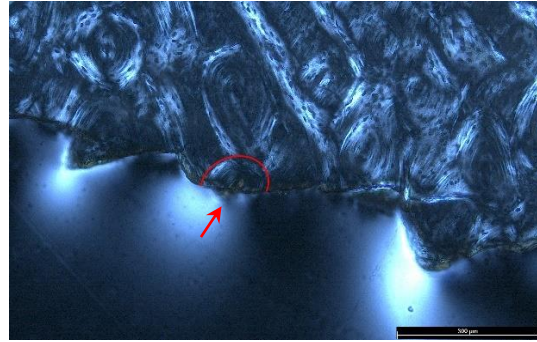
Fig. 7.17: Sample B. Fracture cutting right through the osteon (red arrow); the osteon is outlined by the red line. Magnification 100×, scale bar 300 µm, polarised light (photo SB).

Fig. 7.18: Sample B. Microcrack penetrating under the surface irregularity indicated by red arrows. Magnification 100×, scale bar 300 µm (photo SB).
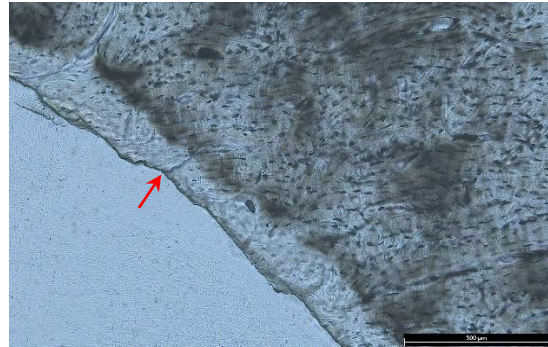
Fig. 7.19: Sample B. Thin and short microcrack perpendicular to the fracture surface indicated by the red arrow. Magnification 100×, scale bar 300 µm (photo SB).
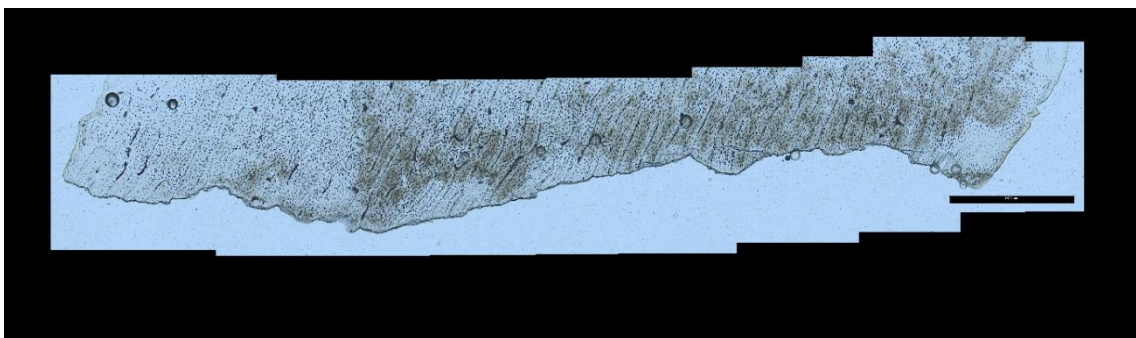
Fig. 7.20: Sample K. Profile of the helical fracture surface in a freshly fragmented sample. Magnification 50×, scale bar 1000 µm (photo SB).

123
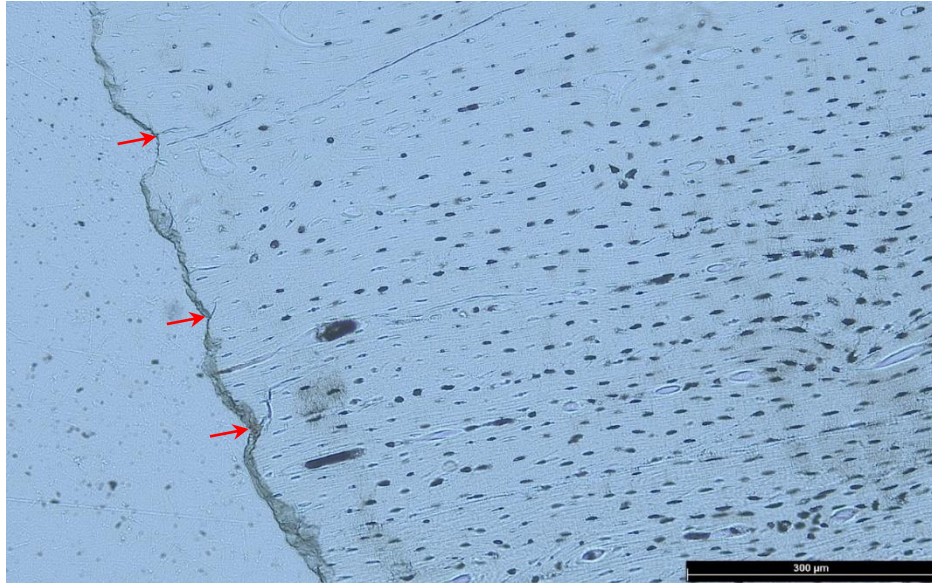
Fig. 7.21: Sample N. The red arrows indicate three depressions in FS. The microcracking starts from all of them and takes a diagonal/oblique course in the same way to the top of the picture. In the case of the uppermost depression, two very thin fractures emerge: one follows the same course as the others, the second runs perpendicular to FS. Magnification 100×, scale bar 300 μm (photo SB).

7.1.6.2 Frozen bones

Longitudinal FS samples generally showed a quite smooth surface. In sample D, the smoothness was not continuous throughout the whole sample. Concerning sample C, in one part of the surface, I observed significant protrusions (Fig. 7.22). These were not due to the structural character of the bone. Deflection of the fracture by the osteon was identified only once in sample C. Microcracking was described again in two types, short and thin capillaceous fractures (Fig. 7.23) present only in sample D, and fractures emerging in surface depressions running obliquely/diagonally, mostly oriented in one way within the sample, were present in both cases (Fig. 7.24).

In the case of spiral FS, both samples showed variable features. The profile of sample E was more shaped, and the surface was also not completely smooth. The stepped line was observed, given by the longitudinal arrangement of lamellae (Fig. 7.25). This was not the case for sample M, where the surface and the profile were very smooth and uniform. In one case, I observed a deflection of the fracture by the osteon (Fig. 7.26). The microfractures were also scarce and short, emerging in surface depressions and taking a diagonal course (Fig. 7.27). In sample M, none of these detailed features was described.

124
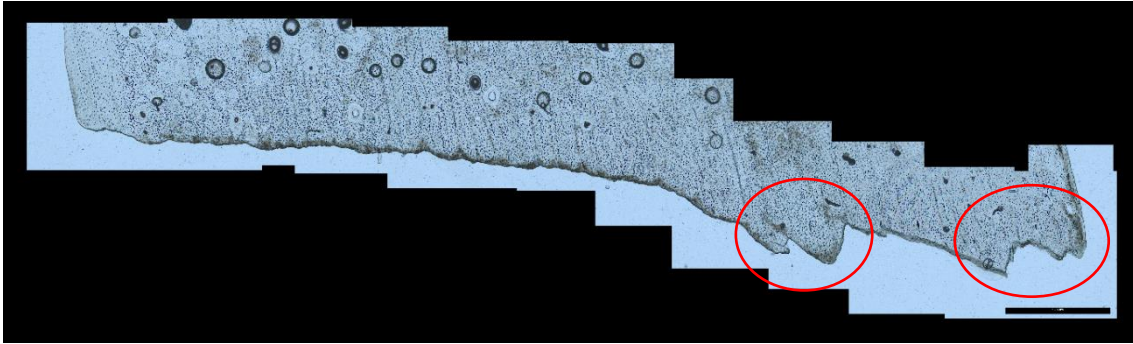
Fig. 7.22: Sample C. Surface irregularities marked by red circles. Magnification 50×, scale bar 1000 µm (photo SB).
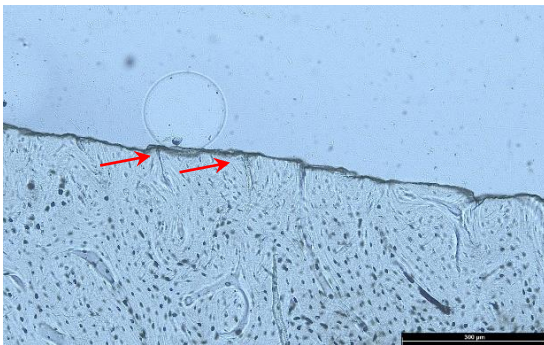
Fig. 7.23: Sample D. Very thin and short microfractures running perpendicular to FS indicated by red arrows. Magnification 100×, scale bar 300 µm (photo SB).
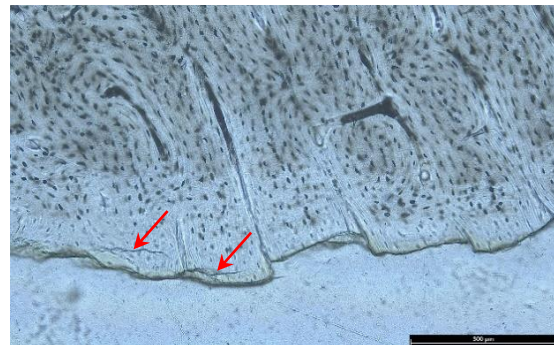
Fig. 7.24: Sample E. Example of microcracking observed in helical FS from frozen bones (red arrows). Magnification 100×, scale bar 300 µm (photo SB).
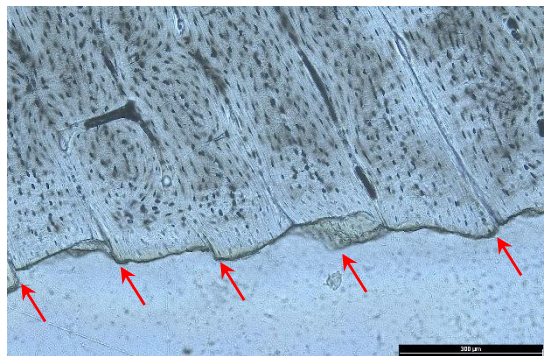
Fig. 7.25: Sample E. Stepped FS respecting the lamellar arrangement. Steps indicated by red arrows. Magnification 100×, scale bar 300 µm (photo SB).

Fig. 7.26: Sample E. Deflection of fracture around concentric lamellae arrangement in the osteon (red arrow). Nevertheless, the deflection is not present in the neighbouring osteon where the fracture cuts right through (red circle). Magnification 100×, scale bar 300 µm (photo SB).

125

Fig. 7.27: Sample C. Microfractures in an area with major surface irregularities indicated by red arrows. Magnification 100×, scale bar 300 µm (photo SB).

7.1.6.3 Dried bones

In the longitudinal samples, in comparison to fresh and frozen samples, the surface profile was markedly shaped and variable. The line of the profile changed from smooth and steep to stepped and gradual transitions (Fig. 7.28). The stepped pattern again follows the lamellar structure of the bone and the spots where they encounter Haversian canals. The microfractures usually start in surface concavities or in places where the surface fracture line changes course, running mostly diagonally but in various ways, unlike in the frozen samples (Fig. 7.29). Capillaceous short cracks heading perpendicular to the FS were also observed.

The transversal FS also had an irregular surface profile but with less pronounced protrusions or depressions significantly disturbing the profile line. The surface was generally rough, as indicated by the inconsistent profile line. The stepped pattern was not observed in transverse FS. Microcracking emerged, as in most of the samples, in surface depressions or around the surface irregularities. Their course is mainly diagonal, not respecting the bone microstructure and similar to that of longitudinal FS heading in various directions. A few perpendicular fractures respecting the lamellar bone structure in their trajectory were identified (Fig. 7.30). Significant cracking was observed in sample J. A massive fracture is present approximately in the middle of the sample, with a path perpendicular to the fracture surface. This crack respects the lamellar bone structure (Fig. 7.31a). Another clearly noticeable fracture cuts through the perpendicular one and is rather horizontal in its trajectory. Contrary to the previous fracture, it does not respect the bone microanatomy and cuts through different structures, under the elevation of the FS (Fig. 7.31b). It appears that this fracture starts with the change of FS diving into the bone, and possibly enters as a thin crack again on the FS (Fig. 7.31c).
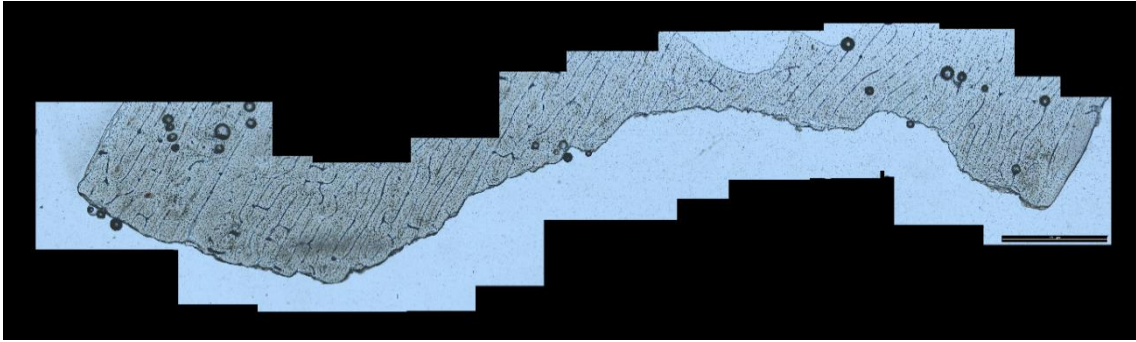
Fig. 7.28: Sample A. Illustration of the changing surface profile in dry longitudinal FS. Magnification 50×, scale bar 1000 μm (photo SB).

Fig. 7.29: Sample G. Diagonally running microfracture in dried longitudinal FS (red arrow). Magnification 100×, scale bar 300 μm (photo SB).
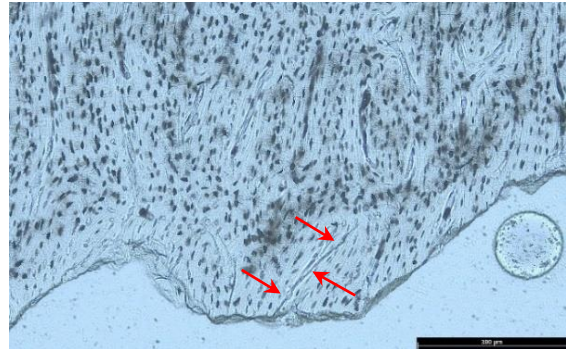
Fig. 7.30: Sample F. Perpendicular microcrack respecting the lamellar bone structure indicated by red arrows. Magnification 100×, scale bar 300 μm (photo SB).
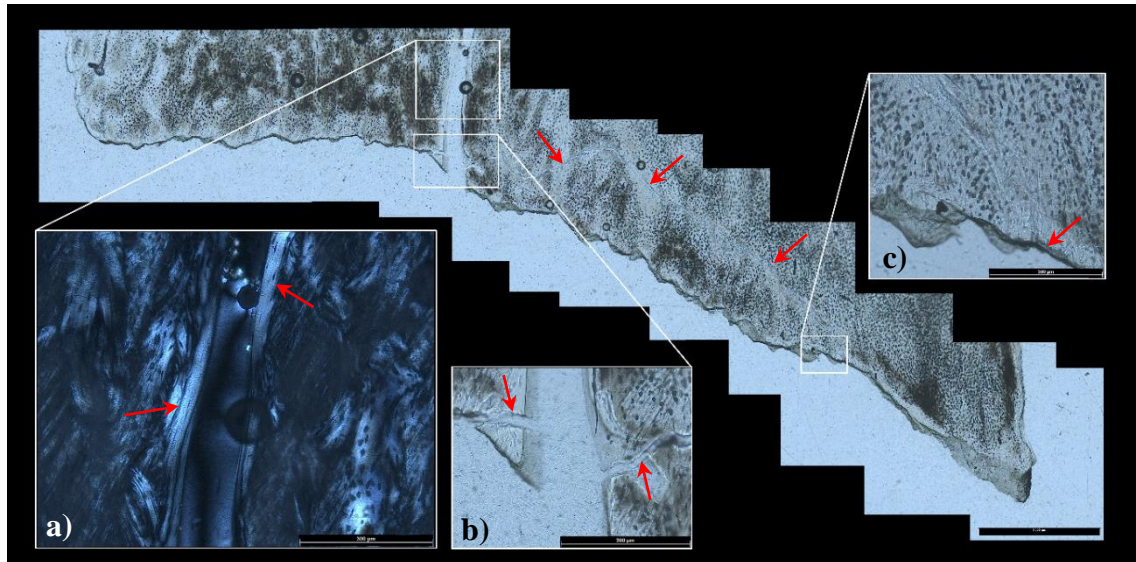
Fig. 7.31: Sample J. Transversal FS with details showing a perpendicular crack respecting the lamellar structure (a), beginning of the horizontal crack crossing the previous one (b) and the horizontal crack entering on the FS (c). The course of the horizontal crack is indicated by red arrows in the overview image. Magnification of overview image 50×, scale bar 1000 μm; magnification of detail images 100×, scale bar 300 μm (photo SB).

127

	Fresh bones (avg. FFI 2.85)		Frozen bones (avg. FFI 2.77)		Dried bones (avg. FFI 4.19)	
	longitudinal FS	*helical FS*	*longitudinal FS*	*helical FS*	*longitudinal FS*	*transversal FS*
SEM *Surface*	uniform, smooth	uniform, smooth	uniform, smooth	mainly uniform, smooth	mainly uniform, rough	irregular, rough
Patterning	linear, respecting microstructure	fan-shaped, crossing the linear pattern	linear, respecting microstructure	fan-shaped, crossing the linear pattern	linear, individual ridges rough and bumpy	not respecting microstructure
Micro fractures	more pronounced, respecting lamellar arrangement	less pronounced, respecting lamellar arrangement	respecting lamellar arrangement; reticulate	respecting lamellar arrangement; reticulate	highly variable thickness and course, mostly respecting lamellar arrangement	highly variable thickness and course, mostly lining surface irregularities
Other features	granular areas	plate-like protrusions	granular areas	plate-like protrusions	granular areas abundant	granular areas scarce
HTS *Surface profile*	uniform, minimal depressions and elevations	uniform, minimal depressions and elevations	mostly uniform, with minimal roughness	ambivalent	shaped and variable	shaped and variable
Surface irregularities	mild	only in individual areas	isolated protrusions	stepped pattern respecting lamellar structure	stepped pattern respecting lamellar structure	mild
Micro fractures	diagonal lining the surface irregularities; thin, perpendicular to FS	diagonal lining the surface irregularities; thin, perpendicular to FS	diagonal lining the surface irregularities; thin, perpendicular to FS	short and thin with diagonal course, emerging in surface depressions	emerging in surface depressions and shifts, diagonal course	diagonal lining the surface irregularities; emerging in surface depressions; thin, perpendicular to FS
Other features	lamellar deflection	none	osteon deflection	osteon deflection	none	extraordinary microcracking in sample J

Tab. 7.2: Table summarising the main surface and microcracking features observed by both microscopic methods in three different states of bone preservation. The most significant differences can be found in the dried samples (author SB).

7.2 Experimental assemblage from intentional human fragmentation (Institute of Archaeology, Brno)

The experiment was planned and conducted at the Institute of Archaeology, Brno (Czech Republic) by the author of the thesis with consultancy (S. Sázelová, A. Outram) in autumn 2020 and 2021 and winter 2022. The experiment was designed to prepare an assemblage of bones deliberately fragmented by humans (in our case, six anonymous experimenters) to simulate the activity of the dynamic impact force of humans on the settlement sites. It focused on the fragmentation of primarily fresh bone with respect to the type of fractures, the number of fragments, the incidence of percussion marks/scars, in connection to the presence of periosteum on the bone. All settings and material were chosen and used with respect to the archaeological material in the interest of this thesis. The material was subjected to macroscopic evaluation and FFI calculation (Chapter 7.2.4) and microscopic imaging and analysis (Chapter 7.2.5 and 7.2.5). Details about the material, environmental and experimental setting are below.

7.2.1 Material

In the experiment, we used long limb bones (*humerus*, *radio-ulna*, *femur*, and *tibia*; left and right elements) of European fallow deer (*Dama dama*) and red deer (*Cervus elaphus*) (Fig. 7.32). Because of their different morphological structure (much thicker compact bone, more consistent through the whole bone length and cross-section, much less variable in overall shape than other limb long bones) leading to different mechanical properties and, therefore, their distinct behaviour in the fragmentation process, metapodials were excluded from the experiment (e.g. *Calapdo – Blumenschine 1994*, 742; *Moclán – Domínguez-Rodrigo – Yravedra 2019*, 4665). Wild species were chosen in relation to the archaeological material of interest (see e.g. *Pickering – Egeland 2006*, 460). As the most related and at the same time the best available, we decided to work with bones of medium-sized cervids as the closest analogue to reindeer (*Rangifer tarandus*) highly abundant in Pavlov I archaeozoological assemblages (see Chapter 8). Resulting the fragmentation itself at a certain level) are different than in domesticates, and if from different physical loads, the morphology and robustness of the bones (influencing available, the wild species in this case present a more accurate analogy.

Fig. 7.32: Fresh bones of *Cervus elaphus* before the fragmentation process. A pair of *humeri* and *radio-ulnae* without (left) and with (right) periosteum, scale bar 30 cm (photo SB).

The bones were collected from local hunters and the killing and processing of the body were according to the legislative requirements of the Czech Republic and Slovakia. Skeletal elements were mainly deprived of soft tissues (fur, muscle). The age of four individuals varied from 18 months to 5 years (age stated by hunters), represented by both male and female individuals. All the bones came from freshly hunted animals, were stored outside in plastic refuse bags (temperatures less than 10°C) and fragmented a maximum of four days after death. In all cases, the season of death respects the hunting season of the individual species in the respective regions (late summer - mid-winter). Demographic information (sex, age) about the individuals providing the bones was recorded, and in the case of age determination then according to epiphyseal fusion (*Heinrich 1991*; *Carden – Hayden 2006; Emra et al. 2022*;) completed the information obtained by the hunters. The inventory and details concerning the data for the fragmented bones can be found in the supplementary material (Supplement 7).

7.2.2 Environmental setting

All the bones in this experiment were fragmented in a fresh state. Half of them were fragmented a) without the periosteum and the other half, b) with the periosteum to evaluate the effect of its presence on fracture surface morphology and the abundance of percussion marks. The amount of other soft tissues on the bones was reduced in both cases to the minimum possible in the fresh bone state. The actual fragmentation of the bones took place outside in autumn weather conditions (average temperature: 7.4°C;

average humidity: 84.5%; weather: mostly cloudy, with mild wind, two of the four experimental days foggy; precipitation: mostly without rain, slight rain present only during one of the four experimental days).

7.2.3 Experimental procedure

Six anonymous experimenters were involved in the fragmentation experiments. They participated in the experiment and provided their demographic and photographic personal data voluntarily (Supplement 8); all the data used in this thesis are anonymised. Men and women were equally represented, the average age was 37 years old (standard deviation 12.1), including various body types. None of them had previous experience with bone fragmentation, although three had extensive experience with bone anatomy (anthropologists/archaeozoologists). Full information about the participants can be found in the supplementary material (Supplement 9). Each of them fragmented four bones – two with and two without periosteum. Weighing of the bones and removal of remnant soft tissues and periosteum were performed immediately before breakage. Fragmentation took place outside in autumn weather conditions which were also recorded, only in the case of rain was the experiment moved under an outdoor shelter. The experimenters were instructed to use a flat sharp-edged anvil placed on solid ground (concrete pavement) and a pebble as an unmodified hammerstone (Fig. 7.33 and 7.34).

Fig. 7.33: Outside working area prepared before experiment, scale bar 30 cm (photo SB).

Fig. 7.34: Sheltered working area during experiment (photo SB).

The pebbles were from quartz, the anvil was sharp-edged and from fine-grained metamorphic rock. The participants had the option to choose from five pebbles of different weights (Supplement 10) and shapes according to their personal preferences (Fig. 7.35). They were also allowed to switch the hammerstones between individual bones; however, I only observed this situation sporadically. Only brief instructions were

given concerning the bone breakage. The participants were told to break the bone, aim their hits approximately in the middle of the bone (avoid epiphyses), how to place the bone on the anvil (so the place of impact would be touching the anvil) and use as many hits as necessary to open the marrow cavity. The number of hits and the time taken to open the cavity were again recorded (Fig. 7.36).

Fig. 7.35: Pebbles for bone fragmentation. The weight of the pebbles varied between ca 630 g to 1420 g, scale bar 30 cm (photo SB).

Fig. 7.36: Experiment in progress. Observer (left) recording the data, and participant (right) in action (photo M. Novák).

After opening the marrow cavity, brief pictures of the situation were taken, and then all fragments were collected and stored together. Bone marrow from long bone cavities was extracted using surgical instruments (probe, tweezers) and the weight was noted. The whole experiment was photodocumented and the experimental protocols (Supplement 11) were filled in carefully. Individual bones and their fragments were cleaned separately so the fragments would not become mixed. They were boiled in solution of Vyvasol powder and water for trophy cleaning for approximately one hour and only in a few cases did this procedure take longer or was repeated when necessary. The method of cleaning was chosen based on other experimental studies (e.g. *Galán et al. 2009*, 777; *Moclán – Domínguez-Rodrigo – Yravedra 2019*, 4665) aimed to the best preservation of the fracture surface (FS). After this treatment, the bones and fragments were left to dry at 15°C to be prepared for further analyses. To control the influence of the post-experimental treatment on the fracture surface preservation and microfracture abundance, we also prepared control samples that did not undergo the cleaning/boiling and dehydrating process prior to SEM imaging and histological thin sectioning.

7.2.4 Macroscopic observation

The results obtained from this experiment are reported separately for bones with and without periosteum (see Chapter 7.2.2). All three outlined methods for the FFI score calculation (see Chapter 6.2) were used to ensure that the observed values and differences truly reflect the fragmentation response. For the mean FFI value calculation in this experiment, we also included the FFI values obtained from the epiphyseal ends as they bear a significant part of the preserved bone shaft. Altogether, over 100 bone fragments were observed and evaluated. To control if the presence of FFI scores from epiphyseal fragments has any impact on the final average value, the mean FFI was also calculated without them. The obtained mean values were the same. The FFI values and measurements of individual fragments analysed can be found in the supplementary material (Supplement 12). The proportional representation of FFI values for bones with periosteum on and off is pictured in Graph 7.2. In this experiment, all fragments were due to the different experimental procedures assigned to the specific skeletal part (Fig. 7.37).
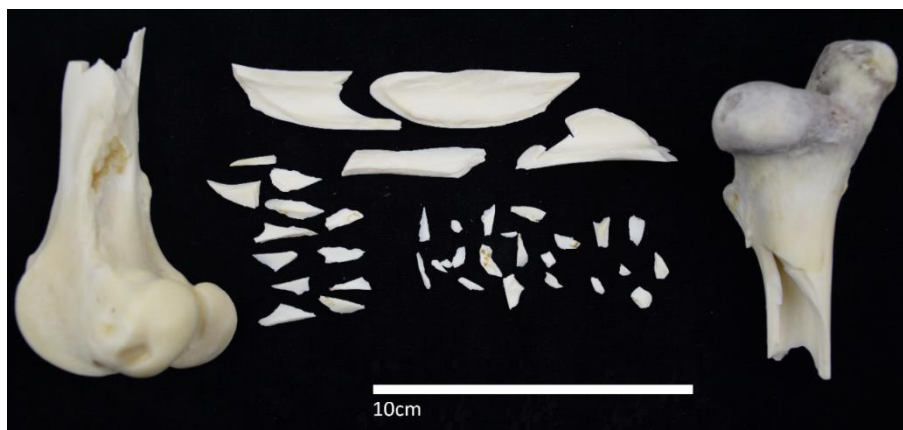
Fig. 7.37: Specimen 09_1_05. Example of a bone and its fragments broken by the hammerstone-to-anvil technique (photo SB).

Alongside the FFI, other variables (number of fragments in specific size categories, number of hits needed to open the marrow cavity, number of identified impact and rebound points) are reported to relate the observed differences in individual traits to the effect of periosteum presence/absence on bone during fragmentation process. The first is the number of bone fragments in size categories 0-0.9 cm, 1-1.9 cm, 2-2.9 cm, 3-3.9 cm, diaphysis fragments ≥4 cm and the number of epiphyses regardless of their size. The category of "other" fragments is also shown and includes fragments ≥4 cm not suitable for FFI scoring (malleolar bone, fragment of ulnar or fibular body). The second observed

variable is the number of hits needed to open the marrow cavity. The last reported trait is the number of identified impact and rebound points. The bones in both sets generally respected the fresh bone fracturing pattern, i.e. spirally shaped fracture outlines with a smooth surface and acute/obtuse angles of the FS to the cortical bone surface. In all cases the epiphyses remained in one piece and the fracture front was dispersed or deflected by cancellous bone (Fig. 7.38).
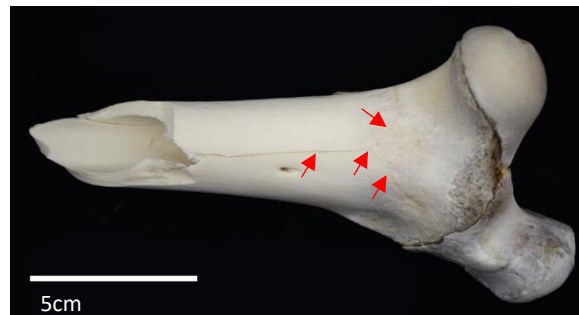
Fig. 7.38: Specimen 01_2_01. Dispersion of the fracture front approaching the epiphysis indicated by red arrows (photo SB).

7.2.4.1 Fresh bones with the periosteum

Altogether, 12 long bones (3 *femora*, 3 *tibiae*, 3 *humeri*, 3 *radio-ulnae*) were fragmented by 6 experimenters (2 bones each). For the fracture freshness index, altogether 34 diaphysis fragments ≥ 4 cm and 24 epiphyseal fragments mainly with joined midshaft parts were evaluated. The mean FFI value for the fresh bones with periosteum is **1.9**, the modus value is **1**. The result was also obtained by methods considering the length of the fracture surfaces. The number of fragments in the individual size categories is summarised in Tab. 7.3. The overall number of resulting fragments is significantly higher than in bones without periosteum although the proportion of individual size categories is very similar (Graph 7.3). The average number of hits necessary to open the marrow cavity of the bone is 6.2. The highest number of impacts per bone is 27 (first attempt by an inexperienced experimenter), and the lowest number of impacts is 1. The number of identified points of impact is 11 (8 bones), mainly represented by complete or double overlapping notches. In three cases, rebound points (creating double opposite notches with the initial impact point according to nomenclature by *Vettese et al. 2020*) were observed (Fig. 7.39).
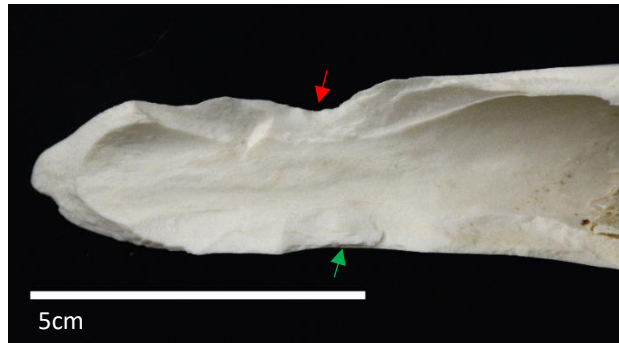
Fig. 7.39: Specimen 01_1_01. Bigger complete normal notch (red arrow) and smaller rebound notch on fragment of diaphysis still attached to the epiphyseal end of bone (green arrow) (photo SB).

7.2.4.2 Fresh bones without periosteum

In this set, 12 long bones (3 *femora*, 3 *tibiae*, 3 *humeri*, 3 *radio-ulnae*) were again fragmented (2 bones per experimenter). For the FFI index, altogether 20 diaphysis fragments ≥ 4 cm and 24 epiphyseal fragments mainly with joined midshaft parts were evaluated. The mean FFI value for fresh bones without periosteum is **1.6**. The same result was also obtained by method A; method B provided a slightly higher result of **1.7**. The modus value is **1**. The number of fragments in the individual size categories is summarised in Tab. 7.3. The total number of resulting fragments in this set is much lower than in the bones with periosteum. The proportion of the individual fragment size categories in both experimental settings is homogenous (Graph 7.3). The average number of hits necessary to open the marrow cavity of the bone is 2.2. The highest number of impacts per bone is 5; the lowest number of impacts is 1. Impact points originating from percussion by hammerstone were observed in 8 cases (7 bones), represented mainly by complete normal notches (Fig. 7.40). No rebound points were identified.
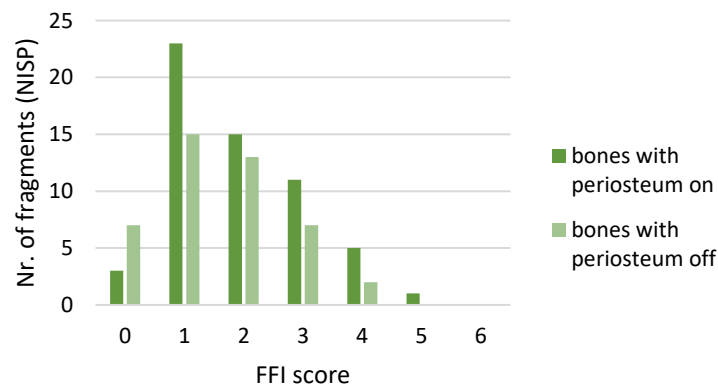
Graph 7.2: Proportion of FFI scores in bones with and without periosteum. The range of represented scores is almost the same in both experimental sets. A slight difference can be observed in the distribution of individual scores, especially for score 0 and 1 (author SB).

135

	Bones with periosteum on	Bones with periosteum off
fr. 0-0.9	452	270
fr. 1-1.9	110	62
fr. 2-2.9	34	21
fr. 3-3.9	9	15
other fr.	4	2
diaphysis fr. ≥4 cm	34	20
prox.	12	12
dist.	12	12
TOTAL	**667**	**414**

Tab. 7.3: Quantitative record for individual fragment size/type categories observed in our experiment. "prox." and "dist." stand for proximal and distal epiphysis (author SB).
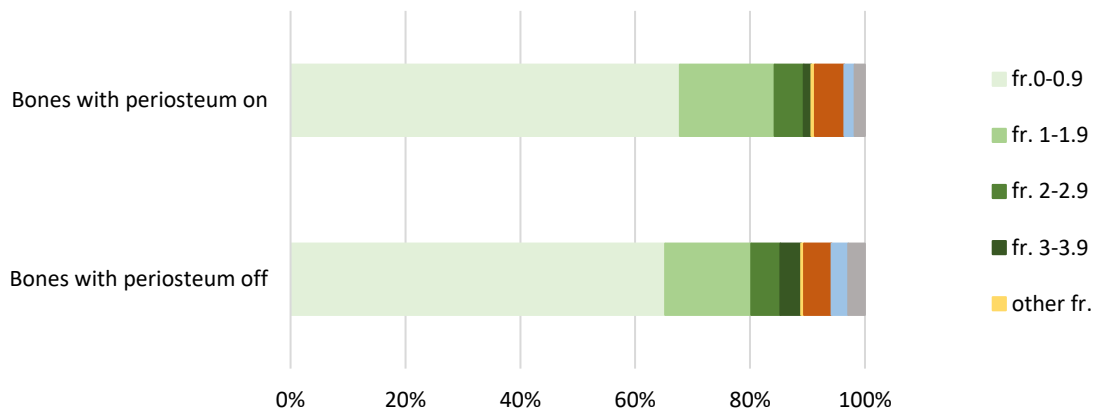
Graph 7.3: Very close proportional representation of individual fragment size categories in experimental set with periosteum on and off the bone. The biggest proportional difference (over 2%) is observable in fragment size categories 0-0.9 cm and 3-3.9 cm. "prox." and "dist." stand for proximal and distal epiphysis (author SB).
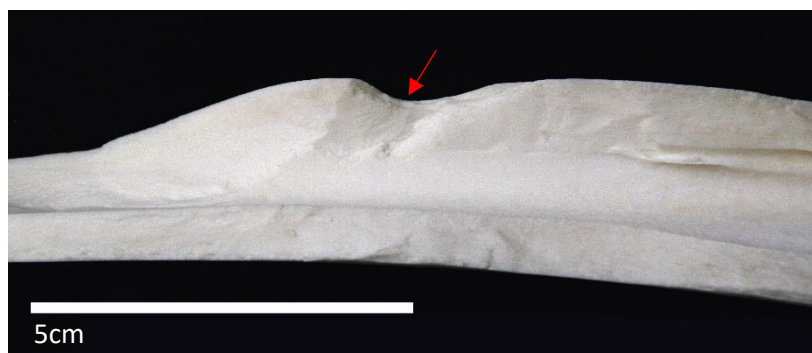
Fig. 7.40: Specimen 10_2_01. Complete normal notch (red arrow) on fragment of diaphysis (photo SB).

7.2.5 SEM analysis

In this experimental set, I focus on the potential differences caused by the presence of periosteum on fresh bone during the fragmentation process. In each setting (periosteum on, and off the bone) 12 samples were taken and observed, half representing longitudinal and half representing spiral fracture surfaces. The list of samples and their description are in Tab. 7.4. Since the bones were fragmented separately one by one, it was possible to keep all the fragments from one bone together and assign them to a specific skeletal element. To verify that post-experimental processing and pre-SEM preparation did not influence the final FS morphology, we prepared and observed two control samples. One was prepared without boiling in the cleaning solution, and the second was, moreover, not dehydrated in alcohol row. No noticeable differences in FS preservation were observed between the control and experimental samples (Fig. 7.41 and 7.42). A summary of the main features observed by electron microscopy can be found in Tab. 7.5 at page 151.

Sample	State of preservation	Skeletal element	Fracture surface (FS)	Histological section thickness
O	fresh with periosteum	*humerus*	spiral	67 μm
P	fresh with periosteum	*tibia*	spiral	73 μm
Q	fresh with periosteum	*radio-ulna*	spiral	70 μm
R	fresh with periosteum	*femur*	spiral	65 μm
S	fresh with periosteum	*femur*	longitudinal	93 μm
T	fresh with periosteum	*tibia*	longitudinal	70 μm
U	fresh with periosteum	*radio-ulna*	longitudinal	72 μm
V	fresh with periosteum	*humerus*	spiral	78 μm
W	fresh with periosteum	*femur*	spiral	85 μm
X	fresh with periosteum	*tibia*	longitudinal	86 μm
Y	fresh with periosteum	*radio-ulna*	longitudinal	85 μm
Z	fresh with periosteum	*humerus*	longitudinal	53 μm
ALFA	fresh without periosteum	*tibia*	longitudinal	93 μm
BETA	fresh without periosteum	*radio-ulna*	longitudinal	80 μm
GAMA	fresh without periosteum	*tibia*	spiral	72 μm
DELTA	fresh without periosteum	*humerus*	spiral	93 μm
EPSILON	fresh without periosteum	*femur*	longitudinal	70 μm
ZETA	fresh without periosteum	*femur*	spiral	93 μm
ETA	fresh without periosteum	*tibia*	spiral/longitudinal	95 μm
THETA	fresh without periosteum	*humerus*	spiral	83 μm
IOTA	fresh without periosteum	*radio-ulna*	longitudinal	70 μm
KAPPA	fresh without periosteum	*humerus*	longitudinal	76 μm
LAMBDA	fresh without periosteum	*femur*	spiral	118 μm
MI	fresh without periosteum	*radio-ulna*	spiral	79 μm

Tab. 7.4: List of samples from the hammerstone experiment subjected to SEM and histological treatment and analysis. Designation of the sample (simple without coding), state of preservation and presence of periosteum in the fragmentation process, skeletal element, type of observed fracture surface, and the thickness of the section are listed (author SB).

Fig. 7.41: Control sample prepared without boiling. Overview picture (magnification 37×, scale bar 100µm) with close up (magnification 250×, scale bar 100 µm) (photo Z. Pokorná and SB).

Fig. 7.42: Control sample prepared without boiling and dehydration. Overview picture (magnification 37×, scale bar 100 µm) with close up (magnification 350×, scale bar 50µm) (photo Z. Pokorná and SB).

7.2.5.1 Fresh bones with the periosteum

The overall surface characteristics in FSs from fresh bones with periosteum greatly correspond with features observed in fresh bones fragmented by rockfall. The morphology of the surface is mainly smooth, as is the texture in areas with longitudinal patterning. The longitudinal patterning is variably abundant and pronounced. In some cases, it covers almost the whole FS (e.g. sample S; Fig. 7.43), and in others, it was identified only in isolated areas (e.g. sample P). Nevertheless, this kind of surface pattern was observed in all samples. It appeared mostly on the periosteal side (Fig. 7.44). In places with more pronounced morphology, the texture is rather coarse with transversal ridges, plate-like laminations, and isolated granular areas (e.g. sample Y). These features are focused on the endosteal part of the sample (Fig. 7.44) although in a few cases they were identified regardless of their position within the sample. Microcracking had two main forms. The first was longitudinal cracking, mostly respecting the lamellar structure of the bone, usually interacting with Haversian canals penetrating their walls and interconnecting them (Fig. 7.45). These fractures were variably wide, long, and deep. The other form was fracturing lining the plate-like protrusions, also respecting the laminar bone structure but having a transversal or irregular course (Fig. 7.46). Although the fractures were variable in their width, depth and length, no standardised differences were identified between longitudinal and helical fracture surfaces. Since this experimental assemblage was sampled for microscopic analysis of individual FS types to a large extent, the differences that could be observed were more systematic so will be described separately.

In all the samples from the longitudinal surfaces, the longitudinal pattern covered at least approximately 40% of the studied surface and greater overall uniformity of the surface was observed. The granularity in these samples was mostly visible on higher magnifications (around 80×, Fig. 7.47). The exception was sample Y, where the areas were also clearly identifiable in the overview picture. A greater number of plate-shaped laminations was also identified in this sample, and unlike in the other samples, they were oriented in two opposing ways. I also identified fan-shaped surface patterning present in five of the longitudinal samples. However, it was not very well pronounced, sometimes visible only on higher magnification, and in some cases, it had a more diagonal than arcuate outline (Fig. 7.48).

In comparison to longitudinal FS, the helical FS were less regular in their surface morphology. In half the samples, the longitudinal pattern covered minor parts of the surface. Granularities were already observable in the overview pictures, especially in samples Q and V. Plate-like laminations had a uniform orientation within the sample; only in sample O did the lamination change its course from transversal to longitudinal. The characteristic fan-shaped pattern was observed in five samples. Compared to the longitudinal surfaces, the pattern is mostly well pronounced (Fig. 7.49), formed by a few larger prominent ridges. Higher magnification was only needed in one case to identify the presence of this pattern.
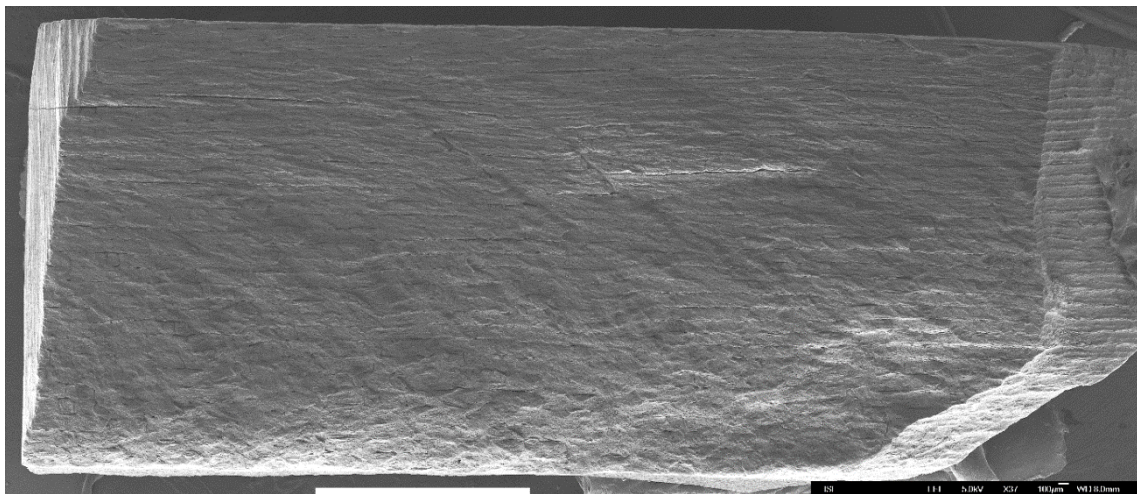
Fig. 7.43: Sample S. Linear patterning apparent in a major part of FS in the sample from longitudinal FS. Magnification 37×, scale bar 100 μm (photo Z. Pokorná and SB).
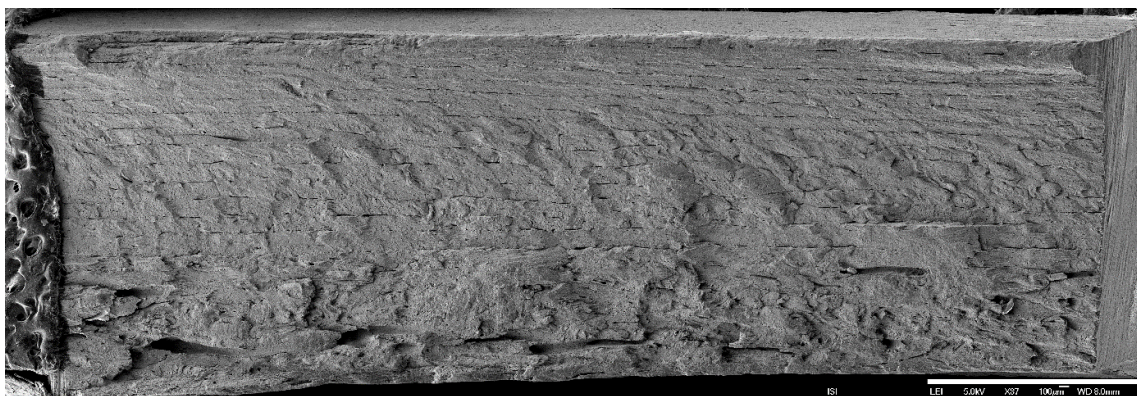
Fig. 7.44: Sample U. Linear pattern on the periosteal side of the fragment (upper part of the picture) in comparison to the highly irregular design present on the endosteal side (lower part of the picture). Magnification 37×, scale bar 100 μm (photo Z. Pokorná and SB).
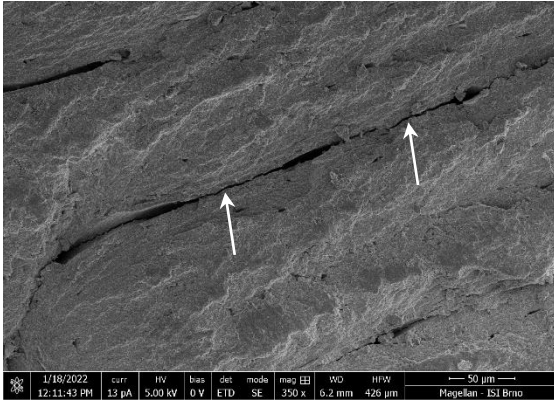
Fig. 7.45: Sample Q. Longitudinal cracking (white arrows) interacting with Haversian canals. Magnification 350×, scale bar 50 µm (photo SB).
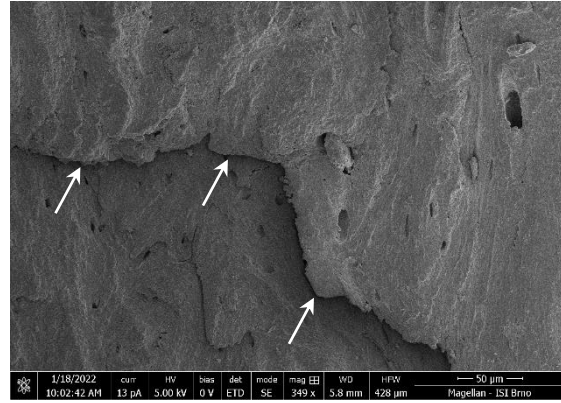
Fig. 7.46: Sample O. Irregular cracking (white arrows) lining the plate-like lamellar protrusion. Magnification 349×, scale bar 50 µm (photo SB).
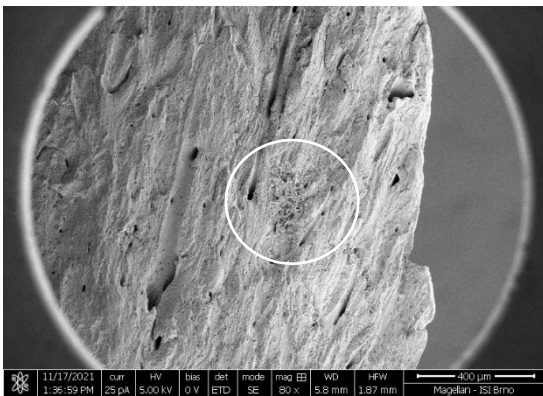
Fig. 7.47: Sample Z. Granular surface area indicated in the white circle. Magnification 80×, scale bar 400 µm, (photo SB).
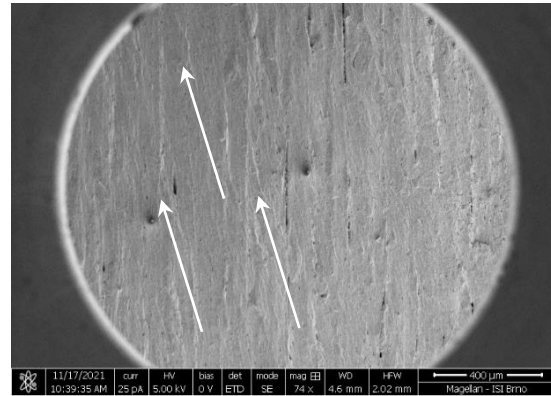
Fig. 7.48: Sample X. Subtle diagonal surface patterning (white arrows). Magnification 74×, scale bar 400 µm (photo SB).
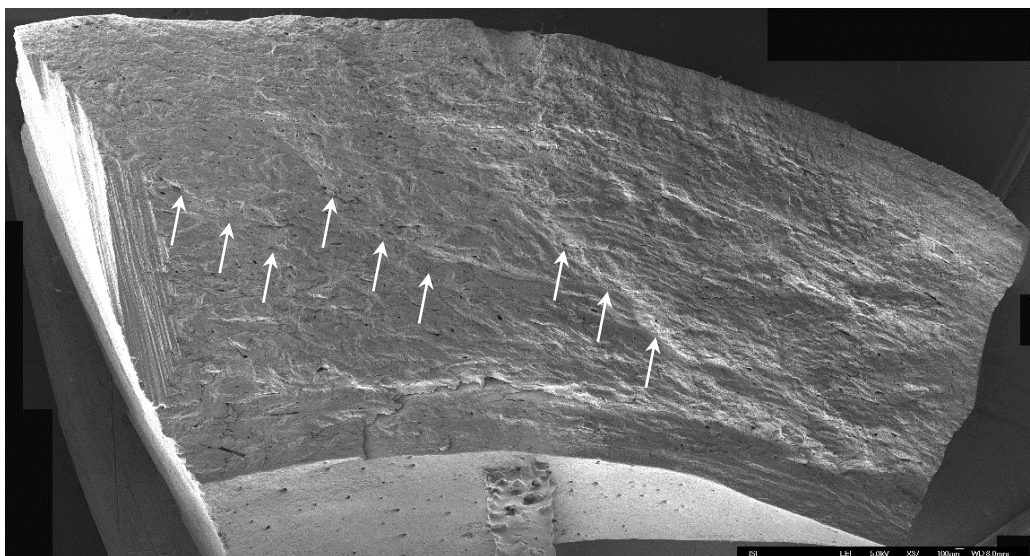
Fig. 7.49: Sample O. Fan-shaped design in the helical FS (white arrows). Magnification 37×, scale bar 100 µm (photo Z. Pokorná and SB).

7.2.5.2 Fresh bones without periosteum

In the majority of the observed and described traces and patterns, there was a consistency in both the fresh bones fragmented with and without periosteum. The surface was mainly smooth in texture and morphology and the linear pattern was represented in a variable range in all the samples. Transversally oriented ridges, plate-like protrusions, and scarce granular areas were also present. Microcracking took two main forms with longitudinal fractures and fractures lining plate-like laminations more transversal in their course.

The longitudinal fractures are variable in their length, depth and width, mostly interacting with Haversian canals and osteons and connecting them in their longitudinal and transversal orientation (Fig. 7.50). Both types commonly respect the laminar bone structure and have smooth edges (Fig. 7.51). Granular areas were also present in both types of FS although they were less abundant than in samples with periosteum. In samples from longitudinal surfaces, the linear pattern was easily readable and covered a major part of the studied surface (Fig. 7.52). The surface was mainly uniform, with more significant shaping only observed in sample IOTA with transversal ridges and numerous steps of the surface on the periosteal side of the sample. Granular areas were only scarce, more obvious, and already identifiable in the overview images in the IOTA and EPSILON samples. In the case of IOTA, they were concentrated along the arcuate ridges (Fig. 7.53). In the longitudinal samples, I also identified fan-shaped surface patterning. However, this was only in three out of six specimens. In one case it was well pronounced, reminding rather a helical FS (Fig. 7.53).

In the helical FS, the surface patterning was comparable to the longitudinal samples. The linear pattern was easily identifiable in a major part of the samples. The overall uniformity of the surface was apparent; only two samples (samples ZETA and MI) showed more distinct morphology. Granularities were rare and observable in small, enclosed areas. The fan-shaped pattern was present in four samples out of six, and in one case was restricted only to a small part of the sample (Fig. 7.54). The intensity and form of this pattern were comparable to the longitudinal FS from both fresh bones with and without periosteum rather than the spiral FS from fresh bones with periosteum. In the helical samples, I also observed minor irregularities concerning micro fracturing. In the MI and LAMBDA samples, the longitudinal cracking was much more pronounced than in the other helical or longitudinal FS from this experimental setting. In the sample

GAMA, I observed rough edges/walls of cracks (Fig. 7.55), and in the ZETA sample, cracking with a variable course was present (Fig. 7.56).
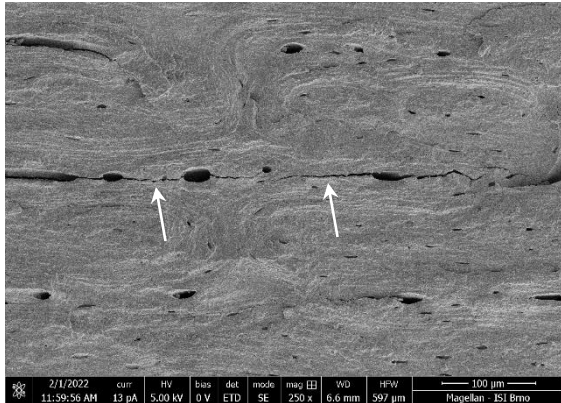
Fig. 7.50: Sample KAPPA. Example of longitudinal cracking connecting individual Haversian canals (white arrows). Magnification 250×, scale bar 100 μm (photo SB).
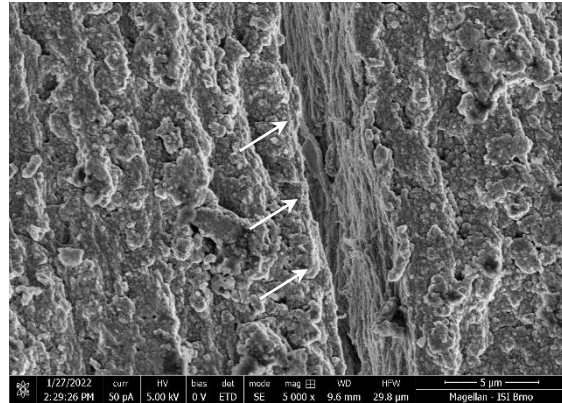
Fig. 7.51: Sample EPSILON. Smooth edge and wall of microfracture (white arrows), orientation of the fibrillary structures tends to be linear to the longitudinal fracture axis. Magnification 5000×, scale bar 5 μm (photo SB).
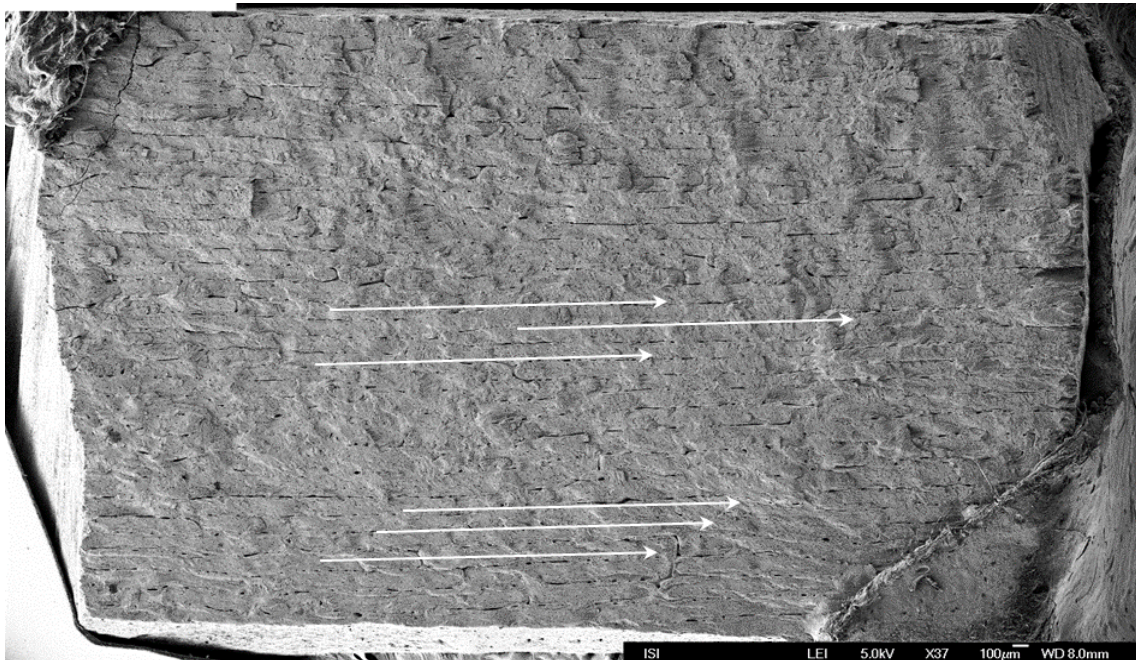
Fig. 7.52: Sample KAPPA. Longitudinal pattern apparent all-over the sample surface (white arrows). Magnification 37×, scale bar 100 μm (photo Z. Pokorná and SB).

Fig. 7.53: Sample IOTA. Granular areas (white circles) near to clearly visible arcuate ridges forming the fan-shaped pattern (white arrows). Magnification 37×, scale bar 100 µm (photo Z. Pokorná and SB).
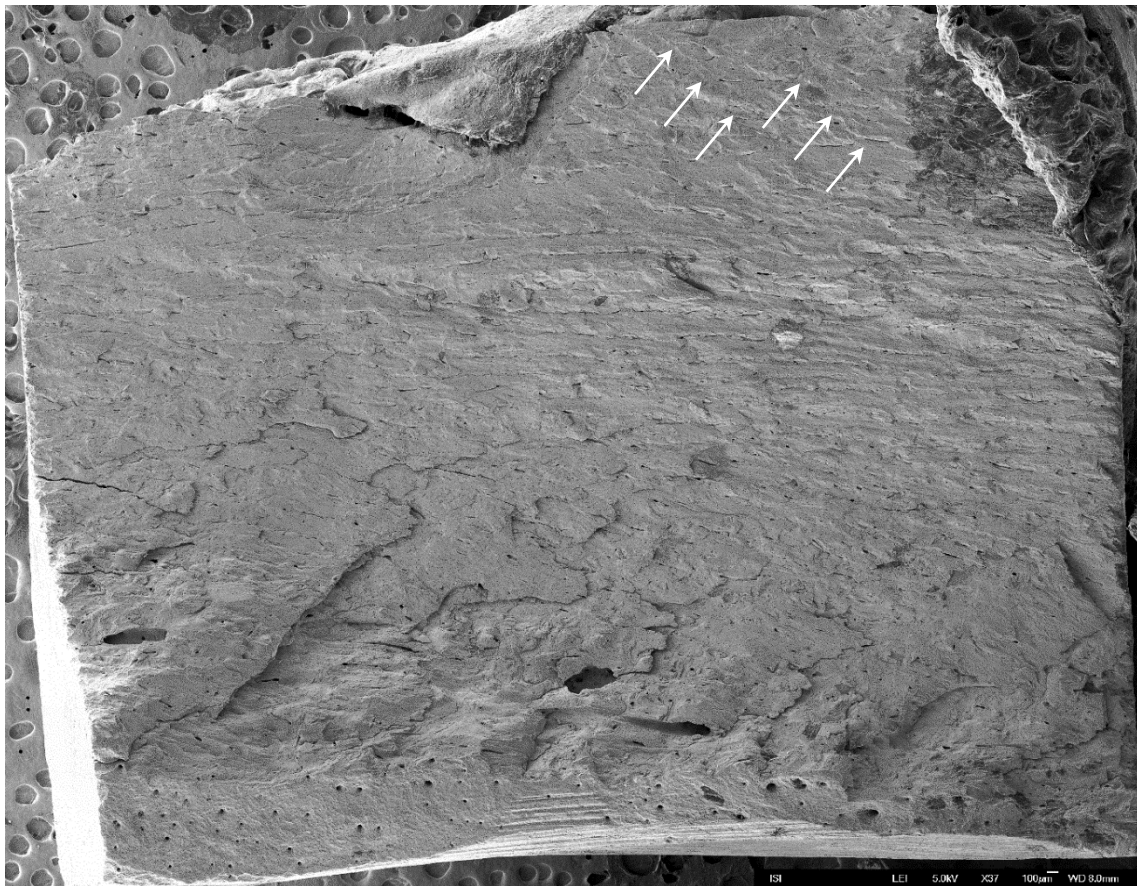
Fig. 7.54: Sample ZETA. Fan-shaped patterning in the upper right corner of the sample. The ridges do not significantly protrude and have a more diagonal course (white arrows). Magnification 37×, scale bar 100 µm (photo Z. Pokorná and SB).
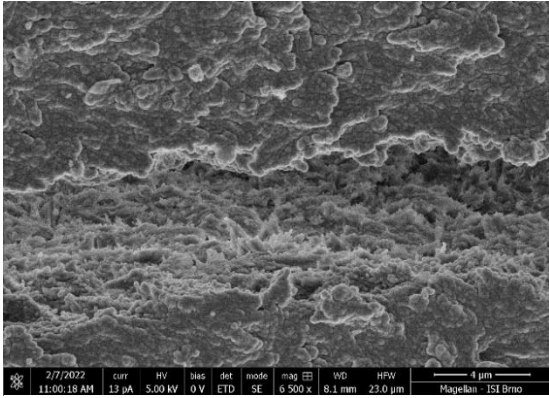
Fig. 7.55: Sample GAMA. Coarse surface of fracture wall with fibrillary projections with seemingly transversal orientation. Magnification 6500×, scale bar 4 μm (photo SB).
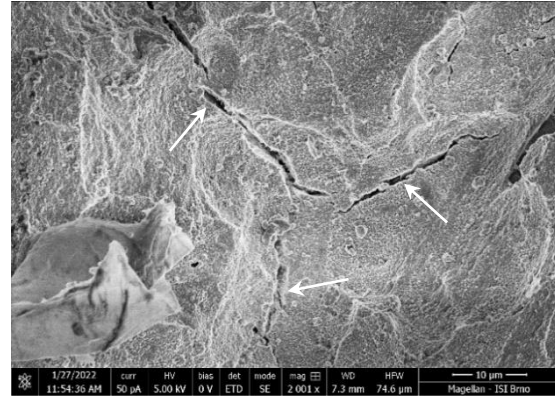
Fig. 7.56: Sample ZETA. Irregular cracking (white arrows). Magnification 2001×, scale bar 10 μm (photo SB).

7.2.6. HTS analysis

The treatment and preparation process were the same as described in Chapter 7.1.6. Again, transmitted and polarised light techniques were used to observe the changes. The final thicknesses of the sections are stated in Tab. 7.4. To control the influence of post-experimental processing and the pre-SEM preparation on the presence of microfractures and character of the fracture surface profile, two samples (one non-boiled, one non-dehydrated) were again prepared for HTS. In these samples, I did not observe any cracking penetrating under the surface, lining the surface irregularities or deflection around the osteons. The tendency to deflect at the boundaries of the canals or lamellae was observed (Fig. 7.57 and 7.58). The summary of the main features observed on the histological thin sections can be found in Tab. 7.5 at page 151.
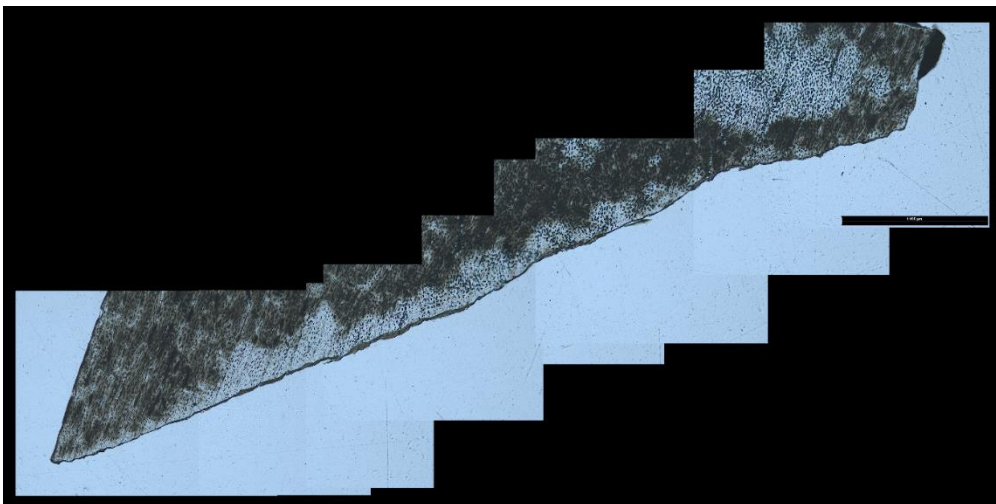
Fig. 7.57: Spiral fracture surface from non-boiled control sample. Magnification 50×, scale bar 1000 μm (photo SB).
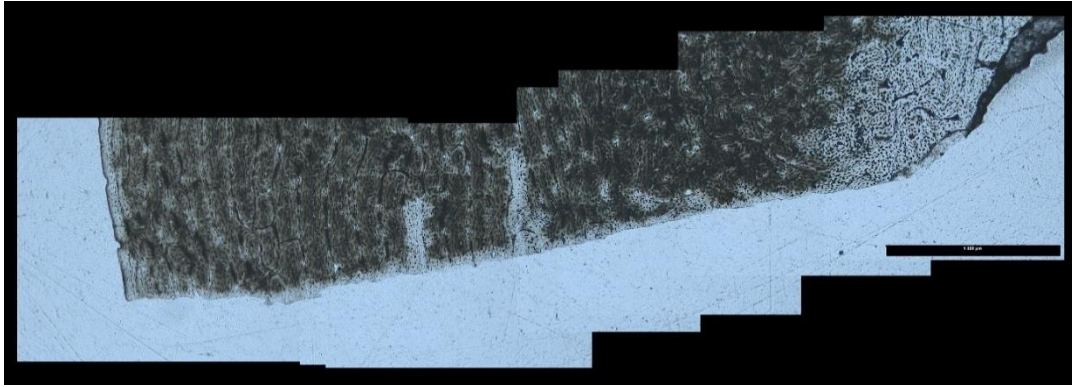
Fig. 7.58: Spiral fracture surface from non-boiled and non-dehydrated control sample. Magnification 50×, scale bar 1000 μm (photo SB).

7.2.6.1 Fresh bones with the periosteum

In the longitudinal samples, the surface showed a very smooth and uniform profile in most of the cases (5 out of 6). The shaping was mainly due to the underlying microstructure, which caused small irregularities in the profile, which was usually observed in the places of Haversian canals or cement lines (Fig. 7.59). Similarly, as in the SEM pictures, the endosteal and periosteal sides of the sample had a different morphology, with a more regular profile on the periosteal side and a more shaped profile on the endosteal side (Fig. 7.60). Despite the morphological smoothness of the surface, in some cases, I assume that the texture was quite rough, due to the inconsistent profile line (Fig. 7.61). Deflection by osteonal structures was not observed, the fracture front mostly cut right through the osteons (Fig. 7.62). Microcracking was very scarce and had two distinct forms. Microfractures perpendicular to the FS, typically very thin and short, and microfractures diagonal in their course and with a variable length (Fig. 7.63).

In the helical samples, the observed features were identical. The surface profile is generally smooth, without any significant depressions or protrusions, respecting the underlying bone microstructure. Deflection was mainly present in the interaction with the Haversian canals and in the case of osteons, the fracture front went right through. Microcracking was again infrequent, in the form of cracking perpendicular to or diagonal to the FS. In one case, the diagonal crack entering back to FS was identified (Fig. 7.64).

146
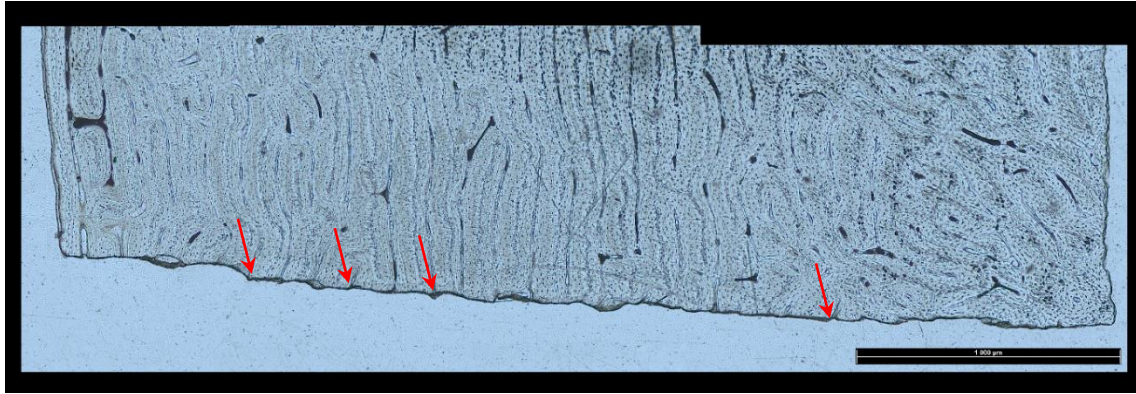
Fig. 7.59: Sample T. Narrow FS profile. Irregularities observed mainly in places where the fracture front encounters the Haversian canal or cement line (red arrows). Magnification 50×, scale bar 1000 µm (photo SB).
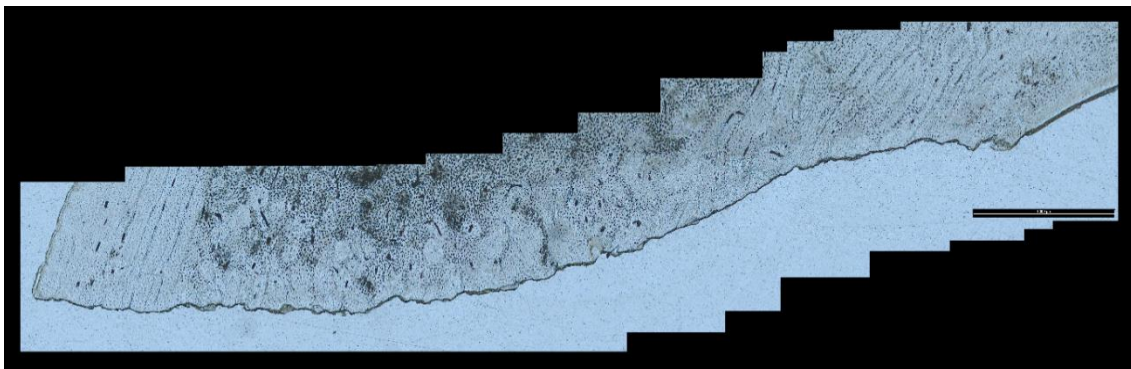
Fig. 7.60: Sample Q. Periosteal side (left) of the sample showing regular surface profiling in area with longitudinally/lamellarly arranged bone tissue. Towards endosteal side (right) more significant shaping and changes in surface morphology can be observed. Magnification 50×, scale bar 1000 µm (photo SB).
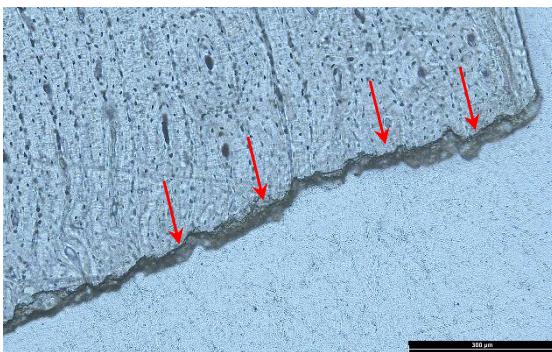
Fig. 7.61: Sample V. Morphologically variable and rough line of the surface profile (red arrows). Magnification 200×, scale bar 200 µm (photo SB).
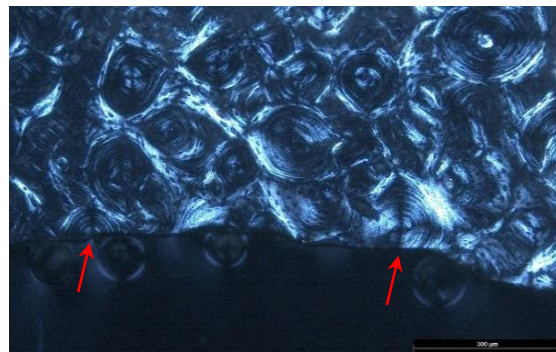
Fig. 7.62: Sample Y. Fracture cutting through the osteons without deflection (red arrows). Magnification 100×, scale bar 300 µm, polarized light (photo SB).

147
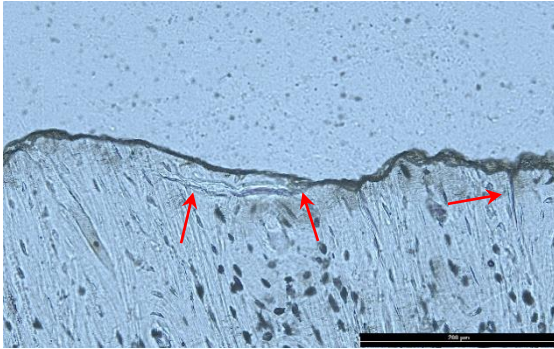
Fig. 7.63: Sample O. Diagonal (left and middle red arrow) and perpendicular (right red arrow) microfracturing. In the diagonal one, a slight deflection by concentric lamellae in the osteon can be identified. Magnification 200×, scale bar 200 μm (photo SB).

Fig. 7.64: Sample Z. Diagonal cracking starting in a surface depression and mouthing back to FS (red arrows). Magnification 100×, scale bar 300 μm (photo SB).

7.2.6.2 Fresh bones without periosteum

The longitudinal FS again showed a uniform profile, only in two cases out of six did I observe a more pronounced shaping (Fig. 7.65). The regularity of the FS was influenced by the underlying microstructure. Therefore, in areas with the osteonal organization of bone, the profile line was less smooth and curvy in its course. In areas with the lamellar organisation of bone (e.g. the periosteal side) a straighter profile line with small shifts respecting the lamellar structure was observed (Fig. 7.66). Deflection of the fracture front by osteons was not observed; the main fracture front and the microcracking penetrating under the FS went through the osteons (Fig. 7.67). The microfractures had two common forms previously recognised in other experimental samples – thin and short fractures perpendicular to the FS and fractures with a diagonal or parallel course, usually originating in surface depressions (Fig. 7.68). In one sample (IOTA), the perpendicular microcrack was unusually long (Fig. 7.69). Generally, in all the longitudinal samples observed, microcracking was quite scarce.

The FS profiles in spiral fractures showed more shaped morphology in comparison with the longitudinal ones (Fig. 7.70). The arrangement of the underlying bone structure was distinguished by the shape of the profile line. In some samples, inconsistency and blurring of the profile line were observed. Deflection by osteons was not observed. Microcracking was present in the form of thin perpendicular and diagonal fractures penetrating under the surface although these were longer and more variable in their course compared to longitudinal samples. A third form of cracking was represented by long, wide-open fractures at the beginning and narrowing towards the end. Some

respected the bone microstructure (Fig. 7.71) and some had a diagonal course, starting in a surface depression and cutting through the lamellar arrangement of the bone (Fig. 7.72). In two cases, (ETA and ZETA samples) this type of cracking caused a complete separation of the surface fragment from the rest of the sample.
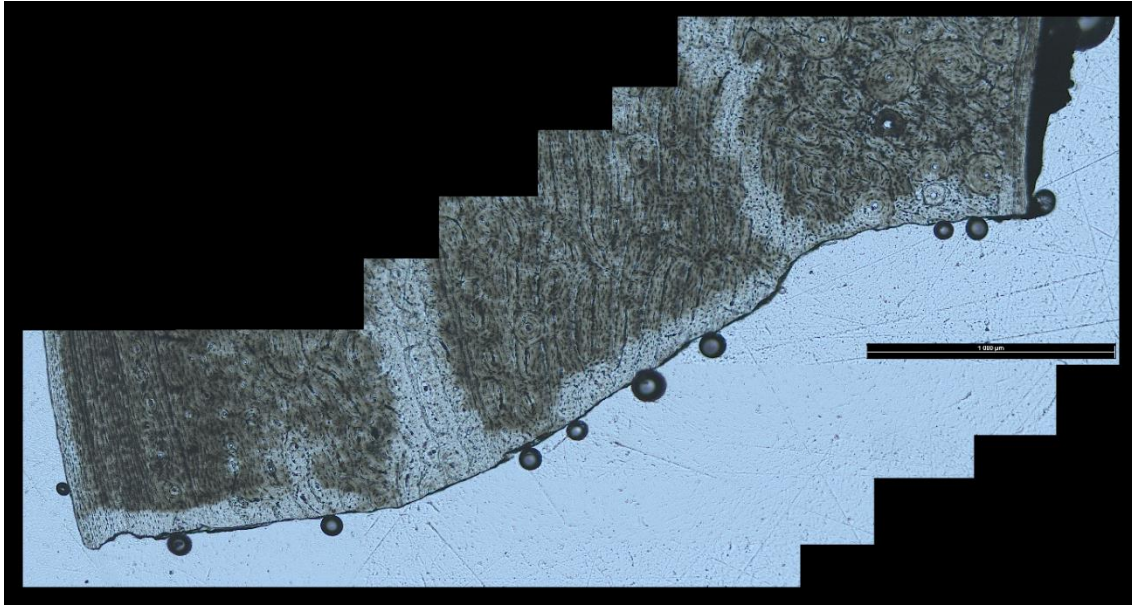
Fig. 7.65: Sample IOTA. More pronounced shaping of the surface profile. Magnification 50×, scale bar 1000 µm (author SB).
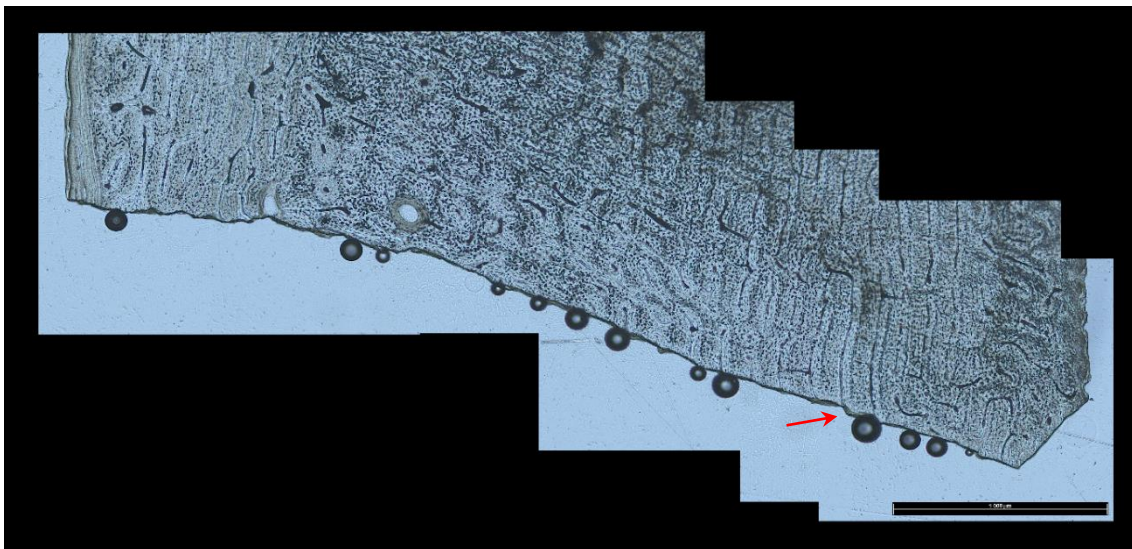
Fig. 7.66: Sample ALPHA. Straight profile line with small shifts indicated by the red arrow. Magnification 50×, scale bar 1000 µm (author SB).
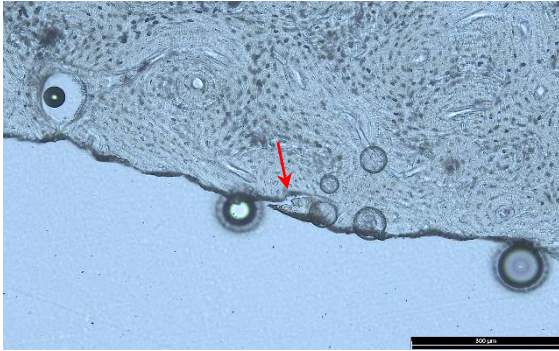
Fig. 7.67: Sample BETA. Microfracture cutting right through the osteon indicated by the red arrow. Magnification 100×, scale bar 300 µm (author SB).
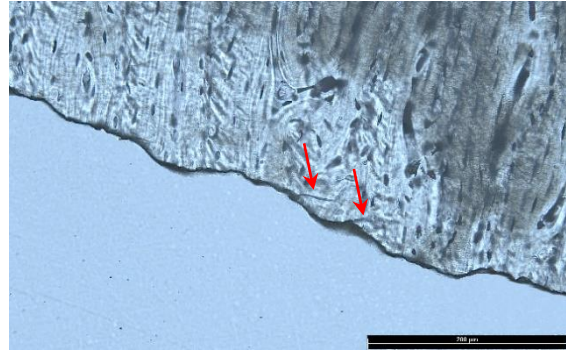
Fig. 7.68: Sample EPSILON. Short and thin diagonal microcracking indicated by the red arrows. Magnification 200×, scale bar 200 µm (author SB).
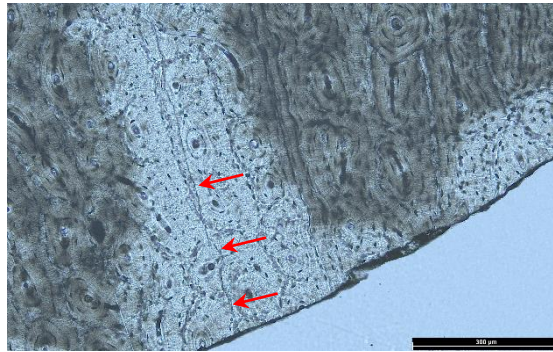
Fig. 7.69: Sample IOTA. Microfracture perpendicular to the FS indicated by the red arrows. Magnification 100×, scale bar 300 µm (author SB).
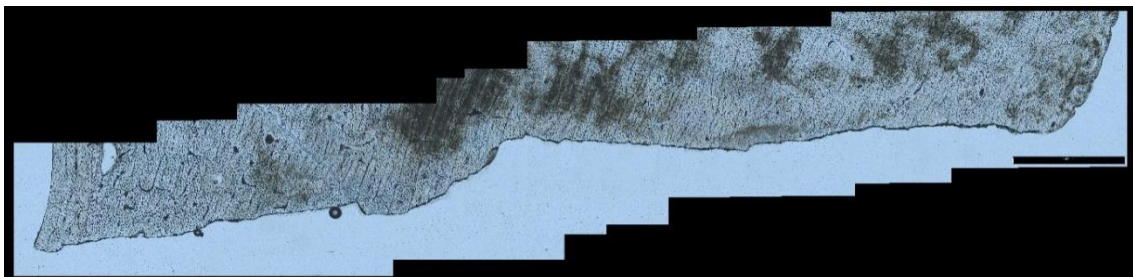
Fig. 7.70: Sample MI. Shaping of the FS profile in spiral fractures. Magnification 50×, scale bar 1000 µm (author SB).
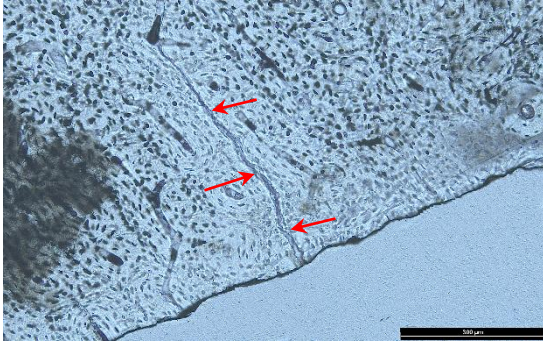
Fig. 7.71: Sample GAMA. Wide perpendicular cracking narrowing towards the end of the crack indicated by the red arrow. Magnification 100×, scale bar 300 μm (author SB).
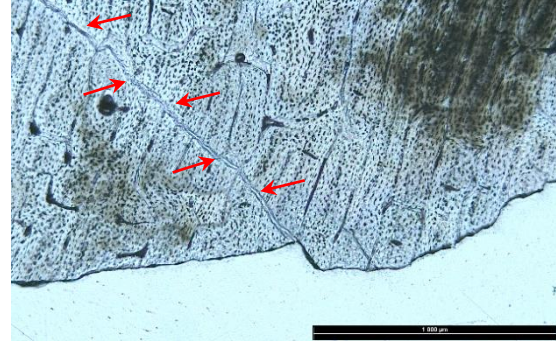
Fig. 7.72: Sample MI. Wide diagonal crack cutting through the bone microstructure, starting in surface irregularity (red arrows). Magnification 50×, scale bar 1000 μm (author SB).

	FB with periosteum (avg. FFI 1.9)		FB without periosteum (avg. FFI 1.6)	
	longitudinal FS	*helical FS*	*longitudinal FS*	*helical FS*
SEM				
Surface	uniform, smooth	less regular morphology, smooth	uniform, smooth	uniform, smooth
Patterning	linear prevalent; fan-shaped poorly pronounced	linear scarce; fan-shaped well pronounced	linear prevalent; fan-shaped poorly pronounced	linear scarce; fan-shaped poorly pronounced
Microfractures	mainly longitudinal, respecting lamellar arrangement	mainly longitudinal, respecting lamellar arrangement	mainly longitudinal, respecting lamellar arrangement	variable with irregularities, mainly respecting lamellar arrangement
Other features	granular areas scarce; plate-like protrusions	granular areas abundant; plate-like protrusions	granular areas scarce, larger; plate-like protrusions	granular areas scarce, smaller; plate-like protrusions
HISTOLOGY				
Surface profile	uniform, mostly narrow	uniform, minimal depressions and elevations	uniform, mostly narrow	uniform, curved morphology
Surface irregularities	very scarce	mild in parts with irregular bone arrangement	very scarce; inconsistent profile line	mild; inconsistent profile line
Microfractures	diagonal lining the surface irregularities; thin, perpendicular to FS	diagonal lining the surface irregularities; thin, perpendicular to FS	diagonal lining the surface irregularities; thin, perpendicular to FS	diagonal lining the surface irregularities; thin, perpendicular to FS; variably long
Other features	lamellar deflection	none	lamellar deflection	wide and long microcracking with a narrowing pattern

Tab. 7.5: Table summarising the main surface and microcracking features observed by both microscopic methods in fresh bones (FB) fragmented with and without the *periosteum*. Certain differences between longitudinal and spiral FS are noticeable, differences between periosted and de-periosted bones are scarce, mainly in the histological features (author SB).

7.3 Discussion of the experimental results

The **macroscopic analysis** of the experimentally obtained assemblages allowed me to observe several phenomena. The mean FFI value in fresh and frozen bones was almost the same, while the representation of specific values varied a little. In the frozen bones, I observed a higher representation of lower scores, similar to other authors, in samples frozen for a shorter period (around one week). The increase in the score that exceeded the fresh bones was documented after several weeks (*Karr – Outram 2012a*). The phenomenon described could be explained by the fragmentation of the bones in the frozen state. In this case, the influence of frozen marrow on specific force transmission within them must also be considered. According to some authors, the thawing process primarily influences the final fracture morphology and increases the index value (e.g. *Grunwald 2016*; *Outram 2002*), while degradation in the frozen state takes a very slow pace, preserving the properties of the fresh bone. The thawing process introduces more significant changes in the bone microstructure, and thus modifies the fragmentation pattern towards the dry state of bone preservation (see also *Boriová et al. in press*). The dried samples showed a significantly different representation of the index values, comparably to the notably distinct morphology observed by microscopic methods. Rapid moisture loss accelerates bone degradation, alters its natural response to applied stress, and makes it more susceptible to transverse failure. My observations are again consistent with the results of other experimental works addressing the state of preservation and using the FFI evaluation system (e.g. *Outram 2001*; *2002; Karr 2012*; *Karr – Outram 2012a*; *2015*).

Examination of the experimental samples under **SEM** proved its usefulness in the analysis of surface morphology. It allowed me to observe a mainly smooth and uniform surface in fresh and frozen bones on one hand and a variable, shaped and rough surface in dried bones on the other. The surface pattern showed characteristic features for individual types of fracture outlines. In the longitudinal and spiral types of FS, the pattern was mainly linear given by the bone microanatomy and longitudinally oriented osteons. This is consistent with the observations of static bone loading by three-point bending, where surface patterning showed similar traces for longitudinal and radial FS, and distinct ones for transverse FS (*Li – Abdel-Wahab – Silberschmidt 2013*, 456, Fig. 5). In spiral FS, an additional fan-shaped patterning was present, crossing the linear one. However, the character of this feature was slightly different in the two experimental sets. In the

rockfall experiment, the fan-shaped patterning was exclusively present only in spiral fractures. In the hammerstone broken assemblage, I identified this patterning in both types of FS. In the longitudinal fractures, the pattern was present only as fine, indistinct, arcuate or diagonal ridges. In the spiral fractures, the pattern was well pronounced and represented by a few clearly shaped arcs. Since the fan-shaped pattern occurred in both the observed assemblages, I assume that this pattern could be characteristic of dynamic impact. To confirm this hypothesis, it is necessary to examine other variables that may influence the result of the fragmentation process, such as the type of percussor (modified/unmodified), the type of raw material (hard/soft/inorganic/organic), and the application of other than dynamic force (e.g. *Galán et al. 2009*; *Hutson et al. 2018b*). However, the type and intensity of surface patterning may also be influenced by the bone portion (anterior/posterior/medial/lateral) from which the sample originates. In their experiments, *Li – Abdel-Wahab – Silberschmidt* (*2013*) stated that the surfaces from the anterior and posterior cortex positions generally tend to be smoother than those from lateral and medial positions. They attribute this distinction to the variable toughening mechanisms present in bone tissue (*Li – Abdel-Wahab – Silberschmidt 2013*, 455). Regarding the microcracking observed on the surface, I noticed small differences between the various types of bone preservation, mainly in their course. Longitudinal fractures and cracks were present in all the samples observed. In frozen bones, a few cases of reticular cracking were described. Higher variability was present in dried samples, where cracks also lined the surface irregularities. However, the differences described were not systematic and were usually documented in individual cases, so it is difficult to tell if they truly reflect the changes in bone preservation related to the fragmentation process or another activity unrelated to fragmentation (e.g. freezing/drying process, post-processing, preparation for analysis).

Concerning the traits reported by *Shipman* (*1981*), in my experiments, I was able to recognise the Type I spiral fracture. The surface characteristics that she described were consistent with what I observed in my spiral samples from fresh and frozen bones '*The fracture plane apparently lies between two adjacent bundles of collagen fibers, which can be seen on the fracture surface as elongate, stringlike structures. The parallel laminae and the intervening networks…*' (*Shipman 1981*, 372). As other authors also conclude, this type of smooth surface respecting the predominantly longitudinal orientation of collagen bundles/osteons results from the lower levels of fracture energy applied (e.g.

Lynn – Fairgrieve 2009, 795-796; *Li – Abdel-Wahab – Silberschmidt 2013*, 455). Only an amount of energy high enough to exceed the longitudinal strength of the osteons (which is greater than their transverse strength) can lead to the appearance of rough surfaces, described by *Shipman* (*1981*, 372) as Type II. She argues that only an active process, such as intentional human fragmentation, is strong enough to cause a Type II spiral fracture. Yet, we suggest that the typicality of Type I and Type II for different fragmentation actors (human vs. non-human) is highly dependent on the amount of strength the actor can apply and the strength of the bone given by its characteristic size, shape and microstructure.

The **histological analysis** by transmitted light microscopy revealed the relation between surface profile shaping/morphology and the state of bone preservation. This trait was significantly different for fresh and frozen bones, where it was mainly smooth, without significant protrusions or depressions. In the case of dried samples, the profile was shaped and variable, many times with an inconsistent blurred profile line, which could be an expression of irregular and rough surface. However, this trait was also observed in fresh samples fragmented without periosteum. It could be influenced by the thickness of the thin section or the variable thickness of the conductive layer from the SEM analysis. The observed differences and roughness may be just more pronounced and visible in comparison to previous samples and not necessarily connected to the fragmentation process. The profile of the surface also allowed me to distinguish between longitudinal and spiral surfaces, but again the character of the distinction was experiment-dependent. In the rockfall-broken material the longitudinal FS have a more regular and smooth profile, whereas in spiral FS more shaping and irregularities are present. In the hammerstone-broken assemblage, the longitudinal FS mainly show narrow morphology, while the spiral FS have a more wave-shaped profile. Wide and long microfractures, mostly penetrating deep under the surface, were observed in the dried samples so represent the characteristic feature of this type of bone preservation. However, this trait may be much more related to the actual state of preservation rather than to the fragmentation process itself. I was also able to describe other repeating types of microcracking. Very thin and short cracks, usually with a diagonal or perpendicular course, were mostly respecting the bone microstructure. The other type originates in places of surface irregularities, that is, depressions, protrusions, and places of fracture front deflection (see also *Boriová et al. in press*). Nevertheless, their presence or

frequency was not standardized among the samples subjected to microscopic analysis. Moreover, its appearance was not characteristic or systematic for any type of preservation or fracture outline. I did not observe the bending of the fracture penetrating under the FS by cement line or osteon concentric lamellae in any of the samples, as described, for example, by *Tang et al.* (*2015*, 29). However, it is important to note that the setting and procedure in Tang's study and my experiments were significantly different so represent a complex package of potential variables that can cause this discrepancy. The signs of such deflection were observed in the case of the main fracture propagation path, represented by the stepped fracture profile outline or the isolated osteon deflection (see Chapter 7.1.6 and 7.2.6).

In the range of experimental samples that I observed, I was unable to describe any systematic differences between bones fragmented with and without soft tissues/periosteum in any of the microscopic methods tested.

The results of the FFI analysis allowed me to observe similar sensitivity in recognising the state of bone preservation in the resulting bone fragments compared to the microscopic methods. Both the macroscopic and microscopic methods reliably distinguished the dried bones from the rest of the samples, based on morphological traits. The level of differentiation between frozen and fresh samples was low with both methods although the FFI was able to highlight small differences. The FFI even proved to be more sensitive to recognition of the presence of soft tissues/periosteum on bone during the fragmentation process. The differences in the mean FFI values between bones with and those without soft tissues were present in both experimental assemblages although with a different intensity and contradictory pattern. While in the rockfall assemblage the bones cleaned from the soft tissues and periosteum always reached a significantly higher mean value of the index, in the hammerstone assemblage the bones without the periosteum scored lower and with only a slight deviation from the bones with the periosteum. Again, there are more possible explanations for the observed differences. The first may be the different pre-experimental treatment and storage conditions, underlining the larger differences in the mean index values in the case of the rockfall experiment. The second may be the influence of different dynamic force implementations. The repeated random impact in the rockfall experiment can cause additional microcracking, introduce a wider variety of fragmentation damage and surface modifications, and influence the final FFI score if compared to single hits in controlled marrow extraction. The third may be the use

of different animal species. The size of the animal plays an important role. The smaller the animal, the relatively greater the force that the dynamic effector (falling rock or hammerstone) can be transmitted to the fractured element. This increases the probability of exceeding bone plasticity and may lead to rough and transverse fractures, even in fresh bones (*Blasco et al. 2014; Gifford-Gonzalez 2018*). Furthermore, the different skeletal requirements in domestic and wild species may also influence the macro and microscopic bone structure, and therefore, the response to applied stress (see Chapter 2.3). The fourth is the presence of soft tissues and the periosteum. These influence the number of hits required to open the marrow cavity and so possibly the frequencies of the accompanying BSM (e.g. *Blasco et al. 2014*). This plays an important role in the process of bone alteration, regulating the rate of moisture loss and so the final fracture pattern (*Outram 2002*; *Karr – Outram 2012b*). The fifth is the actual amount of soft tissues present during the fragmentation process. Since they cushion the impact applied and lower the amount of energy affecting the bone (e.g. *Galán et al. 2009*, 783; *Lynn – Fairgrieve 2009*, 796), they lead to a smoother FS (as mentioned earlier in this chapter) and so may decrease the final FFI. The higher the amount of soft tissues present, the more significant difference in obtained values. There are traits, on which the presence of periosteum or remnant soft tissues may have a notable impact, but not necessarily on all of them. An example of such a trait, resulting from our experiment, is the number of fragments in individual size classes (see Chapter 7.2.4). Whether with periosteum or not, their proportion was nearly the same, although we would expect to observe proportional differences due to the variable mean number of impacts needed to break the bone.

One of the crucial variables that were already tested in certain aspects of my experiment is the influence of post-experimental processing. I prepared testing samples to verify the gentleness of the cleaning and preparation methods in relation to surface preservation. Their examination and comparison with the samples from both experiments under the SEM showed no significant changes in the surface morphology. This proved that even different types of post-experimental treatment (see Chapter 7.1.3 and 7.2.3) if they are of a gentle nature, do not notably influence the surface, and the observed changes are truly related to the process of fragmentation or the state of bone preservation prior to the experiment. A similar kind of control for microcracking was performed, the control thin sections showed no microcracking penetrating under the surface. However, such a state was also observed in individual experimental samples, so therefore, more systematic

and extensive sampling would be desirable. Since I was unable to distinguish any pattern in the abundance or frequency of individual cracking types, there is a possibility that some of these may be remnants after cleaning treatment or the preparation process for microscopic analyses.

As the facts stated above illustrate, further comprehensive experimental work is needed to describe the influence of the different variables affecting the resulting traces to test the authenticity of observed (especially micro but also macroscopic) traits. The differences I observed and described are many times indefinite and scarce, but the fact that they are present should encourage further experimental activities and testing. With the growing number of samples and specimens originating from various well-documented fragmentation settings, the use of other more rigorous numerical/analytical methods (e.g. statistics, machine learning (ML), artificial intelligence (AI)) would be applicable. In the last decade, ML and AI methods have been tested and applied in BSM analysis with high precision and reliability (e.g. *Moclán – Domínguez-Rodrigo – Yravedra 2019*; *Domínguez-Rodrigo et al. 2020*; *2021*; *Pizarro-Monzo et al. 2022).* As the fragmentation traces of my interest also fall into the category of BSMs, these methods could similarly serve for their further study. The implementation of ML and AI in the analysis of image data obtained from SEM or histology could improve the accuracy or even identify other distinctive traces undistinguishable by the human eye. Furthermore, using systematic documentation and consistency in pre and post-experimental treatment will eliminate other potential sources of surface damage, especially in the case of microscopic surface features (e.g. *Karr – Outram 2015*).

The degree of applicability and reliability of the methods used in the archaeological material will be tested in the following chapters. These archaeological samples are highly specific due to the wide range of post-depositional processes to which they are exposed. Similarly, as post-experimental or pre-microscopy treatment, they may be a major influence on the fracture surface preservation or introduce other types of microcracking patterns. The ability to differentiate these features from those directly related to the fragmentation process should be one of the main goals in the further research of this topic.

8. Archaeological material

In the series of experiments, we proved that the microscopic methods were useful in identifying traces most possibly related to the fragmentation process and its conditions. Moreover, they correlate with the well-established macroscopic method of fragmentation analysis. To fully integrate this kind of approach into archaeozoological analysis, it is necessary to test if they can be successfully applied to material affected by weathering, fossilisation, and post-excavation treatment. I decided to test these methods on osteological material from the Gravettian site Pavlov I (*Svoboda – Novák – Sázelová 2016*; *Svoboda et al. 2016*). The importance of bone fragmentation analysis in the context of Paleolithic sites was already discussed in the introductory chapters of this thesis. The archaeozoological material used in this thesis comes from the new phase of excavations in 2013-2015. Three chosen areas from the site of interest were subjected to macro and microscopic fragmentation analysis, two activity zones - area A and G, and one settlement area SE014 (*Svoboda – Novák – Sázelová 2014; 2016*; *Svoboda et al. 2015; 2016;* see Chapter 8.1.1, Fig. 8.2). In area G, I calculated the FFI value and prepared a fragmentation history profile (FHP; see Chapter 8.3) for all long bones fragmented within the area. The analysis was then performed separately for two specific animal species. These were reindeer, representing the basis of the subsistence strategy and wolves, if hunted, most probably for other than dietary reasons. I wanted to see if this kind of approach can reflect the variability in animal body treatment and exploitation and reveal the potential intervention of post-depositional processes in the obtained mean index values. Macroscopic fragmentation patterns for chosen species were also studied in area A and area SE014 (with settlement units S1, S2, and the surrounding area) with a greater amount of identifiable material. First, they served as a control for the results obtained in area G. Second, area SE014 represents an area with different utilisation and therefore possibly also different fragmentation patterns. The test for microscopic analysis applicability and verification was performed only on material from area G. The final number of samples subjected to microscopic analysis was given by the state of preservation and the financial and time demands concerning the possible results.

8.1 Pavlov I Site

8.1.1 Location, history and significance

The Pavlov I site is located in the area surrounding the Pavlov hills and is one of many campsites in the Dolní Věstonice-Pavlov- Milovice settlement region (South Moravia, Czech Republic) (Fig. 8.1). This area is represented by a series of sites, located in 190-240 m.a.s.l., above the floodplains of the Thaya River on northern and northeaster slopes of the Pavlov hills Pavlov I, together with the neighbouring campsite Dolní Věstonice I represents one of the most significant settlement areas in the European Upper Paleolithic period. It has an altitude of 190-205 m.a.s.l. at a gentle northeast slope of the Pavlov hills inclining towards the lower reservoir of Nové Mlýny, and a small side valley of the active Pavlov creek. The subsoil of the slope is made of flysch sandstone and claystone of the Ždánice-Hustopeče formation from the Ždánice unit of the external group of Carpathian nappes. It is covered by marls of neogenic origin and Quaternary loess (*Svoboda 2002*, 33; *Svoboda ed. 2005*, 25; *Svoboda – Novák – Sázelová 2016*, 33).
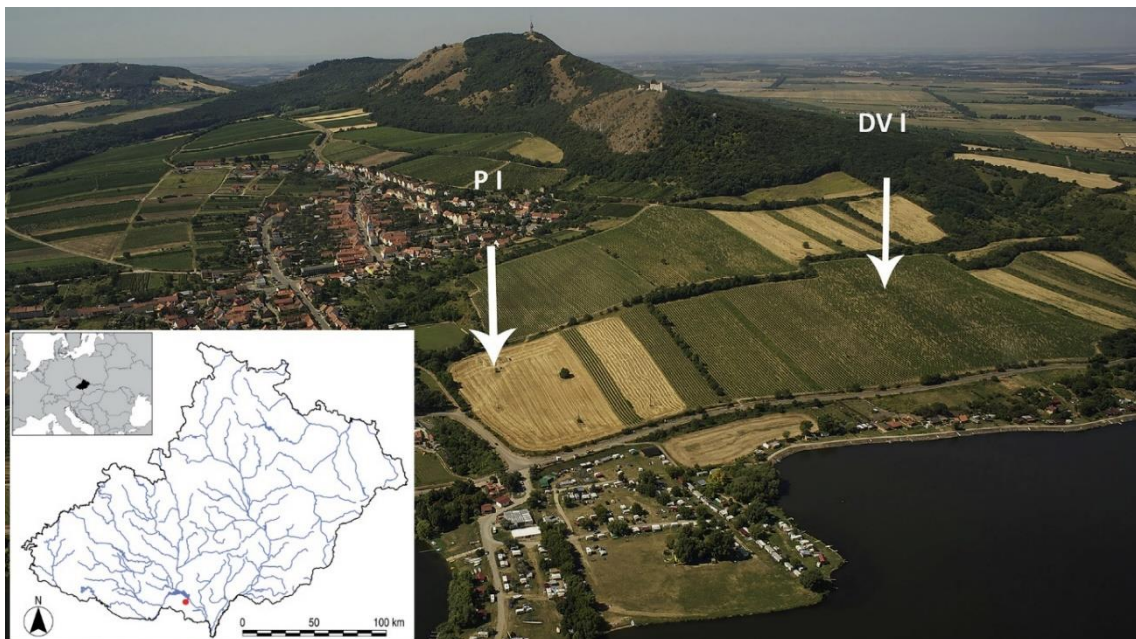
Fig. 8.1: Position of the Pavlov I and Dolní Věstonice I sites in larger context (lower left corner) and locally under the Pavlov hills (*Svoboda – Novák – Sázelová 2016*, 33, Fig. 1; *Svoboda et al. 2016*, 96, Fig. 1, modified by SB).

The site was seen as promising already in early 1950´s and was excavated in two phases. First, were the systematic continuous excavations ongoing in the following seasons from 1952 to 1972. These excavations were led by B. Klíma (*Klíma 1954*; *1959*; *1962*; *1963*; *1964*; *1971*; *1972; 1997*; *Svoboda ed. 1994*; *1997*; *2005).* The site was

159

divided into three parts, southeast, central and northwest. The main occupation zone was located on the small ridge with an east-west orientation, running below the present slope, which was most probably preferred due to the drier and possibly warmer type of subsoil. The peripheral areas and the waste deposit were located in the surrounding gullies (*Svoboda et al. 2016*, 96). The area of the discovered campsite consists of numerous dwellings, various activity zones and workshops often accompanied by hearths or cooking pits. These are mostly represented by shallow depressions around 5 m in diameter, lined by a concentration of larger stones and bones. Some of these units/objects overlap and form a complicated palimpsest (*Verpoorte 2000*; see Chapter 8.1.2). The numerous research seasons and the large area of occupation in Pavlov yielded an enormous number of archaeological finds, including lithic artefacts, bone tools, and symbolic and decorative objects made of ivory or ceramics. There were also rich archaeozoological finds that mostly represent hunted prey. Extra-large and large herbivorous species (such as woolly mammoths and rhinoceroses, bison/aurochs, reindeer and or horses) were present alongside carnivores of different size categories (lions, bears, wolves, wolverines, foxes) (*Musil 1955*; *1994*; *2005a*; *Wojtal et al. 2012*; *Wilczyński et al. 2020*). Among the others were hares, representing a large number of hunted prey, occasionally birds and fish (e.g. *Musil 2005a; Bochenski et al. 2009*). Finally, there were human remains. In 1957, the burial of an adult male (Pav 1) was found in the northwest sector of the site. The partial skeleton was flexed, retaining the anatomical but disarticulated position. The burial was associated with large mammoth bones, which partially covered the human body. The whole finding was affected by downslope redeposition. In addition to this burial, numerous isolated human remains were found and identified either at the site or during the further processing of the material. Among the most prominent we can mention several human teeth of which two are pierced and an isolated hand and pedal pairs identified among the animal material in later processing (*Svoboda 2006*; *Sázelová et al. 2018*; *Sázelová – Hromadová 2020*; *Trinkaus – Sázelová – Svoboda* 2019; *Trinkaus et al. 2009*).

After more than 40 years, the site was opened again in the second phase in 2013. This phase lasted from 2013 to 2015 as an extensive rescue excavation before the construction of the Archeopark Pavlov modern historical museum. This was led by *J. Svoboda* (*Svoboda – Novák – Sázelová 2014*; *2016*; *Svoboda et al. 2015*; *2016*) in three seasons: in 2013 as exploratory research and excavation; in 2014 as a planned rescue

excavation; and in 2015 as a final rescue excavation examining the peripheral/marginal areas of planned construction (Fig. 8.2). The newly excavated area completed the large oval accumulation of units originally excavated by *Klíma* in the southeast sector, by adding newly uncovered unit S1 and pit S2. The new research phase also examined the still unexplored southwest sector of the site. This part was examined by four exploratory trenches (A-D), which in their eastern parts encountered the edge of the old *Klíma's* excavations and allowed for more precise localisation and planning of ongoing research (Fig. 8.2).
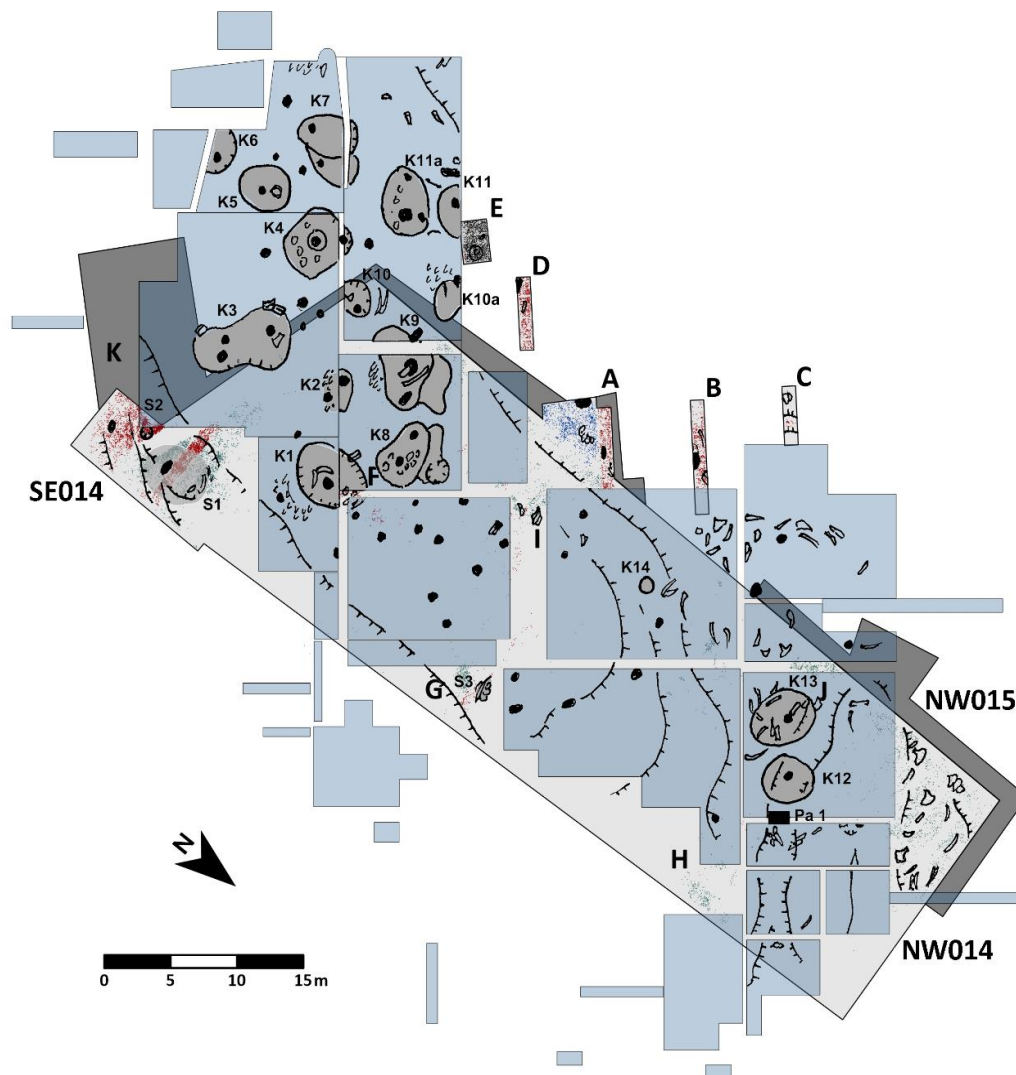
Fig. 8.2: Pavlov I. Excavation plan from the 2013-2014 season (pale grey) with the distribution of 3D recorded finds, 2015 (dark grey on margins), and Klima's trenches from 1952-1972 (transparent blue squares). K1-K14 are units uncovered during 1952-1972 by Klíma, S1-S3 are units uncovered by Svoboda during 2013-2015 (*Svoboda – Novák – Sázelová 2016*, 34, Fig.2; *Svoboda et al. 2016*, 98, Fig. 3; modified by SB).

Further excavation in the southwestern part revealed the unique burial of a wolf individual (*Sázelová et al. 2020*). The excavation works in the central sector uncovered several situations corroborating the remains of the control blocks and objects between the trenches from 1960-1965. The newly documented situations serve as a partial substitute for the original planographic documentation for the central part, which has not yet been found. The northwest sector was widened by exploring the adjoining area in the western direction, where the original surface dives deep under the loess. A large but loosely dispersed mammoth bone deposit, whose location within the Pavlov I site remained unrevealed, was identified as a continuation of scattered mammoth bones and male burial in the northwest part of the site. Part of the mammoth deposit was preserved and is incorporated into the exposition at Archeopark Pavlov (*Svoboda – Novák – Sázelová 2016*, 34-35; *Svoboda et al. 2016*, 96).

With the present data obtained from both old and new excavations, we are still unable to reliably determine whether the site represents one intensive long-term occupation with zones where multiple activities took place or occupation of a short-term character but repeating nature.

8.1.2 Stratigraphy and chronology

Pavlov I represents a site consisting of numerous extensive and intersecting settlements, objects, and hearths. Their overlap and creation of more complex units, the richness of the cultural layers mainly in the southeast of the site, together with the very thin layers of loess separating individual occupational events contribute to creating the stratigraphically complex and difficult-to-read palimpsest. Therefore, the emphasis in stratigraphic analyses was placed on the microstratigraphy of observed cultural layers (for further information on stratigraphic information see e.g. *Klíma 1971*; *1972*; *Svoboda ed. 1997*; *Verpoorte 2000; Svoboda ed. 2005*; *Rejšek 2014*; *Svoboda – Novák – Sázelová 2014*; *2016; Svoboda et al. 2016*; *2019*).

The cultural layers are deposited between the last glacial maximum (LGM) loess above, and the loess, or redeposited Cenozoic marls, beneath, similar to other sites in the Dolní Věstonice-Pavlov-Milovice region. At the top is irregularly thick LGM loess where the thickness varies between none in places where the cultural layers appear on the surface, up to 8 m documented by distant boreholes. The cultural layer lies at the base of the LGM loess. Predominantly, it consists of a 20-40 cm thick dark layer that contains

bones, artefacts and charcoals. In certain positions (e.g. trenches A, B, D, E), it is divided into two or more layers separated by light ochre loess, with the overall thickness reaching 70cm. Finally, the subsoil consists of Jurassic limestone of variable fraction and Neogene marls in an ochre, blueish or greenish colour. In all the layers mentioned, the process of cryogenic and slope movement is documented, proving the existence of permafrost and its movement in the periods before, during and after the Gravettian (*Svoboda – Novák – Sázelová 2016*, 37-39; *Svoboda et al. 2015*, 138; *2016*, 98-102). Poof of its presence, such as frost heaves, ice wedges and polygons, is vital, not just concerning variously disturbed stratigraphic context of the cultural layer. The state of bone preservation, spatial pattern or different modifications on bones may also result from the cryogenic processes or by movements of soil induced by these processes (see Chapter 3.1 and 5.2.3).

The radiocarbon dates obtained from Klima's excavations are from the central parts of the site and date the site to the Middle Gravettian, or the Pavlovian in the short-range around 29-31 ky calBP. The dating of newly excavated situations is focused on microstratigraphy. The sequence of 12 continuous dates taken from trenches A, B, D and E demonstrate the continual formation of a cultural layer from 29 to 33ky calBP (Middle to Early Gravettian). In trenches E and D, dates reaching 36-38 ky calBP (Early Upper Paleolithic) were obtained from the subsoil. In all cases, the dates were obtained from charcoal (*Svoboda – Novák – Sázelová 2016*, 39-40; *Svoboda et al. 2016*, 103-104).

8.1.3 Selected areas

8.1.3.1. Area G

This area was located in the central sector of the location excavated from 1960-1965. The documentation for this area was lost after the death of *B. Klíma*, so the new excavations served to revise this part of the site. The remnants of control blocks, layers with artefacts, the bases of some hearths and individual pits were observed in newly excavated 1 m wide strips. Area G was described as one of the significant situations in this area, situated quite shallow under the topsoil. It is represented by an oval depression designated as S3, with dimensions of 160×70 cm and a maximum depth of 15-20 cm (Fig. 8.2). In its central part was a notably dark-coloured infill. The most significant archaeozoological material was a large part of a mammoth tusk (*Mammuthus primigenius*), fragments of antlers, skulls, vertebrae, ribs and limb bones of reindeer (*Rangifer tarandus*) in articulated but also dispersed positions, articulated metapodials

and phalanges of wolf (*Canis lupus*), mandible fragment of fox (*Vulpes vulpes/lagopus*) and the proximal part of horse (*Equus ferus*) humerus (Fig. 8.3) (*Svoboda – Novák – Sázelová 2016,* 43; *Svoboda et al. 2016*, 98). The osteological material from this area was completely analysed for the purpose of this thesis, and the proposed microscopy methods .of fragmentation analysis were also applied.

Fig. 8.3: Pavlov I, area G. Described feature with articulated skeletal parts of wolf and reindeer. Fragmented osteological material also belonging to other animal species is present, which is scattered in the area (photo M. Novák).

8.1.3.2 Area A

Area A lies in the southeast sector of the site and was gradually excavated over all three years of the last excavation season. In 2013, it only had the form of an exploratory trench, 7.4 m long and around 1 m wide, with cultural layers in 2.5-3.4 m (the uppermost layer) and 3-3.9 m (the lowermost layer). It contained hearths and accumulations of osteological material. In the summer of 2014, the trench was widened on the east side to a triangle with length of cathetuses 7.5 m and 5 m. In 2015, another 1 m was added to this triangle. The area is described as an activity zone with an oval hearth (0.8×0.6 m) with a maximum depth of 15 cm and group of small pits at its base. Another two kettle-shaped pits with a depth of 12-13 cm and filled with bones were located in the area (*Svoboda – Novák – Sázelová 2016*, 42; Fig. 8.4).
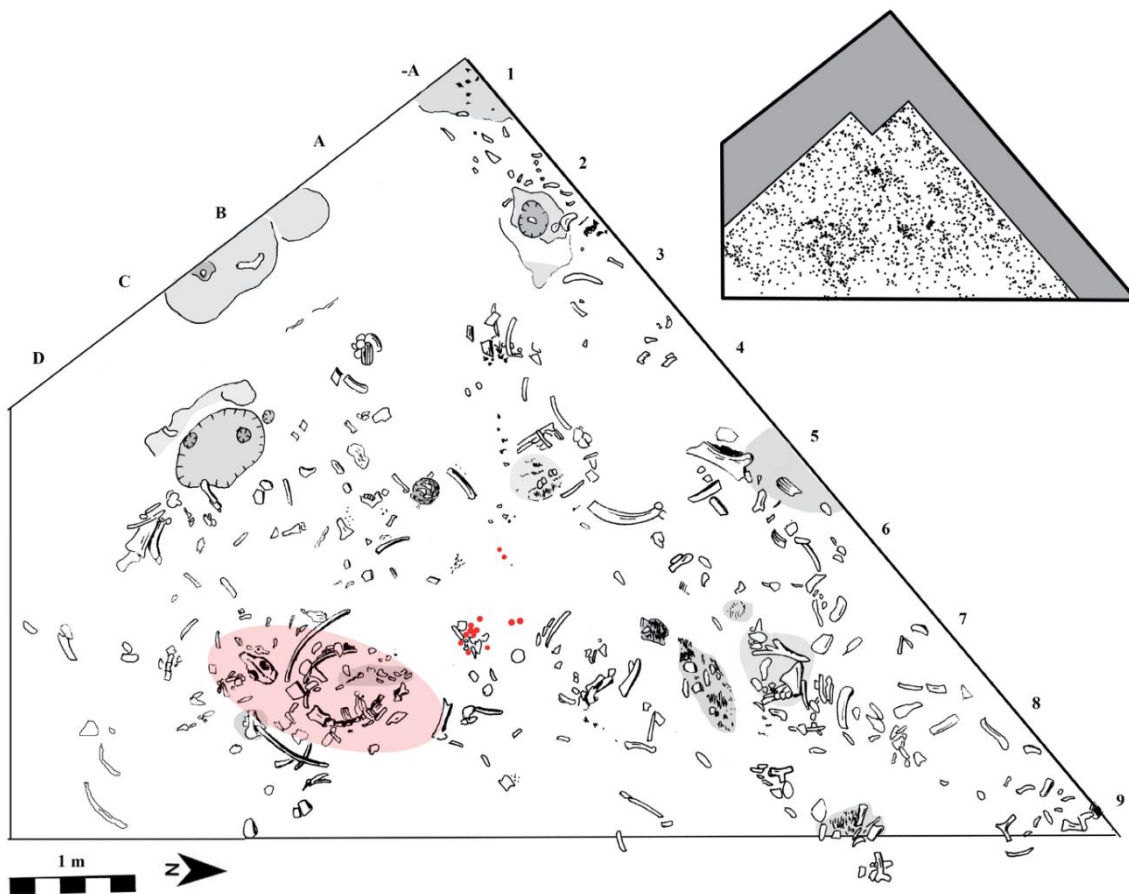
Fig. 8.4: Pavlov I, area A. Plan of the whole area A excavated in 2013-2015 (bigger plan, left) and density of 3D recorded finds from 2013-2014 (smaller plan, upper right) with area extension in 2015 (smaller plan, upper right, dark grey). The red oval represents the find of a wolf skeleton and its surrounding, red dots are recorded finds of shells, the grey areas represent hearth and charcoal concentrations (*Svoboda – Novák – Sázelová 2016*, 45, Fig. 16).

A significant feature of this area is the almost complete articulated wolf skeleton (*Canis lupus*) deposited approximately 1.2 m from the hearth (Fig. 8.5). A wolf skull, lying approximately 40 cm from the skeleton most probably belongs to the same individual. As further analysis showed, this individual suffered from blunt force trauma, later associated with inflammatory processes in both the middle and inner ears, tympanic bullae and the surrounding area. He most probably survived long enough (i.e. several weeks) for the healing process in the skull to progress significantly, however its behavioural expression must have been different and might have attracted the attention of the hunter-gatherers (*Sázelová et al. 2020*, 9-12). The surrounding of the wolf skeleton was circumscribed by a few mammoth ribs. Outside this area was an accumulation of dentalia shells (*Fissidentalium badense*) covered with ochre. However, they were deposited only about 80 cm from the wolf skeleton, so their association cannot be

165

excluded. Other fragments of animal skeletons were also dispersed in the area, namely fragments of ribs and long bones of mammoth (*Mammuthus primigenius*) and fragments of antlers and long bones of reindeer (*Rangifer tarandus*) (*Svoboda – Novák – Sázelová 2016*, 42; *Svoboda et al. 2016*, 97). As the area contains a huge amount of osteological material (to date around 10,000 NISP), which is still being processed, only long bones and their fragments belonging to reindeer (*Rangifer tarandus*) and wolf (*Canis lupus*) were analysed for fragmentation by the macroscopic method.

Fig. 8.5: Pavlov I, area A. Picture of partially complete postcranial skeleton of a wolf *in situ* most possibly belonging to the pathological skull deposited nearby (*Svoboda – Novák – Sázelová 2016*, 46, Fig. 17).

8.1.3.3 Area SE014

Settlement area SE014 is in the southeast part of the site and contains settlement unit S1 and the smaller pit S2 with adjacent activity zones (Fig. 8.6), and spatially complements the large oval agglomeration of objects K1-11 from the old excavation by *Klíma*. Settlement unit S1 is a shallow circle-shaped depression with a diameter of 5-6 m and is filled with anthropogenic sediments reaching 15-20 cm in the central part. Inside this unit is an asymmetrically located hearth around 70 cm in diameter, with a higher density of artefacts and charcoals (Fig. 8.7). The stratigraphy revealed two stages of filling, with fully developed Pavlovian on top (dated around 31 ky calBP) and older Gravettian at the bottom (dated around 33 ky calBP). The unit S2 is represented by an oval pit 1.2 m long and approximately 50 cm deep. Its depth makes it one of the rare cases in the Dolní Věstonice-Pavlov-Milovice settlement region. The feature was chaotically

filled with bones, sediment, artefacts, and ochre with a slightly red-coloured tusk fragment at the bottom. Dating confirmed relatively rapid filling of this pit around 30.1-31.6 ky calBP. Further to the east, another small and irregular hearth was found in the centre of the adjacent activity zone. In this whole area were dispersed fragments of molars, ribs and long bones of mammoth (*Mammuthus primigenius*), fragments of the axial skeleton and apical parts of the limbs of reindeer (*Rangifer tarandus*) and fragments of bones and teeth of various carnivore species (e.g. wolf, wolverine, fox) (*Svoboda – Novák – Sázelová 2016*, 40-41; *Svoboda et al. 2016*, 96-97). Since the amount of material and the state of processing is similar to that of area A, only long bones and their fragments belonging to reindeer (*Rangifer tarandus*) and wolf (*Canis lupus*) were subjected to fragmentation analysis by the macroscopic method.
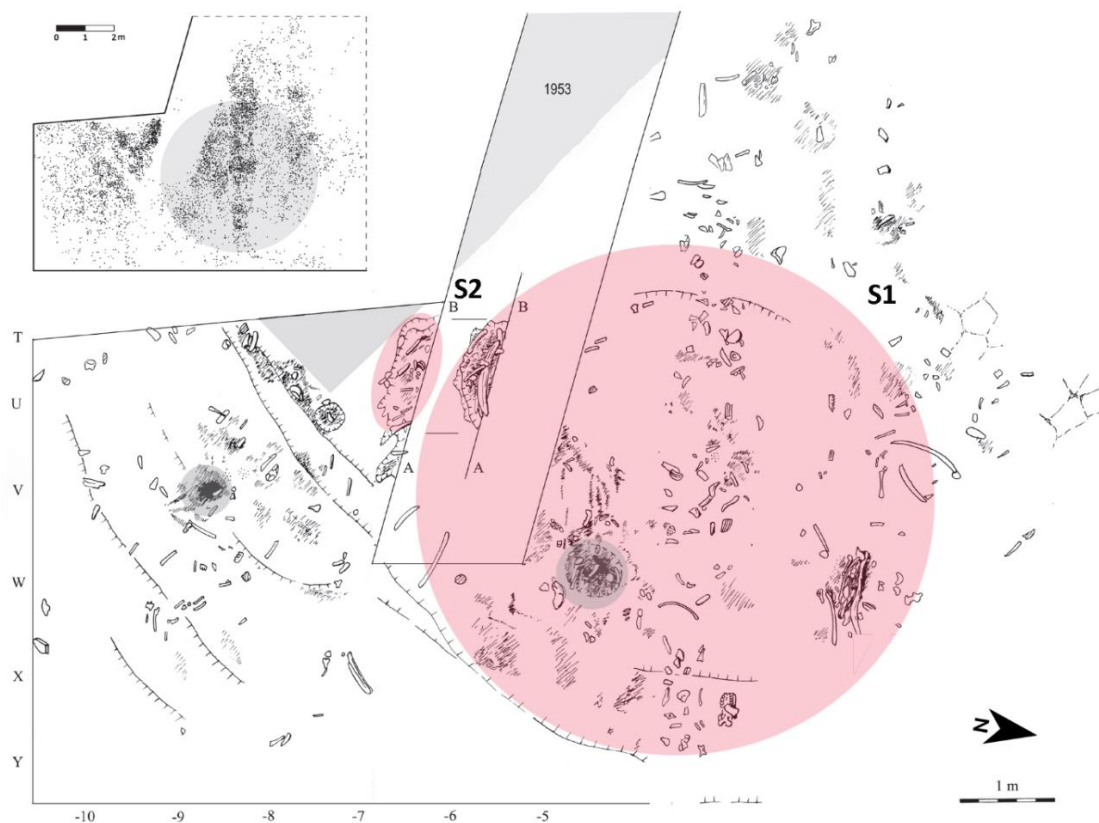
Fig. 8.6: Pavlov I, area SE014. Plan of the whole area with settlement unit S1and eccentrically placed hearth, pit S2, and adjacent activity zone with another hearth on the left. Units marked with a red circle/oval, hearths with grey circle. The distribution of 3D recorded finds is pictured in the upper left corner (*Svoboda – Novák – Sázelová 2016*, 43, Fig. 13, modified by SB).

Fig. 8.7: Pavlov I, area SE014. Eccentrically placed hearth with dense concentration of objects within settlement unit S1 (photo R. Hadacz).

8.2 Primary osteological data evaluation

Methods for the evaluation of primary data from archaeological assemblages used in this chapter are described in Chapter 6.1.

8.2.1 Area G

The osteological assemblage consisted of 1128 (NISP) bones, teeth, tusks, antlers and their fragments. More than 50% (NISP) of the assemblage was taxonomically identifiable. The unusually high proportion of taxonomically identifiable elements is given by the small range of the assemblage (asymmetry in the overall number of bones, teeth, antlers, tusks and their fragments) from this area in comparison to other areas, and the high representation of articulated skeletal elements in the find situation (see Fig. 8.2). From the identified species, the spectrum was dominated by woolly mammoth (*Mammuthus primigenius*), followed by significantly less represented species such as reindeer (*Rangifer tarandus*), wolf (*Canis lupus*), fox (*Vulpes vulpes/lagopus*), hare (*Lepus* sp.) and wolverine (*Gulo gulo*). Taxonomically unidentifiable material was classified into mammal size categories, from extra-large-sized mammals to microfaunal remains. The most abundant was the medium-sized mammal category. Fragments indeterminate to taxa, anatomical parts, or the animal size category represent almost 30%

168

(NISP) of the material. These were sorted into categories according to length in the longest axis of the fragment. The precise numbers and proportional representation are summarised in Tab. 8.1. All identified animal species, except for reindeer and fox, were represented by a minimum of one adult individual. In the case of reindeer, the MNI is 2, which is represented by juvenile individuals aged approximately between 15 and 48 months (according to bone fusion; *Takken Beijersbergen – Hufthammer 2012*). In the case of fox, one individual was a juvenile, under 6.5 months of age (according to bone fusion; *Harris 1978*); the second individual was an adult.

Species	NISP	NISP%	MNE	MNE%	MNI
Canis lupus	17	1.5	16	1.5	1
Gulo gulo	1	0.1	1	0.1	1
Vulpes vulpes/lagopus	10	0.9	10	1	2
Mammuthus primigenius	438	38.8	422	40.7	1
Rangifer tarandus	118	10.5	86	8.3	2
Lepus sp.	2	0.2	1	0.1	1
subtotal	**585**	**51.9**	**536**	**51.7**	**8**
extra-large sized mammal	5	0.4	5	0.5	0
extra/large-sized mammal	20	1.8	12	1.2	0
large-sized mammal	20	1.8	16	1.5	0
large/middle sized mammal	10	0.9	8	0.8	0
medium-sized mammal	129	11.4	105	10.1	0
medium/small-sized mammal	14	1.2	12	1.2	0
small-sized mammal	8	0.7	7	0.7	0
microfauna	2	0.2	2	0.2	0
subtotal	**209**	**18.5**	**168**	**16.2**	**0**
indeterminate bone fr. 10-5cm	4	0.4	4	0.4	0
indeterminate bone fr. 5-3cm	21	1.9	20	1.9	0
indeterminate bone fr. 3-2cm	48	4.3	48	4.6	0
indeterminate bone fr. 2-1cm	76	6.7	76	7.3	0
indeterminate bone fr. 1-0cm	184	16.4	184	17.8	0
indeterminate tooth fr. 1-0cm	1	0.1	1	0.1	0
subtotal	**334**	**29.6**	**332**	**32.1**	**0**
TOTAL	**1128**	**100**	**1036**	**100**	**8**

Tab. 8.1: Pavlov I, area G. Representation of the identified taxa, mammal size categories and indeterminate fragments, with basic quantitative information (author SB).

The fragmentation ratio (NISP:MNE; *Lyman 1994*) was highest for bones assigned to mammal size categories (1.24), followed by identified species (1.13; after removal of complete skeletal elements) and indeterminate fragments (1.01). The lower/closer to 1 the score, the higher the fragmentation intensity and fewer fragments

are assignable to a specific element or bone portion. The weathering stage was evaluated on 250 (MNE) specimens, containing the whole bones of larger fragments. Unequivocally prevalent were Stages 0 and 1, identified in more than 85% (MNE) of the analysed material (Tab. 8.2), suggesting a short time of exposition of the material on the surface and therefore good preservation. The intensity of root etching was evaluated in 269 (MNE) specimens. The total number of evaluated specimens is higher than in the weathering because it also includes fragments of antlers, teeth and tusks. The most prevalent are Stages 1-3, present in more than 70% (MNE) of the cases (Tab. 8.2). The observed stages may suggest that most of the affected fragments were shallow under the surface, reachable for the plant root systems, but not exposed to intensive plant corrosion. Mineral surface concretions were quite common. Their presence was recorded in bones identifiable in the taxon or mammal size category. Manganese concretions were present in 223 (NISP)/164 (MNE) bones and their fragments in various forms, from individual small dots consisting of a few crystals to continuously covered parts of the surface of manganese lines.

	wsNISP	wsNISP%	wsMNE	wsMNE%	reNISP	reNISP%	reMNE	reMNE%
Stage 0	136	42.6	120	48.0	36	10.5	30	11.2
Stage 1	119	37.4	93	37.2	112	32.7	92	34.2
Stage 2	29	9.1	19	7.6	91	26.5	75	27.9
Stage 3	25	7.8	12	4.8	87	25.4	59	21.9
Stage 4	10	3.1	6	2.4	8	2.3	7	2.6
Stage 5	0	0	0	0	9	2.6	6	2.2
TOTAL	**319**	**100**	**250**	**100**	**343**	**100**	**269**	**100**

Tab. 8.2: Pavlov I, area G. Summary of observed weathering (ws) and root etching (re) stages (author SB).

Concerning other taphonomical changes, I observed different levels of burning. Together, 95 (NISP) bone and tusk fragments showed signs of burning. All six stages (*Stiner et al. 1995*) were represented. The most abundant was the highest (6) level of burning, which included altogether 39 (NISP) fragments, followed by level 5 with 21 (NISP) fragments, level 3 with 15 (NISP) fragments, level 2 with 9 fragments, level 4 with 8 (NISP) fragments and finally level 1 with 3 (NISP) fragments. The representation of fragments including compact, spongy and both types of bony tissue is illustrated in Graph 8.1. The burnt tusk fragment was identified in only one case, in level 2, and was added to the group of compact bone fragments.
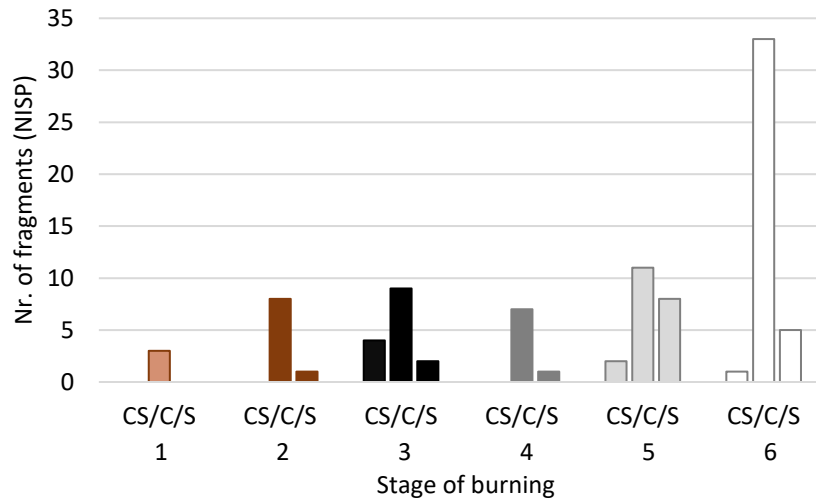
Graph 8.1: Pavlov I, area G. Representation of individual burning stages according to *Stiner et al.* (*1995*) in the observed assemblage. CS = fragments including compact and spongy bone, C = fragments including only compact bone, S = fragments including only spongy bone (author SB).

There were only a few taphonomic traces of intentional human activity. Cutmarks were identified in the tooth fragment of a large-sized carnivore (Fig. 8.8a) and the lumbar vertebra fragment of a juvenile medium-sized mammal (Fig. 8.8b). Possible points of impact were present in five (MNE) cases of bone and tusk fragments (Fig. 8.9). Gnawing by carnivores was scarcely present and was identified on 17 (MNE) fragments of bones, antlers and tusk (Fig. 8.10).
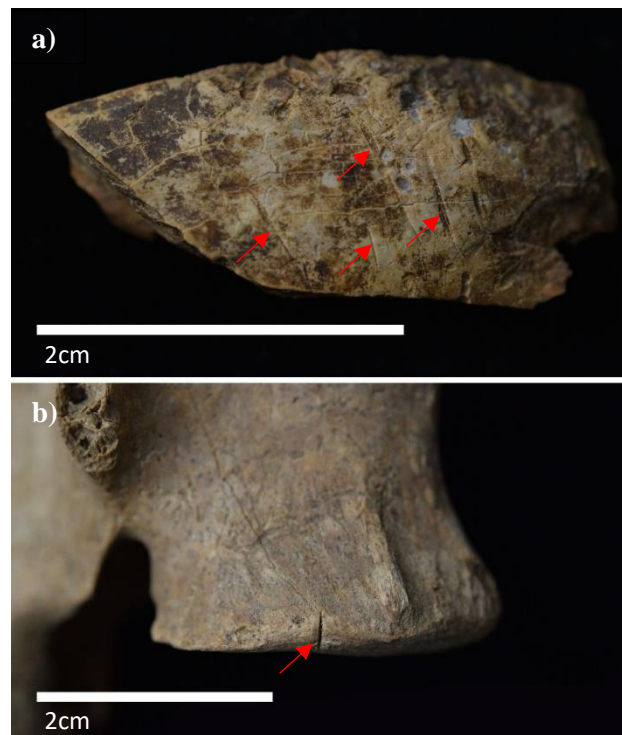
Fig. 8.8: Pavlov I, area G. Cutmarks on fragment of a tooth (a) and caudal extremity of lumbar vertebra (b), indicated by red arrows (photo SB).

Fig. 8.9: Pavlov I, area G. Percussion pit of ovoid shape on the left and percussion notch with heavily corroded inner bevelling on the right are indicated by red arrows (photo SB).

Fig. 8.10: Pavlov I, area G. Fragment of antler bearing marks, most possibly, caused by carnivore gnawing on both sides, indicated by red arrows (photo SB).

I state the specific skeletal representation, for the two chosen species. From the reindeer bones, I identified a few skull and antler fragments and from teeth only one fragmentary deciduous lower fourth premolar was present. The most represented was the axial skeleton including the *atlas*, *axis*, cervical and thoracic vertebrae. From the front limb, I identified fragments of the humerus, radio-ulna, and the third metacarpal. From the hind limb, fragments of the femur, tibia, patella, and tarsal bones were present. All types of phalanges were present, including accessorial phalanges. One fragment of closely unidentified metapodial and two sesamoid bones were also present. The side

determination can be found in Tab. 8.3. In the wolf material, I identified one permanent lower first incisor. The rest of the material contained all three types of phalanges and metacarpal bones I-V. Their summary and side determination are listed in Tab. 8.4.

The abundance of specific skeletal parts in the context of all three observed archaeological areas is presented in Fig. 8.11. The percentage of proportional representation was calculated in the context of the overall abundance from the area richest in identified reindeer and wolf bones (for both species area SE014). The low representation of skeletal parts present, the maximum up to 3.8% for reindeer and 1.3% for wolf, reflects the small size of the area and the small number of bones identified in these species. In the case of reindeer, representation of a wider variety of skeletal elements can be observed, whereas, for wolf, the scope of representation is very narrow and specific.

	NISP dx.	MNE dx.	NISP sin.	MNE sin.	NISP indet.	MNE indet.
Cranium	0	0	0	0	17	14
Antler	0	0	0	0	13	8
Atlas	0	0	0	0	1	1
Axis	0	0	0	0	1	1
Vertebra **C**	0	0	0	0	9	5
Vertebra **Th**	0	0	0	0	14	5
Humerus	0	0	1	1	0	0
Radio-ulna	3	1	4	2	0	0
Metacarpus III	0	0	0	0	1	1
Femur	0	0	6	3	1	1
Patella	0	0	0	0	1	1
Tibia	5	3	0	0	0	0
Os tarasale	2	2	5	5	0	0
Phalanx I	5	5	3	3	0	0
Phalanx II	3	3	4	4	0	0
Phalanx III	3	3	2	2	0	0
Metapodium III	0	0	0	0	1	1
Os sesamoideum	0	0	0	0	5	5
Accessory *phalanx*	0	0	0	0	4	4
Dens **dp**	3	1	0	0	0	0

Tab. 8.3: Pavlov I, area G. List of identified skeletal elements of reindeer, dx. = dexter, sin. = sinister, indet. = indeterminate to side, dp = deciduous premolar (author SB).

	NISP dx.	MNE dx.	NISP sin.	MNE sin.	NISP indet.	MNE indet.
Phalanx I	0	0	4	4	0	0
Phalanx II	0	0	3	3	0	0
Phalanx III	0	0	0	0	1	1
Metacarpal I	1	1	0	0	0	0
Metacarpal II	0	0	1	1	0	0
Metacarpal III	0	0	1	1	0	0
Metacarpal V	0	0	3	2	0	0
Dens I	1	1	0	0	0	0

Tab. 8.4: Pavlov I, area G. List of identified skeletal elements of wolf, dx. = dexter, sin. = sinister, indet. = indeterminate to side (author SB).

8.2.2 Area A

The osteological assemblage from this area is still being subjected to processing and therefore the stated information serves only to describe the character of the assemblage. The area contains more than 10,000 (NISP) bones, teeth, tusks, antlers and their fragments recorded in a 3D system or recovered from wet sieving. The spectrum of identified species is much wider compared to area G. From the herbivorous species, I identified woolly mammoth (*Mammuthus primigenius*), woolly rhinoceros (*Coelodonta antiquitatis*), moose (*Alces alces*), reindeer (*Rangifer tarandus*), horse (*Equus* sp.) and alpine ibex (*Capra ibex*). Carnivorous species are represented by wolf (*Canis lupus*), fox (*Vulpes vulpes/lagopus*), and wolverine (*Gulo gulo*). Bones from hare (*Lepus* sp.) and birds were also identified. The proportion of taxonomically identifiable specimens is approximately 23%, and is significantly lower in comparison to area G. Nevertheless, the proportion of individual species within this category is very similar. The most represented is the woolly mammoth, notably dominating the assemblage. This is followed by reindeer and wolf, whose abundance seems to be balanced in the current state, with a slight predominance of reindeer. Different stages of weathering, root etching, mineral staining and burning are being also identified in the assemblage from this area although they are not presented in this thesis.

In the series of reindeer bones, I identified multiple cutmarks, present in the bones of the hind limb in the tarsal articulation, one vertebra and an antler fragment. Their position suggests that they are remnants of butchering or skinning activities. In a few cases, impact points were also identified, again mostly on bones of hind limb (*tibia*,

metatarsus III). In wolf bones, intentional human activity was identified through a series of cut marks present on the distal part of the humerus and two perforated incisal teeth.

The proportional representation of individual skeletal parts within these two species is illustrated in Fig. 8.12. The representation of cranial and postcranial skeletal parts is quite balanced in both species, and the percentages are also in the lowest given category. In the case of reindeer, there is a significantly higher proportion of antlers represented in this area. This could indicate selective or specialised processing of reindeer remains in this area. For wolf remains, a higher proportion can be recognised in the thoracic part of the axial skeleton. This may be caused by the presence of the nearly complete wolf skeleton/burial, which allowed me to assign the vertebrae and ribs specifically to this species. The preliminary estimated minimum number of individuals is 10 (MNI) for reindeer and 5 (MNI) for wolves. In both cases, juvenile individuals are also represented.

8.2.3 Area SE014

Similarly, as in area A, the archaeozoological assemblage from this area is subjected to current processing as a part of project realisation, and the final data are therefore not available. To illustrate at least the character of the assemblage in comparison to previous areas, the following information is stated. The area contains over 16,000 (NISP) bones, teeth, tusks, antlers and their fragments recorded in the 3D system or recovered from wet sieving. The representation of individual species is very similar to the one observed in area A with a denser amount of osteological material. Herbivore species are represented by woolly mammoth (*Mammuthus primigenius),* reindeer (*Rangifer tarandus*), horse (*Equus sp.*), and alpine ibex (*Capra ibex*). Carnivorous species include wolf (*Canis lupus*), wolverine (*Gulo gulo*), and fox (*Vulpes vulpes/lagopus*). From other species, I identified bones belonging to hares (*Lepus* sp.) and birds. Information about the weathering stage, the intensity of root etching and mineral staining, and the levels of burning are being collected, however, are not presented in this thesis.

To date, in the reindeer bone assemblage, I mainly observed sets of cut marks mainly on tarsal (e.g. *os centroquartale*) and metapodial bones. The impact points were identified in multiple cases, again mainly on metapodial bones, and individually on tibia and radio-ulna. In the case of wolf bones, no significant traces indicating intentional human manipulation have yet been identified.

The proportional representation of individual skeletal parts for reindeer and wolf is pictured in Fig. 8.13. As this area represents the most abundant assemblage of material assigned to the two chosen species, the percentages for specific skeletal elements are the highest of the three areas of interest. For reindeer, antlers, tarsal bones, and phalanges were more significantly represented. The rest of the skeleton is represented within the lowest percentage category, and the bones of the *pelvis* are completely missing. For wolf remains, the situation is slightly different. The most represented are the first phalanges and the tarsal bones, followed by the second phalanges, the tibia, the bones of limb girdles, the caudal vertebrae, the skull and the lower premolars. Higher representation of these skeletal elements is interesting since in most cases they represent bones with high amounts of spongious bone and/or a thin layer of compact bone, making them more prone to taphonomic destruction. The higher number of small autopodial bones could also indicate a specific type of body treatment/exploitation within this species. The estimated minimum number of individuals is 13 (MNI) for reindeer, and 7 (MNI) for wolves. Juvenile individuals were also present in both cases.

Fig. 8.11: Pavlov I, area G. Silhouettes of reindeer (left) and wolf (right) showing the representation of individual skeletal elements. The percentage ranges of representation from the total highest amount of identified bones for reindeer is given on the left side of the legend; for wolf on the right side of the legend. Representation of repetitive skeletal elements (e.g. *vertebrae*, *ossa carpalia*, *ossa tarsalia*, *phalanges*) were evaluated and marked in generalised groups. The ribs were always assigned only to the mammal size category, and so are not displayed in the scheme to avoid false species-specific under/over representation of this skeletal part. Note the very specific representation in wolf, narrowed to the front paw and one lower incisor (silhouettes from *ArchéoZoo - Vectorised skeletons*; modified by SB).

Fig. 8.12: Pavlov I, area A. Silhouettes of reindeer (left) and wolf (right) showing the representation of individual skeletal elements. The percentage ranges of representation from the total highest amount of identified bones for reindeer is given on the left side of the legend, for wolf on the right side of the legend. Representation of repetitive skeletal elements (e.g. *vertebrae*, *ossa carpalia*, *ossa tarsalia*, *phalanges*) were evaluated and marked in generalised groups. In the case of area A, only ribs from the articulated wolf skeleton were considered, as they were easily assignable to the species. Note the high representation of antlers in reindeer and the slightly higher representation of thoracic column in wolf (silhouettes from *ArchéoZoo - Vectorised skeletons*; modified by SB).

178

Fig. 8.13: Pavlov I, area SE014. Silhouettes of reindeer (left) and wolf (right) showing the representation of individual skeletal elements. The percentage ranges of representation from the total highest amount of identified bones for reindeer is given on the left side of the legend, for wolf on the right side of the legend. The representation of repetitive skeletal elements (e.g. *vertebrae*, *ossa carpalia*, *ossa tarsalia*, *phalanges*) were evaluated and marked in generalised groups. Ribs were always assigned only to the mammal size category, and so are not displayed in the scheme to avoid false species-specific under/over representation of this skeletal part. Note the higher representation of antlers, tarsal bones, and phalanges in reindeer. A significantly higher representation can be observed in autopodial elements, tibia, caudal vertebrae and in the flat bones of wolf (silhouettes from *ArchéoZoo - Vectorised skeletons*; modified by SB).

179

8.3 Detailed analysis of fragmentation

The macroscopic method of fragmentation analysis (FFI) was applied to all previously mentioned areas from the Pavlov I site. Besides FFI, the data were complemented by fracture history profiling (*Johnson – Parmenter – Outram 2016*). This method is based on the proportional representation of different types of fractures (fresh, dry, mineralised) and their combinations. In this way, it is possible to capture the range of fragments which have undergone the fragmentation process more than once, in different kinds of preservation and so represent a comprehensive record of a wider variety of taphonomic activities influencing the material or site as a whole (*Johnson – Parmenter – Outram 2016*, 624). The microscopic methods were tested on chosen fragments from area G. The small range of the sample/set for microscopic analysis was given by the setting of the external cooperation and availability of electron microscopes influenced by Covid-19 restrictions. I found the number of 10 samples to be satisfactory for verifying the applicability of the chosen methods to archaeological material. Even sample of this range displayed the potential of the presented approach in the archaeological analysis, however, guided by further experimental practice and extension of the comparative collection for its meaningful application. The treatment concerning the preparation for SEM and histological analysis was almost identical to the experimental samples; the minor differences are reported in the respective chapter (9.3.2).

8.3.1 Macroscopic observation

8.3.1.1 Area G

In area G, all long bone fragments ≥ 2cm were evaluated for FFI calculation and fragmentation history profiling. Altogether, 113 (NISP) fragments (10% of the whole assemblage) were analysed; the list can be found in the supplementary material (Supplement 13). The mean FFI value is **3.7**, which is slightly higher than the limit value for fresh bone fragmentation. The most represented index value (modus) was **6**, followed by a significantly lower value of 2 (Graph 8.2). From the index representation I would expect the fragmentation in this area to be mainly in the dry state by depositional and post-depositional activities. Nevertheless, if visualising the fragmentation history profile, it can be observed that more than 50% of the material is bearing fresh fractures or a combination of fresh with dry or mineralised fractures (Graph 8.3).
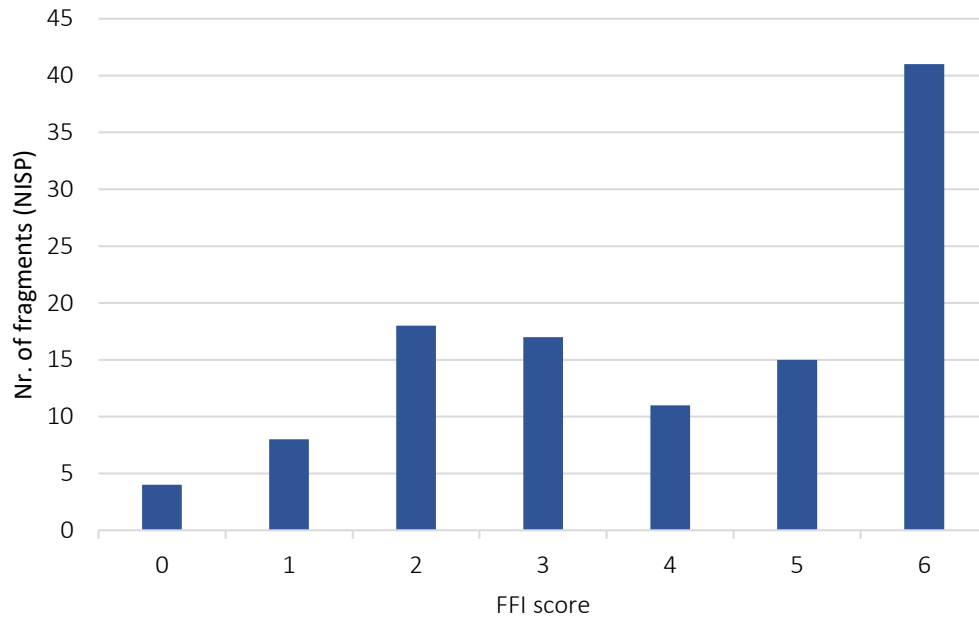
Graph 8.2: Pavlov I, area G. Proportion of FFI representation in the group of all evaluated fragments (author SB).
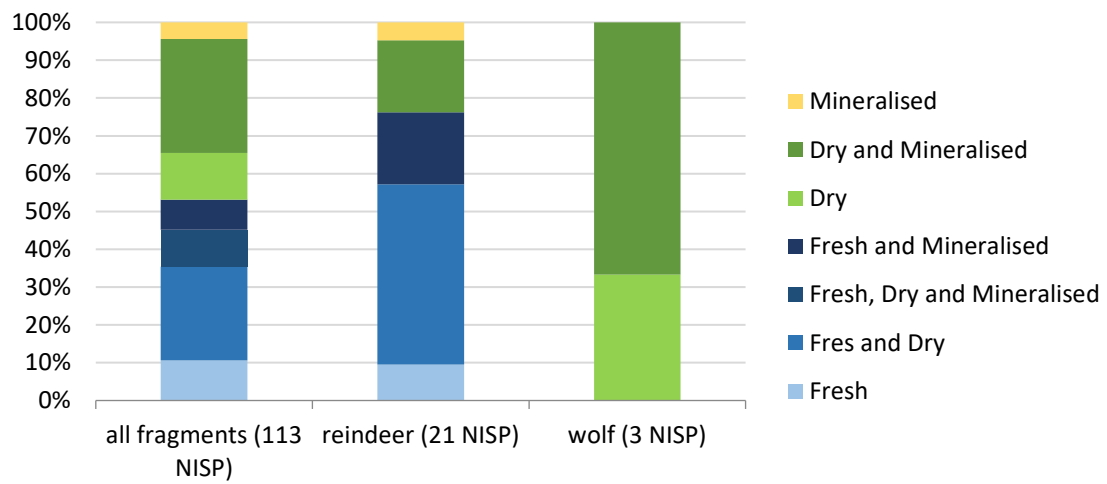
Graph 8.3: Pavlov I, area G. Fragmentation history profiles for all fragments and chosen animal species (author SB).

The proportional index representation changes significantly if considering reindeer and wolf bones separately. In the case of reindeer, 21 (NISP) fragments were evaluated. The mean value is **2.7**, which corresponds better with fresh bone fragmentation and exploitation. The modus value is **3**, and also greatly represented are values lower than 3 (Graph 8.4). The proportion of bones bearing fresh fractures or their combination is around 75% (Graph 8.3). In the case of wolves, only 3 (NISP) fragments were indexed, the mean value is **5.5**, represented are values **5** (modus value) and 6 (Graph 8.4). These values match with the dry depositional or post-depositional nature of fragmentation. The fragmentation history profile similarly showed only fragmentation in a dried and mineralised state (Graph 8.3).
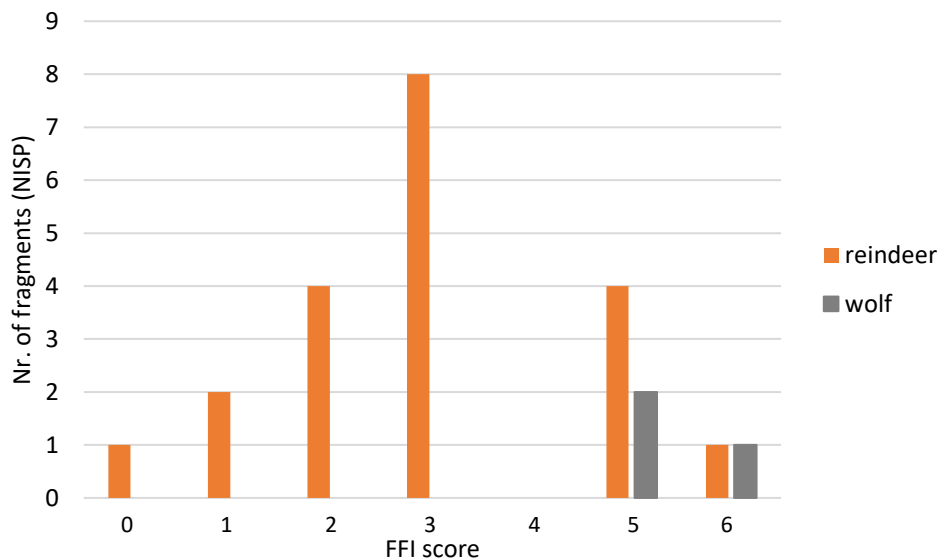
Graph 8.4: Pavlov I, area G. Representation of individual index values in reindeer and wolf bones (author SB).

8.3.1.2 Area A

In this area I analysed long bones and their fragments ≥ 2 cm belonging to reindeer and wolf (Supplement 14). In the case of reindeer, I calculated the mean index value from 96 (NISP) fragments and obtained the score **4**. This value is higher than would be expect in assemblage fragmented in the fresh state. However, the representation of individual values shows that the most represented (modus value) was score **3**, followed by score 6 (Graph 8.5). The fragmentation history profiling indicates that more than 50% of the observed material possesses the characteristics of fresh bone fragmentation (Graph 8.6). This means that the high average value of the index is caused by the rich taphonomic

history of the assemblage. In the case of wolves, I examined 46 (NISP) fragments obtaining the mean FFI value **5.4**, the modus value is **6**. The average and the proportional representation of FFI scores are virtually the same as observed in area G (Graph 8.5). The fragmentation history profile shows the representation of dry and mineralised fracture characteristics. In less than 5% of the material also characteristics of fresh bone fragmentation were identified (Graph 8.6). In comparison to area G, the wolf material from this area also bore other traces after intentional human manipulation, such as cutmarks at the long bone epiphyses or perforation of the teeth.
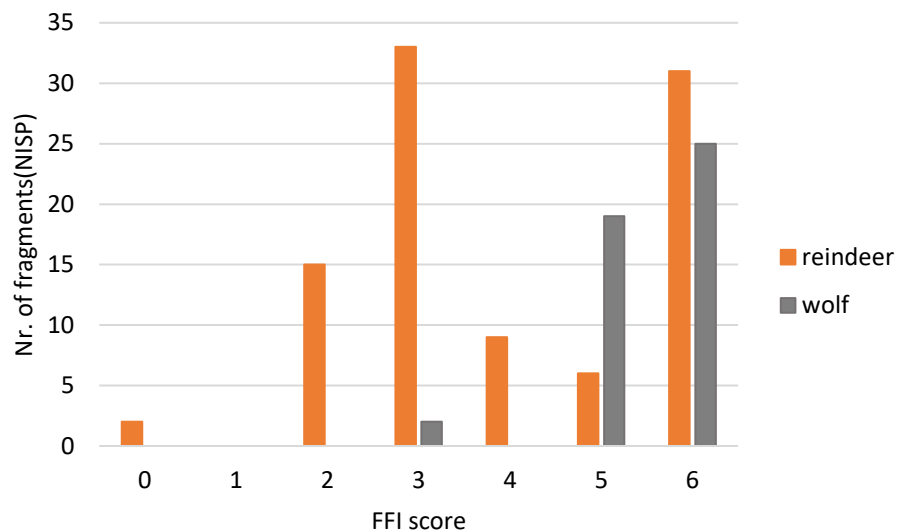
Graph 8.5: Pavlov I, area A. Representation of individual index values in reindeer and wolf bones (author SB).
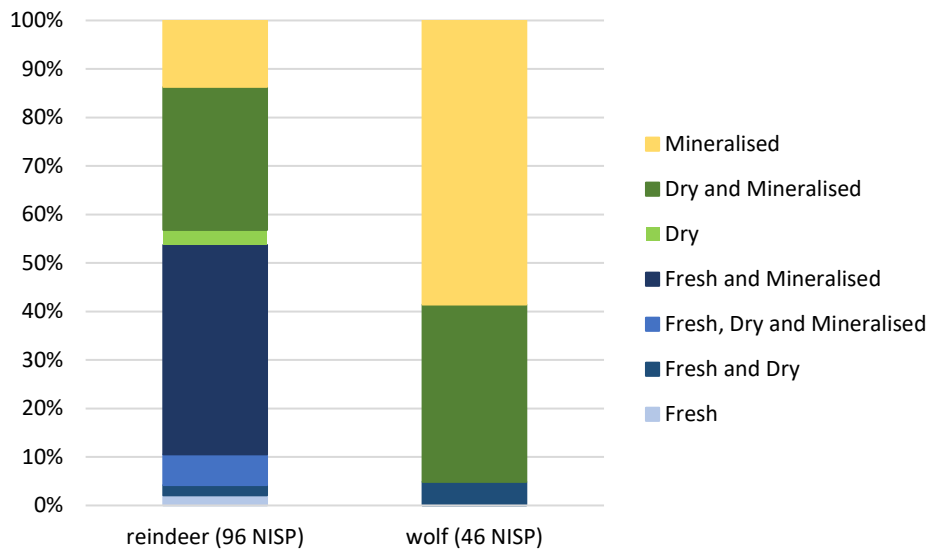
Graph 8.6: Pavlov I, area A. Fragmentation history profiles for chosen animal species (author SB).

8.3.1.3 Area SE014

Concerning this area, I again analysed the reindeer and wolf long bones and their fragments ≥ 2 cm (Supplement 15). The mean value of the index for reindeer was calculated from 107 (NISP) fragments and is **3.8**, the modus value is **6**. The mean value is higher similar to area A although other traces of intentional human activity such as cut marks or impact points were present in osteological reindeer material. The distribution of the individual index values is concentrated around the score 3, and also quite abundant is score 6 (Graph 8.7). The profile of fragmentation history shows that around 50% of the material possesses the characteristics of fresh fragmentation (Graph 8.8). In the case of wolves, together 78 (NISP) fragments were evaluated and the mean FFI in this area is **5.2**, the modus value is **6**. The mean value is slightly lower than in the previously observed areas. The distribution of individual values also differs an also represented are low values of the index (Graph 8.7). The fracture history profile indicates that more than 10% of the observed fragments bear characteristics of the fresh fracturing (Graph 8.8).
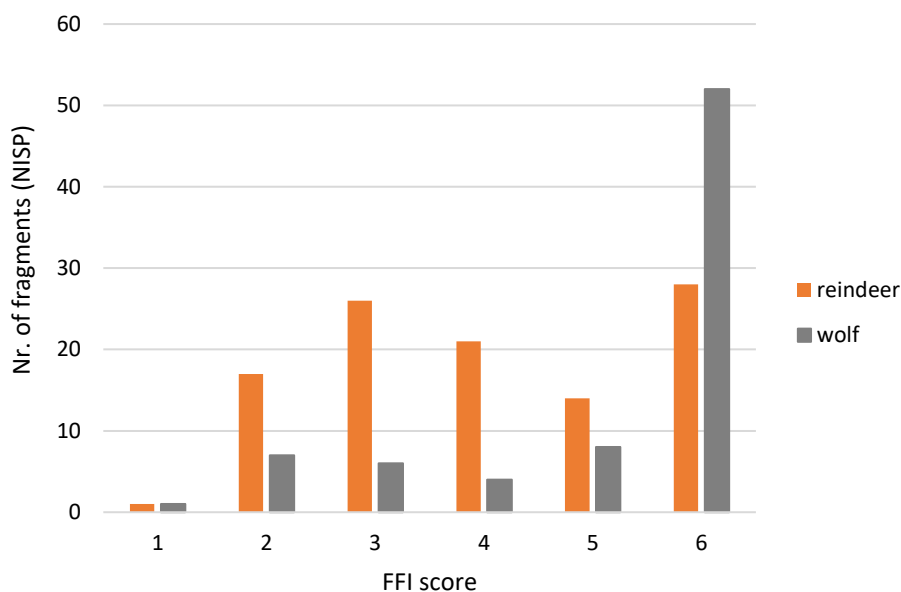
Graph 8.7: Pavlov I, area SE014. Representation of individual index values in reindeer and wolf bones (author SB).
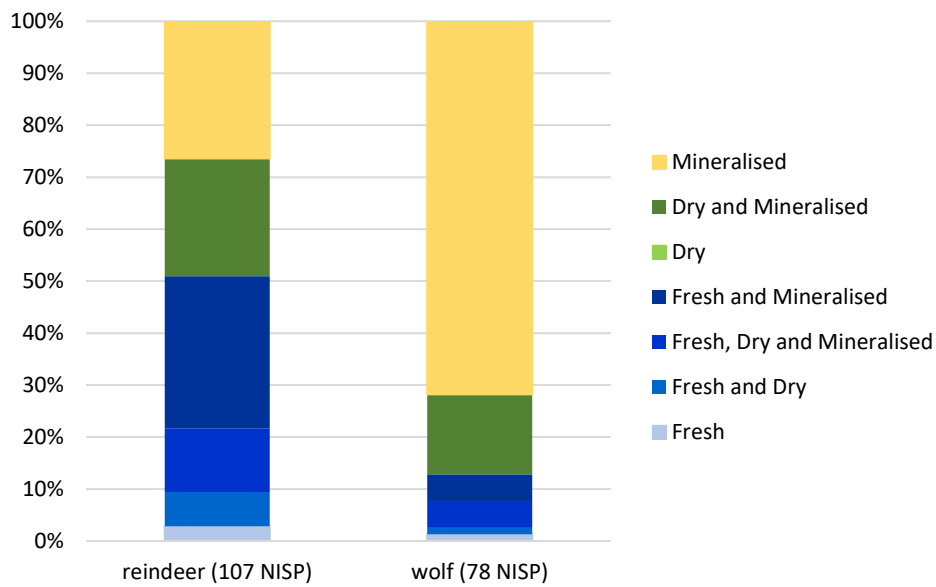
Graph 8.8: Pavlov I, area SE014. Fragmentation history profiles for chosen animal species (author SB).

Since this area provided the highest amount of fragmented material for both the observed species, I tested whether there is any relationship between the spatial placement of individual fragments and their FFI value. Fig. 8.14 illustrates that there is a certain accumulative tendency for individual species. Reindeer bones form a small concentration near the hearth; the rest are more or less evenly dispersed within the area. On the contrary, wolf bones tend to accumulate on the periphery and outside of the settlement area. However, no clear pattern can be recognised when observing the distribution of individual index values (see also *Boriová et al. in press*).
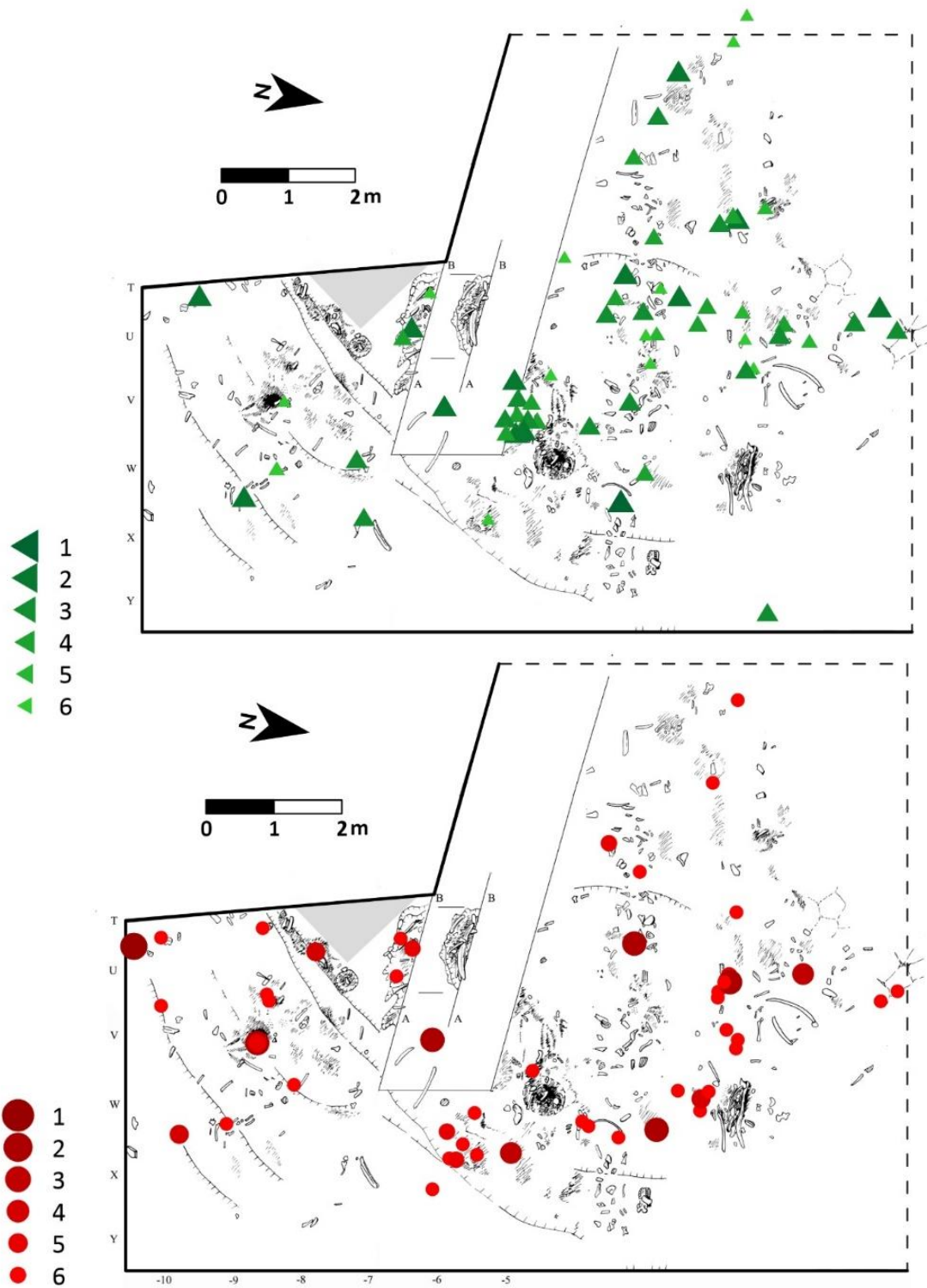
Fig. 8.14: Pavlov I, area SE014. Spatial placement of fragments evaluated by FFI. The upper diagram is for reindeer bones (green triangles), the lower diagram for wolves (red dots) (*Svoboda – Novák – Sázelová 2016,* 43, Fig. 13; modified by M. Novák and SB).

186

8.3.2 SEM analysis, area G

I chose ten samples (A1-A10) for a detailed analysis. Closely unidentified long bone diaphysis fragments were sampled; the only exceptions were samples A5 and A8 (see Tab. 8.5). Longitudinal and spiral fracture surfaces are represented although their proportion is unbalanced. The choice of fragments suitable for detailed analysis was limited by the state of the fracture surface preservation. In the selection process, I used a stereomicroscope Nikon SMZ1500 with a Nikon D7000 camera to ensure that the selected specimens have at least some of the original fracture surfaces preserved (Fig. 8.15).

Fig. 8.15: Sample A3. State of surface preservation in an archaeological sample. The red arrows point to areas with surface corrosion. The areas in red circles represent the original preserved structure of FS, scale bar 1000 µm (photo SB).

In many cases, the surface was most possibly modified by plant root corrosion or sediment movement/contact. These changes are reported in the results (Chapter 8.3.2 and 8.3.3). In general, the manipulation of archaeological material in the preparation process (cleaning, sampling, mounting in SEM) was more complicated due to its state of preservation. The additional wet cleaning before sampling caused further widening of weathering cracks or introduced a new one. These were causing other difficulties while cutting or dehydrating the samples for SEM and histological analysis (cracking of the samples and falling apart). The list of samples and their description is in Tab. 8.5. The

summary of the main features observed by electron microscopy can be found in Tab. 8.6 at the end of Chapter 8.3.3.

Sample	Skeletal element	Species/mammal size category	FFI score	Fracture surface (FS)	Histological section thickness
A1	LB diaphysis fragment	MSM	2	spiral	66 μm
A2	LB diaphysis fragment	MSM	3	spiral	60 μm
A3	LB diaphysis fragment	MSM	1	longitudinal	49 μm
A4	LB diaphysis fragment	M-LSM	1	longitudinal	69 μm
A5	*humerus*	MSM	3	spiral	67 μm
A6	LB diaphysis fragment	MSM	1	spiral	57 μm
A7	LB diaphysis fragment	MSM	1	spiral	62 μm
A8	*radius*	*Rangifer tarandus*	2	spiral	68 μm
A9	LB diaphysis fragment	MSM	4	longitudinal	68 μm
A10	LB diaphysis fragment	MSM	2	spiral	68 μm

Tab. 8.5: List of samples from the Pavlov I site, area G, subjected to SEM and histological treatment and analysis. Designation of the sample (simple without coding), skeletal element, species/mammal size category, FFI score, type of observed fracture surface and thickness of the section are listed. Abbreviations: LB = long bone, MSM = medium-sized mammal, M-LSM = medium to large-sized mammal (author SB).

All the observed samples were burdened by surface modifications most probably related to depositional and post-depositional taphonomic changes. These were represented by oval or polymorph-shaped depressions clearly bordered from the rest of the surface. These depressions are most reminiscent of root imprints on the macroscopic level. In the depressions, numerous microcracks are present, and generally respect the lamellar bone structure and have rather rounded edges (Fig. 8.16). In one case, the presence of fibre (possibly a root remnant) in such a depression was observed (Fig. 8.17). Another trait is represented by thin and shallow scratches/imprints with various parallel and subparallel orientations (Fig. 8.18). These could be related to the movements in sediment. Also, the overall smoothness of surface texture, sometimes more expressed in individual areas and not generally on the surface, was assigned to depositional and post-depositional modification (Fig. 8.19). In many cases, granular areas were observed (Fig. 8.20), although these were also present in experimental samples and therefore are most probably not related to the depositional and post-depositional changes. Due to the above-mentioned changes, it was difficult to systematically observe the traits noticed in the experimental samples.
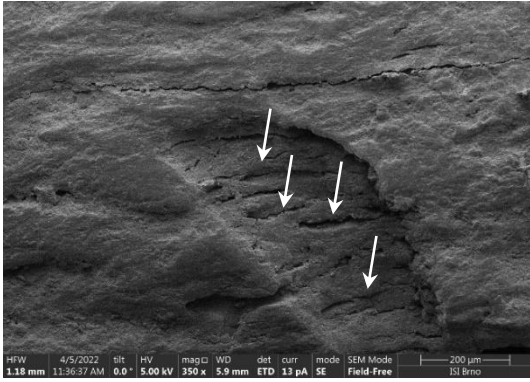
Fig. 8.16: Sample A5. Oval depression in FS with a concentration of microcracks parallel to the lamellar orientation (white arrows). Magnification 350×, scale bar 200 µm (photo SB).

Fig. 8.17: Sample A5. Remnant of fibre-like unit/body (white arrows) present in a surface depression. Magnification 1500×, scale bar 50 µm (photo SB).

Fig. 8.18: Sample A1. Parallel and subparallel lines (white arrows) present on the fracture surface. Magnification 142×, scale bar 500 µm (photo SB).

189
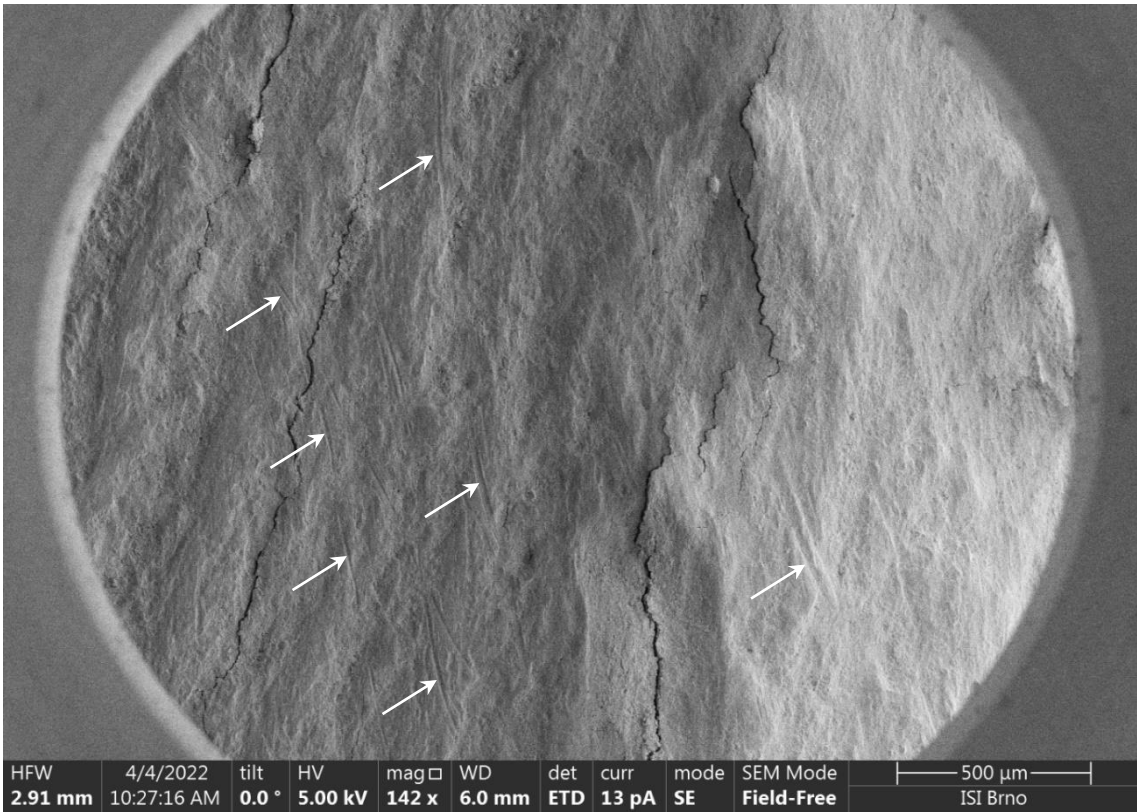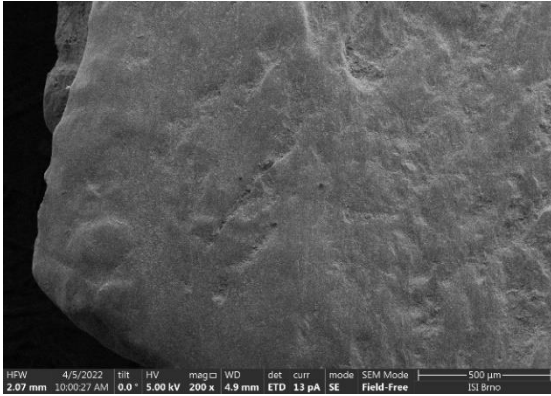
Fig. 8.19: Sample A9. Surface texture most probably smoothened by post-/depositional taphonomic changes. Magnification 200×, scale bar 500 µm (photo SB).
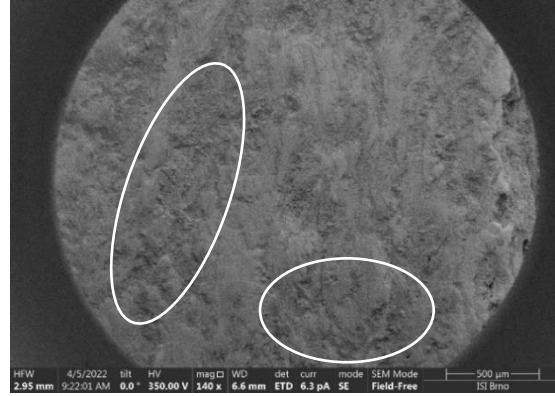
Fig. 8.20: Sample A9. Granularities marked by white ovals. Magnification 140×, scale bar 500 µm (photo SB).

In samples from longitudinal FS, the linear pattern was present only locally and no fan-shaped pattern was identified. Transversally oriented surface ridges forming a tidal wave surface pattern (Fig. 8.21) were present. The microcracking was highly variable in width, length and course. In most cases, the cracks respected the lamellar structure of the bone although an irregular and twisting course of fractures was also present (Fig. 8.22 and 8.23). The biggest microfracture concentrations were observed in surface depressions related to post/depositional changes. In comparison to other microfractures, they have mostly rounded and granular edges and so it can be assumed that they may have emerged before or at the same time as the depressions and are somehow related (Fig. 8.24). In some cases, small granules or crystals were present in the cracks, possibly representing grains of sediment. The long and wide longitudinal fractures mostly had very smooth walls and sharp edges distinct from those observed in surface depression microcracking (Fig. 8.23). In cases where the orientation of the fibres in a crack was observable, it was usually parallel with the course of the fracture. I did not observe any relation of these fractures to Haversian canals, Volkmann canals or osteons as reported in experimental samples. I suppose these longitudinal wide fractures are related to drying/weathering of the bone *in situ* or during post-excavation treatment they may have been further widened by cleaning and preparation for detailed analysis. In the overview images of longitudinal FS, the microfracturing was less apparent in comparison to spiral FS.
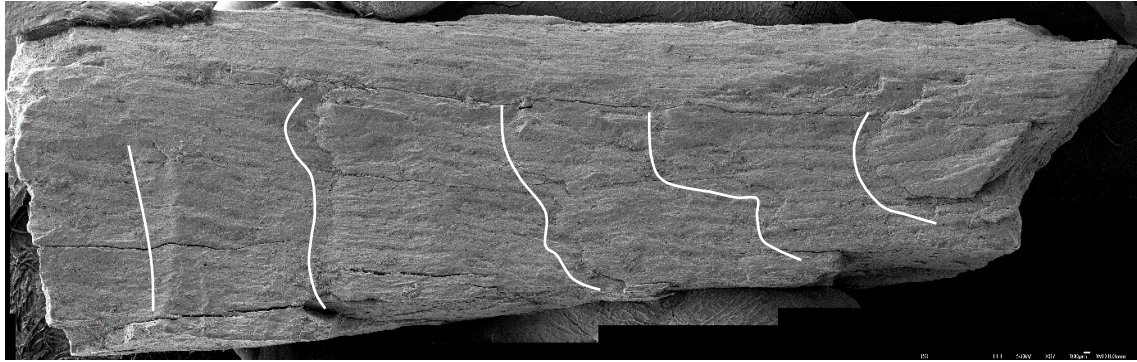
190

Fig. 8.21: Sample A4. Transversally oriented ridges on longitudinal FS indicated by white lines. Magnification 37×, scale bar 100 μm (photo Z. Pokorná and SB).
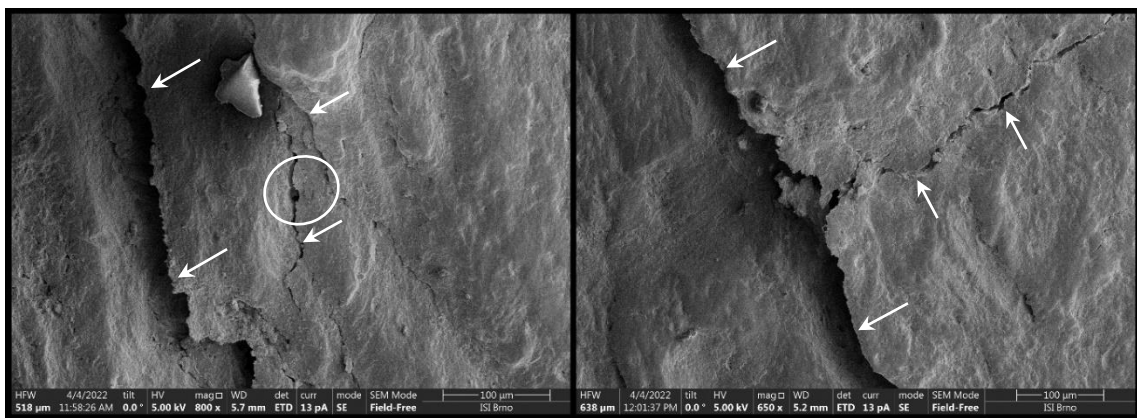
Fig. 8.22: Sample A2. The white arrows point toward microfractures with variable width and course. Interaction of microfracture with most probably the Haversian canal in the white circle. Magnification 800× (left), 650× (right), scale bar 100 μm (photo SB).
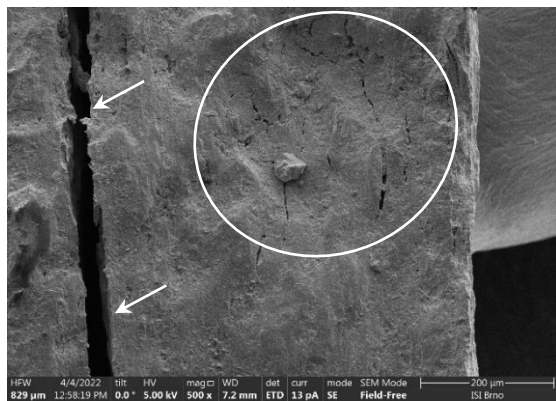
Fig. 8.23: Sample A10. Wide microfracture with sharp edges and smooth walls (white arrows). Thinner cracks with an irregular course present in surface depression (white oval). Magnification 500×, scale bar 200 μm (photo SB).
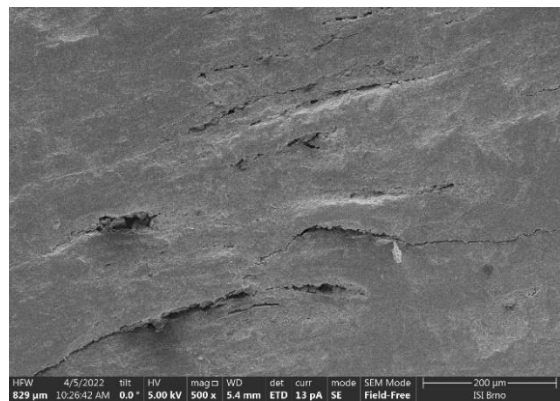
Fig. 8.24: Sample A3. Microcracks with rounded and granular edges present in the surface depression. Magnification 500×, scale bar 200 μm (photo SB).

In samples from spiral FS, the surface is mainly smooth in texture and variable in morphology. In some samples, the morphological shaping is more pronounced than in others although this can be caused by the variable intervention of post/depositional processes. The linear pattern was better preserved and widely observable throughout most of the sample surfaces (e.g. Fig. 8.25). The fan-shaped pattern typically observed in spiral FS from freshly fragmented bones was present in only three out of seven samples. Well pronounced and shaped was this pattern in sample A6 (Fig. 8.26), observable to the naked eye. In the other two samples (A1 and A5), only isolated signs of this pattern were identified. Similar to samples from longitudinal FS, more or less pronounced transversally oriented ridges and plate-like laminations were observed, in some cases lined by cracking (Fig. 8.27). As they were also present in experimental samples, I assume that they are related to the fragmentation process. Concerning microfracturing, the patterns were identical to those observed in samples from longitudinal FS. The relation of microcracking to Haversian canals or osteons was identified only scarcely. In sample A2, the microfracture cut right through what was probably the Haversian canal (Fig. 8.22), in sample A7, the openings of HC are present in the depression cracking (Fig. 8.28).
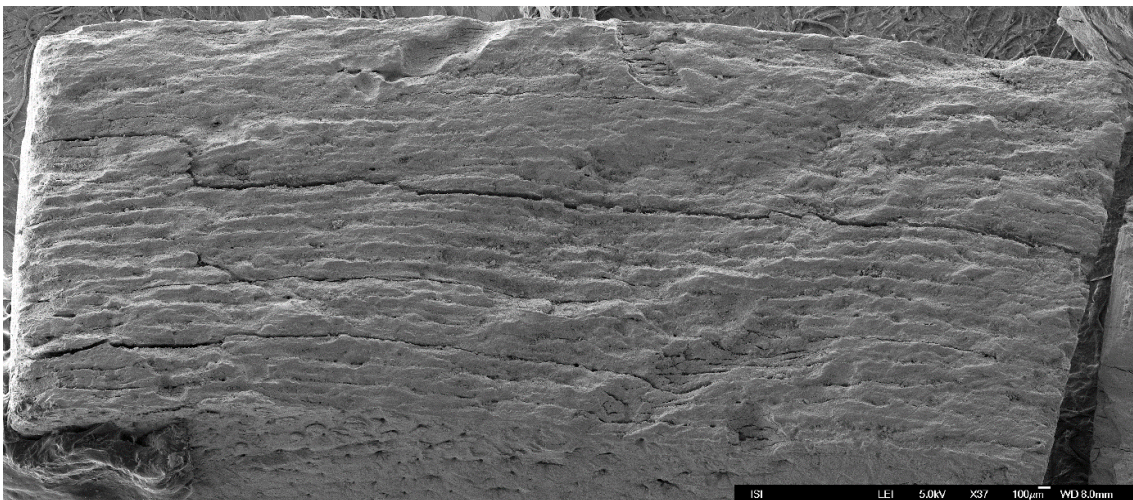
Fig. 8.25: Sample A5. Linear patterning of the surface clearly visible throughout the whole sample. Magnification 37×, scale bar 100 μm (photo Z. Pokorná and SB).

192
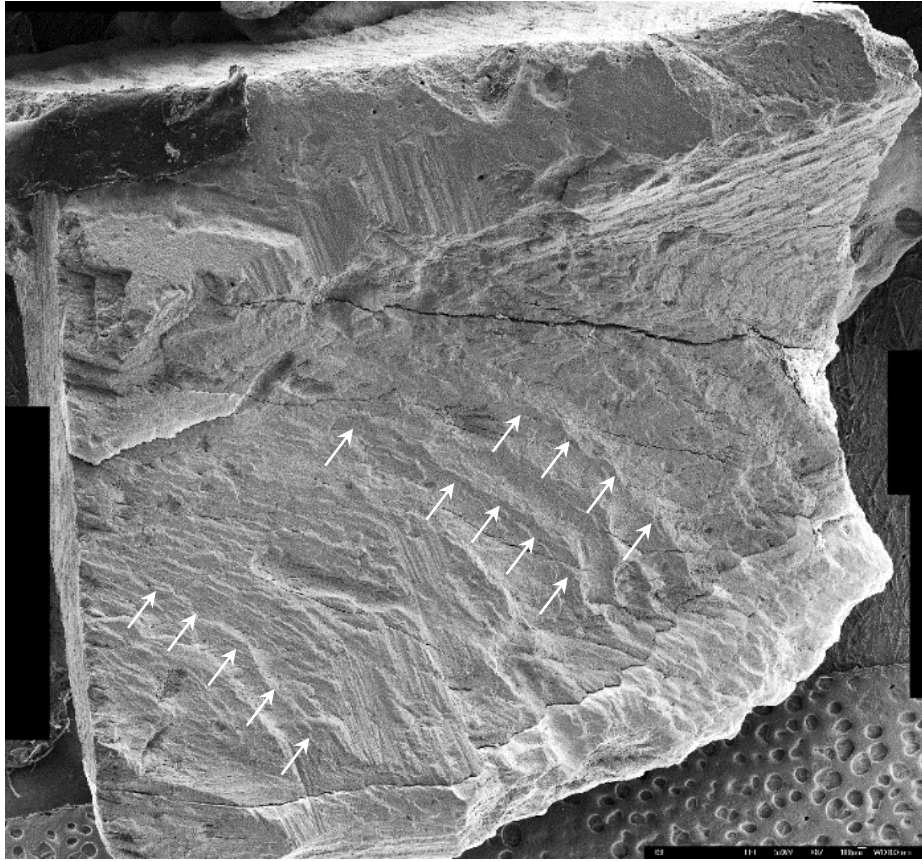
Fig. 8.26: Sample A6. Well pronounced fan-shaped pattern on the sample from helical FS (white arrows). Magnification 37×, scale bar 100 µm (photo Z. Pokorná and SB).

Fig. 8.27: Sample A8. Plate-like protrusion lined by cracking (white arrows). Magnification 37×, scale bar 100 µm (photo Z. Pokorná and SB).
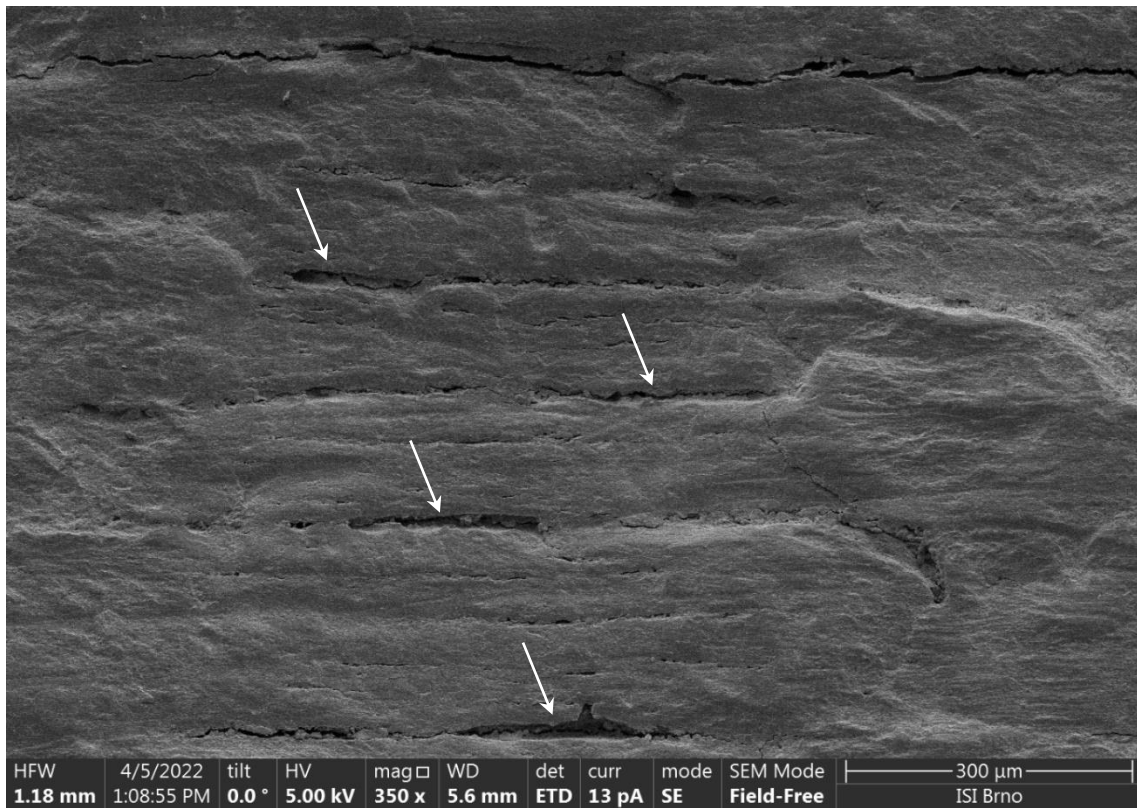
Fig. 8.28: Sample A7. Series of open Haversian canals in surface depressions, microcracking most possibly related to corrosive changes (white arrows). Magnification 350×, scale bar 300 μm (photo SB).

8.3.3 HTS analysis, area G

The treatment and preparation process followed the same steps as in the experimental samples. The fragments used for SEM analysis were also used for HTS preparation, the cutting plane was perpendicular to the observed fracture surface. Again, transmitted and polarised light imaging techniques were used. The list of samples and final thicknesses of the sections are stated in Tab. 8.5. The summary of the main features observed on histological thin sections can be found in Tab. 8.6 at the end of Chapter 9.3.3.

The samples all showed significant traces after post-depositional taphonomic changes. In a few cases, small smoothly shaped depressions with different colourations (Fig. 8.29) were observed. I assume that these could represent the surface depression caused by the corrosion observed by SEM. The colour changes (Fig. 8.30) are usually visible and were, most probably caused by saturation of the sample by minerals or their oxides such as manganese or iron. Another observed phenomenon is dark, cloud-like patches. These mostly avoid the marginal parts of the samples and the parts adjacent to canals or cracks. In some areas, they seem to follow the lamellar arrangement although

in others they continuously cover larger parts of the bone (Fig. 8.31). In polarised light, the patches have a foggy appearance and a grey colour; the only recognisable structures they do not cover are lacunae (Fig. 8.32). Another commonly observed trait was extensive cracking running through the whole sample, branching into different paths that followed but also crossed the bone microstructural units (Fig. 8.33). These cracks had already been observed on a macroscopic level and some of them emerged during the final cleaning before SEM observation. I suggest that most of these wide and continuous cracks are related to weathering and post-depositional changes rather than the actual fragmentation process.
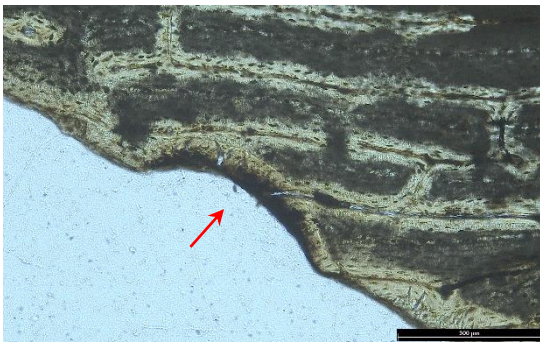
Fig. 8.29: Sample A1. Shallow surface depression with different colouring (red arrow). Magnification 100×, scale bar 300 μm (photo SB).
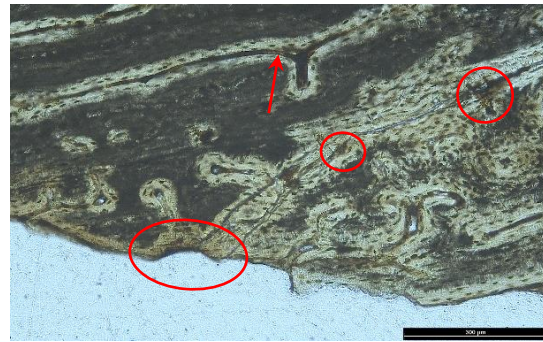
Fig. 8.30: Sample A1. Colour changes most probably caused by iron staining (red circles), also filling the Haversian canals (red arrow). Magnification 100×, scale bar 300 μm (photo SB).
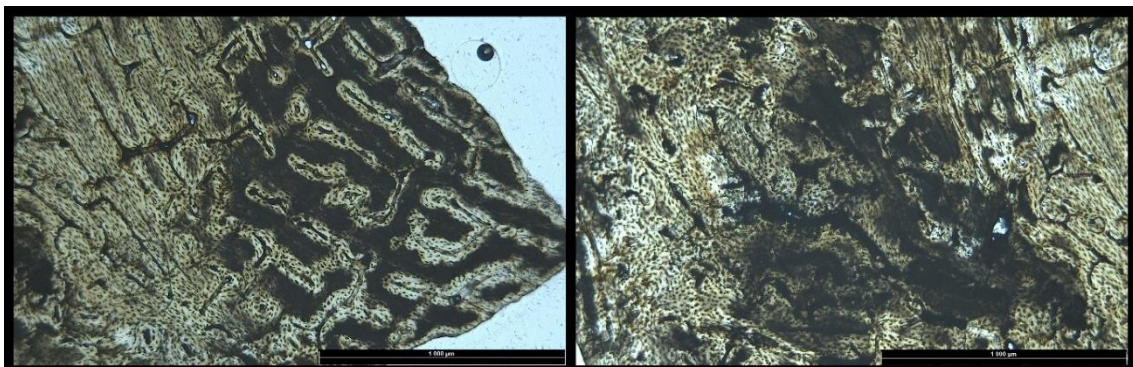
Fig. 8.31: Sample A9. Bounded dark colouring of bone avoiding the Haversian canals (left), and boundless cloud-like colouring spreading through the sample without any reference to the bone microstructure (right). Magnification 50×, scale bar 1000 μm (photo SB).

Fig. 8.32: Sample A4. Foggy appearance of dark coloration in polarised light. Lacunae are represented by the dots in the foggy areas (red circles). Red arrows indicate the iron colouring of the Haversian or Volkmann canals. Magnification 50×, scale bar 1000 µm (photo SB).
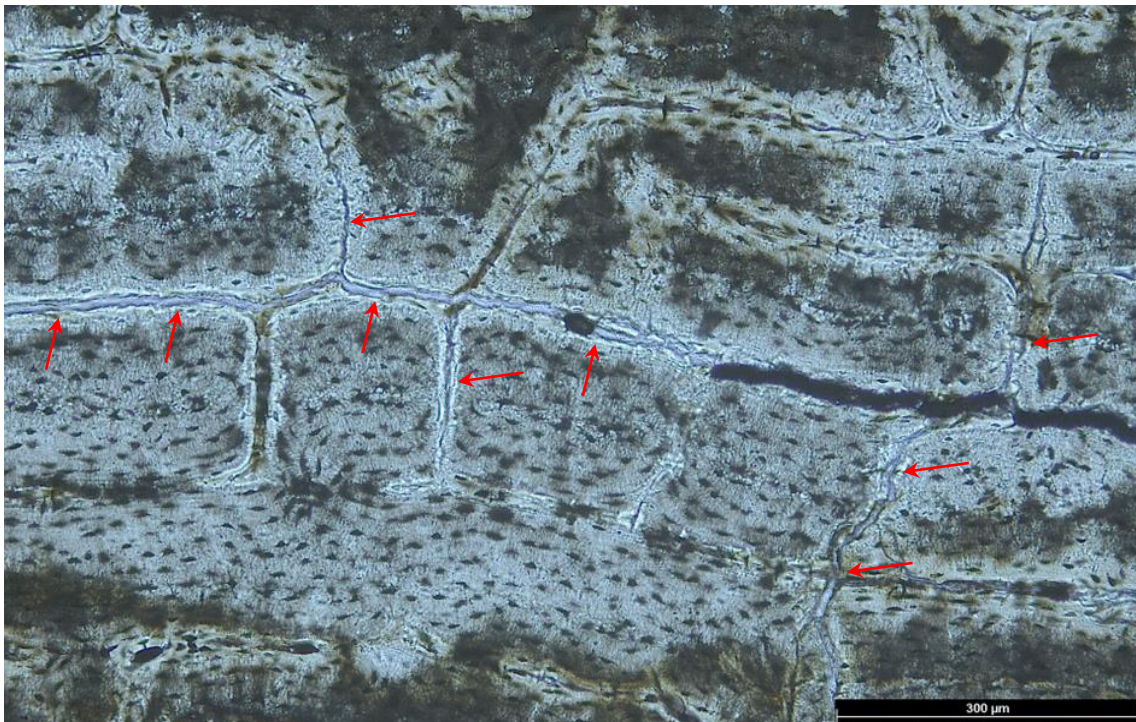
Fig. 8.33: Sample A3. Microcrack running along the Haversian canal, branching in various directions (red arrows). Magnification 100×, scale bar 300 µm (photo SB).

In the longitudinal samples, the surface was quite smooth and uniform without any significant protrusions or depressions. The profile of sample A9 was more irregularly shaped, most probably due to the less regular arrangement of the underlying bone in comparison to the other two samples (Fig. 8.34). No obvious shift of the fracture front related to the microscopic bone structure was observed. In a few cases, small smoothly shaped depressions with different colourations were observed. Microcracking penetrating the FS was scarce and was represented by the range described in the experimental samples. In the case of sample A9, a couple of short diagonal cracks (Fig. 8.35) were observed, and in sample A4 a series of fractures perpendicular to FS was described (Fig. 8.36). A system of wider cracks crossing the whole sample was observed. These fractures respect the lamellar arrangement of the bone and travel along the canals, starting or ending on the FS. Nevertheless, at some point they branch out and travel through the bone crossing osteons, canals, and other fractures (Fig. 8.37). A similar type of cracking was only observed in experimental assemblages in sample J (dried samples).
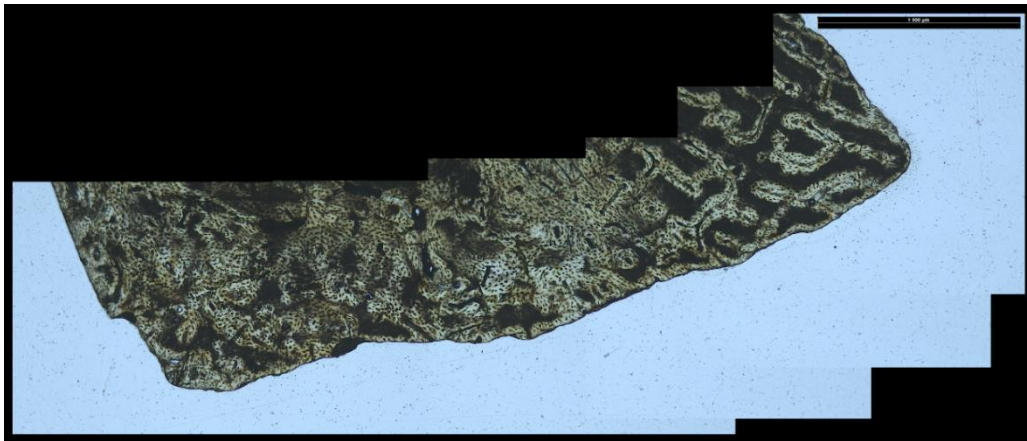
Fig. 8.34: Sample A9. Irregular FS due to the underlying bone microstructure. Magnification 50×, scale bar 1000 μm (photo SB).
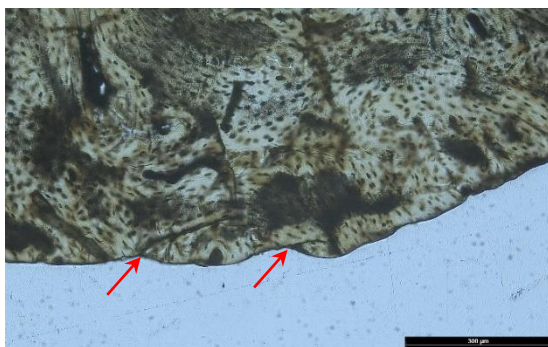
Fig. 8.35: Sample A9. Thin and short diagonal microcracks (red arrows). Magnification 100×, scale bar 300 μm (photo SB).
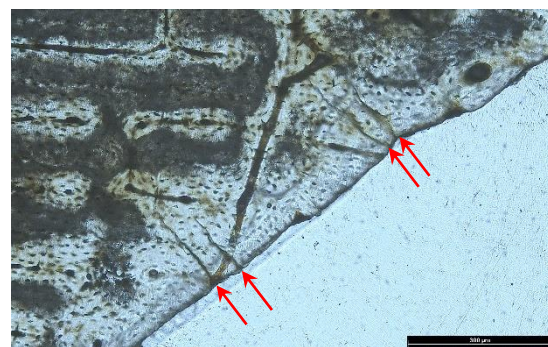
Fig. 8.36: Sample A4. A couple of microfractures perpendicular to FS (red arrows). Magnification 100×, scale bar 300 μm (photo SB).
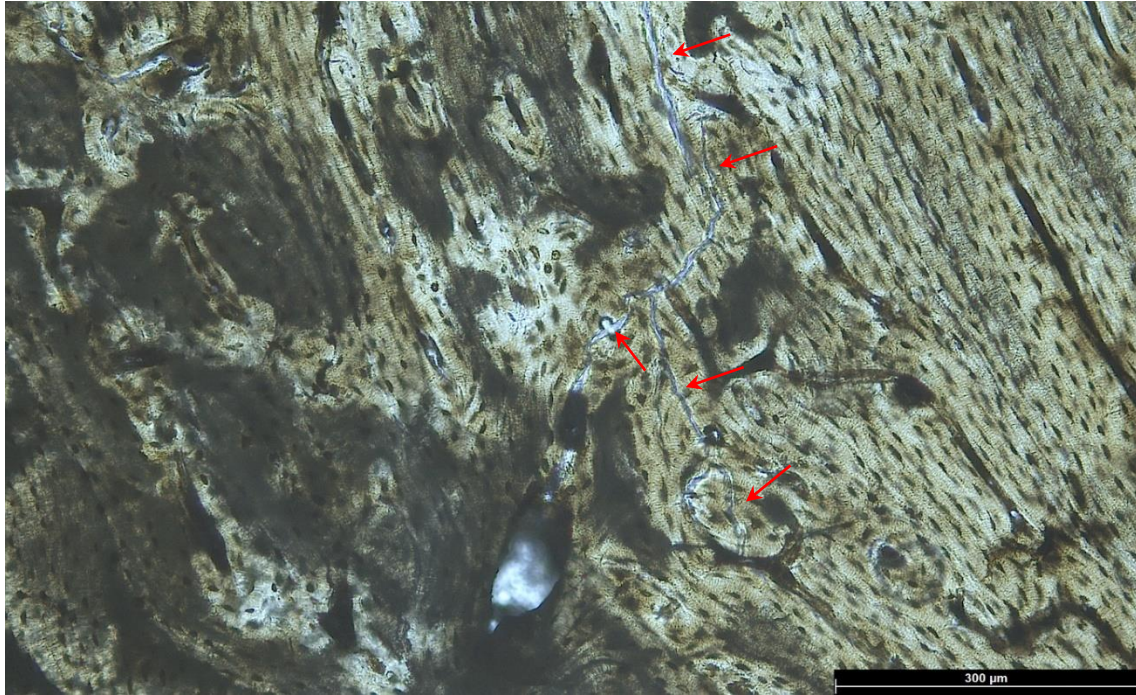
Fig. 8.37: Sample A9. Branching of open crack indicated by red arrows. Magnification 50×, scale bar 1000 μm (photo SB).

In the helical samples, I observed high variability in the shape of the FS profile. In samples A1 and A2, the profile was significantly smooth with a convex form (Fig. 8.38). On the surface of A1, a shallow depression with a darker colour was observed, most probably representing the surface corrosion (Fig. 8.29). In samples A5, A7 and A8, the profile was more or less straight although more shaped with small protrusions (Fig. 8.39). The shift of the fracture plane was typically observed again when encountering a canal or cement line. In comparison to fracture front deflection in experimental samples, the shifts are less pronounced and rounded, most probably due to FS corrosion. In samples A6 and A10, the FS profile is shaped and variable (Fig. 8.40). Microcracking was represented by wide branching fractures (Fig. 8.41) as described in the longitudinal FS. In sample A6 and A8, highly irregular and curvy fractures perpendicular to FS were present (Fig. 8.42). No other forms of microcracking penetrating the FS were recognised.
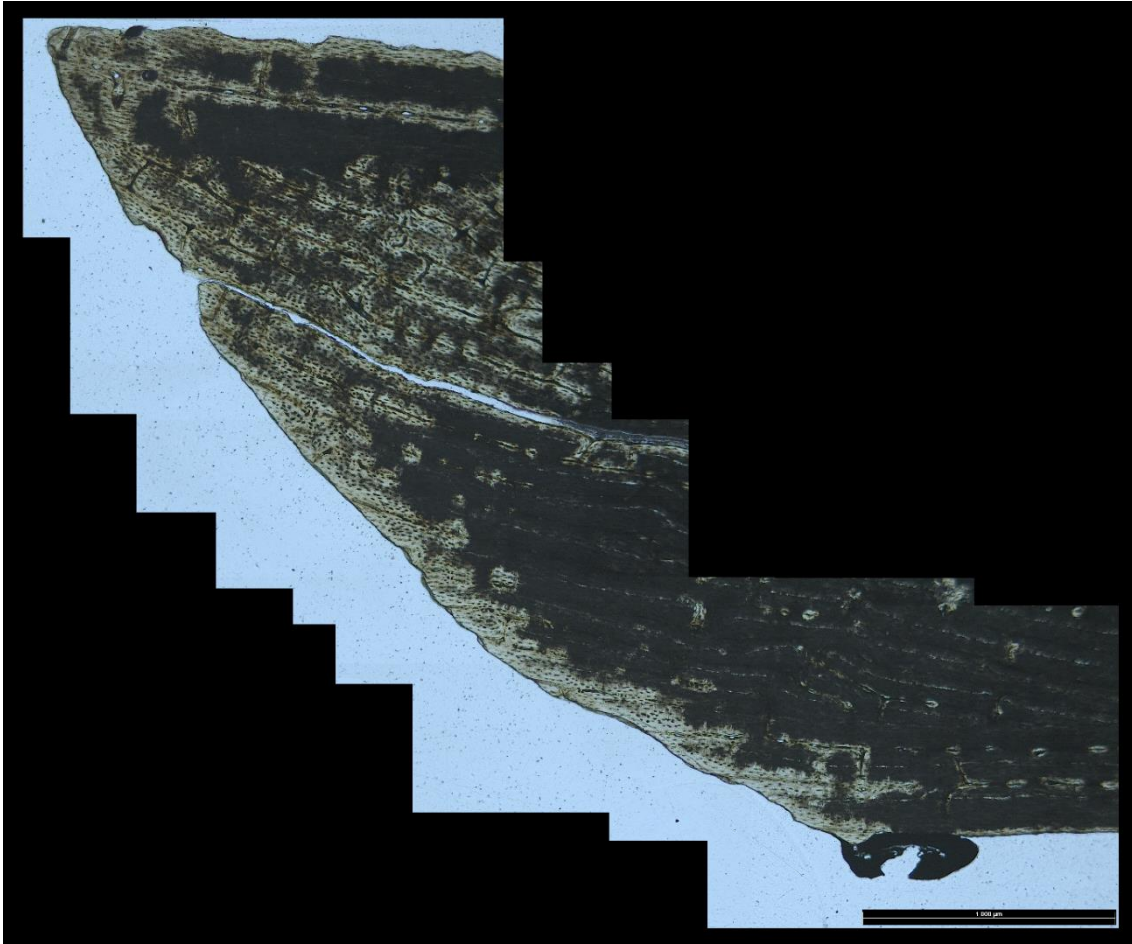
Fig. 8.38: Sample A2. Convex FS on sample from spiral fracture. Magnification 50×, scale bar 1000 μm (photo SB).

Fig. 8.39: Sample A7. Straight profile shaping with slight surface irregularities. Magnification 50×, scale bar 1000 μm (photo SB).

199
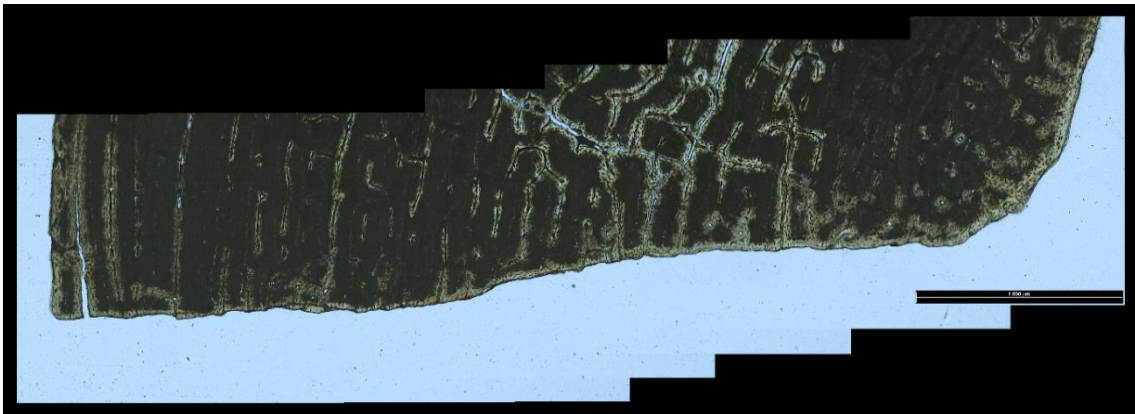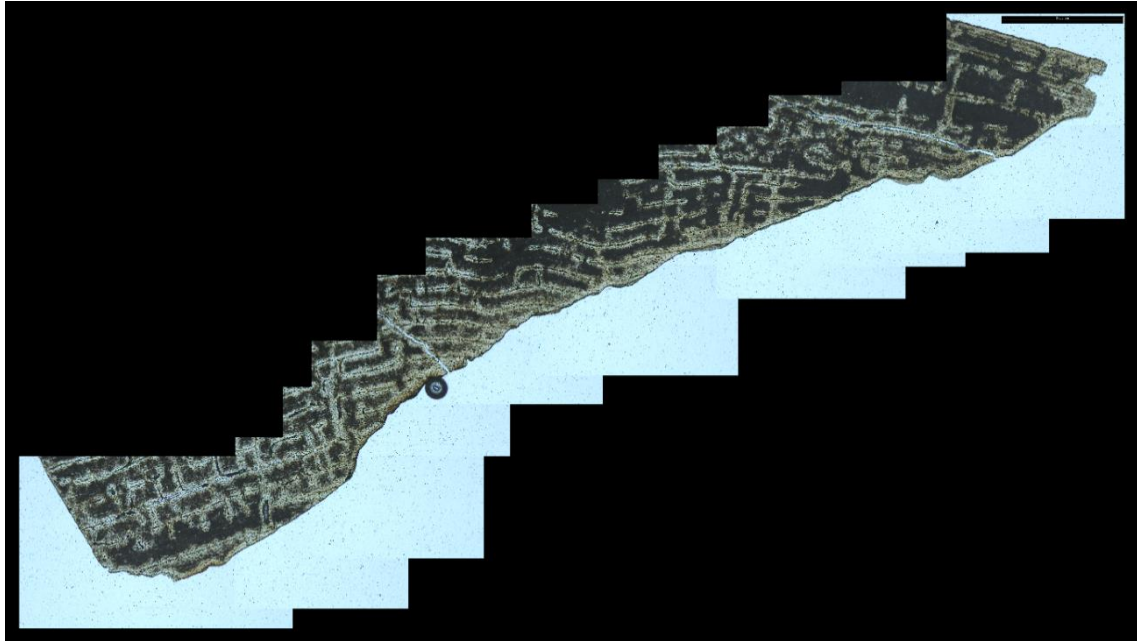
Fig. 8.40: Sample A6. Variable and shaped surface in spiral FS. Magnification 50×, scale bar 1000 µm (photo SB).
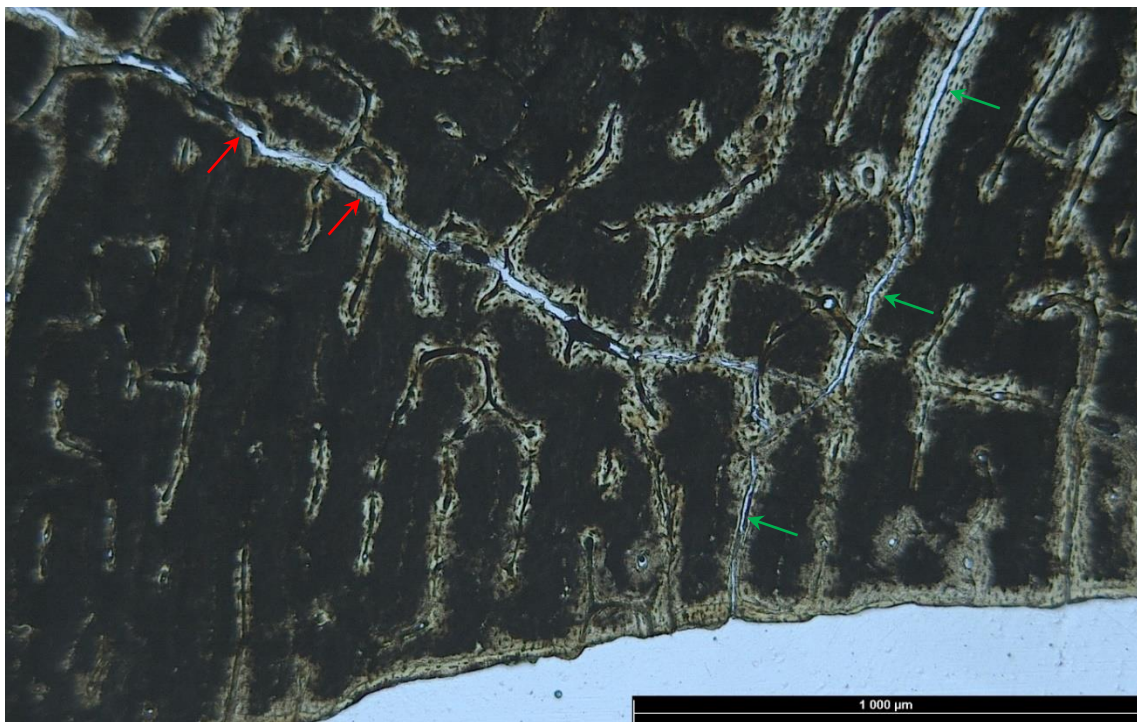
Fig. 8.41: Sample A7. Wide cracking and branching. Green arrows indicate cracks respecting the bone structure; red arrows indicate those that cut through the canals. Magnification 50×, scale bar 1000 µm (photo SB).
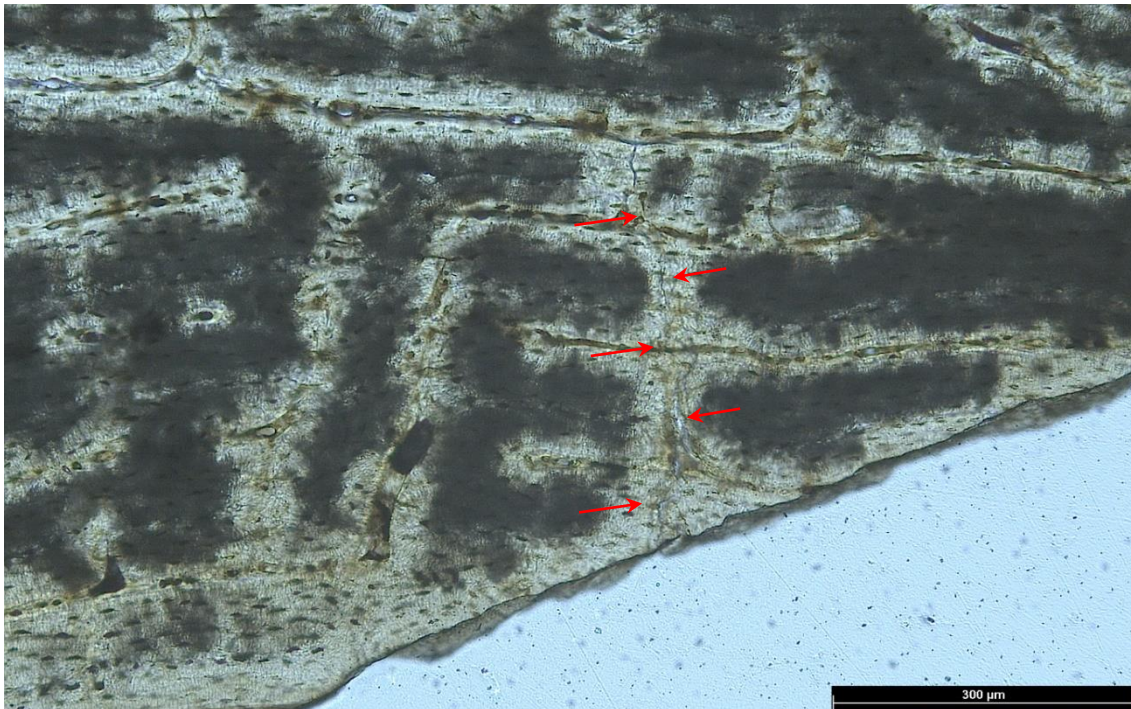
Fig. 8.42: Sample A6. Sinuous crack perpendicular to FS indicated by red arrows. Magnification 200×, scale bar 300 μm (photo SB).

	longitudinal FS	*helical FS*
SEM *Surface*	less regular morphology, smooth texture	less regular morphology, smooth texture
Patterning	linear scarce	linear; fan-shaped scarce
Microfractures	variable with irregularities, mainly respecting the lamellar arrangement	variable with irregularities, mainly respecting the lamellar arrangement
Other features	surface corrosion; granular areas; transversal ridges	surface corrosion; granular areas; transversal ridges; plate-like protrusions
HISTOLOGY *Surface profile*	smooth, uniform	variable
Surface irregularities	isolated	mild
Microfractures	short and thin, diagonal, and perpendicular; wide and branching	curvy perpendicular; wide and branching
Other features	surface corrosion	surface corrosion

Tab. 8.6: Main traits observed by SEM and transmitted light microscopy in archaeological samples (author SB).

8.4 Discussion of the fragmentation analysis in the archaeological assemblage

To greater extent, the **macroscopic method** was applied to variable areas within the site so the informative value of the results is more specific than in the case of microscopic analysis. The calculation of the index was successfully applied to reindeer and wolf long bones from the areas of interest. The fragmentation history profiling allowed me to assess the proportion of the material affected by multiple fragmentation events and describe the rate of post-depositional taphonomical intervention in material preservation, which in all three cases was around 50%.

The final comparison of the FFI value distribution for specific species within the areas shows a slight difference between area SE014 containing the settlement unit S1 and the activity zones in areas A and G (see also *Boriová et al. in press*; Fig. 8.43). Lower index values in reindeer bones are consistent with its function as one of the main subsistence resources. High index values are mainly present in wolf bones and point more to the depositional and post-depositional causes of fragmentation than intentional human intervention. In area G, the reindeer bones mainly show lower values with an average value of 2.7, which may suggest fragmentation of these bones in a fresh state. The presence of impact points, albeit in small numbers, also suggest this interpretation. On the other hand, wolf bones only reached high index values, pointing toward fragmentation in a greatly altered state and not fresh for any kind of exploitation. This is consistent with the overall state of wolf material preservation, which is mostly represented by whole-bone specimens.

In area A, the results were very similar to area G. In reindeer bones, the average FFI is slightly higher and the proportion of higher value representation is greater. The simultaneous presence of low values suggests that fragmentation of the fresh bones could have taken place although the primary area of such processing was most probably elsewhere. This suggestion also correlates with the specific skeletal part representation in this area (see Fig. 8.12), dominated by fragments of antlers, which unlike the bones could be primarily processed here. Wolf bones, analogically as in area G, show a high fragmentation index. What is different is the presence of other traces suggesting intentional human manipulation and modification of wolf bones, such as a series of cutmarks or teeth perforations. Together with possible burial of pathological wolf individual, these traces prove that people paid extraordinary attention to this species.
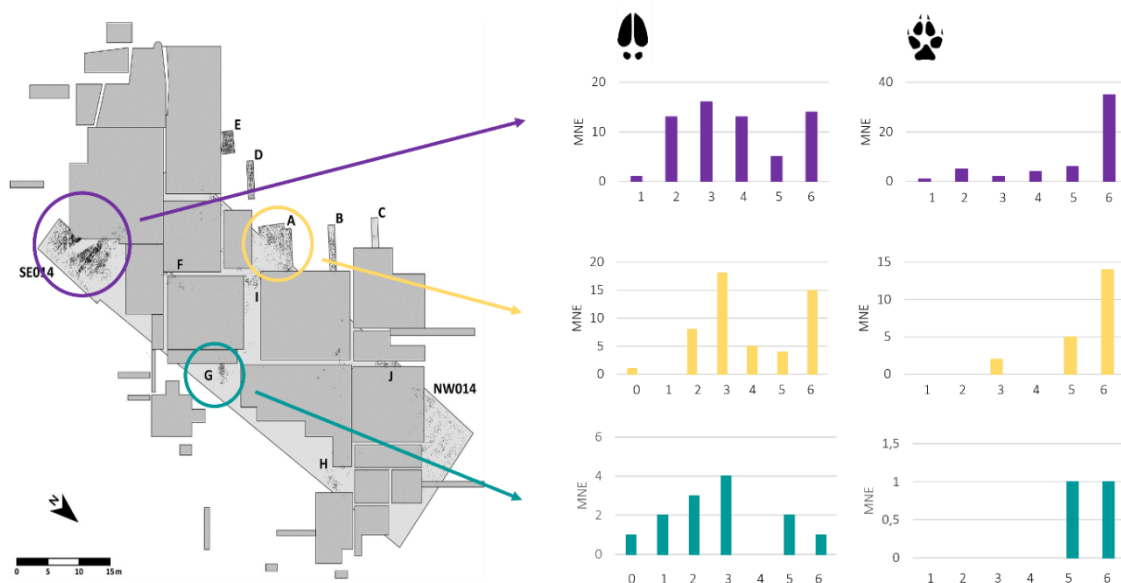
Fig. 8.43: Comparison of FFI value representation in reindeer and wolf in the studied areas (*Svoboda – Novák – Sázelová 2016*, 34, Fig.2; modified by SB).

In area SE014, the tendency is similar as in previous areas although small differences can be observed. In the case of reindeer, all the index values are represented, meaning a wide scale of fragmentation events. However, the accompanying traces such as cut marks and impact points suggest that at least part of these bones represent a remnant after butchering and exploitation activities. In the case of wolf bones, all FFI values are also represented. Even though the low values are present only in small numbers, in comparison to the previous areas they make a significant difference. This area, in comparison to areas G and A, differs in the different wolf bone representations (see Fig. 8.13) with prevailing flat bones and small caudal and paw bones. Nevertheless, the absence of any other traces after human intentional modification complicates the interpretation of the observed trend. A hypothetical explanation could be given by the overlap of the two settlement events, wherein in each event, a different strategy of animal body exploitation could prevail. As the complex processing of the material from this area is still ongoing, the closer inspection of stratigraphy and the differentiation of the two possible settlement phases remains to be examined.

The consistency in represented FFI values within reindeer and wolf bones (Fig. 8.43) suggests that both species played a consistent role in human society, which was reflected in how people manipulated/modified/exploited their bodies. Nevertheless, the

tiny differences and deviations from the observed standard can make a notable difference in the actual area/unit interpretation.

Concerning the site of interest, comments on bone fragmentation were also made by previous researchers. *R. Musil* (*2005a*) analysed the animal bones from old excavation seasons from the southeast part of the site. In his analyses, he reports a high level of fragmentation in the bones of hunted species from years 1952 and 1953, mentioning longitudinal splitting and transversal splintering in the case of small mammals. The strong disproportion of the proximal and distal halves of long bones suggests human involvement and the use of less represented proximal parts for further utilisation (*Musil 2005a*, 191-192). In the material from 1954 and 1956, he divided the species into three groups according to the intensity of fragmentation. Group I included species whose bones were fragmented to a great extent, including most of the body elements. Group II includes species that besides broken bones, display a high number of complete elements. Group III includes complete bones and is reserved for only occasionally hunted species, such as lions or wolverines (*Musil 2005a*, 212). Within this division, he also categorised these two species into different groups. Reindeers belonged to Group I, with longitudinally and transversally broken long bones with a great disproportion of proximal and distal halves and no complete specimens. Wolves belonged to Group II with a notable disproportion in the proximal and distal halves but a considerable amount of whole specimens. The outline of a fracture was mostly transversal, in one case a longitudinally broken metapodial was identified. He also reported a different spatial deposition of reindeer and wolf bones suggesting the seasonal character of the prey and species-specific treatment. This observation is contradictory to those from areas excavated in 1952 and 1953 where the concentrations of reindeer and wolf bones were almost the same, similar to foxes and hares, indicating species-specific areas of animal body processing (*Musil 2005a*, 191). The intentional bone fragmentation was naturally also a matter of other hunted species belonging to small or large/extra-large sized mammals.

As the previous chapters demonstrated, applying **microscopic methods** to archaeological material is possible. However, the fragility of the material and the variety of post-depositional changes and modifications bring certain limitations, not only in the process of sample preparation but also in the process of qualitative analysis. This is where the control of the samples under the stereomicroscope is a crucial step in the selection of specimens suitable for detailed analysis. The main morphological features observed under

SEM and in HTS were consistent with those identified in fresh and frozen experimental samples, corresponding to the specific type of fracture surface. The results of the microscopic observations agree with the calculated FFI values. To the extent presented, the detailed analysis of the archaeological samples did not bring any further information in comparison to the macroscopic methods. However, by comparing the images from archaeological and experimental samples, we proved that the described FS morphological changes are truly caused by the fragmentation process and its conditions, and to a certain extent, are preserved and observable in archaeological samples. This is one of the key premises in the further methodological development for archaeological data evaluation.

The methods used bring several invasive or limiting steps into the process of sample preparation, such as cutting the bone specimen to fit into the limited working space of SEM, coating the FS with conductive layers for better image output, and the lengthy process of thin section preparation to obtain only one profile section from the sample. These are of particular concern when dealing with archaeological samples and may cause many inconveniences. To reduce the destructiveness and increase the data gain/return in archaeological bone analysis, I propose testing other methods with similar imaging capabilities. For example, modern 3D scanning microscopes or confocal profilometers provide larger manipulation space with significantly less demanding observation conditions. This means the samples do not have to be cut out of the original specimen, placed into a vacuum or coated with a conductive layer. The 3D surface microscopy or confocal profilometry could provide detail of the fracture surface and the pattern instead of the overall pictures from SEM. The accessories usually allow numerous types of lightning with various filters reducing the surface reflection while the relevant software allows for sectioning the observed area digitally in numerous places to show the transformation of the FS profile with the option to measure or quantify the observed changes (e.g. *Bello – De Grotte – Delbarre 2013; Pante et al. 2017*; *Casanova – Roldán – Subirà 2020*; *Göldner – Karakostis – Falcucci 2022*). However, these methods do not have the option to observe surface microcracking at the level of collagen bundles to replace the highly detailed imaging obtained by SEM, nor an observation of the internal microcracking penetrating under the FS. The internal microcracking could be non-destructively pictured via micro-CT scanning. This method could provide more complex picture of the internal microcracking patterns in the whole bone or fragment context (e.g. *Boschin et al. 2015*; *Carlson et al. 2022*). Nevertheless, the microcracking traces observed

so far were not very systematic and well pronounced, therefore using the financially and time-demanding micro-CT scanning method could be at the current state of knowledge not worth the obtained results.

Since the topic of bone fragmentation in archaeology comprise wide-ranging problem related to many taphonomic processes, its analysis represents a more specialised and deeper level of research than the common standard in the basic material description. Despite this, the level or character of bone fragmentation in the archaeological assemblages from the Gravettian generally tends to be at least briefly addressed, even in works focused on the basic processing and description of archaeozoological assemblages. It illustratively reflects the importance of this type of analysis in interpreting past human activities. However, as the summary of the chosen open-air sites (Tab. 8.7) shows, the level of fragmentation analysis employed on specific sites varies significantly. I compared studies describing the bone material from neighbouring sites in the Dolní Věstonice-Pavlov-Milovice area with similar dating and also examples of related sites around Napajedla Gate and the Central Bohemia region were included. Examples of sites close/similar in dating, regional setting or comparable faunal assemblages from Slovakia and Austria are stated.

In most cases, I observed that the bone fragmentation topic is addressed at least with a **brief verbal description** (e.g. *Fladerer – Salcher 2004; Nývltová-Fišáková – Pokorný – Šída 2008*). The description mostly concerned the type or size of fragments in relation to the preservation state and in other cases, the type of breaks occasionally present on bones in relation to possible fragmentation agents or the state of bone preservation when fragmented. This type of description is usually complemented by notes on the presence of impact points/scars/flakes or **other traces related to the fragmentation process** (e.g. *Vlačiky 2012*; *Wilczyński et al. 2015*). Nevertheless, this description is also variably detailed. I encountered the numerical or graphic evaluation of these observations offering a more accurate idea about the fragmentation pattern at the site slightly less. The evaluation using **NISP:MNE ratio** precisely was quite rare (*Sázelová 2016*) although, in several studies, the NISP and MNE count for specific species or a skeletal part were stated, so in the case of interest the ratio can be easily calculated (e.g. *Brugère – Fontana – Olivia 2009*; *Bosch et al. 2012*; *Wojtal et al. 2018*; *Wilczyński et al. 2021*). Some authors (e.g. *Musil 2005a*; *Sázelová 2016*) introduce their **own methods** for evaluation of fragmentation patterns or categorising the different observed phenomena, as illustrated in

the previous paragraph concerning the earlier Pavlov I bone material analysis (p. 204). This type of approach was the most detailed and interpretative among the works cited in Tab. 8.7. Nevertheless, it reflects the specific research questions and scopes addressed by specific authors and thus their results are hardly comparable to the data published by other researchers aiming their research questions and goals differently. The use of **established methods for the analysis of bone fragmentation** (e.g. Chapter 2.3.1) was not observed in any of the inspected publications, and similarly, we did not observe the use of any **microscopic techniques** for the analysis of fragmented bones or assemblages.

As this summary (see Tab. 8.7) illustrates, the topic of bone fragmentation is considered in most cited studies and it is mostly discussed in the context of intentional human activities involving bone processing for dietary or utilitarian purposes. However, as the level of analytical approach addressing this topic is extremely variable and, in many cases, custom-made for the specific site, research question or the desired depth of the acquired knowledge of a specific subject, the mutual comparison of observed patterns is complicated. In the summarised studies I observed that a generalised evaluation inspired by standardised fragmentation methodology was used. However, it is important to emphasise, that the stated studies were dealing, except for *Vlačiky 2012*, with a basic description of the archaeozoological material from the respective sites and were not directly aimed at bone fragmentation analysis. I am fully aware that the level of processing and the methods chosen for each site are largely dependent not only on the aim of the study but also on the state of bone preservation and that the application of specialised methods in specific cases may be inefficient. The submitted approach represents an example of a study aimed at fragmentation analysis using established macroscopic methodology combined and correlated with newly introduced and tested methods. The summary should illustrate that there is a broad awareness of the significance of bone fragmentation patterns although works specialising in this type of bone modification in a deeper sense are lacking. Further, it should emphasise the importance of uniform use of the accepted approaches in the description of fragmentation patterns, to better understand and describe the specific traces left by different fragmentation agents or more complex human or non-human taphonomic activities leading to bone fragmentation.

Country	Site	Level of information on bone and tooth fragmentation	Sources
CZ	Dolní Věstonice I-III	1, 3, 5, 7, 8	*West 2001; Nývltová-Fišáková 2001; Wilczyński et al. 2015; Sázelová 2016; Wojtal - Wilczyński - Wertz 2016; Wojtal et al. 2018*
CZ	Pavlov I-VI	1, 2, 3, 5, 6, 8	*Musil 1994; 1997; 2005a; Wojtal – Nývltová-Fišáková – Wilczyński 2011; Wojtal et al. 2012; Wojtal – Wilczyński – Svoboda 2017*
CZ	Milovice I, IV	0, 1, 3, 4	*Brugère – Fontana – Oliva 2009; Brugère – Fontana 2009; Svoboda et al. 2011*
CZ	Předmostí Ia, Ib	1, 3, 5	*Nývltová-Fišáková 2001; Wojtal – Wilczyński 2013; Germonpré et al. 2017*
CZ	Spytihněv	2	*Škrdla – Nývltová-Fišáková 2004; Nývltová-Fišáková 2005; Škrdla et al. 2005*
CZ	Boršice	-	*Nývltová-Fišáková – Nývlt – Škrdla 2006*
CZ	Jarošov II	3, 5, 6	*Škrdla - Musil 1999; Musil 2005b*
CZ	Lubná	1, 2, 3, 5	*Nývltová-Fišáková – Pokorný – Šída 2008; Šída ed. 2009; Šída 2015; Wilczyński et al. 2021*
SK	Trenčianske Bohuslavice	1, 3, 4, 5, 6	*Karol 2005; Pošvancová 2005; Vlačiky 2005; Vlačiky 2009; Vlačiky 2008; Vlačiky 2012*
SK	Moravany - Lopata II	1, 3, 4, 5, 6	*Lipecki – Wojtal 1998; Vlačiky 2009; Vlačiky 2012*
PL	Krakow Spadzista	1, 3, 5	*West 1996; Wojtal – Sobczyk 2003; 2005; Wilczyński et al. 2012; Lipecki – Wojtal 2015; Wojtal – Wilczyński 2015; Wojtal – Sobczyk – Wilczyński 2015*
AT	Grub/ Kranawetberg	1, 3	*Antl – Fladerer 2004; Antl-Weiser et al. 2010; Bosch et al. 2012; Antl – Bosch 2015*
AT	Krems-Hundsstieg/ Wachtberg	0, 2, 3, 4, 5	*Fladerer 2001a; 2001b; Fladerer – Salcher 2004; Fladerer – Salcher Jerdasiak 2008; Fladerer – Salcher Jedrasiak 2010; Fladerer – Salcher Jerdesiak – Händel 2014; Fladerer at al. 2010*
AT	Willendorf II	-	*Nigst 2006; 2014; Nigst et al. 2008a; 2008b*

Tab. 8.7: Summary of studies considering the chosen open-air sites and the level of fragmentation evaluation/analysis of the bone and tooth material. The categories given for the character of fragmentation processing are following: - = without any note on fragmentation; 0 = description of bone fragment size categories with relation to overall preservation of the material; 1 = NISP and MNE counts stated without relation to fragmentation; 2 = brief verbal description with relation to the character of fractures; 3 = verbal description with relation to character of fractures, state of bone and possible fragmentation agents; 4 = same as for category 3 but with numeric or graphic evaluation; 5 = description of other traces related to fragmentation (e.g. impact points/scars, impact flakes); 6 = proximal:distal part count/ratio; 7 = NISP:MNE ratio addressing fragmentation directly; 8 = categorisation of observed fragmentation patterns with individual methods. Studies dealing with antler or ivory material were not considered (author SB).

Conclusion

The analyses I conducted on experimental and archaeological assemblages allowed me to fulfil the aims of the dissertation thesis as follows.

I confirmed that **a)** both the chosen microscopy methods are suitable for observation of the fracture surface character and the distinction of morphological differences in experimental and to a certain extent, archaeological assemblages. Nevertheless, the testing and application of other methods with similar imaging abilities could reduce the destructiveness of the proposed methodological approach, which is essential in the case of archaeological samples.

I verified that **b)** the results obtained by micro and macroscopic methods correspond and have a similar sensitivity in the differentiation of altered states of bone in the fragmentation process. In comparison to microscopic methods, the FFI calculation showed even higher discernment concerning the presence of soft tissues on bone during the fragmentation process. Implementation of the FFI method to the archaeological material allowed me to not only identify different body treatments for the chosen medium-sized mammal species but even reflected the differences between the examined activity and the settlement zones to a certain extent. The broader application of the FFI method in context of spatial distribution and observation of fragmentation patterns, especially for closely unidentifiable bone fragments, could be beneficial.

I proved that **c)** the chosen methods of observation at the microscopic level apply to archaeological material although a systematic approach and control of the fracture surface preservation in the sample selection process are required to prevent worthless destructive sampling and financially and time-consuming microscopic analysis. The level of reliability and interpretational potential of the tested microscopic methods is at the current state significantly limited by the wide range of other variables influencing the final fracture surface morphology. To justify the meaningfulness of such an analysis for archaeological assemblages, it is important to systematically broaden the experimental practice concerning the number of samples and the range of influencing variables such as bone preservation state or the character of the force applied. The comparative collections resulting from controlled experiments can help us to identify and eliminate traces not directly related to the fragmentation itself but rather connected to post-depositional or post-experimental processes and treatment.

The proposed methods of fragmentation analysis complement the existing wide range of analytical approaches concerning this topic in archaeological contexts. Conditioned by further research, they have the potential to address the fragmentation topic in assemblages where the application of present methods might be problematic or strengthen the knowledge of those thoroughly examined.

References

Abe, Y. 2005: Hunting and Butchery Patterns of the Evenki in Northern Transbaikalia, Russia. Stony brook University.

Agenbroad, L. D. 1989: Spiral fractured mammoth bone from nonhuman taphonomic processes at Hot Springs Mammoth site. In: R. Bonnichsen, and M. A. Sorg (eds), Bone Modification. Orono, Center for the Study of the First Americans, 139-147.

Ager, J. W. – Balooch, G. – Ritchie, R. O. 2006: Fracture, ageing, and disease in bone. Journal of Materials Research 21, 1878-1892.

Agnew, A.M. – Bolte IV, J.H. 2012: Bone Fracture. Biomechanics and Risk. In: C. Crowder – S. Stout eds., Bone Histology. An Anthropological Perspective. CRC Press, Boca Raton, 221-233.

Alcántara-García, V. – Barba Egido, R. – Barral del Pino, J. M. – Crespo Ruiz, A. B. – Eiriz Vidal, A. I. – Falquina Aparicio, Á. – Herrero Calleja, S. – Ibarra Jiménez, A. – Megías González, M. – Pérez Gil, M. – Pérez Tello, V. – Rolland Calvo, J. – Yravedra Sáinz de los Terreros, J. – Vidal, A. – Domínguez-Rodrigo, M. 2006: Determinación de procesos de fractura sobre huesos: un sistema de análisis de los ángulos de los planos de fracturación como discriminador de agentes bióticos, Trabajos de Prehistoria 61(1), 25-38.

Alhaique, F. 1997: Do Patterns of Bone Breakage Differ Between Cooked and Uncooked Bones? An Experimental Approach. Anthropozoologica 25-26, 49-56.

Almeida, N.J. – Saladié Balleste, P. 2014: Long bones dynamic fracturation: a comparison of Bos taurus impact flakes made with modified and unmodified hammerstones. Antrope 1, 244-253.

Alunni-Perret, V. – Muller-Bolla, M. – Laugier, J.P. - Lupi-Pègurir L. Bertand, M.F. – Staccini, P. – Bolla, M. – Quatrehomme, G. 2005: Scanning electron microscopy analysis of experimental bone hacking trauma. Journal of Forensic Science*s* 50(4), 796-801.

Antl, W. – Fladerer, F.A. 2004: Outlook to the East: The 25 Ky BP Gravettian Grub/Kranawetberg capsite (Lower Austria). In: J. Svoboda – L. Sedláčková eds., The Gravettian along Danube. Proceedings of the Mikulov Conference, 20.-21. November 2022. The Dolní Věstonice Studies 11. Academy of Sciences of the Czech Republic, Institute of Archaeology, Brno, 116-130.

Antl, W. – Bosch, M. 2015: The Use of Ivory at the Gravettian Site Grub/Kranawetberg, Lower Austria. Anthropologie LIII/1–2, 233-244.

Antl-Weiser, W. – Fladerer, F.A. – Nigst, P.R. – Verpoorte, A. 2010: Grub/Kranawetberg (Lower Austria) - insights into a Gravettian micro-region in Eastern Austria. In: C. Neugebauer-Maresch – L.R. Owen eds., New Aspects of the Central and Eastern European Upper Palaeolithic - Methods, Chronology, Technology and Subsistence. Mitteilungen der Prähistorischen Kommission 72, 231-243.

Arilla M. – Rosell, J. – Blasco, R. – Domínguez-Rodrigo, M. – Pickering, T.R. 2014: The ''Bear'' Essentials: Actualistic Research on Ursus arctos arctos in the Spanish Pyrenees and Its Implications for Paleontology and Archaeology. PLoS ONE 9(7), e102457. DOI: 10.1371/journal.pone.0102457.

Arriaza, M.C. – Domínguez-Rodrigo, M. – Yravedra, J. – Baquedano, E. 2016: Lions as bone accumulators? Paleontological and ecological implications of a modern bone assemblage from Olduvai Gorge. PLoS One 11(5), e0153797. DOI: 10.1371/journal.pone.0153797.

Ascenzi, A. – Bonucci E. 1964: The ultimate tensile strength of single osteons. Acta Anatomica 58, 160-183.

Backwell, L. – d'Errico, F. 2014: Bone Tools, Paleolithic. In: C. Smith ed., Encyclopedia of Global Archaeology. Springer, New York, NY. DOI: 10.1007/978-1-4419-0465-2_702.

Bancroft, J.D. – Stevens, A. – Turner, D.R. 1996: Theory and Practice of Histopathological Techniques, fourth eds. Churchill Livingstone, New York, London, Madrid.

Behrensmeyer, A.K. 1975: The taphonomy and paleoecology of Plio-Pleistocene vertebrate assemblages east of Lake Rudolph, Kenya. Bulletin of the Museum of Comparative Zoology 146, 473–578.

Behrensmeyer, A.K. 1978: Taphonomic and ecologic information from bone weathering. Paleobiology 4(2), 150-162.

Behrensmeyer, A.K. – Gordon, K.D. – Yanagi, G.T. 1986: Trampling as a cause of surface bone damage and pseudo-cutmarks. Nature 319, 768-771.
DOI: 10.1038/319768a0.

Bell, L.S. 2012: Histotaphonomy. In: C. Crowder – S. Stout eds., Bone Histology. An Anthropological Perspective. CRC Press, Boca Raton, 241–251.

Bello, S.M. – Galway-Witham, J. 2019: Bone taphonomy inside and out: Application of 3-dimensional microscopy, scanning electron microscopy and micro-computed tomography to the study of humanly modified faunal assemblages. Quaternary International 517, 16-32. DOI: 10.1016/j.quaint.2019.02.035.

Bello, S.M. – De Groote, I. – Delbarre, G. 2013: Application of 3-dimensional microscopy and micro-CT scanning to the analysis of Magdalenian portable art on bone and antler. Journal of Archaeological Science 40(5), 2464-2476. DOI:10.1016/j.jas.2012.12.016

Bendrey, R. 2011: Identification of metal residues associated with bit-use on prehistoric horse teeth by scanning electron microscopy with energy dispersive X-ray microanalysis. Journal of Archaeological Science 38, 2989-2994. DOI: 10.1016/j.jas.2011.06.016

Bertoglio, B. – Messina, C. – Cappella, A. – Maderna1, E. – Mazzarelli, D. – Lucheschi, S. – Sardanelli, F. – Sconfienza, L.M. – Sforza, Ch. – Cattaneo, C. 2021: Bone tissue preservation in seawater environment: a preliminary comparative analysis of bones with different post-mortem histories through anthropological and radiological perspectives. International Journal of Legal Medicine 135, 2581-2594. DOI: 10.1007/s00414-021-02636-6.

Biddick, K.A. – Tomenchuk, J. 1975: Quantifying Continuous Lesions and Fractures on Long Bones. Journal of Field Archaeology 2(3), 239-249, DOI: 10.1179/009346975791491042.

Bird, F. – Becker, H. 1966: Report No. ARA 322-2. Concord, Massachusetts: Allied Research Associates.

Binford, L.R 1978: Nunamuit ethnoarchaeology. New York: Academic Press.

Binford, L.R. 1981: Bones: ancient man and modern myths. San Diego: Academic press.

Binford, L.R. 1983: In Pursuit of the Past: Decoding the Archaeological Record. University of California Press.

Binford, L. R. – Bertram, J.B. 1977: Bone frequencies – and attritional processes. In: L.R. Binford ed., For theory building in archaeology: essays on faunal remains, aquatic resources, spatial analysis, and systemic modelling. New York: Academic Press, 77-153.

Blasco, R. - Fernández Peris, J. 2012: Small and large game: human use of diverse faunal resources at Level IV of Bolomor Cave (Valencia, Spain), Comptes Rendus Palevol 11, 265-82. DOI: 10.1016/j.crpv.2012.01.003

Blasco, R. – Rosell, J. - Dominguez-Rodrigo, M. – Lozano, S. – Pastó, I. – Riba, D. – Vaquero, D. – Fernández Peris, J. – Arsuaga, J.L. - Bermúdes de Castro, J.M. – Carbonell, E. 2013a: Learning by Heart: Cultural Patterns in the Faunal Processing Sequence during the Middle Pleistocene. PlosOne 8(2), e55863. DOI: 10.1371/journal.pone.0055863.

Blasco, R. - Rosell, J. - Fernández Peris, J. - Arsuaga, J. L. - Bermúdez de Castro, J. M. - Carbonell, E. 2013b: Environmental availability, behavioural diversity and diet: a zooarchaeological approach from the TD10-1 sublevel of Gran Dolina (Sierra de Atapuerca, Burgos, Spain) and Bolomor Cave (Valencia, Spain). Quaternary Science Reviews 70, 124-144. DOI: 10.1016/j.quascirev.2013.03.008

Blasco, R. - Domínguez-Rodrigo, M. – Arilla, M. - Camarós E. - Rosell J. 2014: Breaking Bones to Obtain Marrow: A Comparative Study Between Percussion by Batting Bone on an Anvil and Hammerstone Percussion. Archaeometry 56(6), DOI: 1085-1104 10.1111/arcm.12084.

Blasco, R. – Rosell J. – Arilla M. - Margalida A. - Villalba D. - Gopher A. - Barkai R. 2019: Bone marrow storage and delayed consumption at Middle Pleistocene Qesem Cave, Israel (420 to 200 ka). Science Advances 5, eaav9822. DOI: 10.1126/sciadv.aav982.

Blumenschine, R.J. 1986: Early Hominid Scavenging Opportunities. Implications of Carcass Availability in the Serengeti and Ngorongoro Ecosystems. BAR International Series, 283. Oxford.

Blumenschine, R.J. 1988: An experimental model of the timing of hominid and carnivore influence on archaeological bone assemblages. Journal of Archaeological Science 15, 483-502. DOI: 10.1016/0305-4403(88)90078-7.

Blumenschine, R.J. 1995: Percussion marks, tooth marks, and experimental determinations of the timing of hominid and carnivore access to long bones at FLK Zinjanthropus, Olduvai Gorge, Tanzania. Journal of Human Evolution 29, 21-51. DOI:10.1006/JHEV.1995.1046.

Blumenschine, R.J. – Selvaggio, M.M. 1988: Percussion marks on bone surfaces as a new diagnostic of hominid behaviour. Nature 333, 763-765. DOI: 10.1038/333763a0.

Blumenschine, R.J. – Selvaggio, M.M. 1991: On the marks of marrow bone processing by hammerstones and hyaenas: their anatomical patterning and archaeological implications. In: J.D. Clarke ed., Cultural Beginnings: Approaches to Understanding Early Hominid Life-ways in the African Savanna. Dr Rudolf Habelt GMBH, Bonn, 17-32.

Blumenschine, R.J. – Prassack, K.A. – Kreger, D.C. – Pante, M. 2007: Carnivore tooth-marks, microbial bioerosion, and the invalidation of Domínguez-Rodrigo and Barba's (2006) test of Oldowan hominin scavenging behaviour. Journal of Human Evolution 53, 420-426. DOI: 10.1016/j.jhevol.2007.01.011.

Bochenski, Z.M. – Tomek, M. – Wilczyński, J. – Svoboda, J. – Wertz, K. – Wojtal, P. 2009: Fowling during the Gravettian: the avifauna of Pavlov I, the Czech Republic. Journal of Archaeological Science 36, 2655–2665. DOI: 10.1016/j.jas.2009.08.002.

Bosch, M. – Nigst, P.R. – Fladerer, F. – Antl-Weiser, W. 2012: Humans, bones and fire: Zooarchaeological, taphonomic, and spatial analyses of a Gravettian mammoth bone accumulation at Grub-Kranawetberg (Austria). Quaternary International 252, 109-121. DOI: 10.1016/j.quaint.2011.08.019.

Boschin, F. – Zanolli, C. – Bernardini, F. – Princivalle, F. – Tuniz, C. 2015: A Look from the Inside: MicroCT Analysis of Burned Bones. Ethnobiology Letters, 6(2):258-266. DOI: 10.14237/ebl.6.1.2015.365.

Bouvier, M. – Ubelaker, D. 1977: A comparison of two methods for the microscopic determination of age at death. American Journal of Physical Anthropology 46, 391-394. DOI: 10.1002/ajpa.1330460303.

Bonfield, W. – Li, C. H. 1966: Anisotropy of nonelastic flow in bone. Journal of Applied Physics 38(6), 2450-2455. DOI: 10.1063/1.1709926

Bonnichsen, R. 1973: Some operational aspects of human and animal bone alteration. In: M. Gilbert ed., Mammalian osteoarchaeology: North America. Columbia, Miss: Missouri Archaeological Society, 9-24.

Bonnichsen, R. 1979: Pleistocene bone technology in the Beringian Refugium. Archaeological Survey of Canada Paper, Mercury Series (Paper No. 89). Ottawa: National Museum of Canada.

Bonnichsen, R. 1982: Bone technology as a taphonomic factor: An introductory statement. In: E. Johnson – R. Bonnichsen eds., Bone technology: Experimentation, assemblage, and non-human modification. Canadian Journal of Anthropology 2(2), 137-144.

Bonnichsen, R. – Will, R. 1980: Cultural modification of bone: The experimental approach in faunal analysis. In: M.B. Gilbert ed., Mammalian Osteology. Laramie, Wyoming: B. Miles Gilbert, Publisher, 7-30.

Boriová, S. – Sázelová, S. – Novák, M. – Štelcl, J. – Svoboda, J. 2020: Human and non-human taphonomic effects on faunal remains from the Late Upper Paleolithic: A case study from the Stránská skála IV site, Czech Republic. International Journal of Osteoarchaeology 30(2), 155-169. DOI: 10.1002/oa.2843.

Boriová, S. – Outram, A.K. – Pokorná, Z. – Sázelová S. in press: Bone fractures under the microscope. An experimental approach to Mid-Upper Paleolithic faunal remains. Študíjne zvesti 69(2).

Braidotti, P. – Bemporad, E. – D'Alessio, T. – Sciuto, S. A. – Stagni, L. 2000: Tensile experiments and SEM fractography on bovine subchondral bone. Journal of Biomechanics 33(9), 1153-1157. DOI: 10.1016/S0021-9290(00)00074-9.

Brain, C.K. 1967: Hottentot food remains and their meaning in the interpretation of fossil bone assemblages. Scientific Papers of the Namib Desert Research Station No. 32, 1-11.

Brain, C.K. 1969: The contribution of Namib Desert Hottentots to an understanding of Australopithecine bone accumulations. Scientific Papers of the Namib Desert Research Station 39, 13-22.

Brain, C.K. 1976: Some principles in the interpretation of bone accumulations associated with man. In: Human origins: Louis Leakey and the East African evidence, edited by Glynn LI. Isaac and Elizabeth R. McCown. Reading, Pennsylvania: W. A. Benjamin, Inc.

Brain, C.K. 1981: The hunters or the hunted? An Introduction into the South African cave taphonomy. Chicago: University of Chicago Press.

Breuil, H. 1938: The use of bone implements in the Old Paleolithic period. Antiquity 12, 56-67.

Breuil, H. 1939: Bone and antler industry of the Choukoutien Sinanthropus site. Palaeontologia Sinica, n. s. D., No. 6, Peking.

Brönnimann, D. – Portmann, C. – Pichler, S.L. – Booth, T.J. – Röder, B. – Vach, W. – Schibler, J. – Rentzel, P. 2018: Contextualising the dead: combining geoarchaeology and osteoanthropology in a new multi-focus approach in bone histotaphonomy. Journal of Archaeological Science 98, 45-58. DOI:10.1016/J.JAS.2018.08.005.

Brothwell, D. 1969: The study of archaeological materials by means of the scanning electron microscope: an important new field. In: D. Brotherwell – E. Higgs eds., Science in archaeology: a comprehensive survey of progress and research, 2nd edition. London: Thames and Hudson, 546-566.

Brugère, A. – Fontana, L. 2009: Mammoth origin and exploitation patterns at Milovice (area G excepted). In: M. Oliva ed., Sídliště mamutího lidu u Milovic pod Pálavou. Otázka struktur s mamutími kostmi. Studies in Anthropology, Palaeothnology, Palaeontolgy and Quaternary Geology 27(19), Moravské Zemské Muzeum, Brno, 51-105.
Brugère, A. – Fontana, L. – Oliva, M. 2009: Mammoth procurement and exploitation at Milovice (Czech Republic): new data for the Moravian Gravettian. In: L. Fontana – F. Chauvière – A. Bridault, In search of Total Animal Exploitation. Case Studies from the Upper Palaeolithic and Mesolithic, John and Erica Hedges, BAR International series 2040, 45-69.

Buckland, W. 1823: Reliquiae Diluvianae; or observations on the organic remains contained in caves, fissures, and diluvial gravel, and on other geological phenomena attesting the actions of a universal deluge. London: John Murray. New York: Arno Press. (Reprinted 1978).

Bunn, H.T. 1981: Archaeological evidence for meat-eating by Plio-Pleistocene hominids from Koobi Fora and Olduvai Gorge. Nature 291(5816), 574-576. DOI: 10.1038/291574a0.

Bunn, H.T. 1983: Comparative analysis of modern bone assemblages from a San hunter-gatherer camp in the Kalahari Desert, Bostwana, and from a spotted hyena den near Nairobi, Kenya. In: J. Clutton-Brock – C. Grigson eds., Animals and Archaeology, Hunters and Their Prey, vol. 1, British Archaeological Reports International Series 163. London, 143-148.

Bunn, H.T. 1989: Diagnosing Plio-Pleistocene hominid activity with bone fracture evidence. In: R. Bonnichsen – M. Sorg eds., Bone modification. Orono, ME: Center for the Study of the First Americans, Institute for Quaternary Studies, University of Maine, 299-315.

Burch E.S. 1972: The Caribou/Wild Reindeer as a Human Resource. American Antiquity 37(3), 339-368. DOI: 10.2307/278435.

Byers, D.A. – Keith, J.P. – Breslawski, R.P. 2020: Impact scar frequency, bone density and marrow utility: An experimental study. International Journal of Osteoarchaeology 30, 557–564. DOI: 10.1002/oa.2870.

Cáceres, I. – Bravo, P. – Esteban, M. – Expósito, I. – Saladié, P. 2002: Fresh and heated bones breakage. An experimental approach. In: M. de Rienzi – V. Pardo Alonso – M. Belinchón – E. Peñalver – P. Montoya – A. Márquez-Aliaga eds., Current topics on taphonomy and fossilization. Valencia, 471-481.

Campmas, E. – Beauval, C. 2008: Osseous carnivores consumption: Results of the study of the carcasses of cattle (Bos taurus) exploitation by captive wolves. Annales de Paléontologie 94, 167-186. DOI: 10.1016/j.annpal.2008.06.001.

Capaldo, S.D. 1997: Experimental determinations of carcass processing by Plio-Pleistocene hominids and carnivores at FLK 22 (Zinjanthropus), Olduvai Gorge, Tanzania. Journal of Human Evolution 33, 555-597. DOI: 10.1006/jhev.1997.0150.

Capaldo, S.D. – Blumenschine, R.J. 1994: A quantitative diagnosis of notches made by hammerstone percussion and carnivore gnawing in bovid long bones. American Antiquity 59(4), 724-748. DOI: 10.2307/282345.

Carden, F.R. – Hayden, T.J. 2006: Epiphyseal Fusion in the Postcranial Skeleton as an Indicator of Age at Death of European Fallow Deer (Dama dama dama, Linnaeus, 1758). In: D. Ruscillo ed., Recent Advances in Ageing and Sexing Animal Bones. Proceedings of the 9th Conference of the International Council of Archaeozoology, Durham, August 2002, Oxbow books, 227-236.

Carlson, K.S.D. – Mandl, K. – McCall, A. – Brönnimann, D. – Teschler-Nicola, M. – Weiss-Krejci, E. – Metscher, B. 2022: 3D visualization of bioerosion in archaeological bone. Journal of Archaeological Science 145, 105646. DOI: 10.1016/j.jas.2022.105646.

Carson, E.A. – Stefan, V.H. – Powell, J.F. 2000: Skeletal manifestations of bear scavenging. Journal of Forensic Science 45(3), 515-526. DOI:10.1520/jfs45305j.

Caruso, V. – Marinoni, N. – Diella, V. – Berna, F. – Cantaluppi, M. – Mancini, L. – Trombino, L. - Cattaneo, C. – Pastero, L. – Pavese, A. 2020: Bone diagenesis in archaeological and contemporary human remains: an investigation of bone 3D microstructure and minero-chemical assessment. Archaeological and Anthropological Sciences 12(8), 162. DOI:10.1007/s12520-020-01090-6.

Casanova, X. – Roldán, M. – Subirà, M.E. 2020: Analysis of cut marks on ancient human remains using confocal profilometer. Journal of Historical Archaeology & Anthropological Sciences 5(1), 18-26. DOI: 10.15406/jhaas.2020.05.00213.

Cattaneo, C. – Dimartino, S. – Scali, S. – Craig, O.E. – Grandi, M. – Sokol, R.J. 1999: Determining the human origin of fragments of burnt bone: a comparative study of histological, immunological, and DNA techniques. Forensic Science International. 102, 181-191. DOI: 10.1016/s0379-0738(99)00059-6.

Cattaneo, C. – Porta, D. – Gibelli, D. – Gamba, C. 2009: Histological determination of the human origin of bone fragments. Journal of Forensic Sciences 54(3), 531-533. DOI: 10.1111/j.1556-4029.2009.01000.x.

Coe, M. 1978: The decomposition of elephant carcasses in the Tsavo (East) National Park, Kenya. Journal of Arid Environments l(l), 71-86. DOI:10.1016/S0140-1963(18)31756-7.

Cohen, H. – Kugel, Ch. – May, H. – Medlej, B. – Stein, D. – Slon, V. – Hershkovitz, I. – Brosh, T. 2016: The impact velocity and bone fracture pattern: Forensic perspective. Forensic Science International 266, 54-62. DOI: 10.1016/j.forsciint.2016.04.035.

Coil, R. – Tappen, M. – Yezzi-Woodley, K. 2017: New Analytical Methods for Comparing Bone Fracture Angles: A Controlled Study of Hammerstone and Hyena (Crocuta crocuta) Long Bone Breakage. Archaeometry 59(5), 900–917. DOI: 10.1111/arcm.12285.

Conard, N. 2003: Palaeolithic ivory sculptures from southwestern Germany and the origins of figurative art. Nature 426, 830-832. DOI: 10.1038/nature02186.

Costamagno, S. – David, F. 2009: Comparaison des pratiques bouchères et culinaires de différents groupes sibériens vivant de la renniculture. Archaeofauna 18, 9–25.

Courtenay, L.A. – Yravedra, J. – Huguet, R. – Aramendi, J. – Maté-González, M.Á. – González-Aguilera, D. – Arriaza, M.C. 2019: Combining machine learning algorithms and geometric morphometrics: A study of carnivore tooth marks. Palaeogeography, Palaeoclimatology, Palaeoecology, 522, 28-39. DOI: 10.1016/j.palaeo.2019.03.00.

Crowder, C. – Stout, S. eds. 2012: Bone Histology. An Anthropological Perspective. CRC Press, Boca Raton.

Cuijpers, A.G.F.M. 2006: Histological identification of bone fragments in archaeology: telling humans apart from horses and cattle. International Journal of Osteoarchaeology 16, 465-480. DOI: 10.1002/oa.848

Cummaudo, M. – Cappella, A. – Giacomini, F. – Raffone, C. – Marquez-Grant, N. – Cattaneo, C. 2019: Histomorphometric analysis of osteocyte lacunae in human and pig: exploring its potential for species discrimination. International Journal of Legal Medicine. DOI: 10.1007/s00414-018-01989-9.

Currey, J.D. 1964: Three analogies to explain the mechanical properties of bone. Biorheology 2, 1-10. DOI: 10.3233/BIR-1964-2101.

Currey, J.D. 2002: Bones: structures and mechanics. Oxford: Princeton University Press.

Currey, J.D. 2012: The structure and mechanics of bone. Journal of Material Sciences 47, 41-54. DOI: 10.1007/s10853-011-5914-9.

Cruz-Uribe, K. 1991: Distinguishing hyena from hominid bone accumulations. Journal of Field Archaeology 18, 467-486. DOI: 10.1179/009346991791549068.

Čihák, R. 2001: Anatomie 1. Druhé upravené a doplněné vydání. Grada.

Dart, R.A. 1949: The predatory implemental technique of Australopithecus. American Journal of Physical Anthropology, 7(1), 1-38.

Dart, R.A. 1957: The osteodontokeratic culture of Australopithecus prometheus. Memoir of the Transvaal Museum, Pretoria 10, 1-105.

Dart, R.A. 1959: Further light on Australopithecine humeral and femoral weapons. American Journal of Physical Anthropology 17(2), 87-93.

Dart, R.A. 1960: The bone tool-manufacturing ability of Australopithecus prometheus. American Anthropologist 62(1), 134-143.

Daujeard, C. – Falguères, Ch. – Shao, O. – Geraads, D. – Hublin, J.J. – Lefèvre, D. - El Graoui, M. – Rué, M. – Gallotti, R. – Delvigne, V. – Quefellec, A. – Arous, E.B. – Tombret, O. – Mohib, A. – Raynal, J.P. 2020: Earliest African evidence of carcass processing and consumption in cave at 700 ka, Casablanca, Morocco. Scientific Reports 10, 4761. DOI: 10.1038/s41598-020-61580-4.

Davis, K.L. 1985: A taphonomic approach to experimental bone fracturing and applications to several South African pleistocene sites. Binghamton: SUNY Binghamton.

Dean, C. 2017: How the microstructure of dentine can contribute to reconstructing developing dentitions and the lives of hominoids and hominins. Comptes Rendus Palevol. 16 (5-6), 557-571. DOI: 10.1016/j.crpv.2016.10.006.

Delmas, P.D. – Tracy, R.P. – Riggs, B.L. – Mann, K.G. 1984: Identification of the noncollagenous proteins of bovine bone by two.dimensional gelelectrophoresis. Calcified Tissue International 36, 308-316. DOI: 10.1007/BF02405335.

De Juana, S. – Domínguez-Rodrigo, M. 2011: Testing Analogical Taphonomic Signatures in Bone Breaking: A Comparison Between Hammerstone-Broken Equid and Bovid Bones. Archaeometry 53(5), 996-1011. DOI: 10.1111/j.1475-4754.2010.00576.x.

De Lumley, H. 1969: Une cabane AcheuJéenne dans la Grotte du Lazaret. Memoirs de la Société Préhistorique Frangaise, Tome 7. Paris: Société Préhistorique Frangaise.

De Ruiter, D.J. – Berger, L.R. 2000: Leopards as taphonomic agents in Dolomitic caves - implications for bone accumulations in the hominid-bearing deposits of South Africa. Journal of Archaeological Science 27, 665-684. DOI: 10.1006/jasc.1999.0470.

Dirks, W. – Reid, D.J. – Jolly, C.J. – Phillips-Conroy, J.E. – Brett, F.L. 2002: Out of the mouths of baboons: stress, life history, and dental development in the Awash National Park hybrid zone, Ethiopia. American Journal of Physical Anthropology 118, 239-252. DOI: 10.1002/ajpa.10089.

Dixon, E.J. 1984: Context and Environment in Taphonomic Analysis: Examples from Alaska's Porcupine River Caves. Quaternary Research 22, 201-215. DOI: 10.1016/0033-5894(84)90040-1.

Doblaré, M. – García, J.M. – Gómez, M.J. 2004: Modelling bone tissue fracture and healing: a review. Engineering Fracture Mechanics 71, 1809-1840. DOI: 10.1016/j.engfracmech.2003.08.003.

Domínguez-Rodrigo, M. 2002: Hunting and Scavenging by Early Humans: The State of the Debate. Journal of World Prehistory 16(1), 1-54. DOI: 10.1023/A:1014507129795.

Domínguez-Rodrigo, M. – Barba, R. 2006: New estimates of tooth mark and percussion mark frequencies at the FLK Zinj site: the carnivore-hominid-carnivore hypothesis falsified. Journal of Human Evolution 50, 170-194. DOI: 10.1016/j.jhevol.2005.09.005.

Domínguez-Rodrigo, M. – Barba, R. – Egeland, C. P. 2007: Deconstructing Olduvai, Springer, New York.

Domínguez-Rodrigo, M. – de Juana, S. - Galán, A.B. – Rodríguez, M. 2009: A new protocol to differentiate trampling marks from butchery cut marks. Journal of Archaeological Science 36, 2643–2654. DOI: 10.1016/j.jas.2009.07.017.

Domínguez-Rodrigo, M. – Gidna, O.A. – Yravedra, J. – Musiba, Ch. 2012: A Comparative Neo-Taphonomic Study of Felids, Hyaenids and Canids: an Analogical Framework Based on Long Bone Modification Patterns. Journal of Taphonomy 10(3-4), 151-169.

Domínguez-Rodrigo, M. – Cifuentes-Alcobendas, G. – Jiménez-García, B. – Abellán, N. – Pizarro-Monzo, M. – Organista, E. – Baquedano, E. 2020: Artificial intelligence provides greater accuracy in the classification of modern and ancient bone surface modifications. Scientific Reports 10, 18862. DOI: 10.1038/s41598-020-75994-7.

Domínguez-Rodrigo, M. – Gidna, A. – Baquedano, E. – Cobo-Sánchez, L. – Mora R. – Courtenay, L.A. – Gonzalez-Aguilera D. – Mate-Gonzalez M.A. – Prieto-Herráez, D. 2021: A 3D taphonomic model of long bone modifcation by lions in medium-sized ungulate carcasses. Nature: Scientific Reports 11, 4944. DOI: 10.1038/s41598-021-84246-1.

Efremov, I.A. 1940: Taphonomy: a new branch of paleontology. Pan-American Geologist 74, 81-93.

Emra, S. – Benz, M. – Siddiq, A.B. – Özkaya, V. 2022: Adaptions in subsistence strategy to environment changes across the Younger Dryas - Early Holocene boundary at Körtiktepe, Southeastern Turkey. The Holocene 32(5), 390-413. DOI: 10.1177/09596836221074030.

Enloe, J.G. 1993: Ethnoarchaeology of marrow cracking: implications for the recognition of prehistoric subsistence organization. In: J. Hudson ed., From bones to behavior: ethnoarchaeological and experimental contributions to the interpretation of faunal remains. Carbondale: Southern Illinois University, 82-100.

Enlow, D.H. 1966: An evaluation of the use of bone histology in forensic medicine and anthropology. In: F.G. Evans ed., Studies on the anatomy and function of bones and joints. Springer-Verlag: Berlin, 93-112.

Enlow, D.H. – Brown S.O. 1956: A comparative histological study of fossil andrecent bone tissue, part I. Texas Journal of Science 8,405-443.

Eriksen, M.F. 1991: Histological estimation of age at death using the anterior cortex of femur. American Journal of Physical Anthropology 84, 171-179. DOI: 10.1002/ajpa.1330840207.

Evans, F.G. 1957: Stress and strain in bones: Their relation to fractures and osteogenesis. Springfield, Illinois: Charles C. Thomas, Publisher.

Evans, F.G. 1961: Relation of the physical properties of bone to fractures. American Academy of Orthopaedic Surgeons, Instructional Course Lectures 18, 110-121.

Evans, F.G. 1973: Mechanical properties of bone. Springfield, Illinois: Charles C. Thomas, Publisher.

Evennet, P.J. – Hammond, C. 2005: Microscopy. Overview. In: P. Worsfold – A. Townshend – C. Poole eds., Encyclopedia of Analythical Science. Second Edition. Elsevier Publishing,32-41.

Fernández-Jalvo, Y. – Andrews, P. 2011: When human chew bones. Journal of Human Evolution 60 (1), 117-123. DOI: 10.1016/j.jhevol.2010.08.003.

Fernández-Jalvo, Y. – Andrews P. 2016: Atlas of Taphonomic Identifications. Vertebrate Paleobiology and Paleoanthropology. Springer, Dordrecht. DOI: 10.1007/978-94-017-7432-1_1.

Ferretti, M.P. 2007: Evolution of bone-cracking adaptations in hyaenids (Mammalia, Carnivora). Swiss Journal of Geosciences 100, 41-52. DOI: 10.1007/s00015-007-1212-6.

Fiorillo, A.R. 1984: An experimental study of trampling: implications for the fossil record. In: R. Bonnichsen, R. – M.H. Sorg eds., Bone Modification. Orono: Center for the Study of the First Americans, Institute for Quaternary Studies, University of Maine, Maine, 61-72.

Fladerer, F.A. 2001a: Die Faunareste von Krems-Wachtberg, Ausgrabung 1930. Jagwild und Tierkörpernutzung an der Donau vor 27 000 Jähren. Austrian Academy of Sciences, Mitteilungen der Prähistorischen Kommission 39. Wien.

Fladerer, F.A. 2001b: The Krems-Wachtberg campsite: mammoth carcass utilization at the Danube 27ka ago. In: G. Cavarretta – P. Giola – M. Mussi – M.R. Palombo eds., Proceedings of the 1st International Congress (Atti del 1° Congresso Internazionale), The World of Elephants (La Terra degli Elefanti), Rome, 423-438.

Fladerer, F.A. – Salcher, T. 2004: Faunal remains from the Krems – Hundsstied/Wachtberg Gravettian site complex – A difference in research techniques and/or site function? In: J. Svoboda – L. Sedláčková eds., The Gravettian along Danube. Proceedings of the Mikulov Conference, 20.-21. November 2022. The Dolní Věstonice Studies 11. Academy of Sciences of the Czech Republic, Institute of Archaeology, Brno, 100-115.

Fladerer, F.A. – Salcher Jedrasiak T. 2008: Krems-Hundsstieg 2000-2002: Archaeozoologische und taphonomische Unteruchungen. In: C. Neugebauer Maresch, N. ed., Krems-Hundssteig – Mammutjagerlager der Eiszeit, Ein Nutzungsareal palaolithischer Jager- und Sammler (innen) vor 41.000–27.000 Jahren. Austrian Academy of Sciences, Mitteilungen der Prähistorischen Kommission 67, Wien, 216-312.

Fladerer, F.A. – Salcher Jedrasiak, T. 2010: Animal facts and human decisions, 27 ka ago: the Krems-Hundssteig 2000/02 camp periphery. In: C. Neugebauer-Maresch – L.R. Owen eds., New Aspects of the Central and Eastern European Upper Palaeolithic: Methods, Chronology, Technology and Subsistence. Austrian Academy of Sciences, Mitteilungen der Prähistorischen Kommission72, Wien, 163-181.

Fladerer, F.A. – Salcher Jedrasiak T. – Händel, M. 2014: Hearth-side bone assemblages within the 27 ka BP Krems-Wachtberg settlement: Fired ribs and the mammoth bone-grease hypothesis, Quaternary International 351, 115-133. DOI: 10.1016/j.quaint.2012.06.030.

Fladerer, F.A. – Salcher Jedrasiak, T. – Händel, M. – Simon, U. 2010: Evidence of mammoth bone-grease manufacture within a 27 ka BP Gravettian encampment at Krems an der Donau (Lower Austria)? In: J.D. Vigne – M. Patou-Mathis – C. Lefèvre, 11th International Conference of Archaeozoology, ICAZ 2010-Paris, 23–28 August 2010, 132.

Frahm, E. 2014: Scanning Electron Microscopy (SEM): Applications in Archaeology. In: C. Smith ed., Encyclopedia of Global Archaeology, New York: Springer, 6487-6495.

France, D. L. 2009: Human and Nonuhuman Bone Identification: A Color Atlas. Boca Raton: CRC Press.

Freeman, L.G. 1978: Mousterian worked bone from Cueva Morin (Santander, Spain): A preliminary description. In: L.G Freeman ed., Views of the past. The Hague: Mouton, 29-51.

Frison, G. 1970: The Glenrock Buffalo Jump, 48CO304. Plains Anthropologist Memoir No. 7.

Gash, P.J.S. 1971: A study of surface features relating to brittle and semi-brittle fracture. Tectonophysics 12, 349-391. DOI: 10.1016/0040-1951(71)90040-0.

Galán, A.B. – Rodríguez, M. – de Juana, S. – Domínnguez-Rodrigo, M. 2009: A new experimental study on percussion marks and notches and their bearing on the interpretation of hammerstone-broken faunal assemblages. Journal of Archaeological Science 36, 776-784. DOI: 10.1016/j.jas.2008.11.003.

Germonpré, M. – Lázničková-Galetová, M. – Jimenez, E.L. – Losey, R. – Sablin, M. – Bocherens, H. – van den Broeck, M. 2017: Consumption of canid meat at the gravettian Předmostí site, the Czech Republic. Fossil Imprint 73(3-4), 360-382. DOI: 10.2478/if-2017-0020.

Gidna, A. – Yravedra, J. – Domínguez-Rodrigo, M. 2013: A cautionary note on the use of captive carnivores to model wild predator behavior: a comparison of bone modification patterns on long bones by captive and wild lions, Journal of Archaeological Science 40(4), 1903-1910. DOI: 10.1016/j.jas.2012.11.023.

Gifford, D.P. 1977: Observations of modern human settlements as an aid to archaeological interpretation. Ph.D. dissertation, University of California, Berkeley.

Gifford, D.P. 1981: Taphonomy and paleoecology: A critical review of archaeology's sister disciplines. In: M. Schiffer ed., Advances in archaeological method and theory (volume 4). New York: Academic Press, 365-438.

Gifford-Gonzalez, D. 1989: Ethnographic Analogues for Interpreting Modified Bones: Some Cases from East Africa. In: R. Bonnichsen, R. – M.H. Sorg eds., Bone Modification. Orano: University of Maine Centre for the Study of the First Americans, Maine, 179-246.

Gifford-Gonzalez, D. 2018: An Introduction to Zooarchaeology. Springer International Publishing AG. DOI: 10.1007/978-3-319-65682-3.

Gifford-Gonzalez D. – Damrosch D.B. – Damrosch D.R. – Pryor J. – Thunen R.L. 1985: The Third Dimension in Site Structure: An Experiment in Trampling and Vertical Dispersal. American Antiquity 50(4), 803-818. DOI: 10.2307/280169.

Gonzáles Carretero, L. – Wollstonecroft, M. – Fuller, D.Q. 2017: A methodological approach to the study of archaeological cereal meals: a case study at Çatalhöyük East (Turkey). Vegetation History and Archeobotany 26, 415-432. DOI: 10.1007/s00334-017-0602-6.

Göldner, D. – Karakostis, F.A. – Falcucci, A. 2022: Practical and technical aspects for the 3D scanning of lithic artefacts using micro-computed tomography techniques and laser light scanners for subsequent geometric morphometric analysis. Introducing the StyroStone protocol. PLoS ONE 17(4), e0267163. DOI: 10.1371/journal.pone.0267163.

Guthrie, R.D. 1980: The first Americans? The elusive Arctic bone culture. The Quarterly Review of Archaeology 1:2.

Grunwald, A.M. 2016: Analysis of fracture patterns from experimentally marrow-cracked frozen and thawed cattle bones. Journal of Archaeological Science: Reports 8, 356-365. DOI: 10.1016/j.jasrep.2016.06.022.

Haglund, W.D. – Sorg, M.H. 2002: Human Remains in Water Environments. In: W.D. Haglund – M.H. Sorg eds., Advances in forensic taphonomy: Method, Theory, and Archaeological Perspectives. Boca Raton: CRC Press, 201-218.

Hahn, J. 1993: Erkennen und Bestimmen von Stein-und Knochenartefakten. Einführung in die Artefaktmorphologie. Verlag Archaeologica Venatoria Insititut für Urgeschichte, Universität Tübingen.

Hamed, E. – Lee, Y. – Jasiuk, I. 2010: Multiscale modelling of elastic properties of cortical bone. Acta Mechanica 213, 131-154. DOI: 10.1007/s00707-010-0326-5.

Hanson, M. – Cain, C.H.R. 2007: Examining histology to identify burned bone. Journal of Archaeological Science 34, 1902-1913. DOI: 10.1016/j.jas.2007.01.009.

Harris, S. 1978: Age determination in the Red fox (Vulpes vulpes) - an evaluation of technique efficiency as applied to a sample of suburban foxes. Jornal of Zoology 184, 91-117. DOI: 10.1111/j.1469-7998.1978.tb03268.x.

Hart, N.H. – Nimphius, S. – Rantalainen, T. – Ireland, A. – Siafarikas, A. – Newton, R.U. 2017: Mechanical basis of bone strength: influence of bone material, bone structure and muscle action. Journal of Musculoskeletal & Neuronal Interactions 17(3), 114-139.

Hayes, W.C. – Carter, D.R. 1979: Biomechanics of bone. In: D.J. Simmons ed., Skeletal research: An experimental approach. New York: Academic Press, 263-300.

Haynes, G. 1978a: Excavation of a small Virginia cave. Bulletin of the Archaeological Society of Virginia 32(3), 37-41.

Haynes, G. 1978b: Morphological damage and alteration to bone: Laboratory experiments, field studies, and zoo studies. The American Quaternary Association: Abstracts of the Fifth Biennial Meeting. Edmonton.

Haynes, G. 1980: Evidence of carnivore gnawing on Pleistocene and Recent mammalian bones. Paleobiology 6(3), 341-351.

Haynes, G. 1981: Bone modifications and skeletal disturbances by natural agencies: Studies in North America. Unpublished Ph.D. dissertation, Catholic University of America, Washington, D.C.

Haynes, G. 1982: Utilization and skeletal disturbances of North American prey carcasses. Arctic 35(2), 266-281.

Haynes, G. 1983a: Frequencies of spiral and green-bone fractures on ungulate limb bones in modern surface assemblages. American Antiquity 48(1), 102-114. DOI:10.2307/279822.

Haynes, G. 1983b: A guide for diferentiating mammalian carnivore taxa responsible for gnaw damage to herbivore limb bones. Paleobiology 9(2), 164-172.

Haynes, G. 2017: Taphonomy of the Inglewood mammoth (Mammuthus columbi) (Maryland, USA): Green-bone fracturing of fossil bones. Quaternary International 445, 171-183. DOI:10.1016/J.QUAINT.2016.02.034.

Haynes, G. 2000: Mammoths, Measured Time, and Mistaken Identities. Radiocarbon 42(2), 257-269. DOI: 10.1017/S0033822200059063.

Haynes, G. – Klimowicz, J. 2015: A preliminary review of bone and teeth abnormalities seen in recent Loxodonta and extinct Mammuthus and Mammut, and suggested implications. Quaternary International 379, 135-146. DOI: 10.1016/j.quaint.2015.04.001.

Haynes, G. – Krasinski, K. – Wojtal, P. 2020: Elephant bone breakage and surface marks made by trampling elephants: Implications for interpretations of marked and broken Mammuthus spp. Bones. Journal of Archaeological Science: Reports 33, 102491. DOI: 10.1016/j.jasrep.2020.102491.

Haynes, G. – Krasinski, K. – Wojtal, P. 2021: Study of Fractured Proboscidean Bones in Recent and Fossil Assemblages. Journal of Archaeological Method Theory 28, 956–1025. DOI: 10.1007/s10816-020-09486-3.

Hedges, R.E.M. – Millard, A.R. 1995: Bones and Groundwater: Towards the Modelling of Diagenetic Processes. Journal of Archaeological Science 22, 155–164. DOI: 10.1006/jasc.1995.0017.

Heinrich, D. 1991: Untersuchungen an Skelettresten wildlebender Säugetiere aus dem mittelalterlichen Schleswig. Ausgrabungen Schild 1971-1975, Ausgrabungen in Schleswig, Berichte und Studien 9, Neumünster.

Herrmann, G. – Liebowitz, H. 1972: Mechanics of bone fracture. InH. Liebowitz ed., Fracture: An advance treatise, Volume 7. New York: Academic Press, 771-840.

Hidaka, S. – Matsumoto, M. – Ohsako, S. – Toyoshima, Y. – Nishinkagawa, H. – 1998: A histometrical study on the long bones of Raccoon Dogs, Nycterettes procyonoides and Badgers, Meles meles. Journal of Veterinary Science 60 (3), 323-326. DOI: 10.1292/jvms.60.323.

Hill, A.P. 1976: On carnivore and weathering damage to bone. Current Anthropology 17(3), 335-336. DOI:10.1086/201732.

Hiller, L.P. – Stover, S.M. – Gibson, V.A. – Gibeling, J.C. – Prater, C.S. – Hazelwood, S.J. – Yeh, O.C. – Martin, R.B. 2003: Osteon pullout in the equine third metacarpal bone: effects of ex vivo fatigue. Journal of Orthopaedic Research 21, 481-488 DOI: 10.1016/S0736-0266(02)00232-2.

Hillier, M.L. – Bell, L.S. 2007: Differentiating human bone from animal bone: a review of histological method. Journal of Forensic Sciences 52(2), 249-263. DOI: 10.1111/j.1556-4029.2006.00368.x.

Hillson, S. 1992: Mammal Bones and Teeth: an intorductory guide to methods of identification. Institute of Archaeology, University College London.

Hillson, S. 2005: Teeth (II. ed.). New York: Cambridge University Press.

Hollund, H.I. – Blank, M. – Sjogren, K.G. 2018: Dead and buried? Variation in post-mortem histories revealed through histotaphonomic characterisation of human bone from megalithic graves in Sweden. PloS One 13 (10), e0204662. DOI: 10.1371/journal.pone.0204662.

Hollund, H.I. – Jans, M.M.E. – Collins, M.J. – Kars, H. – Joosten, I. – Kars, S.M. 2011: What happened here? Bone histology as a tool in decoding the postmortem histories of archaeological bone from Castricum, The Netherlands. International Journal of Osteoarchaeology 22(5), 537-548. DOI: 10.1002/oa.1273.

Hollund, H.I. – Arts, N. – Jans, M.M.E. – Kars, H. 2015: Are teeth better? Histological characterization of diagenesis in archaeological bone–tooth pairs and a discussion of the consequences for archaeometric sample selection and analyses. International Journal of Osteoarchaeology 25(6), 901-911. DOI: 10.1002/oa.2376.

Horwitz, L.K. – Monchot, H. 2002: Choice cuts: Hominid butchery activities at the Lower Paleolithic Site of Holon, Israel. In: H. Buitenhuis – A.M. Choyke – M. Mashkour – A.H. Al-Shiyab eds., Archaeozoology of the Near East V: Proceedings of the Fifth International Symposium on the Archaeozoology of Southwestern Asia and Adjacent Areas held at Yarmouk University, Irbid, Jordan in 2000. ARC: Groningen, The Netherlands, 48-61.

Howell, F.C. 1965: Early man. New York: Time-Life Books.

Huisman, H. – Ismail-Meyer, K. – Sageidet, B.M. – Joosten, I. 2017: Micromorphological indicators for degradation processes in archaeological bone from temperate European wetland sites. Journal of Archaeological Science 85, 13-29. DOI: 10.1016/j.jas.2017.06.016.

Hupková, A. – Šáliová, S. – Králík, M. – Malček, M. 2016: Nejsou čáry jako čáry: inkrementální linie v mikrostruktuře zubů a jejich využití při analýze kosterních nálezů. Studia archaeologica Brunensia 21(2), 113-138. DOI: 10.5817/SAB2016-2-7.

Hutson, J.M. – García-Moreno, A. – Noack, E.S. – Turner, E. – Villaluenga, A. - Gaudzinski-Windheuser, S. 2018a: The Origins of Bone Tool Technologies. RGZM – TAGUNGEN, Band 35, Mainz.

Hutson, J.M. – Villaluenga, A. – García-Moreno, A. – Turner, E. – Gaudzinski-Windheuser, S. 2018b: On The Use of Metapodials as Tools at Schöningen 13II-4. In: J.M. Hutson – A. García-Moreno – E.S. Noack – E. Turner – A. Villaluenga – S. Gaudzinski-Windheuser eds., The Origins of Bone Tool Technologies. RGZM – TAGUNGEN, Band 35, Mainz, 53-91.

Hromadová, B. 2016: XVI. Bone, Antler and Ivory Tools. In: J. Svoboda ed., Dolní Věstonice II. Chronostratigraphy, Paleoethnology, Paleoanthropology. The Dolní Věstonice Studies 21. Academy of Sciences of the Czech Republic, Institute of Archaeology, Brno, 273-302.

Charlier, P. – Huynh-Charlier, I. – Munoz, O. – Billard, M. – Brun, L. – de la Grandmaison, G.L. 2010: The microscopic (optical and SEM) examination of dental calculus deposits (DCD). Potential interest in forensic anthropology of a bio-archaeological method. Legal Medicine 12, 163-171. DOI: 10.1016/j.legalmed.2010.03.003.

Choyke, A.M. 1997: The Bone Tol Manufacturing Continuum. Anthropozoologica 25-26, 65-72.

Indra, L. – Errickson, D. – Young, A. – Lösch, S. 2022: Uncovering Forensic Taphonomic Agents: Animal Scavenging in the European Context. Biology 11, 601. DOI: 10.3390/biology11040601.

Jans, M.M.E. 2005: Histological Characterisation of Diagenetic Alternation of Archaeological Bone. Geoarchaeological and Bioarchaeological Studies 4. Institute for Geo and Bioarchaeology, Amsterdam.

Jans, M.M.E. – Kars, H. – Nielsen-Marsh, C.M. – Smith, C.I. – Nord, A.G. – Arthur, P. – Earl, N. 2002: In situ preservation of archaeological bone: a histological study within a multidisciplinary approach. Archaeometry 44 (3), 343-352. DOI: 10.1111/1475-4754.t01-1-00067.

Järvinen, T.L.N. – Kannus, P. – Sievänen, H. – Jolma, P. – Heinonen, A. – Järvinen, M. 1998: Randomized controlled study of effects of sudden impact loading on rat femur. J. Bone Miner. Res. 13(9), 14751482. DOI: 10.1359/jbmr.1998.13.9.1475.

Johnson, E. 1985: Current Developments in Bone Technology. Advances in Archaeological Method and Theory 8, 157-235.

Johnson, E.V. – Parmenter, P.C.R. – Outram, A.K. 2016: A new approach to profiling taphonomic history through bone fracture analysis, with an example application to the Linearbandkeramik site of Ludwinowo 7. Journal of Archaeological Science: Reports 9, 623-629. DOI: 10.1016/j.jasrep.2016.08.047.

Jopling, A. V. – Irving, W. N. – Beebe, B. F. 1981: Stratigraphic, sedimentological and faunal evidence for the occurrence of pre-Sangamonian artefacts in Northern Yukon. Arctic 34(1), 3-33.

Karol, M. 2005: Soby (Artiodactyla, Mammalia) z mladopaleolitického táboriska v TrenčianskychBohuslaviciach. Master thesis, manuscript –archive of DGP, Prif UK, Bratislava, 97.

Karr, L.P. 2012: The Analysis and Interpretation of Fragmented Mammoth Bone Assemblages: Experiments in Bone Fracture with Archaeological Applications. Unpublished PhD thesis, University of Exeter.

Karr, L.P. – Outram, A.K. 2012a: Tracking changes in bone fracture morphology over time: environment, taphonomy, and the archaeological record. International Journal of Archaeological Science 39, 555-559. DOI: 10.1016/J.JAS.2011.10.016.

Karr, L.P. – Outram, A.K. 2012b: Actualistic research into dynamic impact and its implications for understanding differential bone fragmentation and survivorship. Journal of Archaeological Science 39(11), 3443-3449. DOI: 10.1016/J.JAS.2012.05.013.

Karr, L.P. – Outram, A.K. 2015: Bone Degradation and Environment: Understanding, Assessing and Conducting Archaeological Experiments Using Modern Animal Bones. International Journal of Osteoarchaeology 25(2), 201-212. DOI: 10.1002/oa.2275.

Karr, L.P. – Outram, A.K. – Hannus, L.A. 2010: A Chronology of Bone Marrow and Bone Grease Exploitation at the Mitchell Prehistoric Indian Village. Plains Anthropologist 55, 215-223. DOI: 10.1179/pan.2010.019.

Karr, L.P. – Short, A.E.G. – Hannus L.A. – Outram A.K. 2015: A bone grease processing station at the Mitchell Prehistoric Indian Village: Archaeological evidence for the exploitation of bone fats. Environmental Archaeology 20(1), 1-12. DOI: 10.1179/1749631414Y.0000000035.

Keenan, S.W. – Engel, A.S. 2017: Reconstructing diagenetic conditions of bone at the Gray Fossil Site, Tennessee, USA. Palaeogeography, Palaeoclimatology, Palaeoecology 471, 48-57. DOI: 10.1016/j.palaeo.2017.01.037.

Kent, S. 1993: Variability in faunal assemblages: The influence of hunting skill, sharing, dogs, and mode of cooking on faunal remains at a sedentary Kalahari community. Journal of Anthropological Archaeology 10, 1-26. DOI: 10.2307/3889030.

Klein, R.G. 1975: Paleoanthropological implications of the nonarchaeological bone assemblage from Swartklip 1, South-Western Cape Province, South Africa. Quaternary Research 5, 275-278.

Klíma, B. 1954: Pavlov, nové paleolitické sídliště na jižní Moravě. Archeologické rozhledy 3, 137-142.

Klíma, B. 1959: Výzkum paleolitického sídliště u Pavlova v roce 1954. Archeologické rozhledy 11, 3-15.

Klíma, B. 1962: Výzkum paleolitického sídliště Pavlov I. Přehled výzkumů 1961, 16-19.

Klíma, B. 1963: Výzkum paleolitického sídliště Pavlov I. Přehled výzkumů 1962, 4-6.

Klíma, B. 1964: Výzkum paleolitického sídliště Pavlov I. Přehled výzkumů 1963, 5-8.

Klíma, B. 1971: Paleolitické výzkumy pod Pavlovskými kopci. Přehled výzkumú 1970 15, 6-8.

Klíma B. 1972: Výzkum paleolitické stanice v Pavlově. Přehled výzkumů 1971, Brno, 11-13.

Klíma, B. 1997: Grabungsgeschichte, Stratigraphie und Fundumstände. In: J. Svoboda ed., Pavlov I – Northwest, The Dolní Věstonice Studies 4. Academy of Sciences of the Czech Republic, Institute of Archaeology Brno, 13-51.

Krajcarz, M. – Krajcarz, M.T. 2012: The red fox (Vulpes vulpes) as an accumulator of bones in cave-like environments. International Journal of Osteoarchaeology 24, 459-475. DOI: 10.1002/oa.2233.

Kyselý, R. 2004: Kvantifikační metody v archeozoologii. Archeologické rozhledy 56(2), 279-296.

Lam, Y.M. 1992: Variability in the behaviour of spotted hyaenas as taphonomic agents. Journal of Archaeological Science 19, 389-406. DOI: 10.1016/0305-4403(92)90057-A.

Lambri, M.L. – Bozzano, P.B. – Giordano, E.D.V. – Bonifacich, F.G. – Gargicevich, D. – Zelada, G.I. – Lambri, O.A. 2018: Denaturation processes of collagen from cow bones as a function of temperature. Revista Matéria 23(2) ISSN 1517-7076 artigo e-12089. DOI: 10.1590/S1517-707620180002.0424.

Lemmers, S.A.M. – Gonçalves, D. – Cunha, E. – Vassalo, A.R. – Appleby, J. 2020: Burned Fleshed or Dry? The Potential of Bioerosion to Determine the Pre-Burning Condition of Human Remains. Journal of Archaeological Method and Theory 27, 972-991. DOI: 10.1007/s10816-020-09446-x.

Li, S. – Abdel-Wahab, A. – Silberschmidt, V.V. 2013: Analysis of fracture processes in cortical bone tissue. Engineering Fracture Mechanics 110, 448-458. DOI: 10.1016/j.engfracmech.2012.11.020.

Li, X. 2018: What did the fox say? Assessing the role of foxes through ethnographic and archaeological contexts. Unpublished dissertation thesis. University of Exeter, Exeter.

Lipecki, G. – Wojtal, P. 1998: Mammal remains. In: J.K. Kozłowski ed., Complex of Upper Palaeolithic sites near Moravany, Western Slovakia. Vol. II. Moravany-Lopata II. (Excavations 1993–1996). Jagellonian University, Institute of Archaeology, Krajów 103-126.

Lipecki, G. – Wojtal, P. 2015: Carnivores from the open-air site Kraków Spadzista. In: P. Wojtal – J. Wilczyński – G. Haynes eds., A Gravettian Site in Southern Poland. Kraków Spadzista. Institute of Systematics and Evolution of Animals of the Polish Academy of Sciences, Kraków, 117-158.

Lord, T.C. – O'Connor, T.P. – Siebrandt, D.C. – Jacobi, R.M. 2007: People and large carnivores as biostratinomic agents in Late glacial cave assemblages. Journal of Quaternary Science 22(7), 681-694. DOI: 10.1002/jqs.1101.

Lorentz, K.O. – Lemmers, S.A.M. – Chrysostomou, C. – Dirks, W. – Zaruri, M.R. – Foruzanfar, F. – Sajjadi, S.M.S. 2019: Use of dental microstructure to investigate the role of prenatal and early life physiological stress in age at death. Journal of Archaeological Science 104, 85-96. DOI: 10.1016/j.jas.2019.01.007.

Lupo, K.D. 2001: Archaeological Skeletal Part Profiles and Differential Transport: An Ethnoarchaeological Example from Hadza Bone Assemblages. Journal of Anthropological Archaeology 20(3), 361-378. DOI: 10.1006/jaar.2000.0378.

Lyman, R.L. 1994: Vertebrate taphonomy. Cambridge University Press, Cambridge Manuals in Archaeology, Cambridge.

Lyman, R.L. – O´Brien, M.J. 1987: Plow-zone zooarchaeology: fragmentation and identifiability. Journal of Field Archaeology 14, 493-498. DOI: 10.1179/jfa.1987.14.4.493.

Lynn, K.S. – Fairgrieve, S.I. 2009: Microscopic Indicators of Axe and Hatchet Trauma in Fleshed and Defleshed Mammalian Long Bones. Journal of Forensic Sciences 54(4), 793-797. DOI: 10.1111/j.1556-4029.2009.01062.x.

Mack, R.W. 1964: Bone - a natural two-phase material. Technical Memorandum, Biomechanics Laboratory, University of California, San Francisco-Berkeley.

Marean, C.W. – Abe, Y. – Frey, C.J. – Randall, R.C. 2000: Zooarchaeological and taphonomic analysis of the Die Kelders Cave 1 Layers 10 and 11 Middle Stone Age larger mammal fauna. Journal of Human Evolution 38, 197-233. DOI: 10.1006/jhev.1999.0356.

Marín, J. – Saladié, P. – Rodríguez-Hidalgo, A. – Carbonell, E. 2017: Neanderthal hunting strategies inferred from mortality profiles within the Abric Romaní sequence. Plos One 12(11), e0186970. DOI: 10.1371/journal.pone.0186970.

Marshall, L.G. 1989: Bone modification and the „lawss of burial". In R. Bonnichsen, R. – M.H. Sorg eds., Bone Modification. Orano: University of Maine Centre for the Study of the First Americans, Maine, 7-24.

Martin, R.B. – Burr, D.B. 1989: Structure, function, and adaptation of compact bone. New York: Raven Press.

Martin, R.B. – Burr, D.B. – Sharkey, N.A. 1998: Skeletal tissue mechanics. New York: Springer.

Martiniaková, M. – Grosskopf, B. – Omelka, R. – Dammers, K. – Vondráková, M. – Bauerová, M. 2006: Differences among species in compact bone tissue microstructure of mammalian skeleton: use of a discriminant function analysis for species identification. Journal of Forensic Sciences 51 (6), 1235-1239. DOI: 10.1111/j.1556-4029.2006.00260.x.

Martiniaková, M. – Grosskopf, B. – Omelka, R. – Dammers, K. – Vondráková, M. – Bauerová, M. 2007: Histological study of compact bone tissue in some mammals: a method for species determination. International Journal of Osteoarchaeology 17, 82-90. DOI: 10.1002/oa.856.

McComb, K. – Baker, L. – Moss, C. 2006: African elephants show high levels of interest in the skulls and ivory of their own species. Biology Letters 2, 26-28. DOI: 10.1098/rsbl.2005.0400.

Merritt, S.R. – Davis, K.M. 2017: Diagnostic properties of hammerstone-broken long bone fragments, specimen identifiability, and Early Stone Age butchered assemblage interpretation. Journal of Archaeological Science 85, 114-123. DOI: 10.1016/J.JAS.2017.06.009.

Miyasaka, Y. – Sakurai, M. – Yokobori, A.T. – Kuroda, S. – Ohyama, M. 1991: Bending and torsion fractures in long bones (a mechanical and radiologic assessment of clinical cases). Biomedical Materials Engineering 1(1), 3-10.

Moclán, A. – Domínguez-Rodrigo, M. 2018: An experimental study of the patterned nature of anthropogenic bone breakage and its impact on bone surface modification frequencies. Journal of Archaeological Science 96, 1-13. DOI: 10.1016/j.jas.2018.05.007.

Moclán, A. – Domínguez-Rodrigo, M. – Yravedra, J. 2019: Classifying agency in bone breakage: an experimental analysis of fracture planes to differentiate between hominin and carnivore dynamic and static loading using machine learning (ML) algorithms. Archaeological and Anthropological Sciences, DOI: 10.1007/s12520-019-00815-6.

Morin, E. 2007: Fat composition and Nunamiut decision-making: a new look at the marrow and bone grease indices. Journal of Archaeological Science 34, 69-82. DOI: 10.1016/j.jas.2006.03.015.

Morlan, R.E. 1980: Taphonomy and archaeology in the Upper Pleistocene of the Yukon Territory: A glimpse of the peopling of the New World. National Museum of Man Mercury Series, Archaeological Survey of Canada Paper 94, 1-380.

Morlan, R.E. 1984: Toward the Definition of Criteria for the Recognition of Artificial Bone Alterations. Quaternary Research 22, 160-171. DOI: 10.1016/0033-5894(84)90037-1.

Morlan, R.E. 1994: Bison Bone Fragmentation and Survivorship: a Comparative Method. Journal of Archaeological Science 21, 797-807. DOI: 10.1006/jasc.1994.1077.

Morley, M.W. – Goldberg, P. – Uliyanov, V.A. – Kozlikin, M.B. – Shunkov, M.V. – Derevianko, A.P. – Jacobs, Z. – Roberts, R.G. 2019: Hominin and animal activities in the microstratigraphic record from Denisova cave (Altai mountains, Russia). Scientific Reports 9(1), 1-12. DOI: 10.1038/s41598-019-49930-3.

Mulhern, D.M. – Ubelaker, D.H. 2001: Differences in osteon banding between human and nonhuman bone. Journal of Forensic Sciences 46(2), 220-222 DOI: 10.1520/JFS14952J.

Mulhern, D.M. – Ubelaker, D.H. 2012: Differentiating human from nonhuman bone microstructure. In: C.M. Crowder – S.D. Stout eds., Bone Histology: an Anthropological Perspective. CRC Press, Boca Raton, 109-134.

Musil, R. 1955: Osteologický materiál z paleolitického sídliště v Pavlově. Acta Academiae Scientiarum Čechoslovenicae, Basis Brunensis 27/318,6, 279-320.

Musil, R. 1994: Hunting game of the Culture Layer of Pavlov. In: Pavlov I. Excavations 1952-1953. ERAUL 66/DVS 2, Liege, 169-196.

Musil, R. 1997: Hunting Game Analysis. In: J. Svoboda ed., Pavlov I – Northwest. The Dolní Věstonice Studies 4. Academy of Sciences of the Czech Republic, Institute of archaeology, Brno, 443-468.

Musil R. 2005a: Animal Prey. In: Pavlov I Southeast. A window Into the Gravettian Lifestyle. Brno: Academy of Sciences of the Czech Republic, Institute of Archaeology at Brno, 190-228.

Musil, R. 2005b: Jarošov-Podvršťa. A faunal Anomaly among Gravettian sites. Osteological Material Analysis. In: P. Škrdla, The Upper Paleolithic on the Middle Course of the Morava River. The Dolní Věstonice Studies 13. Academy of Sciences of the Czech Republic, Institute of Archaeology, Brno, 203-216.

Myers, T.P. – Voorhies, M.R. – Corner, R.G. 1980: Spiral fractures and bone pseudotools at paleontological sites. American Antiquity 45(3), 483-490. DOI: 10.2307/279863.

Nalla, R.K. – Kinney, J.H. – Ritchie, R.O. 2003: Mechanistic fracture criteria for the failure of human cortical bone. Nature Materials 2, 164-168. DOI: 10.1038/nmat832.

Nielsen-Marsh, C. – Gernaey, A. – Turner-Walker, G. – Hedges, R. – Pike, A. - Collins, M. 2000: The chemical degradation of bone. In: M. Cox – S. Mays eds., Human Osteology in Archaeology and Forensic Science. Cambridge University Press, Cambridge, 439-454.

Nigst, P.R. 2006: The first modern humans in the Middle Danube Area? New Evidence from Willendorf II (Eastern Austria). In: N.J. Conard ed., When Neanderthals and Modern Humans Met. Tübingen: Kerns Verlag, 269-304.

Nigst, P.R. 2014: Willendorf II: Geography and Culture. In: C. Smith ed., Encyclopedia of Global Archaeology. Springer, New York, 7824-7833. DOI: 10.1007/978-1-4419-0465-2_1865.

Nigst, P.R. – Viola, T.B. – Haesaerts, P. – Blockley, S. – Damblon, F. – Frank, C. – Fuchs, M. – Götzinger, M. – Hambach, U. – Mallol, C. – Moreau, L – Niven, L. – Richards, M. – Richter, D. – L. Zöller, L. – Trnka, G. – Hublin, J.J. 2008a: New research on the Aurignacian of central Europe: a first note on the 2006 fieldwork at Willendorf II. Quartär 55, 9-15.

Nigst, P.R. – Viola, T.B. – Haesaerts, P. – Trnka, G. 2008b: Willendorf II. Wissenschaftliche Mitteilungen aus dem Niederösterreichischen Landesmuseum 19, 31-58.

Niven, L. – Steele, T.E. – Finke, H. – Gernat, T. – Hublin, J.J. 2009: Virtual skeletons: using structured light scanner to create 3D faunal comparative collection. Journal of Archaeological Science 36(9), 2018-2023. DOI: 10.1016/j.jas.2009.05.021.

Noe-Nygaard, N. 1977: Butchering and marrow fracturing as a taphonomic factor in archaeological. The Paleontological Society 3, 218-237.

Nývltová-Fišáková, M. 2001: Předmostí – vyhodnocení fauny z výzkumu v roce 1992. Archeologické rozhledy 53, 444-451.

Nývltová-Fišáková, M. 2001: Vyhodnocení nálezú fauny na lokalitách Dolní Věstonice II, IIa, IIb, III. Památky archeologické XCII(1), 124-152.

Nývltová-Fišáková, M. 2005: Faunal Remains from the Sites of Spytihněv-Duchonce, Jarošov-Kopaniny and Napajedla-Brickyard. In: P. Škrdla, The Upper Paleolithic on the Middle Course of the Morava River. The Dolní Věstonice Studies 13, Academy of Sciences of the Czech Republic, Institute of Archaeology, Brno, 217-221.

Nývltová-Fišáková, M. 2007: Sezonalita gravetských lokalit na základě studia mikrostruktur zubního cementu. *Přehled výzkumů* 48, 13-23.

Nývltová-Fišáková, M. 2013: Seasonality of gravettian sites in middle Danube region and adjoining areas of central Europe. Quaternary International 294, 120-134. DOI: 10.1016/j.quaint.2011.08.017.

Nývltová-Fišáková, M. – Nývlt, D. – Škrdla, P. 2006: Výzkum mladopaleolitické lokality Boršice u Buchlovic. Zprávy o geologických výzkumech v roce 2006, 85-89.

Nývltová-Fišáková, M. – Pokorný, P. – Šída, P. 2008: Nové poznatky o přírodním prostředí českého gravettienu – bioarcheologie málo prozkoumaného úseku naší minulosti. In: J. Beneš, J. – P. Pokorný eds., Bioarcheologie, České Budějovice – Praha, 115-143.

233

O´Brien, F.J. – Hardiman, D.A. – Hazenberg, J.G. – Mercy, M.V. – Mohsin, S. – Taylor, D. – Lee, T.C. 2005: The behaviour of microcracks in compact bone. European Journal of Morphology 42(1/2), 71-79. DOI: 10.1080/09243860500096131.

O'Connell, J.F. – Hawkes, K. – Blurton Jones, N. 1988: Hadza Hunting, Butchering, and Bone Transport and Their Archaeological Implications. Journal of Anthropological Research, 44(2), 113-161. DOI: 10.2307/3630053.

Okaluk, T.R. – Greenfield, H.J. 2022: Macroscopic Chop Mark Identification on Archaeological Bone: An Experimental Study of Chipped Stone, Ground Stone, Copper, and Bronze Axe Heads on Bone. Quaternary 5, 15. DOI: 10.3390/quat5010015.

Oliver, J.S. 1993: Carcass processing by the Hadza: bone breakage from butchery to consumption. In: J. Hudson ed., From bones to behaviour: ethnoarchaeological and experimental contributions to the interpretation of faunal remains. Center for Archaeological Investigations, Southern Illinois University at Carbondale, 200-227.

Olsen, S.L. 1988a: Scanning Electron microscopy in archaeology. Oxford: British Archaeological Reports Series, London.

Olsen, S.L. 1988b: Applications of Scanning Electron Microscopy in Archaeology. Advances in Electronics and Electron Physics 71, 357-380.

Olsen, S.L. 1988c: The identification of stone and metal tool marks on bone artifacts. In: S.L. Olsen ed., Scanning Electron Microscopy in Archaeology. British Archaeological Reports, BAR International Series 452, Oxford, 337-360.

Olsen, S.L. – Shipman, P. 1988: Surface modification on bone: trampling versus butchery. Journal of Archaeological Science 15, 535-553. DOI: 10.1016/0305-4403(88)90081-7.

Organista, E. – Pernas-Hernández, M. – Gidna, A. – Yravedra, J. – Domínguez-Rodrigo, M. 2016: An experimental lion-to-hammerstone model and its relevance to understand hominin-carnivore interactions in the archeological record. Journal of Archaeological Science 66, 2016, 69-77. DOI: 10.1016/j.jas.2015.12.004.

Ortner, D.J. – Turner-Walker G. 2003: The Biology of Skeletal Tissues. In: D.J. Ortner ed., Identification of Pathological Conditions in Human Skeletal Remains. Second Edition. Academic press An Imprint of Elsevier, 11-35.

Outram, A.K. 1998: The Identification and Palaeoeconomic Context of Prehistoric Bone Marrow and Grease Exploitation, Unpublished PhD Thesis, University of Durham, Durham

Outram, A.K. 1999: A comparison of paleo-Eskimo and medieval Norse bone fat exploitation in Western Greenland. Arctic Anthropology 36(1-2), 103-117.

Outram, A.K. 2001: A New Approach to Identifying Bone Marrow and Grease Exploitation: Why the ''Indeterminate'' Fragments should not be Ignored. Journal of Archaeological Science 28, 401-410. DOI: 10.1006/jasc.2000.0619.

Outram, A.K. 2002: Bone fracture and within-bone nutrients: An experimentally based method for investigating levels of marrow extraction. In: P. Miracle – N. Milner eds., Consuming Passions and Patterns of Consumption. McDonald Institute for Archaeological Research, Cambridge, 51-64.

Outram, A.K. 2005: Distinguishing bone fat exploitation from other taphonomic processes: what caused the high level of bone fragmentation at the Middle Neolithic site of Ajvide, Gotland? In: J. Mulville – A.K. Outram eds., The zooarchaeology of fats, oils, milk and dairying (Proceedings of the 9th ICAZ Conference), Oxbow Books, 32-43.

Owsley, D.W. – Mires, A.M. – Keith, M.S. 1985: Case involving differentiation of deer and human bone fragments. Journal of Forensic Sciences 28, 572-578. DOI: 10.1520/JFS11842J.

Padian, K. – Lamm, E.T. 2013: Bone histology of fossil tetrapods. University of California Press.

Palomares, F. – Ruiz-Villar, H.A. – Morales-González, A. – Calzada, J. – Román, J. – Rivilla, J.C. – Revilla, E. – Fernández-Gil, A. – Delibes, M. 2022: Hyaenids, felids and canids as bone accumulators: Does the natural history of extant species support zooarchaeological inferences? Quaternary Science Reviews 284, DOI: 107459. 10.1016/j.quascirev.2022.107459.

Pante, M.C. – Muttar, M.V. – Keevil, T.L. – Blumenschine, R.J. – Njau, J.K. – Merritt, S.R. 2017: A new high-resolution 3-D quantitative method for identifying bone surface modifications with implications for the Early Stone Age archaeological record. Journal of Human Evololution 102, 1-11. DOI: 10.1016/j.jhevol.2016.10.002.

Parkinson, J. 2018: Revisiting the hunting-versus-scavenging debate at FLK Zinj: A GIS spatial analysis of bone surface modifications produced by hominins and carnivores in the FLK 22 assemblage, Olduvai Gorge, Tanzania. Palaeogeography, Palaeoclimatology, Palaeoecology 511(15), 29-51. DOI: 10.1016/j.palaeo.2018.06.044.

Peretto, C. – Anconetani, A. – Crovetto, C. – Evangelista, L. – Ferrari, M. – Giusberti, G. – Thun Hohenstein, U. – Vianello, F. 1996: Approccio sperimentale alla comprensione delle attività di sussistenza condotte nel sito di Isernia La Pineta (Molise-Italia). La fratturazione intenzionale. In: C. Peretto ed., I reperti paleontologici del giacimento paleolitico di Isernia La Pineta, l'Uomo e l'ambiente. Istituto Regionale per gli Studi Storici del Molise ''V. Cuoco'' Cosmo Iannone Editore, Isernia, 187-452.

Pickering, T.R. 2002: Reconsideration of Criteria for Differentiating Faunal Assemblages Accumulated by Hyenas and Hominids. International Journal of Osteoarchaeology 12, 127-141. DOI: 10.1002/oa.594.

Pickering, T.R. – Egeland, C.P. 2006: Experimental patterns of hammerstone percussion damage on bones and zooarchaeological inferences of carcass processing intensity by humans. Journal of Archaeological Science 33, 459-469. DOI: 10.1016/J.JAS.2005.09.001.

Pickering, T.R. – Clarke, R.J. – Moggi-Cecchi, J. 2004: Role of Carnivores in the Accumulation of the Sterkfontein Member 4 Hominid Assemblage: A Taphonomic Reassessment of the Complete Hominid Fossil Sample (1936–1999). American Journal of Physical Anthropology 125, 1-15. DOI: 10.1002/ajpa.10278.

Pickering, T.R. – Domínguez-Rodrigo, M. – Egeland, C.P. – Brain, C.K. 2005: The Contribution of Limb Bone Fracture Patterns to Reconstructing Early Hominid Behaviour at Swartkrans Cave (South Africa): Archaeological Application of a New Analytical Method. International Journal of Osteoarchaeology 15, 247-260. DOI: 10.1002/oa.780.

Piekarski, K. 1970: Fracture of Bone. Journal of Applied Physics 41, 215–223.

Pilcher, J.R. 1968: Some applications of scanning electron microscopy to the study of modern and fossil pollen. Ulster Journal of Archaeology, 3rd series, 31, 87-91.

Pineda, A. – Saladié, P. – Vergés, J.M. – Huguet, R. – Cáceres, I. – Vallverdú, J. 2014: Trampling versus cut marks on chemically altered surfaces: an experimental approach and archaeological application at the Barranc de la Boella site (la Canonja, Tarragona, Spain). Journal of Archaeological Science 50, 84-93. DOI: 10.1016/j.jas.2014.06.018.

Pizarro-Monzo, M. – Organista, E. – Cobo-Sánchez, L. – Bequedano, E. – Domínguez-Rodigo, M. 2022: Determining the diagenetic paths of archaeofaunal assemblages and their palaeoecology through artificial intelligence: an application to Oldowan sites from Olduvai Gorge (Tanzania). Journal of Quaternary Science 37(3), 543-557. DOI: 10.1002/jqs.3385.

Þórhallsdóttir, R. – Walser, J.W. – Kristjánsdóttir, S. – Anamthawat-Jónsson, K. 2019: SEM analysis of an archaeological hair sample from East-Iceland and comparative samples from nine modern-day species of mammals from the region. Journal of Archaeological Science: Reports 24, 24-29. DOI: 10.1016/j.jasrep.2018.12.022.

Ponting, M. 2004: The scanning electron microscope and the archaeologist. Physics Education 39(2), 166-170. DOI: 10.1088/0031-9120/39/2/004.

Pošvancová, L. 2005: Kone (Equidae, Mammalia) z mladopleistocénnej spraše v Trenčianskych Bohuslaviciach. Diplomová práca. Archív KGP, Prif UK, Bratislava.

Raeisi Najafi, A. – Arshi, A.R. – Eslami, M.R. – Fariborz, S. – Moeinzadeh, M. 2007: Haversian cortical bone model with many radial microcracks: An elastic analytic solution. Medical Engineering and Physics 29, 708-717. DOI: 10.1016/j.medengphy.2006.08.001.

Raggatt, L.J. – Partridge, N.C. 2010: Cellular and Molecular Mechanisms of Bone Remodeling. The Journal of Biological Chemistry 285(33), 25103-25108. DOI: 10.1074/jbc.R109.041087.

Rašková Zelinková, M. 2013: Subsistenční strategie mladopaleolitických lovců-sběračů. Kniha I. Industrie z tvrdých živočišných materiálů ve světle antropologické zooarcheologie. Unpublished dissertation thesis. Masaryk University, Faculty of Sciences.

Rämsch, R. – Zerndt, B. 1963: Vergleichende Untersuchungen der Havers'schen Kanäle zwischen Menschen und Haustieren. Archiv für Kriminologie 131, 74-82.

Rejšek, K. 2014: Komplexní hodnocení čtyř půdních těles studijní plochy Pavlov I, červen-červenec 2014. Rkp. nepublikované pedologické zprávy. Uložení: Archeologický ústav AV ČR Brno.

Reynard, J.P. 2014: Trampling in coastal sites: An experimental study on the effects of shell on bone in coastal sediment. Quaternary International 330, 156-170. DOI: 10.1016/j.quaint.2013.11.007.

Reynard, J.P. – Henshilwood, Ch.S. 2018: Using Trampling Modification to Infer Occupational Intensity During the Still Bay at Blombos Cave, Southern Cape, South Africa. African Archaeological Review 35, 1-19. DOI: 10.1007/s10437-018-9286-2.

Rho, J.Y. – Kuhn-Spearing, L. – Ziopous, P. 1998: Mechanical properties and the hierarchical structure of bone. Medical Engineering & Physics 20, 92-102. DOI: 10.1016/s1350-4533(98)00007-1.

Richardson, P.R.K. 1980: Carnivore damage to antelope bones and its archaeological implications. Palaeontologia Africana 23, 109-125.

Richter, J. 1986: Experimental Study of Heat Induced Morphological Changes in Fish Bone Collagen. Journal of Archaeological Science 13, 477-481. DOI: 10.1016/0305-4403(86)90017-8.

Ritchie, R.O. – Kinney, J.H. – Kruzic, J.J. – Nalla, R.K. 2005: A fracture mechanics and mechanistic approach to the failure of cortical bone. Fatigue and Fracture of Engineering Materials and Structures 28, 345-371. DOI: 10.1111/j.1460-2695.2005.00878.x.

Roberts, S.J. – Smith, C.I. – Millard, A. – Collins, M.J. 2002: The Taphonomy of Cooked Bone: Characterizing Boiling and its Physico-Chemical Effects. Archaeometry 44(3), 485-494. DOI: 10.1111/1475-4754.t01-1-00080.

Roebroeks, W. – Gaudzinski-Windheuser, S. – Baales, M. – Kahlke, R.D. 2018: Uneven Data Quality and the Earliest Occupation of Europe-the case of Untermassfeld (Germany). Journal of Paleolithic Archaeology 1, 5-31. DOI: 10.1007/s41982-017-0003-5.

Rodríguez-Hidalgo, A. – Sanz, M. – Daura, J. – Sánchez-Marco, A. 2020: Taphonomic criteria for identifying Iberian lynx dens in quaternary deposits. Scientific Reports 10, 1-17. DOI: 10.1038/s41598-020-63908-6.

Rosell, J. – Blasco, R. – Arilla, M. – Fernández-Jalvo, Y. 2019: Very human bears: Wild brown bear neo-taphonomic signature and its equifinality problems in archaeological contexts. Quaternary International 517, 67-78. DOI: 10.1016/j.quaint.2019.05.013.

Rozada, L. – Allain, R. – Tournepiche, J.P. 2018: Trampling Experiments on Bones in Fine and Soft Sediments. Quaternaire, 29(1), 39-44. DOI:10.4000/QUATERNAIRE.8593.

Ruangwit, U. 1967: The split line phenomena and the microscopic structure of bone. American Journal of Physical Anthropology 26, 325-334. DOI: 10.1002/ajpa.1330260307.

Sadek-Kooros, H. 1972: Primitive bone fracturing: A method of research. American Antiquity 37, 369-382.

Sadek-Kooros, H. 1975: Intentional fracture of bone description of criteria. In: A.T. Clason ed., Archaeozoological Studies, New York: American Elsevier Publishing Co. Inc. 139-150.

Sala, N. – Arsuaga, J.L. 2013: Taphonomic Studies with Wild Brown Bears (Ursus Arctos) in the Mountains of Northern Spain. Journal of Archaeological Science 40, 1389-1396. DOI: 10.1016/j.jas.2012.10.018.

Sala, N. – Arsuaga, J.L. – Haynes, G. 2014: Taphonomic comparison of bone modifications caused by wild and captive wolves (Canis lupus), Quaternary International 330, 126-135.DOI: 10.1016/j.quaint.2013.08.017.

Saladié, P. – Huguet, R. – Diéz, C. – Rodríguez-Hidalgo, A. – Carbonell, E. 2013: Taphonomic Modifications Produced by Modern Brown Bears (Ursus arctos). Internationa Journal of Osteoarchaeology 23(1), 13-33. DOI: 10.1002/oa.1237.

Sauqué, V. – Rabal-Garcés, R. – Sola-Almagro, C. – Cuenca-Bescós, G. 2014: Bone Accumulation by Leopards in the Late Pleistocene in the Moncayo Massif (Zaragoza, NE Spain). PLoS ONE 9(3), e92144. DOI: 10.1371/journal.pone.0092144.

Sawada, J. – Nara, T. – Nakajima, T. – Saito, Y. – Dodo, Y. – Hirata, K. 2010: Histomorphological discrimination between human and nonhuman bones of fragmentary osteal remains: analyses of burnt bones from the ancient Heian site in the Northern Tohoku district, Japan. Anthropological Science 118, 23-36. DOI: 10.1537/asj.118.23.

Sawada, J. – Nara, T. – Fukui, J. – Dodo, Y. – Hirata, K. 2014: Histomorphological species identification of tiny bone fragments from Paleolithic site in the Northern Japanese Archipelango. Journal of Archaeological Science 46(1), 270-280. DOI: 10.1016/j.jas.2014.03.025.

Sázelová, S. 2016: XI. Small osteological element analysis. Case study of newly excavated faunal remains. In: J. Svoboda ed., Dolní Věstonice II. Chronostratigraphy, Paleoethnology, Paleoanthropology. The Dolní Věstonice Studies 21. Academy of Sciences of the Czech Republic, Institute of Archaeology, Brno, 129-137.

Sázelová, S. – Hromadová, B. 2020: Human teeth pendants from the Mid-Upper Paleolithic sites Pavlov I and Dolní Věstonice I, Czech Republic. Archaeological and Anthropological Sciences 12:41. DOI: 10.1007/s12520-019-01008-x.

Sázelová, S. – Boriová, S. – Šáliová, S. 2021: The Upper Paleolithic hard animal tissue under the microscope: Selected examples from Moravian sites. Quaternary International 587-588, 127-136. DOI: 10.1016/j.quaint.2020.10.027.

Sázelová, S. – Wilczyński, J. – Wojtal, P. – Svoboda, J. – Trinkaus, E. 2018: Puzzling Pairs from Pavlov and Mortuary Diversity in the Mid Upper Paleolithic. Přehled výzkumů 59-1, 69-88.

Sázelová, S. – Lawler, D. – Hladilová, Š. – Boriová, S. – Šáliová, S. – Janoušek, T. – Perri, A. – Hublin, J.J. – Svoboda, J. 2020: A wolf from Gravettian site Pavlov I, Czech Republic: Approach to skull pathology. International Journal of Paleopathology 31, 7-13. DOI: 10.1016/j.ijpp.2020.07.001.

Sázelová, S. – Hromadová, B. – Polanská, M. – Perri, A. 2021: Aspects of hard tissue modifications. Three objects from the Gravettian at Dolní Věstonice II (Czech Republic). Študijné zvesti Archeologického ústavu SAV – Supplementum 2, 129-144. DOI: 10.31577/szausav.2021.suppl.2.9

Seetha, D. – Velraj, G. 2019: FT-IR, XRD, SEM-EDS, EDXRF and Chemometric analyses of Archaeological Artifacts Recently Excavated from Chandravalli in Karnataka State, South India. Radiation Physics and Chemistry 162, 114-120. DOI: 10.1016/j.radphyschem.2019.03.017

Shah, F.A. – Rucsák, K. – Palmquist, A. 2019: 50 years of scanning electron microscopy of bone—a comprehensive overview of the important discoveries made and insights gained into bone material properties in health, disease, and taphonomy. Bone Research 7, 1-15. DOI: 10.1038/s41413-019-0053-z.

Sharir, A. – Barak, M.M. – Shahar, R. 2008: Whole bone mechanics and mechanical testing. The Veterinary Journal 177, 8-17. DOI: 10.1016/j.tvjl.2007.09.012.

Shipman, P. 1981: Applications of scanning electron microscopy to taphonomic problems. In: A.E. Cantwell – J.B. Griffin – N.A. Rothschild eds., The research potential of anthropological museum collections. Annals of the New York Academy of Sciences 376, 357-386.

Shipman, P. – Bolser, W. – Davis, K.L. 1981: Butchering of Giant Geladas at an Acheulian Site. Current Anthropology 22(3), 257-268.

Schmid, E. 1972: Atlas of Animal Bones: For Prehistorians, Archaeologists and Quaternary Geologists. Knochenatlas. Für Prähistoriker, Archäologen und Quartärgeologen. New York: Elsevier Publishing Company.

. *Smith, G.M. 2015*: Neanderthal megafaunal exploitation in Western Europe and its dietary implications: A contextual reassessment of La Cotte de St Brelade (Jersey). Journal of Human Evolution 78, 181-201. DOI: 10.1016/j.jhevol.2014.10.007.

Smith, T.M. – Reid, D.J. – Sirianni, J.E. 2006: The accuracy of histological assessments of dental development and age at death. Journal of Anatomy 208(1), 125-138. DOI: 10.1111/j.1469-7580.2006.00500.x.

Soledad Domingo, M. – Martín-Perea, D. – Domingo, L. – Cantero, E. – Cantalapiedra, J. L. – García Yelo, B.A. – Gómez Cano, A.R. – Alcalde, G.M. – Fesharaki, O. – Hernández Fernández, M. 2017: Taphonomy of mammalian fossil bones from the debris-flow deposits of Somosaguas-North (Middle Miocene, Madrid Basin, Spain), Palaeogeography, Palaeoclimatology, Palaeoecology 465(Part A), 103-121. DOI: 10.1016/j.palaeo.2016.10.023.

Speth, J.D. – Meignen, L. - Bar-Yosef, O. – Goldberg, P. 2012: Spatial organization of Middle Paleolithic occupation X in Kebara Cave (Israel): Concentrations of animal bones. Quat Int. 247: 85–102. DOI: 10.1016/j.quaint.2011.03.001.

St-Pierre, Ch.G. – Walker, R.B. 2007: Bones as Tools: Current Methods and Interpretations in Worked Bone Studies. BAR International Series 1622.

Stančíková, M. 2018: Stopy lidského ohryzu na vybrané archeologické lokalitě: Komparace a experiment. Unpublished master thesis, Masaryk University, Brno.

Stavrova, T. – Borel, A. – Daujeard, C. – Vettese, D. 2019: A GIS based approach to long bone breakage patterns derived from marrow extraction. PlosOne 14(5), e0216733. DOI: 10.1371/journal.pone.0216733.

Stiner, M.C. – Kuhn, S.L. – Weiner, S. – Bar-Yosef, O. 1995: Differential burning, recrystallization, and fragmentation of archaeological bone. Journal of Archaeological Science 22(2), 223-237. DOI: 10.1006/jasc.1995.0024.

Stloukal, M. ed. 1999: Antropologie. Příručka pro studium kostry. Národní muzeum. Praha.

Svoboda, J. ed. 1994: Pavlov I, excavations 1952-53. ERAUL 66/The Dolní Věstonice Studies 2, Liége.

Svoboda, J. ed. 1997: Pavlov I – Northwest. Upper Paleolithic Burial and its Settlement Context. The Dolní Věstonice Studies 4, Brno.

Svoboda, J. 2002: Lovci a sběrači – paleolit a mezolit. In: S. Stuchlík ed., Oblast vodního díla Nové mlýny od pravěku do středověku. Archeologický ústav AVČR Brno, 31-56.

Svoboda, J. ed. 2005: Pavlov I – Southeast. A Window into the Gravettian Lifestyles. The Dolní Věstonice Studies 14, Brno.

Svoboda, J. 2006: The Burials: Ritual and Taphonomy. In: E. Trinkaus – J. Svoboda eds., Early Modern Human Evolution in Central Europe: The People of Dolní Věstonice and Pavlov. The Dolní Věstonice Studies 12. Oxford, New York: Oxford University Press, 15-26.

Svoboda, J. 2017: On landscapes, maps and Upper Paleolithic lifestyles in the central European corridor: the images of Pavlov and Předmostí. Veleia 34, 67-74.

Svoboda, J. – Novák, M. – Sázelová, S. 2014: Pavlov (okr. Břeclav), Lokalita I – Jihozápad. Gravettien. Revize, prospekce a předstihový výskum I Přehled výzkumů 55(1), 146-148.

Svoboda, J. – Novák, M. – Sázelová, S. 2016: Pavlov I. Předběžné výsledky výzkumu v letech 2013-2015. Přehled výzkumů 57(1), 9-33.

Svoboda, J. – Bocheński, Z.M. – Čulíková V. – Dohnalová, A. – Hladilová, Š. – Hložek, M. – Horáček, I. – Ivanov, M. – Králík, M. – Novák, M. – Pryor, A.E. – Sázelová, S. – Stevens, R.E. – Wilczynski, J. – Wojtal, P. 2011: Paleolithic Hunting in a Southern Moravian Landscape: The Case of Milovice IV, Czech Republic. Geoarchaeology: An International Journal 26(6), 838–866. DOI:10.1002/gea.20375

Svoboda, J. – Novák, M. – Sázelová, S. – Demek J. 2015: Pavlov (okr. Břeclav), Lokalita Pavlov I. Počátek mladého paleolitu; gravettien. Záchranný výskum. Přehled výzkumů 56(1), 137-141.

Svoboda, J. – Novák, M. – Sázelová, S. – Demek, J. 2016: Pavlov I: a large Gravettian site in space and time. Quaternary International 406, 95-105. DOI: 10.1016/j.quaint.2015.09.015.

Svoboda, J. – Krejčí, O. – Krejčí, V. – Dohnalová, A. – Sázelová, S. – Wilczyński, J. – Wojtal, P. 2019: Pleistocene landslides and mammoth bone deposits: The case of Dolní Věstonice II, Czech Republic. Geoarchaeology 34(6), 1-14. DOI: 10.1002/gea.21740.

Šída, P. ed. 2009: The Gravettian of Bohemia, Dolnověstonické studie 17, 1-264. Brno.

Šída, P. 2015: Gravetské osídlení v Lubné. Nálezy od roku 1960. Fontes Archaologici Pragenses 42, Národní muzeum, Praha..

Škrdla, P. – Musil, R. 1999: Jarošov II – Nová stanice gravettienu na Uherskohradišťsku, Přehled výzkumů 39, 47-62.

Škrdla, P. – Nývltová-Fišáková, M. 2004: Paleontologický a archeologický výzkum na lokalitě Spytihněv-Duchonce. Zprávy o geologických výzkumech v roce 2003, 76-77.

Škrdla, P. – Nývltová-Fišáková, M. – Novák, M. – Nývlt, D. 2005: SPYTIHNĚV (okr. Zlín). Přehled výzkumu 46, 207-2011.

Takken Beijersbergen, L.M. – Hufthammer, A.K. 2012: Age determination of reindeer (Rangifer tarandus) based on postcranial elements. In: D.C.M. Raemaekers – E. Esser – R.C.G.M. Lauwerier – J.T. Zeiler eds., A bouquet of archaeozoological studies: Essays in honour of Wietske Prummel. Groningen Archaeological Studies 21, 11-20. DOI: 10.2307/j.ctt227285m.

Tang, T. – Ebacher, V. – Cripton, P. – Guy, P. – McKay, H. – Wang, R. 2015: Shear deformation and fracture of human cortical bone. Bone 71, 25-35. DOI: 10.1016/j.bone.2014.10.001.

Tappen, N.C. 1969: The relationship of weathering cracks to split-line orientation in bone. American Journal of Physical Anthropology 31, 191-197. DOI: 10.1002/ajpa.1330310208.

Tappen, N.C. – Peske, R. 1970: Weathering Cracks and Split-Line Patterns in Archaeological Bone. American Antiquity 35(3), 383-386.

Tersigni, M.T.A. 2007: Frozen human bone: a microscopic investigation. Journal of Forensic Sciences 52(1), 16-20. DOI: 10.1111/j.1556-4029.2006.00325.x.

Thomas, C.D.L. – Stein, M.S. – Feik, S.A. – Wark, J.D. – Clement, J.G. 2000: Determination of age at death using combined morphology and histology of the femur. Journal of Anatomy 196, 463-471. DOI: 10.1046/j.1469-7580.2000.19630463.x.

Thompson, J.C. – Carvalho, S. – Marean, C.W. – Alemseged, Z. 2019: Origins of the Human Predatory Pattern. The Transition to Large-Animal Exploitation by Early Hominins. Current Anthropology 60(1), 1-23. DOI: 10.1086/701477.

Thorson, R.M. – Guthrie, R.D. 1984: River ice as a taphonomic agent: An alternative hypothesis for bone "artifacts". Quaternary Research 22(2), 172-188. DOI: 10.1016/0033-5894(84)90038-3.

Todd, L.C. – Rapson, D.J. 1988: Long bone fragmentation and interpretation of faunal assemblages: approaches and comparative analysis. Journal of Archaeological Science 15, 307-325. DOI: 10.1016/0305-4403(88)90067-2.

Trinkaus, E. – Sázelová, S. – Svoboda, J. 2019: Pieces of people in Pavlovian: burials, body parts and bones in the earlier Upper Paleolithic. Human Remains and Violence 5(1), 70-87. DOI: 10.7227/HRV.5.1.6.

Trinkaus, E. – Svoboda, J.A. – Nývltová-Fišáková, M. – Wilczyński, J. 2009: Human remains from the Moravian Gravettian: morphology and taphonomy of additional elements from Dolní Věstonice II and Pavlov I. International Journal of Osteoarchaeology 20(6), 645-669. DOI: 10.1006/JASC.1999.0501.

Tseng, Z.J. – Binder, W.J. 2010: Mandibular biomechanics of Crocuta crocuta, Canis lupus, and the late Miocene Dinocrocuta gigantea (Carnivora, Mammalia). Zoological Journal of the Linnean Society 158, 683–696. DOI: 10.1111/j.1096-3642.2009.00555.x.

Turco, F. – Davit, P. – Cossio, R. – Agostino, A. – Operti, L. 2017: Accuracy improvement by means of porosity assessment and standards optimization in SEM-EDS and XRF elemental analyses on archaeological and historical pottery and porcelain. Journal of Archaeological Science: Reports 12, 54-65. DOI: 10.1016/j.jasrep.2017.01.022.

Turner, C.G. 1983: Taphonomic reconstruction of human violence and cannibalism based on mass burials in the American Southwest. In: G.M. LeMoine – A.S. MacEachern eds., Carnivores, Human Scavengers and Predators: A Question of Bone Technology, University of Calgary Archaeological Association, Calgary, 219-240.

Turner, C. – Wang, T. – Burr, D. 2001: Shear Strength and Fatigue Properties of Human Cortical Bone Determined from Pure Shear Tests. Calcified Tissue International 69, 373-378. DOI: 10.1007/s00223-001-1006-1.

Turner, E. – Humphrey, L. – Bouzouggar, A. – Barton, N. 2020: Bone retouchers and technological continuity in the Middle Stone Age of North Africa. PLoS ONE 15(3): e0230642. DOI: 10.1371/journal.pone.0230642.

Turner-Walker, G. – Jans, M. 2008: Reconstructing taphonomic histories using histological analysis. Palaeogeography, Palaeoclimatology, Palaeoecology 266, 227-235. DOI: 10.1016/j.palaeo.2008.03.024.

Udoni, M.M. – Pokines, J.T. – Moore, T.L. 2021: Experimental Study of Black Bear (Ursus americanus) and Grizzly Bear (U. arctos) Tooth Marks and Other Gnawing Damage on Bone. Forensic Anthropology 4(2), 71-87. DOI: 10.5744/fa.2020.0035.

Urbanová, P. 2003: Rozlišení zvířecích a lidských kostí: Histologická komparativní studie pro forenzní antropologii a kriminalistiku. Unpublished master thesis, Masaryk University.

Urbanová, P. – Novotný, V. 2005: Distinguishing between human and non-human bones: histometric method for forensic anthropology. Anthropologie XLIII/1, 77-85.

Vergès, J.M. – Morales, J.I. 2014: The gigapixel image concept for graphic SEM documentation.Applications in archeological use-wear studies. Micron 65, 15-19. DOI: 10.1016/j.micron.2014.04.009.

Verpoorte, A. 2000: Pavlovian reflexes and the Pompeii premise: A spatial analysis of stone artefacts from Pavlov I (Moravia, Czech Republic). Archeologické rozhledy 52, 577-594.

Vettese, D. 2019: Approche techno-culturelle de la fracturation des os longs chez les Néandertaliens (Sud-Ouest de l'Europe, MIS 5-3): une systématisation des gestes. Partialy published PhD thesis. Università degli Studi di Ferrara.

Vettese, D. – Daujeard, C. – Blasco, R. – Borel, A. – Caceres, I. – Moncel, M.H. 2017: Neandertal long bone breakage process: Standardized or random patterns? The example of Abri du Maras (Southeastern France, MIS 3). Journal of Archaeological Science Reports 13, 151-163. DOI: 10.1016/j.jasrep.2017.03.029.

Vettese, D. – Blasco, R. – Cáceres, I. – Gaudzinski-Windheuser, S. – Moncel, M.H. – Hohenstein, U.H. – Daujeard, C. 2020: Towards an understanding of hominin marrow extraction strategies: a proposal for a percussion mark terminology. Archaeological and Anhtropological Sciences 12,48. DOI: 10.1007/s12520-019-00972-8.

Vettese, D. – Stavrova, T. – Borel, A. – Marín, J. – Moncel, M.H. – Arzarello, M. – Daujeard, C. 2021: A way to break bones? The weight of intuitiveness. PLoS ONE 16(10), e0259136. DOI: 10.1371/journal.pone.0259136.

Végh, E.I. – Czermak, A. – Márquez-Grant, N. – Schulting, R.J. 2021: Assessing the reliability of microbial bioerosion features in burnt bones: A novel approach using feature-labelling in histotaphonomical analysis. Journal of Archaeological Science: Reports 37, 102906. DOI: 10.1016/j.jasrep.2021.102906.

Villa, P. – Mahieau, E. 1991: Breakage patterns of human long bones. Journal of Human Evolution 21, 27-48. DOI:10.1016/0047-2484(91)90034-S.

Villa, P. – Castel, J.Ch. – Beauval, C. – Bourdillat, V. – Goldberg, P. 2004: Human and carnivore sites in the European Middle and Upper Paleolithic: Similarities and differences in bone modification and fragmentation. Revue de Paléobiologie, Genève 23(2), 705-730.

Vlačiky, M. 2005: Mamuty (Proboscidea, Mammalia) z mladopaleolitického sídliska v Trenčianskych Bohuslaviciach. Diplomová práca. Archív KGP, Prif UK, Bratislava.

Vlačiky, M. 2008: Hunting Game of the Gravettian Site in Trenčianske Bohuslavice (SR). Human activities on the Faunal Material. 6th Meeting of the European Association of Vertebrate Palaeontologists. Volume of abstracts, EAVP, Múzeum Spiša, Spišská Nová Ves, 91-93.

Vlačiky, M. 2009: Carnivores from from Trenčianske Bohuslavice – Pod Tureckom and Moravany – Lopata II, two Gravettian open-air sites in Slovakia. Acta carsologica slovaca, Liptovský Mikuláš, 47 (Suppl. 1), 113-124.

Vlačiky, M. 2012: Intencionálna fragmentarizácia kostí v paleolitických kultúrach. Unpublished dissertation thesis. Masaryk University, Brno.

Wang, X. 2011: Cortical Bone Mechanics and Composition: Effects of Age and Gender. In: Silva M. (eds) *Skeletal Aging and Osteoporosis*. Studies in Mechanobiology, Tissue Engineering and Biomaterials, vol 5. Springer, Berlin, Heidelberg. DOI: 10.1007/8415_2011_108.

Wang, X. – Mabrey, J.D. – Agrawal, C.M. 1998: An interspecies comparison of bone fracture properties. Bio-medical Materials and Engineering 8(1), 1-9.

Waterhouse, K. 2013: The effect of weather conditions on burnt bone fragmentation. Journal of Forensic and Legal Medicin*e* 20, 489-495. DOI: 10.1016/j.jflm.2013.03.016.

Weidenreich, F. 1941: The extremity bones of Sinanthropus pekinensis. Palaeontologia Sinica. New Series D. No. 5. Peking.

Weiner, S. – Traub, W. – Wagner, H.D. 1999: Lamellar bone: structure-function relations. Journal of Structural Biology 126, 241-255. DOI: 10.1006/jsbi.1999.4107.

West, D. 1996: Kraków-Spadzista, unit E and unit F. Faunal remains. Folia Quaternaria 67, 21-34.

West, D. 2001: Analysis of the fauna recovered from the 1986/1987 excavations at Dolní Věstonice II, western slope. Památky archeologické XCII(1), 98-123.

White, T.D. 1992: Prehistoric Cannibalism at Mancos 5MTURM-2346. Princeton University Press, Princeton.

White, E.M. – Hannus, L.A. 1983: Chemical weathering of bone in archaeological soils. American Antiquity 48(2), 316-322. DOI: 10.2307/280453.

Wieberg, D.A.M. – Wescott, D.J. 2008: Estimating the Timing of Long Bone Fractures: Correlation Between the Postmortem Interval, Bone Moisture Content, and Blunt Force Trauma Fracture Characteristics. Journal of Forensic Science 53(5), 1-7. DOI: 10.1111/j.1556-4029.2008.00801.x.

Wilczyński, J. – Wojtal, P. – Roblíčková, M. – Oliva, M. 2015: Dolní Věstonice I (Pavlovian, the Czech Republic). Results of zooarchaeological studies of the animal remains discovered on the campsite (excavation 1924-52). Quaternary International 379, 58-70. DOI: 10.1016/j.quaint.2015.05.059.

Wilczyński, J. – Haynes, G. – Sobczyk, L. – Svoboda, J. – Roblíčková, M. – Wojtal, P. 2020: Friend or foe? Large canid remains from Pavlovian sites and their archaeozoological context. Journal of Anthropological Archaeology 59, 101197. DOI: 10.1016/j.jaa.2020.101197.

Wilczyński, J. – Šída, P. – Kufel-Diakowska, B. – Mroczek, P. – Pryor, A. – Oberc, T. – Sobieraj, D. – Lengyel, G. 2021: Population mobility and lithic tool diversity in the Late Gravettian – The case study of Lubná VI (Bohemian Massif). Quaternary International 587-588, 103-126. DOI: 10.1016/j.quaint.2020.08.046.

Wilson, E.E. – Awonusi, A. –Morris, M.D. – Kohn, D.H. – Tecklenburg, M.M. – Beck, L.W. 2006: Three structural roles for water in bone observed by solid-state NMR. Biophysical Journal 90(10), 3722–3731. DOI: 10.1529/biophysj.105.070243

Wojtal, P. – Sobczyk, K. 2003: Taphonomy of the Gravettian site - Kraków Spadzista Street (B). In: J.W.F. Reumer – J. de Vos – D. Mol eds., Advances in Mammoth Research. Proceedings of the Second International Mammoth Conference, May 16–20 1999. Deinsea 9, 557–561.

Wojtal, P. – Sobczyk, K. 2005: Man and woolly mammoth at the Kraków Spadzista Street (B) - taphonomy of the site. Journal of Archaeological Science 32, 193-206. DOI: 10.1016/j.jas.2004.08.005.

Wojtal, P. – Wilczyński, J. 2013: The Faunal record. In: Svoboda, J. - Mikulík, J. – Novák, M. – Polanská, M. – Schenk, Z. - Wilczyński, J. – Wojtal, P. 2013: Předmostí. Building an Authentic Museum. Dolnověstonické studie 19, 35-43, Brno.

Wojtal, P. – Wilczyński, J. 2015: Zooarchaeological studies of large mammal remains from Kraków Spadzista site – trench C2and trench E1 (2011-2012 excavations). In: P. Wojtal – J.Wilczyński – G. Haynes eds., A Gravettian Site in Southern Poland. Kraków Spadzista. Institute of Systematics and Evolution of Animals of the Polish Academy of Sciences, Kraków.

Wojtal, P. – Nývltová-Fišáková, M. – Wilczyński, J. 2011: The Fauna of Pavlov VI. In: J. Svoboda ed., Pavlov. Excavations 2007-2011. The Dolní Věstonice Studies 18. Academy of Sciences of the Czech Republic, Institute of Archaeology at Brno, 61-75.

Wojtal, P. – Sobczyk, K. – Wilczyński, J. 2015: A new look at an old site: Studies of the Kraków Spadzista site 1968–2013. In: S. Sázelová – M. Novák – A. Mizerová eds., Forgotten times and spaces: New perspectives in paleoanthropological, paleoetnological and archeological studies. 1st Edition. Brno: Institute of Archeology of the Czech Academy of Sciences; Masaryk University, 169-190. DOI: 10.5817/CZ.MUNI.M210-7781-2015-15.

Wojtal, P. – Wilczyński, J. – Wertz, K. 2016: Pavlovian hunters among bones. The animal remains. In: J. Svoboda ed., Dolní Věstonice II. Chronostratigraphy, Paleoethnology, Paleoanthropology. The Dolní Věstonice Studies 21, Academy of Sciences of the Czech Republic, Institute of Archaeology at Brno, 105-128.

Wojtal, P. – Wilczyński, J. – Svoboda, J. 2017: Pavlovian Hunters on the Margin – Archaeozoological Analysis of the Animal Remains Discovered at the Pavlov II Site (1966 – 67 excavations). Fossil Imprint 73, 322-331. DOI: 10.2478/if-2017-0018.

Wojtal, P. – Wilczyński, J. – Bocheński, Z.M. – Svoboda, J. 2012: The scene of spectacular feasts: Animal remains from Pavlov I south-east the Czech Republic. Quaternary International 252, 122-141. DOI: 10.1016/j.quaint.2011.06.033.

Wojtal, P. – Wilczyński, J. – Wertz, K. – Svoboda, J. 2018: The scene of a spectacular feast (part II): Animal remains from Dolní Věstonice II, the Czech Republic. Quaternary International 466(B), 194-211. DOI: 10.1016/j.quaint.2016.03.022.

Wolverton, S. 2002: Nisp:Mne And %Whole In Analysis Of Prehistoric Carcass Exploitation. North American Archaeologist 23(2), 85-100. DOI: 10.2190/EGDQ-CQ1Q-LLD2-H3TP.

Yeshrun, R. – Marom, N. – Bar-Oz, G. 2007: Differential Fragmentation of Different Ungulate Body-Size: A Comparison of Gazelle and Fallow Deer Bone Fragmentation in Levantine Prehistoric Assemblages. Journal of Taphonomy 5(3), 137-148.

Zapfe, M. 1939: Lebensspuren der eiszeitlichen Höhlenhyäne: Die urgenschictliche Bedeutung der Lebensspuren knochenfressender Raubtiere. Paleobiologica 7, 111-146.

Zhang, W. – Tekalur, S.A. – Baumann, M. – McCabe, L.R. 2013: The effects of damage accumulation on the tensile strength and toughness of compact bovine bone. Journal of Biomechanics 46, 964-972. DOI: 10.1016/j.jbiomech.2012.12.005.

Zhang, Y. – Huang, W. – Hayashi, C. – Gatesy, J. – McKittrick, J. 2018: Microstructure and mechanical properties of different keratinous horns. Journal of The Royal Society Interface 15, 20180093. DOI: 10.1098/rsif.2018.0093.

Ziegler, R. 2001: An extraordinary small mammoth (Mammuthus primigenius) from SW Germany. Stuttgarter Beiträge zur Naturkunden B 300.

Zioupos, P. – Kirchner, H.O.K. – Peterlik, H. 2020: Ageing bone fractures: the case of ductile to brittle transition that shifts with age. Bone 131, 1-11. DOI: 10.1016/j.bone.2019.115176.

Online sources:
ArcheoZoo [online]. [cit. 2022-07-12]. Dostupné z: https://www.archeozoo.org/archeozootheque/

ArchéoZoo - Vectorised skeletons [online]. [cit. 2022-06-05]. Dostupné z: https://www.archeozoo.org/archeozootheque/index/category/132-mammiferes_langen_mammals_lang_langes_mamiferos_lang_/start-30#content

Laetoli Production [online]. [cit. 2022-07-12]. Dostupné z: https://www.laetoli-production.fr/en/works/12

Specimen - electron-beam interaction [online]. [cit. 2022-07-5]. Dosupné z: https://www.nhm-wien.ac.at/en/research/central_research_laboratories/analytical_electron_microscopy/theory

List of supplementary material

Supplement 1: Table summarizing variables for each fragment analysed from the rockfall experiment, fresh bones without soft tissues. In total 150 samples were analysed. Maximal length (Max. length) in cm and FFI score are stated (author SB). **pp. 249-250**

Supplement 2: Table summarizing variables for each fragment analysed from the rockfall experiment, fresh bones with soft tissues. In total 150 samples were analysed. Maximal length (Max. length) in cm and FFI score are stated (author SB). **pp. 251-252**

Supplement 3: Table summarizing variables for each fragment analysed from the rockfall experiment, frozen bones without soft tissues. In total 126 samples were analysed. Maximal length (Max. length) in cm and FFI score are stated (author SB). **pp. 253-254**

Supplement 4: Table summarizing variables for each fragment analysed from the rockfall experiment, frozen bones with soft tissues. In total 139 samples were analysed. Maximal length (Max. length) in cm and FFI score are stated (author SB). **pp. 255-256**

Supplement 5: Table summarizing variable for each fragment analysed from the rockfall experiment, dried bones without soft tissues. In total 219 samples were analysed. Maximal length (Max. length) in cm and FFI score are stated (author SB). **pp. 257-258**

Supplement 6: Table summarizing variables for each fragment analysed from the rockfall experiment, dried bones with soft tissues. In total 207 samples were analysed. Maximal length (Max. length) in cm and FFI score are stated (author SB). **pp. 259-260**

Supplement 7: Table with inventory of bones used in hammerstone to anvil experiment (IA Brno) and their characteristics. Inventory number (Inv. nr.) consists of three numbers, first number is number of the bone in experimental set (01-12), second number marks the experimental set (1 – set with periosteum on, 2 – set with periosteum off) and third number is identification of the experimenter (01-06). Age (in years) is stated according to hunter´s estimation/osteological age according to methods stated in Chapter 7.2.1. Weight (in grams) was recorded right before the fragmentation process, in case of second experimental set, bones were weighted already without periosteum (author SB). **p. 261**

Supplement 8: Sample of informed consent for participants of the experiment (author SB). **p. 262**

Supplement 9: Table with basic information about probands involved into the experiment, all of them are anonymized according to GDPR policy at the University of Hradec Králové (author SB). **p. 263**

Supplement 10: Characteristics of unmodified hammerstones used in experiment. Total number of probands using them (last column) exceeds number of probands (6) because some of them were switching in between different pebbles for individual bone fragmentation (author SB). **p. 263**

Supplement 11: Example of the protocol for recording fresh bone fragmentation experiments, in this case specifically for humerus (author SB). **pp. 264-265**

Supplement 12: Table summarizing variables for each fragment analysed from hammerstone to anvil experiment. In total 102 fragments were analysed. Inventory number (Inv. nr.), type of fragment, maximal length (Max. length) and length of fracture surface (FS length) in cm, and FFI score are stated. Abbreviations: prox. = proximal, dist. = distal, epi. = epiphysis (author SB). **pp. 266-267**

Supplement 13: Table summarizing fragments from archaeological material, Pavlov I, area G evaluated for FFI calculation. In total 113 fragments were analysed. Abbreviations: fr .= fragment, epi. = epiphysis, prox. = proximal, dist. = distal, indet. = indeterminate, MSM = medium-sized mammal, LSM = large-sized mammal, ELSM = extra-large sized mammal (author SB). **pp. 268-269**

Supplement 14: Table summarizing fragments from archaeological material, Pavlov I, area A evaluated for FFI calculation. In total 96 fragments were analysed. Abbreviations: fr .= fragment, epi. = epiphysis, prox. = proximal, dist. = distal (author SB). **pp. 270-271**

Supplement 15: Table summarizing fragments from archaeological material, Pavlov I, area SE014 evaluated for FFI calculation. In total 107 fragments were analysed. Abbreviations: fr .= fragment, epi. = epiphysis, prox. = proximal, dist. = distal (author SB). **pp. 272-274**

Supplementary material

Supplement 1: Table summarizing variables for each fragment analysed from the rockfall experiment, fresh bones without soft tissues. In total 150 samples were analysed. Maximal length (Max. length) in cm and FFI score are stated (author SB).

Fresh without tissues (pce.)	Max. length (cm)	FFI score	Fresh without tissues (pce.)	Max. length (cm)	FFI score	Fresh without tissues (pce.)	Max. length (cm)	FFI score
1	14.5	1	1	6.0	1	1	4.0	2
1	13.0	2	1	5.5	3	1	4.0	2
1	12.5	3	1	5.5	6	1	4.0	3
1	12.0	4	1	5.5	3	1	4.0	5
1	12.0	3	1	5.5	6	1	4.0	2
1	11.5	3	1	5.5	5	1	4.0	3
1	11.0	1	1	5.5	5	1	6.5	4
1	11.0	5	1	5.5	5	1	6.5	4
1	11.0	1	1	5.5	3	1	6.5	2
1	10.0	2	1	5.5	2	1	6.5	3
1	10.0	2	1	5.5	1	1	6.5	5
1	10.0	3	1	5.5	1	1	6.0	4
1	10.0	2	1	5.5	4	1	6.0	5
1	10.0	3	1	5.5	4	1	6.0	5
1	9.5	4	1	5.0	6	1	6.0	2
1	9.5	5	1	5.0	3	1	6.0	3
1	9.5	2	1	5.0	5	1	6.0	6
1	9.0	4	1	5.0	4	1	6.0	2
1	9.0	2	1	5.0	2	1	6.0	3
1	9.0	3	1	5.0	4	1	6.0	4
1	9.0	3	1	5.0	2	1	6.0	2
1	9.0	2	1	5.0	3	1	6.0	5
1	8.5	5	1	5.0	4	1	6.0	4
1	8.5	3	1	5.0	6	1	4.0	2
1	8.5	2	1	5.0	2	1	4.0	5
1	8.0	5	1	5.0	3	1	4.0	2
1	8.0	6	1	5.0	2	1	4.0	1
1	8.0	2	1	5.0	2	1	4.0	6
1	8.0	1	1	5.0	1	1	4.0	3
1	8.0	1	1	5.0	3	1	4.0	5
1	8.0	4	1	5.0	2	1	4.0	1
1	8.0	5	1	5.0	0	1	4.0	1
1	8.0	2	1	4.5	4	1	4.0	2
1	7.5	2	1	4.5	2	1	4.0	1
1	7.5	3	1	4.5	6	1	4.0	3
1	7.5	4	1	4.5	5	1	4.0	1
1	7.5	4	1	4.5	5	1	4.0	4

Fresh without tissues (pce.)	Max. length (cm)	FFI score	Fresh without tissues (pce.)	Max. length (cm)	FFI score	Fresh without tissues (pce.)	Max. length (cm)	FFI score
1	7.5	5	1	4.5	6	1	4.0	5
1	7.5	4	1	4.5	2	1	4.0	1
1	7.5	1	1	4.5	5	1	4.0	2
1	7.5	5	1	4.5	3	1	4.5	0
1	7.0	3	1	4.5	4	1	4.0	4
1	7.0	3	1	4.5	3	1	4.0	3
1	7.0	4	1	4.5	5	1	4.0	2
1	7.0	4	1	4.5	6	1	6.5	3
1	7.0	2	1	4.5	3	1	6.5	5
1	7.0	4	1	4.5	2	1	6.5	5
1	7.0	2	1	4.5	3	1	6.5	3
1	7.0	4	1	4.5	4	1	6.5	3
1	7.0	4	1	4.5	4	1	4.5	4

Supplement 2: Table summarizing variables for each fragment analysed from the rockfall experiment, fresh bones with soft tissues. In total 150 samples were analysed. Maximal length (Max. length) in cm and FFI score are stated (author SB).

Fresh with tissues	Max. length (cm)	FFI score	Fresh with tissues	Max. length (cm)	FFI score	Fresh with tissues	Max. length (cm)	FFI score
1	18.0	2	1	7.0	4	1	4.0	2
1	14.0	2	1	7.0	3	1	4.0	4
1	14.0	3	1	7.0	4	1	4.0	6
1	14.0	3	1	7.0	3	1	4.0	4
1	13.0	2	1	7.0	2	1	4.0	6
1	13.0	3	1	6.5	2	1	4.0	4
1	13.0	5	1	6.5	0	1	8.0	2
1	13.0	4	1	6.5	0	1	8.0	3
1	12.5	5	1	6.5	4	1	8.0	0
1	12.0	1	1	6.0	1	1	8.0	3
1	12.0	2	1	6.0	0	1	8.0	3
1	12.0	2	1	6.0	1	1	8.0	4
1	12.0	5	1	6.0	5	1	8.0	3
1	11.5	3	1	6.0	0	1	8.0	4
1	11.5	5	1	6.0	0	1	7.5	1
1	11.0	1	1	6.0	3	1	7.5	2
1	11.0	3	1	6.0	4	1	7.5	3
1	10.5	4	1	6.0	1	1	7.5	4
1	10.5	6	1	6.0	1	1	7.5	5
1	10.5	1	1	6.0	2	1	7.5	1
1	10.0	1	1	6.0	5	1	7.0	2
1	10.0	1	1	6.0	2	1	7.0	2
1	10.0	0	1	6.0	2	1	7.0	1
1	10.0	2	1	6.0	2	1	7.0	1
1	10.0	2	1	6.0	2	1	7.0	0
1	10.0	2	1	6.0	1	1	7.0	0
1	10.0	1	1	5.5	0	1	7.0	1
1	9.5	3	1	5.5	4	1	7.0	0
1	9.5	2	1	5.5	4	1	5.0	3
1	9.5	2	1	5.5	3	1	5.0	4
1	9.0	3	1	5.5	2	1	5.0	2
1	9.0	1	1	5.5	1	1	5.0	2
1	9.0	3	1	5.5	5	1	5.0	6
1	9.0	2	1	5.5	4	1	5.0	1
1	9.0	3	1	5.5	3	1	5.0	2
1	9.0	0	1	5.0	5	1	5.0	3
1	9.0	1	1	5.0	0	1	5.0	5

Fresh with tissues	Max. length (cm)	FFI score	Fresh with tissues	Max. length (cm)	FFI score	Fresh with tissues	Max. length (cm)	FFI score
1	9.0	5	1	5.0	1	1	5.0	3
1	9.0	5	1	5.0	0	1	5.0	2
1	9.0	5	1	5.0	5	1	5.0	4
1	9.0	4	1	5.0	0	1	4.5	3
1	8.5	0	1	5.0	2	1	4.5	5
1	8.5	4	1	5.0	0	1	4.5	2
1	8.5	5	1	5.0	1	1	4.5	5
1	8.0	2	1	5.0	0	1	4.5	1
1	8.0	3	1	5.0	3	1	4.5	3
1	8.0	3	1	5.0	1	1	4.0	4
1	8.0	0	1	5.0	3	1	4.0	0
1	8.0	2	1	5.0	0	1	4.0	4
1	8.0	1	1	5.0	2	1	4.0	2

Supplement 3: Table summarizing variables for each fragment analysed from the rockfall experiment, frozen bones without soft tissues. In total 126 samples were analysed. Maximal length (Max. length) in cm and FFI score are stated (author SB).

Frozen without tissues (pce.)	Max. length (cm)	FFI score	Frozen without tissues (pce.)	Max. length (cm)	FFI score
1	19.0	3	1	6.0	5
1	17.0	3	1	6.0	2
1	15.0	5	1	6.0	3
1	15.0	4	1	6.0	2
1	14.0	5	1	6.0	2
1	13.5	4	1	6.0	3
1	13.5	2	1	6.0	3
1	12.5	3	1	6.0	2
1	12.0	4	1	5.5	6
1	11.0	3	1	5.5	6
1	11.0	3	1	5.5	4
1	11.0	3	1	5.5	4
1	11.0	4	1	5.5	4
1	11.0	5	1	5.5	4
1	11.0	2	1	5.5	3
1	11.0	5	1	5.5	4
1	11.0	3	1	5.5	4
1	11.0	5	1	5.5	4
1	10.5	4	1	5.5	5
1	10.5	4	1	5.5	5
1	10.0	4	1	5.0	4
1	10.0	4	1	5.0	1
1	10.0	4	1	5.0	4
1	10.0	5	1	5.0	2
1	10.0	5	1	5.0	3
1	9.5	3	1	5.0	3
1	9.5	6	1	5.0	4
1	9.5	5	1	5.0	5
1	9.0	2	1	5.0	3
1	9.0	3	1	5.0	3
1	9.0	1	1	5.0	6
1	9.0	1	1	5.0	6
1	9.0	6	1	5.0	4
1	9.0	6	1	5.0	4
1	8.5	4	1	5.0	2
1	8.5	3	1	5.0	5
1	8.5	5	1	5.0	5
1	8.0	3	1	4.5	6
1	8.0	6	1	4.5	0
1	8.0	5	1	4.5	3
1	8.0	4	1	4.5	4
1	8.0	3	1	4.5	2

Frozen without tissues (pce.)	Max. length (cm)	FFI score	Frozen without tissues (pce.)	Max. length (cm)	FFI score
1	8.0	1	1	4.5	3
1	8.0	4	1	4.5	4
1	8.0	5	1	4.5	4
1	7.5	5	1	4.5	4
1	7.5	4	1	4.5	2
1	7.5	2	1	4.0	5
1	7.5	5	1	4.0	2
1	7.5	5	1	4.0	1
1	7.5	3	1	4.0	6
1	7.5	3	1	4.0	1
1	7.5	2	1	4.0	3
1	7.0	4	1	4.0	4
1	7.0	6	1	7.0	6
1	7.0	5	1	6.5	4
1	7.0	5	1	6.5	5
1	7.0	4	1	6.5	3
1	7.0	6	1	6.5	5
1	7.0	5	1	6.5	4
1	7.0	3	1	6.0	5
1	7.0	4	1	6.0	5
1	7.0	4	1	6.0	3

Supplement 4: Table summarizing variables for each fragment analysed from the rockfall experiment, frozen bones with soft tissues. In total 139 samples were analysed. Maximal length (Max. length) in cm and FFI score are stated (author SB).

Frozen with tissues (pce.)	Max. length (cm)	FFI score	Frozen with tissues (pce.)	Max. length (cm)	FFI score
1	18.5	2	1	5.5	0
1	15.0	1	1	5.5	0
1	14.0	2	1	5.5	1
1	13.0	2	1	5.5	2
1	12.0	3	1	5.5	2
1	11.0	1	1	5.5	2
1	11.0	1	1	5.0	0
1	10.0	1	1	5.0	1
1	10.0	1	1	5.0	1
1	10.0	1	1	5.0	0
1	10.0	1	1	5.0	0
1	9.5	2	1	5.0	3
1	9.0	4	1	5.0	2
1	9.0	2	1	5.0	1
1	9.0	2	1	5.0	2
1	9.0	2	1	5.0	2
1	9.0	4	1	5.0	1
1	9.0	1	1	5.0	1
1	8.5	4	1	5.0	0
1	8.5	4	1	5.0	1
1	8.5	3	1	5.0	3
1	8.5	2	1	5.0	1
1	8.5	1	1	5.0	1
1	8.5	1	1	5.0	0
1	8.5	1	1	5.0	3
1	8.0	3	1	5.0	3
1	8.0	2	1	5.0	3
1	8.0	0	1	5.0	5
1	8.0	1	1	5.0	0
1	8.0	1	1	5.0	3
1	8.0	1	1	5.0	3
1	8.0	3	1	5.0	4
1	8.0	0	1	5.0	0
1	8.0	0	1	5.0	5
1	7.5	4	1	5.0	2
1	7.0	1	1	5.0	2
1	7.0	3	1	4.5	1
1	7.0	2	1	4.5	3
1	7.0	0	1	4.5	3
1	7.0	1	1	4.5	0
1	7.0	3	1	4.5	0
1	7.0	1	1	4.5	5

Frozen with tissues (pce.)	Max. length (cm)	FFI score	Frozen with tissues (pce.)	Max. length (cm)	FFI score
1	7.0	2	1	4.5	1
1	7.0	1	1	4.5	1
1	7.0	0	1	4.5	1
1	7.0	3	1	4.5	1
1	7.0	4	1	4.0	4
1	7.0	2	1	4.0	1
1	7.0	1	1	4.0	2
1	7.0	1	1	4.0	2
1	6.5	1	1	4.0	3
1	6.5	3	1	4.0	3
1	6.5	0	1	4.0	3
1	6.5	2	1	4.0	0
1	6.5	0	1	4.0	2
1	6.0	0	1	4.0	2
1	6.0	2	1	4.0	0
1	6.0	0	1	4.0	1
1	6.0	2	1	4.0	1
1	6.0	2	1	4.0	1
1	6.0	2	1	4.0	5
1	6.0	1	1	4.0	0
1	6.0	3	1	4.0	1
1	6.0	1	1	4.0	1
1	6.0	4	1	4.0	3
1	6.0	5	1	4.0	1
1	6.0	2	1	4.0	6
1	6.0	0	1	4.0	4
1	6.0	1	1	6.0	1
1	6.0	1	1	6.0	0

Supplement 5: Table summarizing variables for each fragment analysed from the rockfall experiment, dried bones without soft tissues. In total 219 samples were analysed. Maximal length (Max. length) in cm and FFI score are stated (author SB).

Dried without tissues (pce.)	Max. length (cm)	FFI score	Dried without tissues (pce.)	Max. length (cm)	FFI score	Dried without tissues (pce.)	Max. length (cm)	FFI score
1	14.0	5	1	6.5	6	1	5.0	4
1	12.5	6	1	6.5	5	1	5.0	4
1	12.5	5	1	6.5	5	1	5.0	6
1	12.5	2	1	6.5	5	1	5.0	5
1	12.5	5	1	6.5	4	1	5.0	1
1	12.0	5	1	6.5	5	1	5.0	3
1	12.0	6	1	6.5	4	1	5.0	3
1	12.0	5	1	6.5	2	1	5.0	3
1	11.5	4	1	6.5	6	1	5.0	4
1	11.0	5	1	6.5	6	1	5.0	5
1	11.0	4	1	6.5	4	1	5.0	4
1	11.0	4	1	6.5	3	1	5.0	2
1	10.5	5	1	6.0	4	1	5.0	5
1	10.5	6	1	6.0	6	1	5.0	6
1	10.5	4	1	6.0	6	1	5.0	4
1	10.0	5	1	6.0	5	1	5.0	5
1	10.0	5	1	6.0	3	1	5.0	6
1	10.0	4	1	6.0	4	1	5.0	5
1	10.0	3	1	6.0	4	1	5.0	5
1	10.0	6	1	6.0	6	1	5.0	6
1	10.0	3	1	6.0	5	1	5.0	5
1	9.5	5	1	6.0	2	1	5.0	3
1	9.5	5	1	6.0	4	1	5.0	4
1	9.0	3	1	6.0	1	1	5.0	4
1	9.0	6	1	6.0	2	1	5.0	4
1	9.0	5	1	6.0	3	1	5.0	6
1	9.0	6	1	6.0	6	1	4.5	6
1	9.0	5	1	6.0	5	1	4.5	3
1	9.0	3	1	6.0	6	1	4.5	4
1	8.5	2	1	6.0	6	1	4.5	6
1	8.5	6	1	6.0	5	1	4.5	3
1	8.5	3	1	6.0	5	1	4.5	5
1	8.5	3	1	6.0	6	1	4.5	3
1	8.0	4	1	6.0	6	1	4.5	6
1	8.0	5	1	6.0	4	1	4.5	6
1	8.0	5	1	6.0	5	1	4.5	5
1	8.0	5	1	6.0	4	1	4.5	6
1	8.0	6	1	5.5	4	1	4.5	6
1	8.0	3	1	5.5	4	1	4.5	3

Dried without tissues (pce.)	Max. length (cm)	FFI score	Dried without tissues (pce.)	Max. length (cm)	FFI score	Dried without tissues (pce.)	Max. length (cm)	FFI score
1	8.0	6	1	5.5	2	1	4.5	3
1	8.0	3	1	5.5	6	1	4.5	6
1	8.0	5	1	5.5	4	1	4.5	2
1	8.0	5	1	5.5	3	1	4.5	2
1	7.5	4	1	5.5	6	1	4.5	6
1	7.5	3	1	5.5	4	1	4.5	4
1	7.5	5	1	5.5	6	1	4.5	5
1	7.5	5	1	5.5	3	1	4.5	2
1	7.5	6	1	5.5	4	1	4.5	4
1	7.5	3	1	5.5	4	1	4.5	4
1	7.5	2	1	5.5	6	1	4.5	5
1	7.5	1	1	5.5	6	1	4.5	4
1	7.5	5	1	5.5	4	1	4.5	6
1	7.5	5	1	5.5	3	1	4.5	4
1	7.5	4	1	5.5	4	1	4.5	2
1	7.0	3	1	5.5	2	1	4.5	6
1	7.0	6	1	5.5	6	1	4.0	5
1	7.0	6	1	5.5	6	1	4.0	6
1	7.0	4	1	5.5	6	1	4.0	3
1	7.0	4	1	5.5	4	1	4.0	6
1	7.0	2	1	5.5	3	1	4.0	6
1	7.0	4	1	5.5	6	1	4.0	4
1	7.0	5	1	5.0	5	1	4.0	3
1	7.0	2	1	5.0	5	1	4.0	5
1	7.0	6	1	5.0	3	1	4.0	6
1	7.0	2	1	5.0	5	1	4.0	5
1	7.0	6	1	5.0	3	1	4.0	6
1	6.5	5	1	5.0	4	1	4.0	5
1	6.5	4	1	5.0	3	1	4.0	3
1	6.5	5	1	5.0	3	1	4.0	4
1	6.5	5	1	5.0	6	1	4.0	3
1	6.5	5	1	5.0	5	1	4.0	3
1	6.5	6	1	5.0	6	1	4.0	6
1	4.0	4	1	5.0	4	1	4.0	5

Supplement 6: Table summarizing variables for each fragment analysed from the rockfall experiment, dried bones with soft tissues. In total 207 samples were analysed. Maximal length (Max. length) in cm and FFI score are stated (author SB).

Dried with tissues (pce.)	Max. length (cm)	FFI score	Dried with tissues (pce.)	Max. length (cm)	FFI score	Dried with tissues (pce.)	Max. length (cm)	FFI score
1	15.0	5	1	7.0	3	1	5.0	6
1	11.0	5	1	7.0	4	1	5.0	6
1	11.0	2	1	7.0	4	1	5.0	4
1	11.0	2	1	7.0	3	1	5.0	4
1	10.5	4	1	7.0	4	1	5.0	6
1	10.5	6	1	7.0	3	1	5.0	5
1	10.5	4	1	7.0	3	1	5.0	4
1	10.0	5	1	7.0	3	1	5.0	4
1	10.0	5	1	7.0	5	1	5.0	5
1	10.0	5	1	7.0	1	1	5.0	3
1	10.0	4	1	6.5	3	1	5.0	3
1	10.0	5	1	6.5	5	1	5.0	4
1	10.0	5	1	6.5	4	1	5.0	3
1	10.0	3	1	6.5	6	1	5.0	3
1	10.0	3	1	6.5	3	1	5.0	4
1	9.5	5	1	6.5	4	1	5.0	3
1	9.5	5	1	6.5	6	1	5.0	2
1	9.5	3	1	6.5	3	1	5.0	4
1	9.0	4	1	6.5	4	1	5.0	2
1	9.0	3	1	6.5	5	1	5.0	4
1	9.0	4	1	6.5	4	1	5.0	3
1	9.0	5	1	6.5	3	1	5.0	4
1	9.0	5	1	6.5	3	1	5.0	4
1	9.0	4	1	6.0	3	1	5.0	5
1	9.0	2	1	6.0	6	1	5.0	4
1	9.0	5	1	6.0	5	1	5.0	3
1	9.0	3	1	6.0	5	1	5.0	4
1	9.0	2	1	6.0	3	1	5.0	3
1	9.0	5	1	6.0	5	1	5.0	3
1	9.0	5	1	6.0	3	1	5.0	4
1	9.0	3	1	6.0	6	1	5.0	5
1	9.0	1	1	6.0	5	1	5.0	4
1	9.0	3	1	6.0	5	1	4.5	5
1	8.5	1	1	6.0	6	1	4.5	6
1	8.5	5	1	6.0	5	1	4.5	5
1	8.5	3	1	6.0	3	1	4.5	3
1	8.5	4	1	6.0	3	1	4.5	3
1	8.5	4	1	6.0	4	1	4.5	4
1	8.0	6	1	6.0	2	1	4.5	2

Dried with tissues (pce.)	Max. length (cm)	FFI score	Dried with tissues (pce.)	Max. length (cm)	FFI score	Dried with tissues (pce.)	Max. length (cm)	FFI score
1	8.0	4	1	5.5	6	1	4.5	3
1	8.0	5	1	5.5	4	1	4.5	5
1	8.0	3	1	5.5	4	1	4.0	4
1	8.0	4	1	5.5	6	1	4.0	5
1	8.0	5	1	5.5	4	1	4.0	5
1	8.0	4	1	5.5	4	1	4.0	5
1	8.0	1	1	5.5	4	1	4.0	5
1	8.0	3	1	5.5	2	1	4.0	6
1	8.0	4	1	5.5	4	1	4.0	2
1	8.0	3	1	5.5	4	1	4.0	4
1	8.0	1	1	5.5	5	1	4.0	5
1	8.0	1	1	5.5	6	1	4.0	3
1	8.0	2	1	5.5	6	1	4.0	1
1	7.5	4	1	5.5	4	1	4.0	4
1	7.5	5	1	5.5	5	1	4.0	2
1	7.5	6	1	5.5	4	1	4.0	5
1	7.5	6	1	5.5	2	1	4.0	3
1	7.5	5	1	5.5	3	1	4.0	4
1	7.5	2	1	5.5	3	1	4.0	4
1	7.5	4	1	5.5	4	1	4.0	3
1	7.5	3	1	5.5	2	1	4.0	3
1	7.0	3	1	5.5	4	1	4.0	5
1	7.0	5	1	5.5	1	1	4.0	2
1	7.0	6	1	5.5	4	1	5.0	6
1	7.0	6	1	5.5	4	1	5.0	3
1	7.0	5	1	5.5	4	1	5.0	5
1	7.0	4	1	5.0	4	1	5.0	5
1	7.0	2	1	5.0	2	1	5.0	5
1	7.0	5	1	5.0	5	1	7.0	5
1	7.0	3	1	7.0	5	1	7.0	5

Supplement 7: Table with inventory of bones used in hammerstone to anvil experiment (IA Brno) and their characteristics. Inventory number (Inv. nr.) consists of three numbers, first number is number of the bone in experimental set (01-12), second number marks the experimental set (1 – set with periosteum on, 2 – set with periosteum off) and third number is identification of the experimenter (01-06). Age (in years) is stated according to hunter´s estimation/osteological age according to methods stated in Chapter 7.2.1. Weight (in grams) was recorded right before the fragmentation process, in case of second experimental set, bones were weighted already without periosteum (author SB).

Inv. nr.	Species	Anantomy	Side	Sex	Age	Weight (g)	Periosteum	Time after death
01_1_01	*C. elaphus*	*femur*	*dx.*	M	2y/<3y	545.0	present	2 days
02_1_01	*C. elaphus*	*tibia*	*dx..*	M	2y/1.6-3y	534.7	present	2 days
03_1_02	*C. elaphus*	*radio-ulna*	*sin.*	M	2y/1.6-3y	369.1	present	2 days
04_1_02	*C. elaphus*	*humerus*	*sin.*	M	2y/0-1.6y	437.0	present	2 days
05_1_03	*C. elaphus*	*tibia*	*dx.*	M	1.5y/<3y	311.7	present	2 days
06_1_03	*C. elaphus*	*femur*	*dx.*	M	1.5y/<3y	333.2	present	2 days
07_1_04	*C. elaphus*	*radio-ulna*	*dx.*	M	1.5y/1.6-3y	207.9	present	2 days
08_1_04	*C. elaphus*	*humerus*	*dx.*	M	1.5y/0-1.6y	260.5	present	2 days
09_1_05	*D. dama*	*femur*	*sin.*	F	4-5y/>3.3y	224.3	present	4 days
10_1_05	*D. dama*	*tibia*	*sin.*	F	4-5y/>6.3y	201.6	present	4 days
11_1_06	*D. dama*	*humerus*	*sin.*	F	4-5y/>9y	157.1	present	4 days
12_1_06	*D.dama*	*radio-ulna*	*sin.*	F	4-5y/>3.8y	109.6	present	4 days
01_2_01	*C. elaphus*	*femur*	*sin.*	M	2y/<3y	537.5	missing	2 days
02_2_03	*C. elaphus*	*femur*	*sin.*	M	1.5y/<3y	336.9	missing	2 days
03_2_01	*C. elaphus*	*tibia*	*sin.*	M	1.5y/<3y	298.5	missing	2 days
04_2_04	*C. elaphus*	*radio-ulna*	*sin.*	M	1.5y/1.6-3y	200.4	missing	2 days
05_2_04	*C. elaphus*	*humerus*	*sin.*	M	1.5y/0-1.6y	256.3	missing	2 days
06_2_05	*D.dama*	*femur*	*dx.*	F	4-5y/>3.3	218.4	missing	4 days
07_2_05	*D. dama*	*tibia*	*dx.*	F	4-5y/>6.3	192.6	missing	4 days
08_2_06	*D.dama*	*humerus*	*dx.*	F	4-5y/>9	146.0	missing	4 days
09_2_06	*D.dama*	*radio-ulna*	*dx.*	F	4-5y/>3.8	105.8	missing	4 days
10_2_03	*C. elaphus*	*tibia*	*sin.*	F	5y/1.6-3y	509.0	missing	2 days
11_2_02	*C. elaphus*	*humerus*	*sin.*	F	5y/0-1.6y	478.0	missing	2 days
12_2_02	*C. elaphus*	*radio-ulna*	*sin.*	F	5y/1.6-3y	371.0	missing	2 days

Informed consent

Hereby, I agree with participation in bone fragmentation experiment and storage and usage of my personal data.

Prior the experiment we will record information concerning your sex, age, body height, body weight, dominant hand, sport activities and prior experience with performed activity. During the experiment a photographic documentation will be taken. All recorded and used data will be anonymized. They will be stored for period of 5 years, according to standards used at the University of Hradec Králové. The data will be used as a part of research for PhD thesis "*Fragmentation of osteological material in the Upper Paleolithic: Experiment and Archaeology*", further they might be used for presentation and publication of the research results to scientific community via different platforms (conferences, research papers), or to broader public audience as a part of popularization activities. You provide your personal data voluntarily. Consent can be withdrawn at any time, by sending an email to the responsible person.

You have a right to request for copies of your personal data and copy of your signed consent with their processing; right to request for correction of inaccurate or incomplete data; under certain conditions; and right to request to erase any personal data stored by responsible person.

Please provide necessary individual exceptions for this consent if applicable:

Researcher/responsible person:
Mgr. Soňa Boriová,
Department of Archaeology, Faculty of Arts, University of Hradec Králové
sona.boriova@uhk.cz

In Dolní Věstonice, date:

Name of participant: Signature:

Supplement 9: Table with basic information about probands involved into the experiment, all of them are anonymized according to GDPR policy at the University of Hradec Králové (author SB).

Nr.	Sex	Age	Height (cm)	Weight (kg)	Dominant hand	Sports activity	Previous experiences
01	female	26	169	63	right-handed	horse riding, climbing, hiking	none
02	female	36	183	70	right-handed	hiking, outdoor activities	none
03	male	56	173	73	right-handed	fitness activities	none
04	male	26	200	85	right-handed	climbing, bicycle, hiking	none
05	male	46	178	80	right-handed	none	none
06	female	30	183	82	right-handed	none	none

Supplement 10: Characteristics of unmodified hammerstones used in experiment. Total number of probands using them (last column) exceeds number of probands (6) because some of them were switching in between different pebbles for individual bone fragmentation (author SB).

Designation	Weight (g)	Max. width (mm)	Max. length (mm)	Max. height (mm)	Material	Surface	Nr. of probands using
A	629.9	78	103	59	quartz	smooth	3
B	769.7	93	111	62	granite	smooth	1
C	1032.5	84	135	70	quartz	smooth	1
D	1416.9	101	141	83	quartz	smooth	1
E	1101.4	88	133	69	quartz	smooth	2
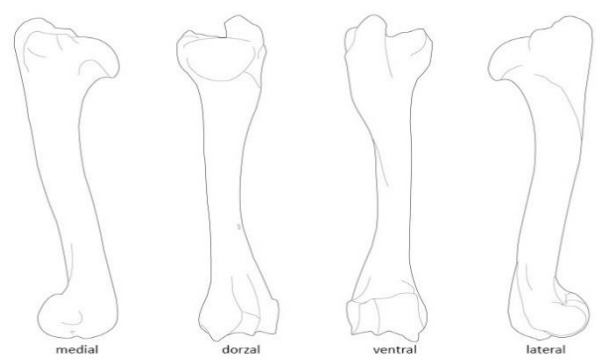
Supplement 11: Example of the protocol for recording fresh bone fragmentation experiments, in this case specifically for humerus (author SB).

Participant n.:	Weight:	Age:	Sex: M □ F □
Name:	Height:	Sports activity:	
Previous experience: none □ intermediate □ expert □			
Notes:			

Pebble n.:	Weight:	Modification:	Anvil:
	Surface:		

Bone n.:	Weight:	Periosteum: on □ off □
Species:	Anatomy: dex □ sin □	Soft tissue: on □ off □
Sex: M □ F □ I □	Age:	Time after death:
Notes:		Bone temp.:

Experiment set n.:	Time to open:
Weather conditions:	N. of hits to open:
temperature: humidity:	Marrow weight:
Number of fragments proximal epiphysis: distal epiphysis: diaphysi:	
Fracture characteristics: Outline: Surface: Angle: FFI:	Impact/rebound point/scar:
Notes:	
placement of hits:	

medial   dorzal   ventral   lateral

Notes:

Supplement 12: Table summarizing variables for each fragment analysed from hammerstone to anvil experiment. In total 102 fragments were analysed. Inventory number (Inv. nr.), type of fragment, maximal length (Max. length) and length of fracture surface (FS length) in cm, and FFI score are stated. Abbreviations: prox. = proximal, dist. = distal, epi. = epiphysis (author SB).

Inv. nr.	Fragment	Max. length (cm)	FS length (cm)	FFI score	Inv. nr.	Fragment	Max. length (cm)	FS length (cm)	FFI score
01_1_01	diaphysis	4.0	12.0	1	01_2_01	diaphysis	4.0	8.0	1
01_1_01	prox. epi	17.0	18.0	1	01_2_01	diaphysis	5.5	11.0	2
01_1_01	dist. epi	15.0	12.0	1	01_2_01	prox. epi	16.5	12.0	1
02_1_01	diaphysis	10.0	23.0	3	01_2_01	dist. epi	18.5	17.0	0
02_1_01	diaphysis	4.0	9.0	1	02_2_03	diaphysis	4.0	7.5	1
02_1_01	diaphysis	4.0	9.0	2	02_2_03	diaphysis	5.5	11.0	0
02_1_01	prox. epi	13.0	11.0	2	02_2_03	prox. epi	13.0	7.0	2
02_1_01	dist. epi	24.0	28.0	1	02_2_03	dist. epi	11.0	7.0	3
03_1_02	diaphysis	4.0	9.5	4	03_2_01	diaphysis	6.5	14.0	3
03_1_02	diaphysis	6.0	12.5	1	03_2_01	diaphysis	6.5	10.0	2
03_1_02	diaphysis	7.0	14.0	3	03_2_01	prox. epi	14.0	13.0	3
03_1_02	prox. epi	16.0	11.5	1	03_2_01	dist. epi	15.5	12.0	1
03_1_02	dist. epi	13.0	14.0	1	04_2_04	diaphysis	4.5	9.5	2
04_1_02	diaphysis	12.5	27.0	2	04_2_04	diaphysis	6.0	13.0	4
04_1_02	prox. epi	15.0	18.0	4	04_2_04	prox. epi	18.0	8.0	3
04_1_02	dist. epi	9.5	14.0	1	04_2_04	dist. epi	11.5	15.0	1
05_1_03	diaphysis	7.5	16.0	2	05_2_04	prox. epi	10.0	11.5	1
05_1_03	diaphysis	8.5	18.0	3	05_2_04	dist. epi	14.0	17.5	2
05_1_03	diaphysis	7.5	16.0	3	06_2_05	diaphysis	6.0	13.0	1
05_1_03	prox. epi	14.0	21.0	2	06_2_05	prox. epi	12.0	14.0	1
05_1_03	dist. epi	11.5	11.0	2	06_2_05	dist. epi	10.5	12.0	2
06_1_03	diaphysis	4.0	8.5	2	07_2_05	diaphysis	6.5	13.0	2
06_1_03	diaphysis	5.0	11.0	1	07_2_05	diaphysis	5.0	10	0
06_1_03	diaphysis	5.0	11.0	1	07_2_05	diaphysis	7.5	15.0	2
06_1_03	diaphysis	4.0	9.0	2	07_2_05	diaphysis	7.0	13.5	3
06_1_03	diaphysis	5.0	12.5	4	07_2_05	prox. epi	11.5	12.0	2
06_1_03	prox. epi	11.0	12.0	0	07_2_05	dist. epi	13.0	18.0	0
06_1_03	dist. epi	10.0	10.5	4	08_2_06	diaphysis	5.0	12.0	1
07_1_04	diaphysis	4.0	9.0	2	08_2_06	diaphysis	4.0	8.0	1
07_1_04	diaphysis	5.0	10.0	1	08_2_06	diaphysis	5.0	13.0	0
07_1_04	diaphysis	6.0	13.5	1	08_2_06	prox. epi	9.0	9.0	2
07_1_04	prox. epi	16.0	17.0	1	08_2_06	dist. epi	8.5	7.0	1
07_1_04	dist. epi	11.0	6.0	5	09_2_06	diaphysis	5.0	10.0	1
08_1_04	diaphysis	5.0	11.0	3	09_2_06	prox. epi	11.5	7.0	0

Inv. nr.	Fragment	Max. length (cm)	FS length (cm)	FFI score	Inv. Nr.	Fragment	Max. length (cm)	FS length (cm)	FFI score
08_1_04	diaphysis	4.5	9.0	2	09_2_06	dist. epi	11.5	8.0	2
08_1_04	diaphysis	5.5	12.5	2	10_2_03	diaphysis	7.0	14.5	1
08_1_04	prox. epi	11.0	12.5	3	10_2_03	diaphysis	23.0	45.0	2
08_1_04	dist. epi	7.0	12.5	1	10_2_03	prox. epi	30.0	45.0	3
09_1_05	diaphysis	5.0	10.5	0	10_2_03	dist. epi	15.0	21.0	1
09_1_05	diaphysis	6.5	13.5	0	11_2_02	prox. epi	20.0	18.0	1
09_1_05	diaphysis	5.5	14.5	1	11_2_02	dist. epi	11.0	14.0	0
09_1_05	diaphysis	4.5	9.0	3	12_2_02	diaphysis	6.0	14.5	3
09_1_05	prox. epi	10.5	12.0	1	12_2_02	prox. epi	22.5	15.0	2
09_1_05	dist. epi	10.5	12.0	2	12_2_02	dist. epi	14.5	9.0	4
10_1_05	diaphysis	4.5	9.0	1					
10_1_05	diaphysis	4.5	9.0	1					
10_1_05	diaphysis	6.0	12.0	3					
10_1_05	diaphysis	5.5	10.5	2					
10_1_05	prox. epi	15.0	17.0	1					
10_1_05	dist. epi	10.0	9.0	3					
11_1_06	diaphysis	4.5	10.0	3					
11_1_06	diaphysis	5.0	10.0	2					
11_1_06	prox. epi	9.0	12.0	4					
11_1_06	dist. epi	8.5	10.0	2					
12_1_06	diaphysis	4.0	9.0	1					
12_1_06	diaphysis	5.0	10.0	1					
12_1_06	prox. epi	11.5	8.0	3					
12_1_06	dist. epi	9.5	7.5	1					

Supplement 13: Table summarizing fragments from archaeological material, Pavlov I, area G evaluated for FFI calculation. In total 113 fragments were analysed. Abbreviations: fr .= fragment, epi. = epiphysis, prox. = proximal, dist. = distal, indet. = indeterminate, MSM = medium-sized mammal, LSM = large-sized mammal, ELSM = extra-large sized mammal (author SB).

Site	Inv. nr./square	NISP	MNE	Anatomical part	Taxon	FFI score
Pavlov I-G	5214	3	1	dist. *radius*	*Rangifer tarandus*	3
Pavlov I-G	1830	3	1	prox. *radius*	*Rangifer tarandus*	2
Pavlov I-G	N24/c	1	1	dist. *femur*	*Rangifer tarandus*	6
Pavlov I-G	5521	1	1	dist. m*etacarpus III*	*Rangifer tarandus*	2
Pavlov I-G	5505	3	1	prox. *tibia*	*Rangifer tarandus*	5
Pavlov I-G	5522	1	1	prox. *radius*	*Rangifer tarandus*	2
Pavlov I-G	5509	1	1	dist. *humerus*	*Rangifer tarandus*	1
Pavlov I-G	5130	1	1	prox. *femur*	*Rangifer tarandus*	0
Pavlov I-G	5196	1	1	dist. *metapodium III*	*Rangifer tarandus*	5
Pavlov I-G	5526	1	1	dist. *tibia*	*Rangifer tarandus*	1
Pavlov I-G	5515	3	2	dist. *femur*	*Rangifer tarandus*	3
Pavlov I-G	5506	2	1	dist. *femur*	*Rangifer tarandus*	3
Pavlov I-G	5530	2	1	prox. *metacarpus V*	*Canis lupus*	5
Pavlov I-G	5530	1	1	dist. *metacarpus V*	*Canis lupus*	6
Pavlov I-G	6299	1	1	long bone epi.	ELSM	6
Pavlov I-G	6265	1	1	fr. of epi.	ELSM	6
Pavlov I-G	6295	1	1	compact bone fr.	L/ELSM	2
Pavlov I-G	5424	1	1	long bone fr.	LSM	5
Pavlov I-G	6335	1	1	*tibia* fr.	LSM	2
Pavlov I-G	6328	3	3	compact bone fr.	LSM	2
Pavlov I-G	5215	1	1	bone fr. 3-5 cm	LSM	0
Pavlov I-G	5215	1	1	bone fr. 5-10 cm	LSM	0
Pavlov I-G	5426	2	1	long bone fr.	LSM	6
Pavlov I-G	5426	3	1	long bone fr.	LSM	6
Pavlov I-G	5426	1	1	bone fr. 5-10 cm	LSM	5
Pavlov I-G	5426	1	1	bone fr. 5-10 cm	LSM	5
Pavlov I-G	5430	1	1	bone fr. 5-10 cm	M/LSM	1
Pavlov I-G	6423	1	1	compact bone fr.	M/LSM	4
Pavlov I-G	5130	1	1	bone fr. 5-10 cm	MSM	3
Pavlov I-G	5130	1	1	bone fr. 2-3 cm	MSM	2
Pavlov I-G	5130	1	1	bone fr. 3-5 cm	MSM	2
Pavlov I-G	5241	1	1	bone fr. 3-5 cm	MSM	4
Pavlov I-G	5241	2	1	bone fr. 2-3 cm	MSM	4
Pavlov I-G	5198	1	1	bone fr. 5-10 cm	MSM	2
Pavlov I-G	5429	1	1	dist. *humerus*	MSM	6
Pavlov I-G	5429	3	1	bone fr. 3-5 cm	MSM	6
Pavlov I-G	5199	1	1	bone fr. 3-5 cm	MSM	5

Site	Inv. nr./square	NISP	MNE	Anatomical part	Taxon	FFI score
Pavlov I-G	5216	1	1	bone fr. 5-10 cm	MSM	1
Pavlov I-G	5131	1	1	bone fr. 5-10 cm	MSM	5
Pavlov I-G	5133	1	1	bone fr. 5-10 cm	MSM	3
Pavlov I-G	N24/c	1	1	long bone fr.	MSM	1
Pavlov I-G	5547	1	1	*humerus* shaft fr.	MSM	3
Pavlov I-G	5522	1	1	prox. *ulna*	MSM	5
Pavlov I-G	6302	2	1	compact bone fr.	MSM	6
Pavlov I-G	6446	2	1	compact bone fr.	MSM	3
Pavlov I-G	6397	2	1	compact bone fr.	MSM	3
Pavlov I-G	5516	1	1	compact bone fr.	MSM	1
Pavlov I-G	5510	2	1	*metapodium* fr.	MSM	6
Pavlov I-G	5527	1	1	accessory *metapodium*	MSM	6
Pavlov I-G	5507	1	1	*femur* fr.	MSM	2
Pavlov I-G	5130	1	1	bone fr. 3-5 cm	MSM	4
Pavlov I-G	5130	1	1	bone fr. 5-10 cm	MSM	2
Pavlov I-G	5199	1	1	bone fr. 2-3 cm	S/MSM	4
Pavlov I-G	1827	1	1	bone fr. 3-5 cm	indet.	5
Pavlov I-G	N24/c	1	1	bone fr. 3-5 cm	indet.	6
Pavlov I-G	N24/c	1	1	bone fr. 2-3 cm	indet.	6
Pavlov I-G	5426	4	4	bone fr. 3-5 cm	indet.	6
Pavlov I-G	5426	9	9	bone fr. 2-3 cm	indet.	6
Pavlov I-G	5426	1	1	bone fr. 2-3 cm	indet.	4
Pavlov I-G	5229	1	1	bone fr. 3-5 cm	indet.	0
Pavlov I-G	5229	1	1	bone fr. 3-5 cm	indet.	2
Pavlov I-G	5229	1	1	bone fr. 2-3 cm	indet.	5
Pavlov I-G	5131	1	1	bone fr. 2-3 cm	indet.	4
Pavlov I-G	5131	1	1	bone fr. 2-3 cm	indet.	3
Pavlov I-G	5215	1	1	bone fr. 3-5 cm	indet.	4
Pavlov I-G	5132	1	1	bone fr. 3-5 cm	indet.	3
Pavlov I-G	5132	1	1	bone fr. 2-3 cm	indet.	1
Pavlov I-G	5132	1	1	bone fr. 2-3 cm	indet.	1
Pavlov I-G	6431	1	1	bone fr. 2-3 cm	indet.	4
Pavlov I-G	5510	1	1	bone fr. 2-3 cm	indet.	6
Pavlov I-G	5510	1	1	bone fr. 3-5 cm	indet.	2
Pavlov I-G	6319	1	1	bone fr. 2-3 cm	indet.	4
Pavlov I-G	6265	2	2	bone fr. 2-3 cm	indet.	6
Pavlov I-G	6265	1	1	bone fr. 2-3 cm	indet.	6
Pavlov I-G	6265	3	3	bone fr. 3-5 cm	indet.	6
Pavlov I-G	N24/c	1	1	bone fr. 2-3 cm	indet.	6
Pavlov I-G	N24/c	1	1	bone fr. 2-3 cm	indet.	5

Supplement 14: Table summarizing fragments from archaeological material, Pavlov I, area A evaluated for FFI calculation. In total 96 fragments were analysed. Abbreviations: fr .= fragment, epi. = epiphysis, prox. = proximal, dist. = distal (author SB).

Site	Inv. nr./square	NISP	MNE	Anatomical part	Taxon	FFI score
Pavlov I-A	Nal 252	1	1	prox. *ulna*	*Rangifer tarandus*	6
Pavlov I-A	Nal 239	1	1	prox. *femur*	*Rangifer tarandus*	6
Pavlov I-A	Nal 239	1	1	prox. *ulna*	*Rangifer tarandus*	6
Pavlov I-A	Nal 246	2	1	prox. *ulna*	*Rangifer tarandus*	6
Pavlov I-A	Nal 339	2	1	*radio-ulna* fr.	*Rangifer tarandus*	3
Pavlov I-A	Nal 339	7	7	*radio-ulna* fr.	*Rangifer tarandus*	3
Pavlov I-A	-A2 a,b	1	1	*ulna* fr.	*Rangifer tarandus*	6
Pavlov I-A	Nal 241	1	1	prox. *metacarpus III*	*Rangifer tarandus*	3
Pavlov I-A	Nal 241	1	1	prox. *femur*	*Rangifer tarandus*	6
Pavlov I-A	A5	3	1	prox. *humerus*	*Rangifer tarandus*	6
Pavlov I-A	A5	1	1	*metapodium III* fr.	*Rangifer tarandus*	6
Pavlov I-A	A5	3	1	dist. *metapodium III*	*Rangifer tarandus*	3
Pavlov I-A	A1	1	1	prox. *metatarsus III*	*Rangifer tarandus*	3
Pavlov I-A	579	1	1	dist. *metapodium III*	*Rangifer tarandus*	5
Pavlov I-A	13065	2	1	*metapodium III* fr.	*Rangifer tarandus*	2
Pavlov I-A	13039	3	1	prox. *metatarsus III*	*Rangifer tarandus*	5
Pavlov I-A	13110	3	1	prox. *metapodium III*	*Rangifer tarandus*	3
Pavlov I-A	12733	2	1	dist. *metapodium III*	*Rangifer tarandus*	3
Pavlov I-A	12760	1	1	*tibia* fr.	*Rangifer tarandus*	2
Pavlov I-A	12799	1	1	dist. *tibia*	*Rangifer tarandus*	4
Pavlov I-A	1423	3	1	dist. *radio-ulna*	*Rangifer tarandus*	4
Pavlov I-A	1336	5	1	prox. *humerus*	*Rangifer tarandus*	6
Pavlov I-A	376	1	1	dist. *humerus*	*Rangifer tarandus*	5
Pavlov I-A	232	1	1	dist. *tibia*	*Rangifer tarandus*	3
Pavlov I-A	318	3	1	prox. *metatarsus III*	*Rangifer tarandus*	6
Pavlov I-A	1273	1	1	dist. *femur*	*Rangifer tarandus*	6
Pavlov I-A	1374	7	1	*metatarsus III* fr.	*Rangifer tarandus*	3
Pavlov I-A	108	1	1	prox. *radius*	*Rangifer tarandus*	2
Pavlov I-A	63	4	1	dist. *metapodium III*	*Rangifer tarandus*	2
Pavlov I-A	133	2	1	prox. *ulna*	*Rangifer tarandus*	6
Pavlov I-A	554	1	1	dist. *metatarsus III*	*Rangifer tarandus*	2
Pavlov I-A	1370	1	1	dist. *radius*	*Rangifer tarandus*	3
Pavlov I-A	13 833	1	1	dist. *radius*	*Rangifer tarandus*	6
Pavlov I-A	13 617	2	1	dist. *tibia*	*Rangifer tarandus*	2
Pavlov I-A	480	3	1	dist. *tibia*	*Rangifer tarandus*	2
Pavlov I-A	sector 5	1	1	dist. *humerus*	*Rangifer tarandus*	4
Pavlov I-A	1302	1	1	dist. *tibia*	*Rangifer tarandus*	2
Pavlov I-A	217	6	1	dist. *metapodium III*	*Rangifer tarandus*	6

Site	Inv. nr./square	NISP	MNE	Anatomical part	Taxon	FFI score
Pavlov I-A	12 925	2	1	dist. *metapodium III*	*Rangifer tarandus*	6
Pavlov I-A	12 969	2	1	dist. *metatarsus III*	*Rangifer tarandus*	0
Pavlov I-A	12922	1	1	*metapodium III* fr.	*Rangifer tarandus*	3
Pavlov I-A	13 487	4	1	dist. *metapodium III*	*Rangifer tarandus*	3
Pavlov I-A	13 205	3	1	prox. *metapodium III*	*Rangifer tarandus*	4
Pavlov I-A	13 326	1	1	prox. *tibia*	*Rangifer tarandus*	5
Pavlov I-A	13 942	11	1	*humerus*	*Canis lupus*	5
Pavlov I-A	13 710	3	1	*metatarsus II*	*Canis lupus*	5
Pavlov I-A	trench A	1	1	*phalanx I*	*Canis lupus*	5
Pavlov I-A	13 943	4	1	*ulna*	*Canis lupus*	6
Pavlov I-A	13 706	1	1	prox. *ulna*	*Canis lupus*	6
Pavlov I-A	13 687	1	1	prox. *ulna*	*Canis lupus*	6
Pavlov I-A	13 532	2	1	*metatarsus II*	*Canis lupus*	5
Pavlov I-A	13 438	3	1	*pelvis* fr.	*Canis lupus*	6
Pavlov I-A	13 511	2	1	*phalanx I*	*Canis lupus*	5
Pavlov I-A	13 441	1	1	*metatarsus I* fr.	*Canis lupus*	3
Pavlov I-A	12767	1	1	prox. *metatarus III*	*Canis lupus*	6
Pavlov I-A	13 397	2	1	*ulna*	*Canis lupus*	6
Pavlov I-A	13 389	1	1	*radius*	*Canis lupus*	6
Pavlov I-A	Nal 103	1	1	*humerus*	*Canis lupus*	6
Pavlov I-A	Nal 516	4	1	*humerus*	*Canis lupus*	6
Pavlov I-A	Nal 239	1	1	dist. *radius*	*Canis lupus*	3
Pavlov I-A	Nal 594	1	1	dist. *tibia* fr.	*Canis lupus*	6
Pavlov I-A	6-Aa	1	1	dist. *humerus* fr.	*Canis lupus*	6
Pavlov I-A	A5-5	1	1	prox. *tibia* fr.	*Canis lupus*	6
Pavlov I-A	973	1	1	prox. *radius* fr.	*Canis lupus*	6
Pavlov I-A	7635	3	1	prox. *femur* fr.	*Canis lupus*	6

Supplement 15: Table summarizing fragments from archaeological material, Pavlov I, area SE014 evaluated for FFI calculation. In total 107 fragments were analysed. Abbreviations: fr .= fragment, epi. = epiphysis, prox. = proximal, dist. = distal (author SB).

Site	Inv. nr. /square	NISP	MNE	Anatomical part	Taxon	FFI score
Pavlov I-SE014	V-5	1	1	prox. *metatarsus III*	*Rangifer tarandus*	2
Pavlov I-SE014	V-5	1	1	dist. *metacarpus III*	*Rangifer tarandus*	2
Pavlov I-SE014	274	2	1	dist. *femur*	*Rangifer tarandus*	5
Pavlov I-SE014	10603	4	1	prox. *femur*	*Rangifer tarandus*	4
Pavlov I-SE014	W	2	1	dist. *radio-ulna*	*Rangifer tarandus*	4
Pavlov I-SE014	U-0	1	1	prox. *ulna*	*Rangifer tarandus*	6
Pavlov I-SE014	P-1	1	1	dist. *humerus*	*Rangifer tarandus*	2
Pavlov I-SE014	3471	1	1	dist. *femur*	*Rangifer tarandus*	6
Pavlov I-SE014	3356	1	1	prox. *metatarsus III*	*Rangifer tarandus*	4
Pavlov I-SE014	3387	1	1	prox. *tibia*	*Rangifer tarandus*	3
Pavlov I-SE014	3386	1	1	prox. *tibia*	*Rangifer tarandus*	6
Pavlov I-SE014	3355	1	1	dist. *tibia*	*Rangifer tarandus*	2
Pavlov I-SE014	3469	1	1	prox. *tibia*	*Rangifer tarandus*	6
Pavlov I-SE014	8488	1	1	dist. *femur*	*Rangifer tarandus*	6
Pavlov I-SE014	9109	1	1	dist. *humerus*	*Rangifer tarandus*	4
Pavlov I-SE014	8307	1	1	prox. *tibia*	*Rangifer tarandus*	6
Pavlov I-SE014	9370	2	1	dist. *metapodium III*	*Rangifer tarandus*	5
Pavlov I-SE014	9370	1	1	prox. *metatarsus III*	*Rangifer tarandus*	6
Pavlov I-SE014	8406	1	1	dist. *radio-ulna*	*Rangifer tarandus*	2
Pavlov I-SE014	7477	1	1	dist. *tibia*	*Rangifer tarandus*	3
Pavlov I-SE014	9475	1	1	dist. *tibia*	*Rangifer tarandus*	3
Pavlov I-SE014	9499	1	1	dist. *metapodium III*	*Rangifer tarandus*	4
Pavlov I-SE014	9288	1	1	*metapodium III* fr.	*Rangifer tarandus*	2
Pavlov I-SE014	7652	1	1	prox. *metacarpus III*	*Rangifer tarandus*	6
Pavlov I-SE014	2623	1	1	dist. *metacarpus III*	*Rangifer tarandus*	1
Pavlov I-SE014	2930	1	1	dist. *metacarpus III*	*Rangifer tarandus*	3
Pavlov I-SE014	3094	1	1	*metapodium III* fr.	*Rangifer tarandus*	3
Pavlov I-SE014	2540	1	1	dist. *tibia*	*Rangifer tarandus*	3
Pavlov I-SE014	2932	2	1	prox. *radius*	*Rangifer tarandus*	4
Pavlov I-SE014	10683	1	1	*metapodium III* fr.	*Rangifer tarandus*	2
Pavlov I-SE014	10239	2	1	*metapodium III* fr.	*Rangifer tarandus*	3
Pavlov I-SE014	10773	1	1	dist. *humerus*	*Rangifer tarandus*	3
Pavlov I-SE014	10588	1	1	prox. *metatarsus III*	*Rangifer tarandus*	3
Pavlov I-SE014	11945	4	1	prox. *metacarpus III*	*Rangifer tarandus*	2
Pavlov I-SE014	11563	4	1	prox. *tibia*	*Rangifer tarandus*	6
Pavlov I-SE014	358	1	1	dist. *humerus*	*Rangifer tarandus*	4
Pavlov I-SE014	427	2	1	dist. *tibia*	*Rangifer tarandus*	5
Pavlov I-SE014	73	3	1	prox. *metatarsus III*	*Rangifer tarandus*	3

Site	Inv. nr. /square	NISP	MNE	Anatomical part	Taxon	FFI score
Pavlov I-SE014	171	4	1	dist. *metapodium III*	*Rangifer tarandus*	3
Pavlov I-SE014	983	2	1	dist. *radio-ulna*	*Rangifer tarandus*	4
Pavlov I-SE014	846	2	1	dist. *radio-ulna*	*Rangifer tarandus*	3
Pavlov I-SE014	833	3	1	*metapodium III* fr.	*Rangifer tarandus*	5
Pavlov I-SE014	569	1	1	prox. *metapodium III*	*Rangifer tarandus*	6
Pavlov I-SE014	1074	5	1	prox. *ulna*	*Rangifer tarandus*	6
Pavlov I-SE014	1171	2	1	*metatarsus III* fr.	*Rangifer tarandus*	4
Pavlov I-SE014	1136	1	1	dist. *metacarpus III*	*Rangifer tarandus*	2
Pavlov I-SE014	1179	1	1	*metacarpus III* fr.	*Rangifer tarandus*	2
Pavlov I-SE014	1222	1	1	dist. *tibia*	*Rangifer tarandus*	2
Pavlov I-SE014	1362	1	1	dist. *tibia*	*Rangifer tarandus*	3
Pavlov I-SE014	1317	2	1	prox. *radius*	*Rangifer tarandus*	4
Pavlov I-SE014	1380	2	1	prox. *metatarsus III*	*Rangifer tarandus*	3
Pavlov I-SE014	1416	5	1	prox. *tibia*	*Rangifer tarandus*	5
Pavlov I-SE014	1584	3	1	prox. *tibia*	*Rangifer tarandus*	3
Pavlov I-SE014	1645	1	1	prox. *ulna*	*Rangifer tarandus*	4
Pavlov I-SE014	1862	1	1	prox. *ulna*	*Rangifer tarandus*	6
Pavlov I-SE014	2086	1	1	dist. *humerus*	*Rangifer tarandus*	3
Pavlov I-SE014	2187	1	1	prox. *metatarsus III*	*Rangifer tarandus*	4
Pavlov I-SE014	2150	8	1	dist. *tibia*	*Rangifer tarandus*	6
Pavlov I-SE014	3297	1	1	dist. *humerus*	*Rangifer tarandus*	2
Pavlov I-SE014	2244	1	1	dist. *humerus*	*Rangifer tarandus*	4
Pavlov I-SE014	2283	1	1	prox. *metatarsus III*	*Rangifer tarandus*	6
Pavlov I-SE014	2305	2	1	prox. *metatarsus III*	*Rangifer tarandus*	2
Pavlov I-SE014	V-1	1	1	dist. *metapodium*	*Canis lupus*	6
Pavlov I-SE014	V-5	1	1	prox. *radius*	*Canis lupus*	2
Pavlov I-SE014	3435	1	1	prox. *metacarpus III*	*Canis lupus*	6
Pavlov I-SE014	3318	1	1	*metatarsus III*	*Canis lupus*	6
Pavlov I-SE014	3312	2	1	*tibia* fr.	*Canis lupus*	6
Pavlov I-SE014	818	2	1	*humerus* fr.	*Canis lupus*	6
Pavlov I-SE014	274	5	1	dist. *humerus*	*Canis lupus*	3
Pavlov I-SE014	518	1	1	*metatarsus III*	*Canis lupus*	6
Pavlov I-SE014	6922	1	1	dist. *metapodium*	*Canis lupus*	6
Pavlov I-SE014	6922	1	1	prox. *metacarpus III*	*Canis lupus*	6
Pavlov I-SE014	8945	1	1	dist. *metapodium*	*Canis lupus*	6
Pavlov I-SE014	7273	1	1	dist. *metapodium*	*Canis lupus*	6
Pavlov I-SE014	8400	2	1	prox. *metatarsus II*	*Canis lupus*	2
Pavlov I-SE014	8400	1	1	prox. *metatarsus III*	*Canis lupus*	4
Pavlov I-SE014	8400	1	1	prox. *metacarpus IV*	*Canis lupus*	5
Pavlov I-SE014	7842	1	1	prox. *metacarpus III*	*Canis lupus*	6
Pavlov I-SE014	6988	1	1	*humerus* fr.	*Canis lupus*	6
Pavlov I-SE014	9934	3	1	prox. *femur*	*Canis lupus*	6
Pavlov I-SE014	11545	1	1	prox. *radius*	*Canis lupus*	4

Site	Inv. nr. /square	NISP	MNE	Anatomical part	Taxon	FFI score
Pavlov I-SE014	12522	1	1	prox. *metatarsus II*	*Canis lupus*	6
Pavlov I-SE014	10618	1	1	prox. *metacarpus III*	*Canis lupus*	5
Pavlov I-SE014	11129	2	1	dist. *humerus*	*Canis lupus*	5
Pavlov I-SE014	2938	1	1	dist. *femur*	*Canis lupus*	5
Pavlov I-SE014	3014	2	1	*metatarsus III*	*Canis lupus*	5
Pavlov I-SE014	2875	2	1	*radius*	*Canis lupus*	6
Pavlov I-SE014	2829	5	1	*femur*	*Canis lupus*	6
Pavlov I-SE014	2976	2	1	*metatarsus IV*	*Canis lupus*	6
Pavlov I-SE014	2885	3	1	*radius*	*Canis lupus*	6
Pavlov I-SE014	2990	1	1	prox. *metatarsus IV*	*Canis lupus*	6
Pavlov I-SE014	3009	1	1	prox. *metacarpus IV*	*Canis lupus*	6
Pavlov I-SE014	T-Y	1	1	dist. *femur*	*Canis lupus*	6
Pavlov I-SE014	T-Y	1	1	prox. *femur*	*Canis lupus*	6
Pavlov I-SE014	6987	2	1	*ulna*	*Canis lupus*	6
Pavlov I-SE014	9154	2	1	dist. *tibia*	*Canis lupus*	6
Pavlov I-SE014	2688	1	1	dist. *femur*	*Canis lupus*	4
Pavlov I-SE014	2655	1	1	prox. *tibia*	*Canis lupus*	6
Pavlov I-SE014	2654	3	1	dist. *tibia*	*Canis lupus*	6
Pavlov I-SE014	11782	1	1	dist. *tibia*	*Canis lupus*	4
Pavlov I-SE014	12617	1	1	prox. *tibia*	*Canis lupus*	1
Pavlov I-SE014	11166	1	1	*tibia*	*Canis lupus*	6
Pavlov I-SE014	551	2	1	dist. *radius*	*Canis lupus*	2
Pavlov I-SE014	P-1	2	1	dist. *metapodium*	*Canis lupus*	6
Pavlov I-SE014	1386	1	1	dist. *tibia*	*Canis lupus*	2
Pavlov I-SE014	1362	1	1	prox. *radius*	*Canis lupus*	2
Pavlov I-SE014	1384	1	1	prox. *metatarsus IV*	*Canis lupus*	5
Pavlov I-SE014	1543	1	1	dist. *radius*	*Canis lupus*	6
Pavlov I-SE014	1601	1	1	prox. *tibia*	*Canis lupus*	6
Pavlov I-SE014	1978	1	1	prox. *metapodium*	*Canis lupus*	6
Pavlov I-SE014	2150	1	1	dist. *metapodium*	*Canis lupus*	6
Pavlov I-SE014	2255	1	1	dist. *metapodium*	*Canis lupus*	6
Pavlov I-SE014	2216	1	1	dist. *humerus*	*Canis lupus*	3
Pavlov I-SE014	2364	1	1	prox. *metacarpus IV*	*Canis lupus*	6
Pavlov I-SE014	1056	1	1	dist. *radius*	*Canis lupus*	6